Hydrogenation of multi-functional compounds

Kathryn Currall
MSc

Submitted in fulfilment of the requirements for the Degree of Doctor of Philosophy

School of Chemistry
College of Science and Engineering
University of Glasgow

2015

Abstract

Selective hydrogenation of a multi-functional compound to achieve high yield of a particular product is often involved in the production of fine chemicals and pharmaceuticals. The control of selectivity can be difficult and can be affected by a number of variables such as the interaction of the reactants and intermediates with the catalyst, the particle size, promoters, steric factors and adsorption geometries. In this study, two selective hydrogenation reactions were studied namely the gas-phase hydrogenation of furfural to furfuryl alcohol and liquid-phase hydrogenation of 4-nitroacetophenone.

The hydrogenation of furfural is the sole production route for furfuryl alcohol which is used widely in the chemical industry. However, a variety of products can be formed through the hydrogenation of furfural depending on the catalyst used. The industrial process is conducted at high temperature and pressure using a copper chromite catalyst. However, the main drawback of this method is the toxicity of the catalyst.

In this study, silica supported copper catalysts proved to be active and selective alternative catalysts for the hydrogenation of furfural to furfuryl alcohol. The higher the copper loading the greater the furfural conversion as more Cu sites were present with both catalysts achieving 98% selectivity for furfuryl alcohol. Ceria was investigated as a promoter for copper catalysts and the incorporation of 1% CeO_x was found to enhance the selectivity towards furfuryl alcohol. The presence of Ce^{3+} sites was thought to polarise the carbonyl bond facilitating nucleophillic attack by dissociated hydrogen present on Cu. However, 5% CeO_x promoter was found to reduce the selectivity of the catalyst possibly by the blocking Cu active sites.

Pd was also investigated as a promoter was found to enhance the activity and selectivity of the catalyst as it activated hydrogen allowing for more facile hydrogenation of the carbonyl group.

Cu1132, a BASF copper-chromite catalyst used for the production of furfuryl alcohol by hydrogenation of furfural exhibited moderate activity but excellent selectivity towards furfuryl alcohol (almost 100%).

For all catalysts, deactivation was observed over time on stream mainly due to carbon laydown. Polyaromatic coke formation on the surface of copper catalysts blocked pores and significantly reduced the activity of the catalyst. 5% Cu + 5% CeO_x/SiO_2 catalyst showed a slow deactivation compared to all of the other catalysts and post-reaction XRD suggested sintering was the cause of deactivation. TPD of 5% Cu + 1% CeO_x/SiO_2 showed desorption of furfural, 2-methylfuran and furan suggesting that the catalyst was poisoned causing deactivation.

An important reaction in the pharmaceutical industry is the hydrogenation of 4-nitroacetophenone (4-NAP) which yields 4-aminoacetophenone (4-AAP); a chemical intermediate used in the production of the hypoglycemic drug acetohexamide. Further hydrogenation of the carbonyl group yields 1-(4-aminophenyl)ethanol (4-APE) which can be dehydrated to give a substituted styrene that can be polymerised. As the consecutive hydrogenation of 4-NAP has not been the subject of significant study, this reaction was systematically investigated using a series of Rh/SiO_2 catalysts.

Functional group hydrogenation followed the order NO_2 >> C=O > Ph > OH with the nitro group being hydrogenated approximately an order of magnitude faster than the carbonyl group, while hydrogenation of either the phenyl ring or the alcohol function is a factor of two slower than carbonyl hydrogenation. This combination of kinetic controls allows high selectivity to 4-AAP (99%) and 4-APE (94%) to be achieved at different times in the reaction. The presence of 4-NAP inhibits 4-AAP hydrogenation due to strong adsorption of the 4-NAP while deuterium studies revealed the presence of a kinetic isotope effect for both 4-NAP and 4-AAP. Full kinetic analysis of the reaction system gave activation energies of ~48 kJ mol^{-1} for 4-NAP and 4-AAP hydrogenation, with orders of reaction of ~1 for hydrogen and a zero order dependence for 4-NAP.

Although 4-NAP inhibits 4-AAP hydrogenation when present, 4-AAP hydrogenation is faster after 4-NAP hydrogenation than over a fresh catalyst. The reason for this may be that 4-NAP adsorption causes a surface reconstruction which allows easier hydrogen transfer or sub-surface hydrogen.

The hydrogenation of both 4-NAP and 4-AAP showed an antipathetic particle size effect with an increase in TOF with increasing metal crystallite particle size. This suggests that the hydrogenation reaction takes place on the plane face surface as opposed to edge and corner sites. However the electronic changes in small metal particles of this size are also significant and it is likely that the antipathetic particle size effect is a combination of both an electronic and geometric effect.

Addition of 4-methylcyclohexylamine (4-MCHA) to 4-NAP and 4-AAP hydrogenation systems results in an enhancement of rate for both reactants. For 4-NAP hydrogenation, this is due to electron donation from the acyclic amine causing a reduction of the reactant-surface bond strength since it is clear that 4-NAP forms a strong bond to the surface as shown by the zero order kinetics and the inhibition of 4-AAP hydrogenation, a reduction in the strength of 4-NAP adsorption would enhance the rate of 4-NAP hydrogenation. However, 4-AAP is not strongly bound to the surface so a weakening the carbonyl interaction is unlikely to lead to an enhanced rate. Just as the rate enhancement observed for 4-AAP hydrogenation after 4-NAP hydrogenation has been attributed to changes in hydrogen concentration in the rhodium by strong adsorption of 4-NAP, 4-MCHA is also strongly adsorbed which means it may promote 4-AAP hydrogenation by a similar process.

Author's Declaration

I declare that, except where explicit reference is made to the contribution of others, that this thesis is the result of my own work and has not been submitted for any other degree at the University of Glasgow or any other institution.

Signature.....

Printed name.....

Contents

List of figures

List of tables

Acknowledgements

First and foremost, thanks must go to my supervisor Prof. David Jackson for his help and guidance over the (many) years; for always being on hand to answer my silly questions, providing words of encouragement and for believing in my abilities. Thank you to Ron Spence and Andy Monaghan for both their technical and moral support and thanks to the rest of the Catalysis Research Group for making my time as a postgrad most enjoyable.

To my family and friends, thank you for your love and support and above all for putting up with me while I was writing up.

Daniel you can stop asking me “is it finished yet?” Thank you for being you because without you I could not have finished it.

1 Introduction

1.1 Background

The production of fine chemicals and pharmaceuticals often involves the selective hydrogenation of a multi-functional compound and commonly a high yield of a specific intermediate is required to form a range of other products. A typical example of such a transformation is the selective hydrogenation of an unsaturated aldehyde to the corresponding unsaturated alcohol [1,2]. Hydrogenation of a carbonyl group is not in itself difficult, however it is difficult to obtain the desired product when another functional group is present due to side reactions such as hydrogenation of the C=C bond which is thermodynamically favoured over the hydrogenation of the carbonyl group [3]. Hydrogenation of these compounds has been studied over a variety of catalysts, for example using copper-chromite catalysts [4-6], as copper will preferentially hydrogenate the carbonyl group [6] whereas noble metals such as platinum favour hydrogenation of the unsaturated carbon bonds [7]. The ability to achieve high selectivity depends on understanding the process and the interaction of the reactants and intermediates with the catalyst. The following examples show how the particle size, promoters, steric factors and adsorption geometries influence selectivities. Acrolein (AC), is the simplest α,ß-unsaturated aldehyde and may be hydrogenated to form allyl alcohol (AOL), propanal (PA) and n-propanol (nPOL) as shown in figure 1.1.

Figure 1.1 Hydrogenation of acrolein

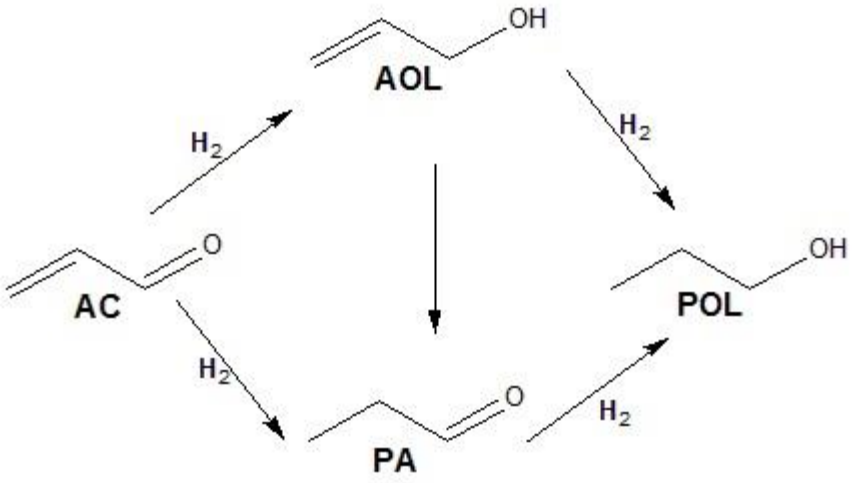

The selective hydrogenation of acrolein to allyl alcohol has been studied using silica supported silver catalysts. The formation of allyl alcohol over propanal was found to increase with increasing particle size suggesting that the orientation of acrolein on the plane face surface of Ag crystals favoured allyl alcohol production [8].

The selectivity to the unsaturated alcohol was found to be governed by the nature of the active metal, metal particle size [9], support effects [10,11] and the presence of promoters or bimetallic phases [12,13]. A study compared the hydrogenation of crotonaldehyde and furfural using a copper chromite catalyst and found copper to an active metal for furfuryl alcohol production but exhibited a poor selectivity (~3%) for crotyl alcohol [14].

The effect of promoters was revealed when CeO_2 and MgO were studied as promoters for ruthenium catalysts used for gas-phase hydrogenation of crotonaldehyde and liquid-phase hydrogenation of citral [15]. MgO did not influence selectivity however the presence of CeO_2 greatly enhanced selectivity for the production of unsaturated alcohols. Ceria can act as a promoter and a reducible support. Its unique ability to store and release oxygen (redox property) makes it attractive for oxide catalysts because it can provide Lattice oxygen and prevent the sintering of noble metals [16,17]. The enhancement in selectivity to the unsaturated alcohols was attributed to the presence of Ce^{3+} sites capable of polarising the carbonyl bond facilitating nucleophillic attack by dissociated hydrogen present on Ru [15-17].

Many studies examining α,β-unsaturated aldehyde hydrogenation have shown that bulky substituents facilitate high selectivity to unsaturated alcohols [2,18-20]. Not only can the substituents sterically hinder the interaction of C=C bonds with the surface of the catalyst but they may also have an inductive effect that deactivates the C=C bond, as was found for the hydrogenation of cinnamaldehyde (CA) (shown in figure 1.2), where excellent selectivity (80-90%) to cinnamyl alcohol (COL) was achieved using platinum [21], ruthenium [22], and cobalt catalysts [23].

Figure 1.2 Hydrogenation of cinnamaldehyde

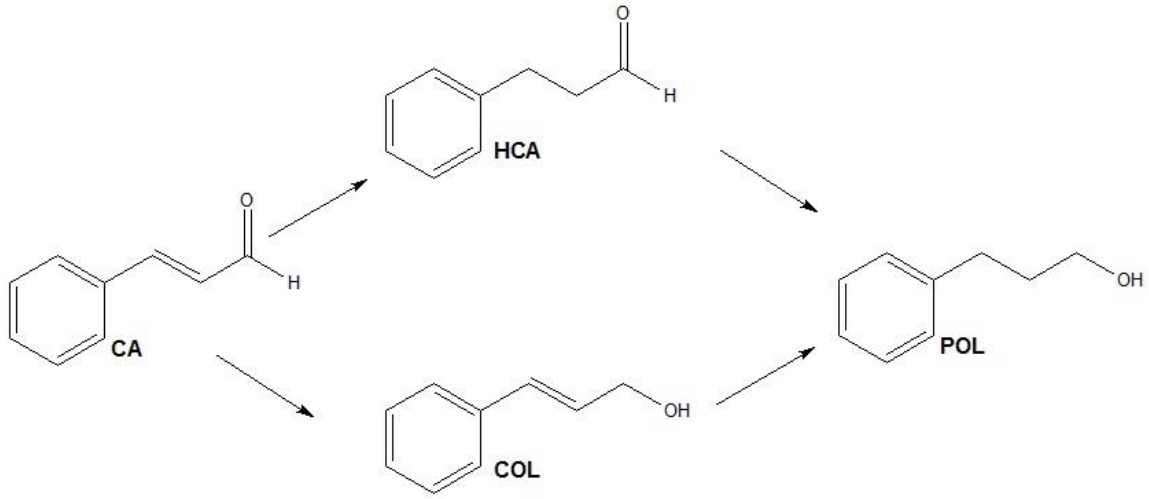

Further hydrogenation of both HCA and COL produced phenyl propanol (POL). Larger particles were found to give a higher selectivity to COL and this was attributed to steric effects [22], where the phenyl group prevents the close approach of the C=C to the surface of a large particle so that the molecule is tilted with C=O closer to the surface and therefore more easily activated [24]. For smaller particles there is nothing to hinder the approach of the phenyl group and so it is more easily hydrogenated resulting in low selectivity to COL.

Adsorption geometries reportedly controlled the competitive hydrogenation of the aromatic ketone acetophenone. Competitive hydrogenation between the phenyl and carbonyl groups was investigated using Pt catalysts and found that pre-treatment conditions had a significant effect on the selectivity [25]. The effect of substituent on the hydrogenation of substituted acetophenones has been studied over nickel and cobalt catalysts [26] and in that study the choice of metal was found to be crucial as the electronic and steric effects of the substituents were greater using the nickel catalyst. This behaviour was suggested to be related to the strength of adsorption and the difference in *d*-electron density of the metals [26].

As can be seen from the above examples the control of selectivity can be difficult and be affected by a number of variables. In this study, two selective hydrogenation reactions were studied namely the gas-phase hydrogenation of furfural to furfuryl alcohol, and liquid-phase hydrogenation of 4-nitroacetophenone. The hydrogenation of furfural can produce various products

depending on the catalyst and reaction conditions used. In this study we have focused on the gas phase reaction over copper catalysts. The selective hydrogenation of 4-nitroacetophenone (4-NAP) has received little attention however the ability to selectivity produce 4-aminoacteophenone (4-AAP) or 1-(4-aminophenyl)ethanol (4-APE) (both of which are employed in a variety of applications) is typical of many liquid phase hydrogenations in the fine chemical industry.

1.2 Hydrogenation of furfural

Furfural is obtained from the dehydration of pentoses, five-carbon sugars, such as xylose and arabinose, commonly obtained by acid-catalysed digestion of hemicellulose-rich agricultural wastes [27]. It has received much attention recently as it can be upgraded to provide valuable biofuel components [28-34]. Hydrogenation remains the most versatile reaction to upgrade furanic components to biofuels [31].

Hydrogenation of furfural is also the sole production route for furfuryl alcohol which is widely employed in the chemical industry [35-39]. It is mainly used in the manufacture of synthetic fibres, rubbers, resins and farm chemicals [35,36]. Additionally, it is used as a chemical intermediate during the manufacture of lysine, vitamin C and lubricants [37-39]. Depending on the catalyst employed, the hydrogenation of furfural can yield a variety of products, such as furfuryl alcohol, 2-methylfuran, furan, tetrahydrofuran, tetrahydrofurfuryl alcohol and even ring-decomposition products, such as pentanols and pentanediols. The possible hydrogenation products of furfural are shown in figure 1.3.

Figure 1.3 Plausible reaction scheme for furfural hydrogenation [40]

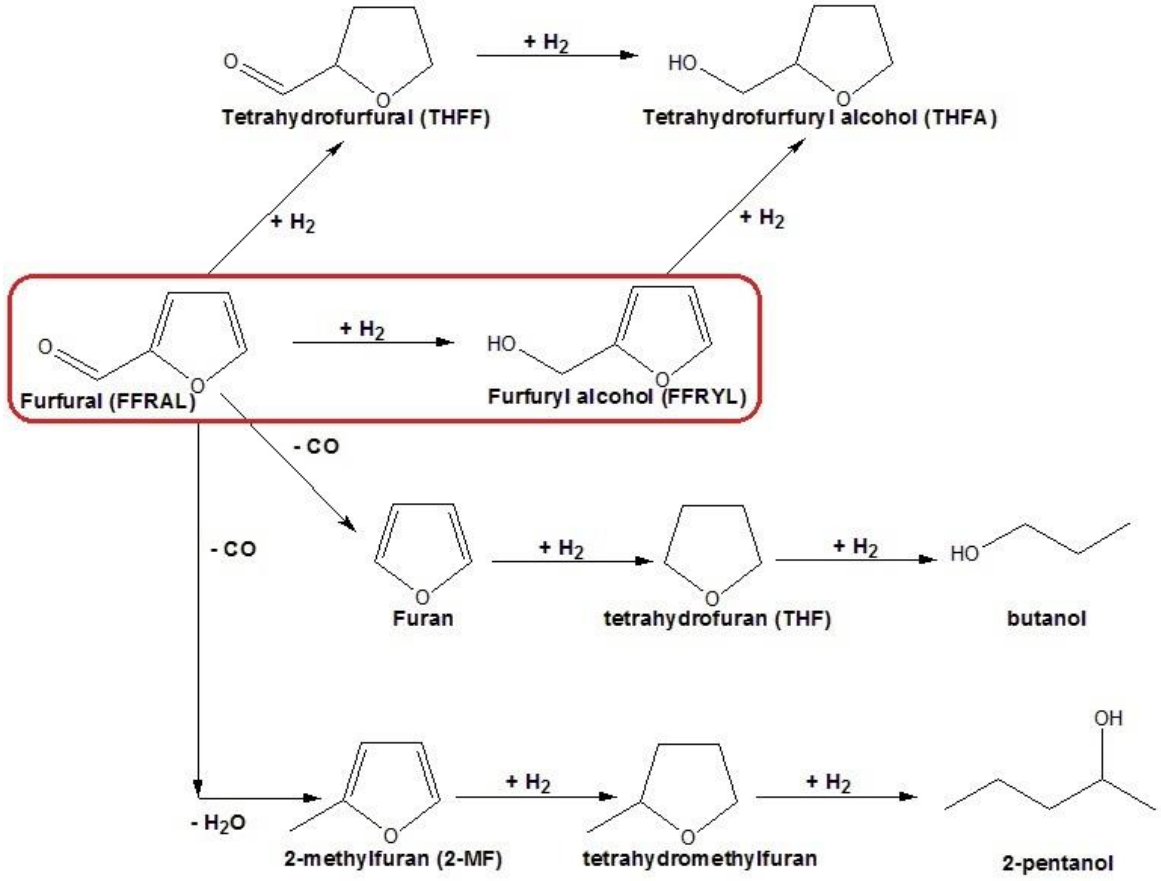

The hydrogenation of furfural to furfuryl alcohol can be carried out in either liquid or vapour-phase [41-43]. A high yield (>96%) of furfuryl alcohol has been reported through liquid phase batch hydrogenation using a copper chromite catalyst ($CuCr_2O_4$-CuO) with and without alkali-earth metal oxide promoters such as CaO, BaO or ZrO [44]. Typically, liquid phase hydrogenation is conducted using mild temperatures (<180°C) but at high hydrogen pressure (70-100 barg) [45-48]. Vannice *et al*. found that copper chromite catalyst, pre-treated at 300°C, converted 64% of furfural with 70% selectivity for furfuryl alcohol [14]. The main drawback of this method is the toxicity of the catalyst due to the presence of CrO_3 [39]. Furthermore, new environmental restrictions state that deactivated copper chromite catalyst cannot be used in landfill sites [41]. Therefore, it is important to design an environmentally friendly, active and selective catalytic system for obtaining furfuryl alcohol.

The hydrogenation of furfural in the liquid-phase has been studied extensively using supported metal and amorphous alloys as catalysts such as Cu, Ni, Mo, Co, Pt, Rh, Ru and Pd [14,38,39,42,50-54] and Ni-P, Ni-B and Ni-P-B ultrafine materials [55].

In 1923, platinum was identified as an active catalyst for furfural hydrogenation [56]. However, supported active palladium oxide has been found to catalyse undesired side reactions such as hydrogenolysis, decarbonylation, hydrogenation of the furan ring and ring opening. Kijenski *et al*. have reported the effect of covering supported Pt catalysts with a monolayer of transition metal oxide [38]. It was found that silica supported Pt covered with partially reducible titania achieved 93.8% selectivity for furfuryl alcohol at atmospheric pressure and temperatures between 150 and 300 °C. Where electron-rich surfaces such as MgO meant weak adsorption of the equally electron-rich substrate promoting furfural conversion, strong adsorption occurred on electron-deficient surfaces such as γ-Al_2O_3 enabling polymerisation and condensation.

In the vapour-phase hydrogenation of furfural the products that can be produced are furfuryl alcohol, 2-methylfuran and tetrahydrofurfuryl alcohol. These arise from the reduction of the C=O group and/or the furan ring [57]. Secondary reactions such as hydrogenolysis of the C=O bond, decarbonylation or furan ring

opening may occur [41]. The formation of some condensation products of high molecular weight has also been reported [38].

Gas-phase hydrogenation of furfural requires much milder conditions than the Liquid-phase reaction and Cu has been studied extensively for this process and found to exhibit high activity and selectivity to furfuryl alcohol [39,42,49,50,52,54,57,58]. A comparison of silica supported Cu, Pd and Ni catalysts for furfural reactions was conducted by Sitthisa and Resasco [50]. At atmospheric pressure and between 210-290°C, high selectivity towards furfuryl alcohol was obtained using Cu/SiO_2 with 2-methylfuran the only by-product. Pd/SiO_2 promoted decarbonylation to produce furan which could further react with hydrogen to form tetrahydrofuran (THF). Finally, over Ni/SiO_2 catalyst ring opening products such as butanal, butanol and butane were formed. The strength of interaction of the furan ring was found to follow the trend Ni > Pd >> Cu and the formation of only the η^1-aldehyde intermediate on the Cu surface [60] was reported to be responsible for the high selectivity towards alcohol formation.

Figure 1.4 η^1-(O)-aldehyde on Cu surface

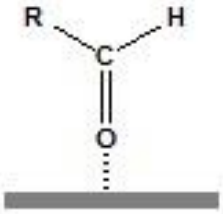

However, the most likely intermediate on Ni and Pd surfaces was thought to be the η^2-adlehyde [61], which can react further with hydrogen to produce either the corresponding alcohol, or decompose to form the acyl intermediate which results in the formation of furan. This means that the selectivity towards furfuryl alcohol was much lower for both Pd and Ni catalysts.

Figure 1.5 η^2-(C-O-)aldehyde and acyl species on Pd and Ni surfaces

The addition of a second metal or promoter has also been found to improve activity and/or selectivity [39,54] by increasing the surface area or acting as a Lewis acid site to polarise the C=O bond. Ni or Co systems containing Mo promoter [59], Ni-Fe, Cu-Ca bimetallic catalysts and Cu-MgO with Co, Zn, Fe, Cr, Pd or Ni promoters have shown high selectivity (98%) and furfural conversion (~100%).

Ce-promoted Ni-B amorphous catalyst has been studied for liquid phase hydrogenation of furfural to furfuryl and found to be more active and selective than Ni-B [62]. An optimum loading of Ce was determined and the Ce^{3+} species was thought to act as a Lewis acid site which would polarise the carbonyl group facilitating nucleophilic attack by hydrogen dissociatively adsorbed on neighbouring Ni active sites [63]. If the Ce content was too high, too many Ni active sites were covered and the catalyst was less active.

Cu-MgO coprecipitated catalysts with various Cu Loadings were studied for vapour-phase hydrogenation of furfural with 98% activity and selectivity achieved using 16 wt.% Cu [39]. In this study, Rao *et al*. proposed that both Cu^0 and Cu^+ species were required for optimum catalytic performance as catalysts with higher Cu loading, containing more Cu^{2+}, were found to be less active.

However, there have been two problems identified with gas-phase hydrogenation, the first being the production of 2-methylfuran by-product at high furfural conversion [44]. Cu-based catalysts operated at high temperature (200-300˚C) and low pressure (~1 bar) and a H_2:furfural molar ratio of 5-8 have reportedly shown high selectivity to 2-methylfuran [64]. Studies of reaction pathways have indicated that furfural is converted to furfuryl alcohol and subsequent dehydration forms 2-methylfuran [39,41,49,50,65]. An alternative reaction pathway for furfural hydrogenation to by-products is shown in figure 1.6.

Figure 1.6 Alternative reaction pathway for furfural hydrogenation

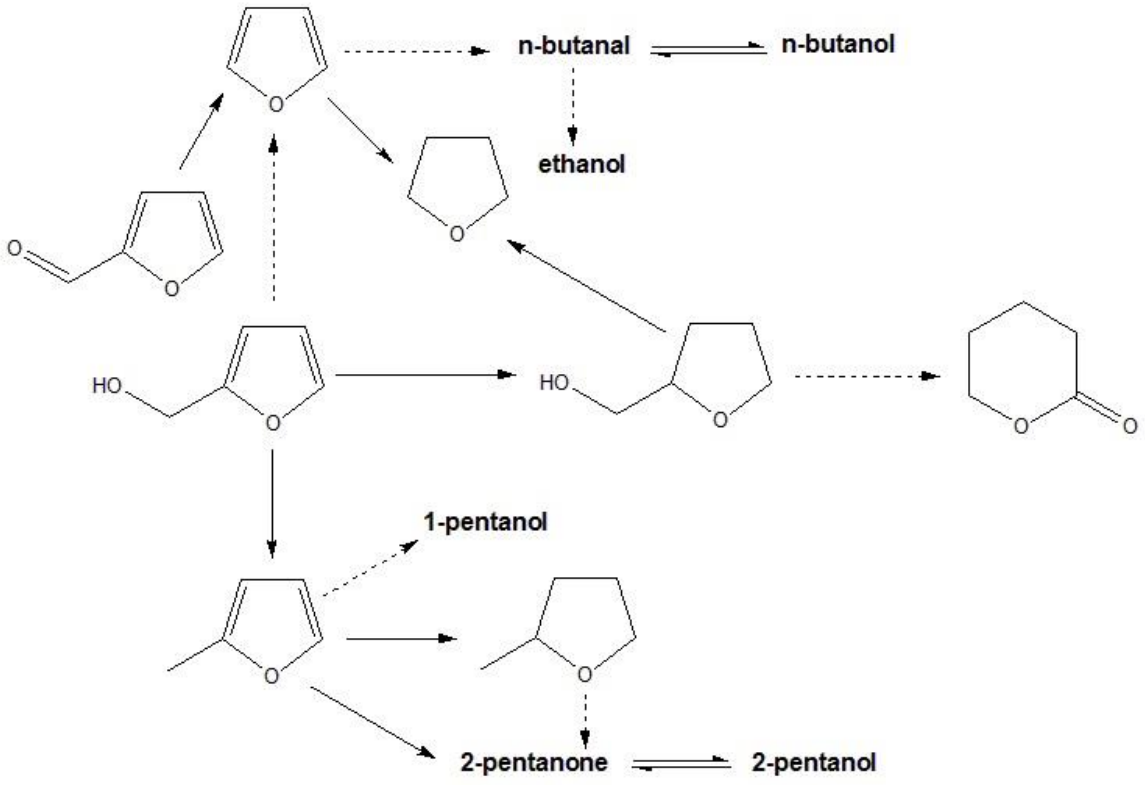

An active alternative to copper chromite catalysts has not yet been developed as most catalysts have been reported unsuitable due to their rapid deactivation [27,66-68]. Deactivation has been observed in all previous studies of furfural hydrogenation [14,41,42,64], and various causes have been proposed, such as poisoning of the catalyst by either a reaction intermediate or by-product, the formation of coke on the catalyst surface, a change in the oxidation state of copper during the reaction or sintering of the catalyst under reaction conditions.

Catalyst deactivation has been found to enhance selectivity in other reactions, e.g. in the hydrogenation of nerol to citronellol using a Rh/Al_2O_3 catalyst [69]. Figure 1.7 shows the possible products of nerol hydrogenation and it is clear that citronellol is only one of a number of possible products.

Figure 1.7 Reaction pathways for hydrogenation of nerol

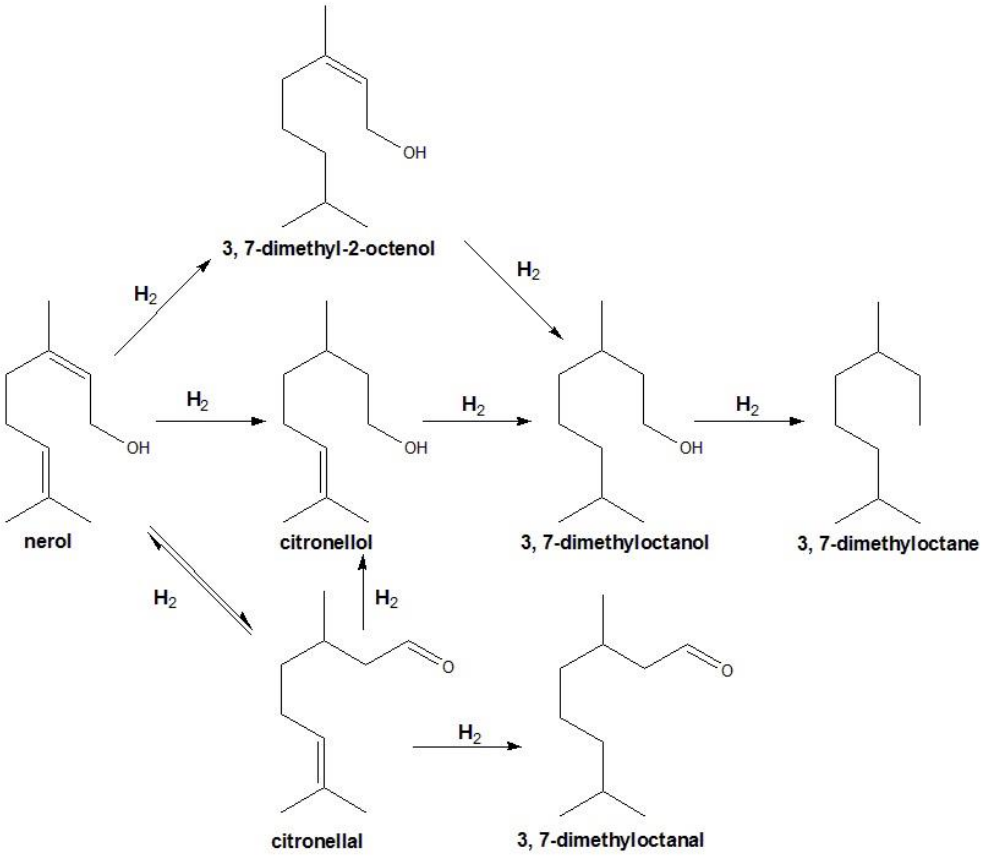

Decarbonylation of nerol was found to cause catalyst fouling and a subsequent decrease in surface area. This inhibited consecutive hydrogenation of citronellol to form 3,7-dimethyloctanol and isomerisation forming cis-3,7-dimethyl-2-octenol.

Contrastingly, catalyst deactivation can have a detrimental effect on the selectivity of a reaction and this has been observed for the selective hydrogenation of 4-isobutylacetophenone (4-IBAP) to 1-(4-isobutylphenyl) ethanol (4-IBPE) which is an intermediate reaction step involved in the synthesis of ibuprofen [70]. Consecutive hydrogenolysis of 4-IBPE to 4-isobutylethylbenzene (4-IBEB) and the product of oligomers causes catalyst fouling and a reduction in 4-IBPE selectivity [71].

Nevertheless selective poisoning of copper catalysts has been used to achieve higher selectivity, for example in the production of crotyl alcohol through the hydrogenation of crotonaldehyde [72-77]. A 5% Cu/Al_2O_3 catalyst was found to preferentially produce 1-butanol however, once dosed with thiophene the product distribution favoured crotyl alcohol formation [72]. It was thought that

modification of the catalyst using sulphur compounds formed Cu-S and Cu^{+}-S sites which were more selective for the hydrogenation of the carbonyl bond than hydrogenation of the C=C bond. Whereas, silica supported Pd-Cu alloy catalyst treated with thiophene has been tested and showed no selectivity towards crotyl alcohol [77]. It was reported that thiophene preferentially poisoned the Cu which left active Pd sites which favoured hydrogenation of the C=C bond.

Therefore the aim of this study was to investigate the extent and cause of deactivation of copper-based catalysts for the selective hydrogenation of furfural to furfuryl alcohol. The reactions were conducted in gas-phase and the reaction parameters optimised to give the highest activity and selectivity to furfuryl alcohol. Ceria was investigated as a catalyst promoter to determine if it can be used to improve the yield of furfuryl alcohol and/or improve resistance to the mechanism of deactivation.

1.3 Hydrogenation of 4-nitroacetophenone

An important reaction in the pharmaceutical industry is the hydrogenation of 4-nitroacetophenone (4-NAP). It has three functional groups that can be hydrogenated: the nitro group, the carbonyl group and the benzene ring. Hydrogenation of the nitro group yields 4-aminoacetophenone (4-AAP) which is used in the production of flavaniline and acetohexamide; an oral hypoglycemic drug [78,79]. Subsequent hydrogenation of the carbonyl present in 4-AAP produces 1-(4-aminophenyl) ethanol (4-APE) which can be dehydrated to give a substituted styrene that can be polymerised [80]. Figure 1.8 shows the full hydrogenation profile for this reaction and includes the formation of 1-(4-cyclohexylamine)ethanol (4-ACHE), 4-ethylaniline (4-EA) and 4-ethylcyclohexylamine (4-ECHA).

Figure 1.8 Reaction scheme for 4-NAP hydrogenation

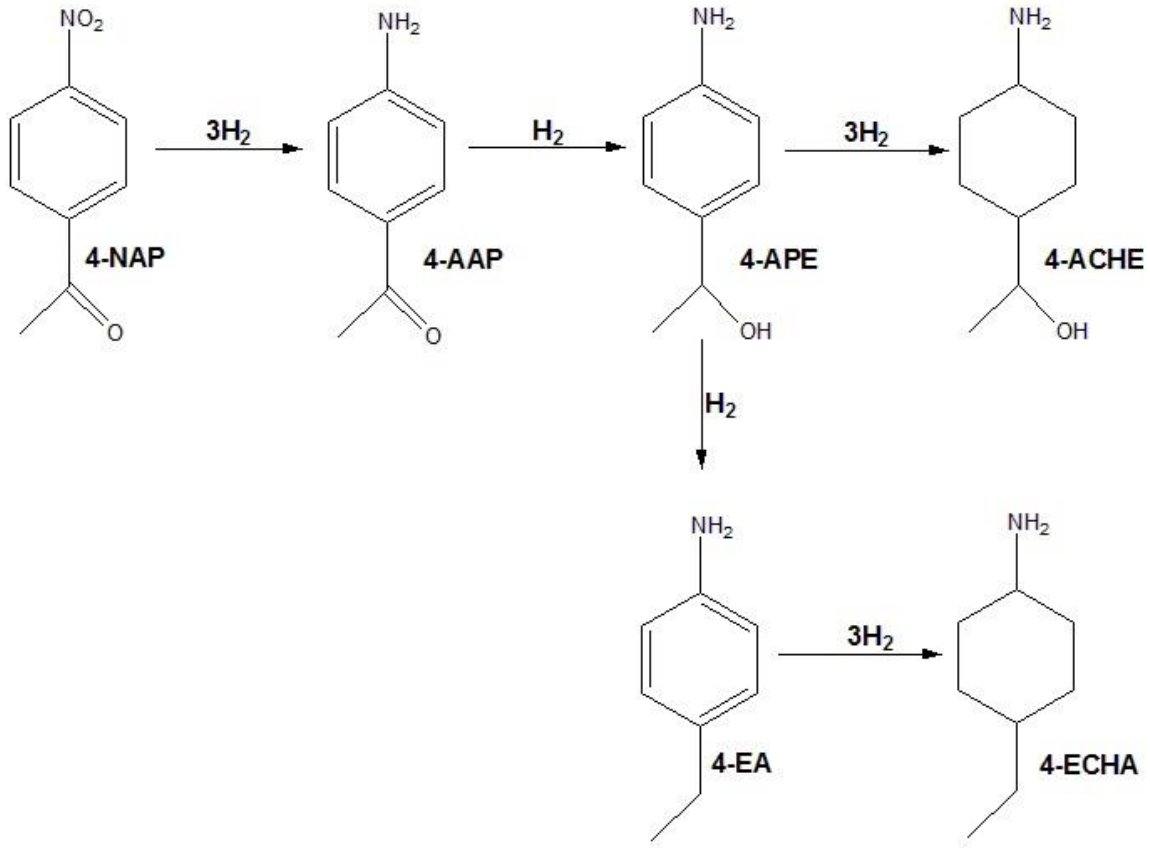

Hydrogenation of a nitro-substituted aromatic compound and the hydrogenation of aromatic ketone often involve the use of either platinum or palladium catalysts. Colloidal rhodium and palladium catalysts have been studied for the hydrogenation para-substitued nitrobenzenes to the corresponding amines [81].

The catalytic performance of rhodium was reportedly affected by the electron donating or withdrawing properties of the substituents, and by the presence of an acid or base, however the performance of the palladium catalyst remained unchanged. The reduction of acetophenone, an aromatic ketone, can be carried out using various catalysts such as platinum, palladium, ruthenium and nickel systems [82-92]. The competitive hydrogenation of C=O and C=C bonds has been studied using both oxidised and reduced Pt/SiO_2 catalysts. The reaction network for acetophenone hydrogenation is shown in figure 1.9.

Figure 1.9 Hydrogenation of acetophenone

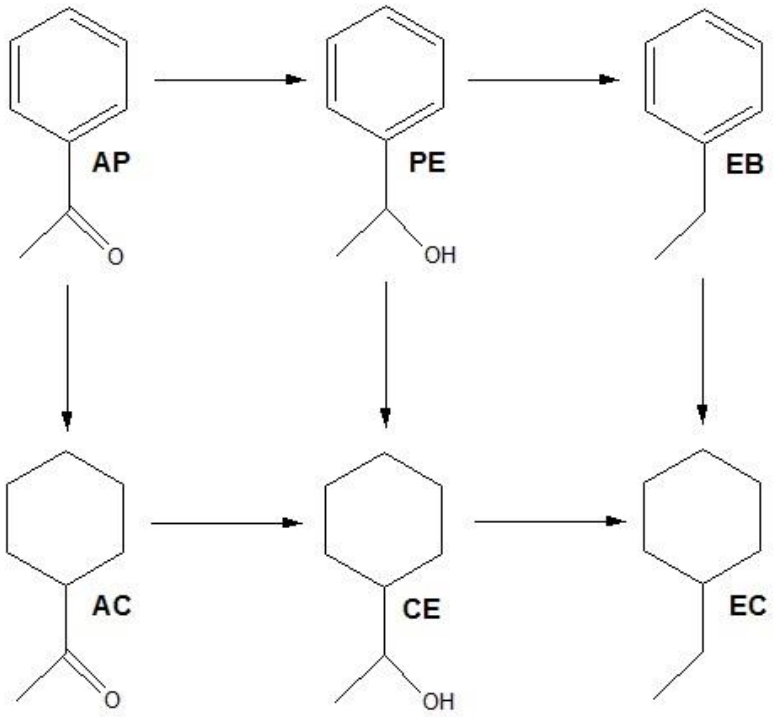

The hydrogenation of acetophenone can produce various products including 1-phenylethanol (PE), ethylbenzene (EB), 1-cyclohexylethanol (CE), acetylcyclohexane (AC) and ethylcyclohexane (EC). The observed 1-phenylethanol selectivity (83%) for reduced Pt/SiO_2 catalyst was reportedly due to fragments from AP dissociation inhibiting the interaction of the phenyl group with the Pt surface [25] and therefore reducing CE formation. The strong adsorption of PE on the Pt surface also suppressed phenyl group hydrogenation. Whereas, the oxidised Pt/SiO_2 was found to activate the C=O group and EB was formed preferentially over CE.

Acetophenone hydrogenation has also been studied using 5% Pd/C and 5% Rh/Al_2O_3, and it was found that a high yield of 1-phenylethanol was achieved using the palladium catalyst (~99.9%) whereas significant hydrogenation of the aromatic ring was observed when the rhodium catalyst was used [90].

Multi-functional compounds such as nitro aromatics containing a ketonic function can be selectively reduced to form an amino ketone. This has been demonstrated by the derivation of Mannich bases from 4-nitroacetophenone (4-NAP) which were reduced using 5% Pd/C in methanol to form 4-aminoacetophenone (4-AAP) [94] . Hawkins and Makowski [95] have used parallel screening to study three separate Pd catalyst formulations and identify the optimum reaction conditions to achieve high selectivity for 4-AAP, 4-APE and 4-EA respectively. A 5% $Pd/CaCO_3/Pb$ catalyst was used at low hydrogen pressure showed 97% selectivity for 4-AAP. At 7 bar hydrogen pressure, 10% Pd/C exhibited 95% selectivity towards 4-APE, and this catalyst dosed with 1.1 molar equivalent of methanesulphonic acid (MsOH) achieved 99% 4-EA selectivity.

Jackson and co-workers studied a 1% Pd/C for the hydrogenation of 2-, 3- and 4-nitroacetophenone to the respective aminoacetophenone. Hydrogenation of 3-NAP exhibited the highest rate of reaction owing to the cooperative position of the electron-withdrawing nitro and carbonyl groups. The slowest rate was observed for 2-NAP however, a nitrogen insertion product, indolinone, was formed which suggested the presence of a $CH_3COPhN(a)$ species on the surface [96].

Figure 1.10 Hydrogenation of 2-nitroacetophenone (2-NAP)

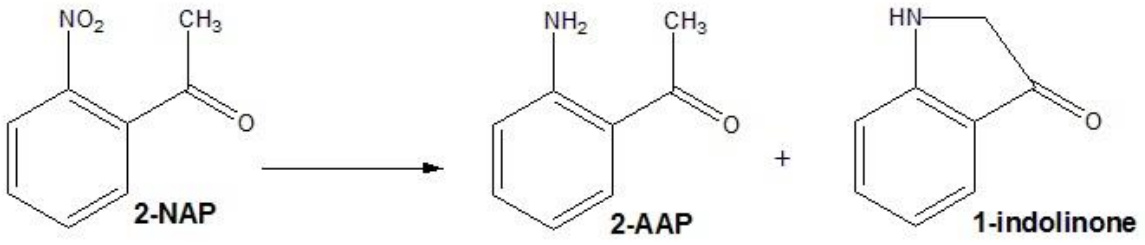

Rhodium catalysts have been used for the hydrogenation of p-toluidine which contains two functional groups namely; an aromatic ring which can be hydrogenated and an amine group which can be cleaved, like 4-ethylaniline (4-EA). An antipathetic size effect was observed as the turnover frequency (TOF)

increased with increasing crystal size suggesting that plane face surface atoms were active sites for ring hydrogenation [97]. Hindle *et al*. also noted that the presence of 4-methylcyclohexylamine (4-MCHA) inhibited p-toluidine hydrogenation as the lone pair on the nitrogen atom forms a strong bond to the active metal [98].

More recently, a study of 3-nitroacetophenone (3-NAP) hydrogenation using ~2.3% Rh/SiO_2 catalysts showed that high selectivity to 3-aminoacetophenone (3-AAP) and 1-(3-aminophenyl)ethanol (3-APE) could be achieved. 3-AAP is used as food flavouring and in synthesising pharmaceutical intermediates such as adrianol, and zaleplon [85]. Earlier studies [99-102] focussed on the hydrogenation of 3-NAP to 3-AAP only, and did not consider the full reaction profile. 3-APE is a useful intermediate in the synthesis of polyester dyestuffs [88]. An antipathetic particle size effect was reported in this study as turnover frequency increased with an increase in the size of the metal crystallites, and it was suggested that the reaction took place on plane face surfaces of the Rh crystals [103].

The hydrogenation of 4-nitroacetophenone (4-NAP) has not been the subject of significant study and is not covered well in the heterogeneous catalysis literature. Moreover, none of the previous work examined the consecutive hydrogenation of 4-NAP to 4-aminoacetophenone (4-AAP) and 4-ethylaniline as shown in figure 1.8.

In the present study, the hydrogenations of 4-NAP and 4-AAP were investigated over a series of Rh/SiO_2 catalysts. As little literature exists surrounding this reaction over heterogeneous catalysts, a systematic study was carried out to investigate the effect of temperature, pressure and reactant concentration. The competitive hydrogenation between 4-NAP and 4-AAP was also investigated as was the effect of an alicyclic amine (4-methylcyclohexylamine) on the reaction activity and selectivity. The catalyst series varied in metal crystallite size and silica support pore size, so metal particle size effects and pore size effects have been investigated. Reactions were also carried out using deuterium instead of hydrogen to determine the role of hydrogen in the rate determining step.

2 Aims

2.1 Gas-phase hydrogenation

The aim of this study was to investigate the extent and cause of deactivation of copper-based catalysts for the selective hydrogenation of furfural to furfuryl alcohol.

Figure 2.1 Hydrogenation of furfural to furfuryl alcohol

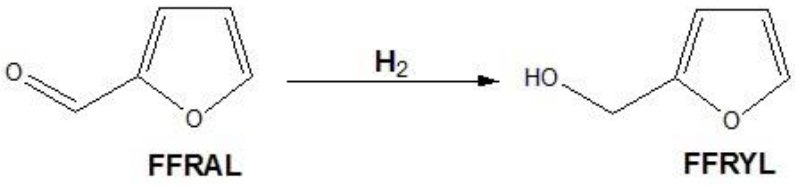

The reactions were conducted in gas-phase and the reaction parameters optimised to give the highest activity and selectivity to furfuryl alcohol. Ceria was investigated as a catalyst promoter to determine if it can be used to improve the yield of furfuryl alcohol and/or improve resistance to the mechanism of deactivation.

2.2 Liquid-phase hydrogenation

The aim of this study was to investigate the Liquid-phase hydrogenation of 4-nitroacetophenone to the corresponding products as shown in figure 2.2.

Figure 2.2 Hydrogenation of 4-NAP

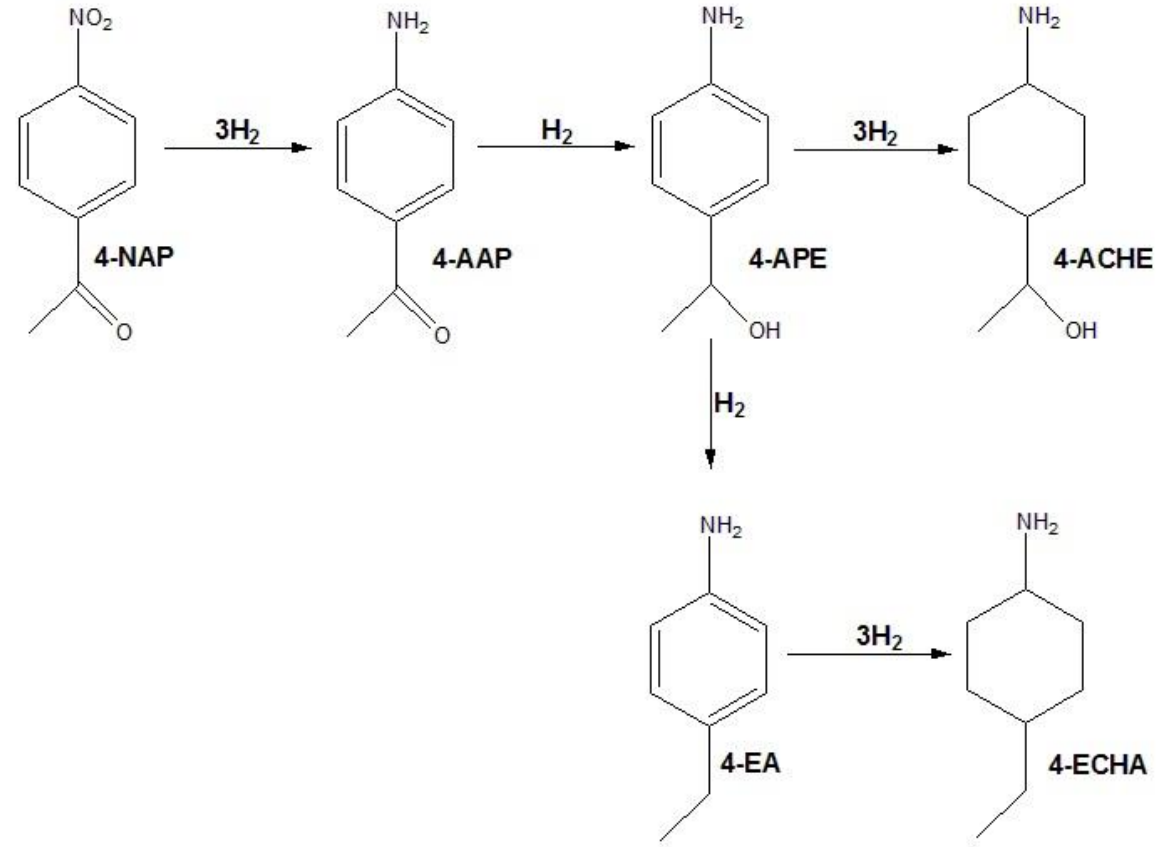

As little literature exists surrounding this reaction over heterogeneous catalysts, a systematic study was carried out to investigate the effect of temperature, pressure, concentration and the presence of an aliphatic amine on the progress of the reaction. Reactions were conducted in the liquid-phase, over a series of 2.5% Rh/SiO_2 catalysts and under both hydrogen and deuterium to determine the rate determining step.

3 Experimental

The following chapter describes the procedures used during experimentation. It includes the analysis of Liquid samples and reactor design.

3.1 Gas-phase hydrogenation

In this section the catalysts, reagents, reactor and analyses used for the gas-phase hydrogenation experiments are described.

3.1.1 Catalysts

A series of silica supported copper catalysts were used for the gas-phase hydrogenation of furfural and these are shown in table 3.1. The catalysts were prepared [104] at the University of Glasgow by spray impregnation using nitrate precursors and dried at 60°C. A BASF copper chromite catalyst, Cu1132, used industrially for the hydrogenation of furfural to furfuryl alcohol was also tested. The exact composition of this catalyst was unknown.

Table 3.1 Catalysts for gas-phase hydrogenation

Catalysts
Cariact Q10 silica
5% Cu/SiO_2
5% CeO_x/SiO_2
5% Cu + 5% CeO_x/SiO_2
5% Cu + 1% CeO_x/SiO_2
10% Cu/SiO_2
10% Cu + 5% CeO_x/SiO_2
10% Cu+ 5% CeO_x + 0.05% Pd/SiO_2
Cu1132

3.1.2 Characterisation

Catalyst characterisation was conducted prior to reaction. Surface area determination, thermogravimetric analysis (TGA) and powder X-ray diffraction (XRD) were carried out to characterise each catalyst.

3.1.2.1 Surface area determination

The surface area and pore size for each catalyst was determined using a Micrometrics Gemini III 2375 Surface Area Analyser. Approximately 0.04 g of the catalyst sample was weighed into a glass tube and degassed in a flow of N_2 overnight at 110°C to remove any adsorbed species from the surface. Measurements were performed using helium as calibrant and nitrogen as the adsorbate at -196°C. Determining the number of molecules needed to form a monolayer is the underlying principle in surface area measurements. In practice however, the molecules may adsorb to form multi-layers. The surface area was calculated using the BET (Brunauer-Emmett-Teller) equation which can be expressed as:

Figure 3.1 The BET equation

$$\frac{P}{V(P_0-P)} = \frac{1}{V_mC} + \frac{(C-1)P}{V_mCP_0}$$

Where P = pressure of the adsorbate gas

P_0 = saturated pressure of adsorbate gas

V = volume of adsorbed gas

V_m = volume of monolayer adsorbed gas

C = BET constant ($C = \exp^{(E_1 - E_L/RT)}$)

E_1 = heat of adsorption on the first Layer

E_L = heat of Liquefaction on second and subsequent Layers

R = ideal gas constant (8.314 J K^{-1} mol^{-1})

Physical adsorption of gas on the surface of the solid is used to determine the specific surface area of the powder by calculating the volume of adsorbate gas

required to form a monolayer (V_m). At least three measurements of P/P_0 can be used to produce a linear plot of $1/V(P_0-P)$ against P/P_0 with a gradient equal to $C-1/V_mC$ and a y-intercept equal to $1/V_mC$. Using the gradient and the intercept, a value of V_m can be calculated using the following method:

$$V_m = 1/(A+B)$$

where A and B are the intercept and gradient respectively. The total surface area of the catalyst can be determined using the following equation:

$$S_{total} = V_m N \sigma / M_v$$

where N = Avogadro's constant (6.022×10^{23} mol^{-1})

Mv = Molar volume of adsorbed gas

σ = cross-sectional area of adsorbed gas (0.162 m^2 for N_2)

The surface area per unit weight of catalyst can then be calculated by dividing the total surface area by the mass of the catalyst ($S = S_{total}/m$).

3.1.2.2 Thermogravimetric analysis

Thermogravimetric analysis (TGA) of each catalyst was performed on pre-reaction samples. The instrument used was a SDT Q600 series combined TGA, DSC instrument with online ESS Evolution Mass Spectrometer. Approximately 0.01 g of sample was used. Each sample was heated from room temperature to 500°C under an O_2/Ar at a flow rate of 100 mL min^{-1} and a heating rate of 10°C min^{-1}. These conditions were used to mimic calcination and mass spectrometry was used to monitor the species with *m/z* equal to 18, 28, 44, which usually correspond to H_2O, CO, and CO_2. Additional species were monitored to investigate the decomposition of the nitrate precursor.

Catalyst samples were also heated from room temperature to 500°C under hydrogen, using the same flow and heating rate as before. Mass spectrometry was used to monitor the same species as above.

3.1.2.3 Powder x-ray diffraction (XRD)

XRD analysis was conducted on all catalysts pre-reaction. The apparatus used throughout was a Siemens D5000 X-ray Diffractometer (40 kV, 40 mA) using a monochromatised CuK_α X-ray source (wavelength 1.5418 Å). The scanning range used was $5^\circ < 2\theta < 80^\circ$ with a step range size of 0.02° and counting time of 1 s per step.

In-situ hot-stage XRD was performed using an Anton Par XRK 900 heated reaction chamber. The unit comprises of a water-cooled, vacuum tight, stainless steel chamber with a beryllium window, shown in figure 3.2.

Figure 3.2 Schematic of hot-stage XRD chamber

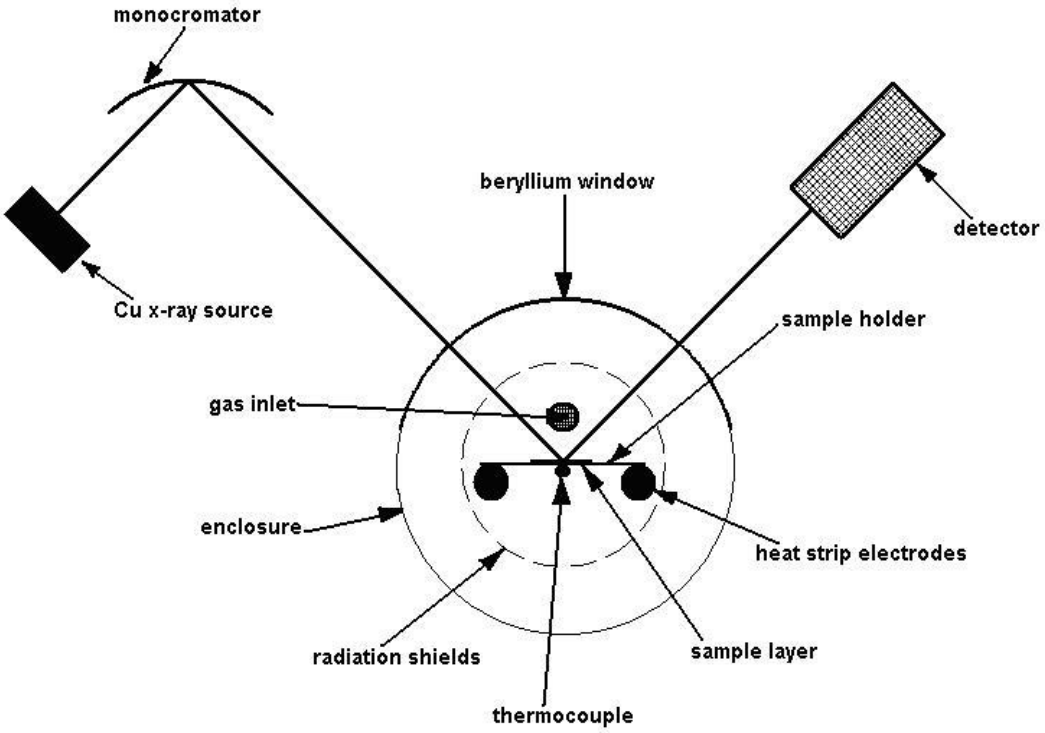

The temperature programme was used to heat pre-calcined catalyst samples under hydrogen flow from room temperature to 200°C at a rate of 12°C min^{-1}. The temperature was held for 2 h to mimic reduction conditions a then a scan performed at scan speed 1. The step size, scanning range and counting time were the same as standard XRD analysis.

From the broadening of the peaks, it is possible to determine an average crystallite size by measuring the full width at half maximum (FWHM) of a peak, then applying the Scherrer equation:

Figure 3.3 The Scherrer equation

$$t = K\lambda / \beta\cos\theta$$

Where: t = Average crystallite size

K = Scherrer constant (0.87-1.0, normally taken to be 1.0)

λ = the wavelength of the X-ray (1.5418 Å)

β = the breadth of a reflection in radians 2θ (FWHM)

This is only an approximation as the results can be influenced by various factors such as lattice distortion and instrumental parameters.

3.1.3 Materials

The following materials, shown in table 3.2, were used in gas-phase hydrogenation reactions without further purification.

Table 3.2 Materials used for gas-phase hydrogenation

Material	Supplier	Purity
Furfural	Sigma Aldrich	98%
Furfuryl alcohol	Sigma Aldrich	98%
2-methylfuran	Sigma Aldrich	99%
Tetrahydrofuran	Sigma Aldrich	99%
Tetrahydrofurfuryl alcohol	Sigma Aldrich	99%
Furan	Alfa Aesar	99%
2-pentanol	Sigma Aldrich	98%
1-butanol	Sigma Aldrich	99.4%
H_2	BOC	99%
N_2	BOC	99.98%
2-propanol	Sigma Aldrich	>99.5%

3.1.4 Reactor

The gas phase hydrogenation of furfural was carried out in a stainless steel fixed bed reactor (600 mm long and 8 mm i.d.) at 5 barg and 200°C. The gas flow rate was controlled by a mass flow controller (Brooks 5850, 0-800 mL min^{-1} H_2, max pressure 100 bar) and the Liquid flow controlled by an HPLC (Gilson 307). Hydrogen, nitrogen and a 2% O_2/Ar were available as gas feed when required.

The temperature of the reaction was measured using a thermocouple located at the outside of the reactor wall positioned at the middle of the reactor tube and in line with the catalyst bed. Control of temperature was achieved by a furnace attached to a DMG temperature controller (West 4400, accuracy ±1°C). Figure 3.4 is a schematic of the fixed bed reactor used for all experiments.

Figure 3.4 Schematic of fixed bed reactor

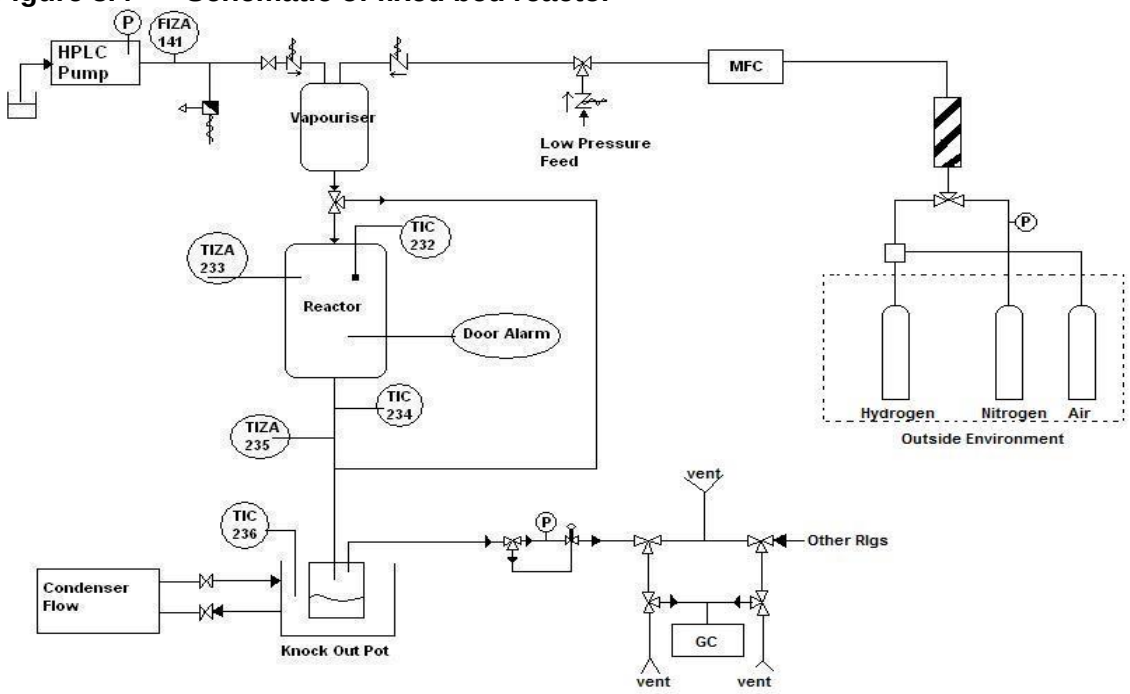

3.1.5 Experimental method

Each catalyst was calcined prior to reaction by heating over 5 h to 300°C then holding at this temperature for 16 h under a 1000 mL min^{-1} flow of air.

Following calcination, the catalyst (0.25 g) was loaded into the reaction vessel between two layers of boiling chips. The reactor was then purged with nitrogen.

The pressure was increased to 6 barg and the system tested for Leaks. The catalyst was then reduced under 50 mL min^{-1} H_2 at 5 barg. The temperature of the reaction vessel was increased at 300°C h^{-1} and maintained at 200°C for 2 h. The vessel was then cooled to reaction temperature at 300°C h^{-1}.

The HPLC pump (Gilson 307) was started and the liquid reactant (furfural) injected into the vaporiser at 1.8 mL h^{-1}**:** the knock-out pot coolant was also switched on. Pressure was kept at 5 barg and reactor temperature was 200°C. Hydrogen flow was set at 100 mLmin^{-1} to give H_2:furfural molar ratio of 16. Liquid samples were collected from the knock-out pot at regular intervals and analysed using gas chromatography.

At the end of the reaction, the liquid flow was stopped and the HPLC pump isolated. The gas was switched to nitrogen. The vaporiser was left on and the reactor/lower trace heating was switched off. The gas flow was then switched to a low pressure exit. The system was then left overnight to cool and then the upper trace heating was switched off. The reactor tube was then removed and the knock-out pot cleared of condensed vapour.

3.1.6 Analysis

Liquid samples were analysed by gas chromatography using a ThermoQuest 2000 series Trace gas chromatograph fitted with a flame ionisation detector and using a 30 m Zebron ZB-Wax plus column with 0.25 mm i.d. and film thickness of 5 µm. An injection temperature of 250°C, a split flow of 14 mL min^{-1} and a split ratio of 10 were used. The oven temperature was 40°C for 5 min and then increased at a rate of 10°C min^{-1} to 230°C for 7 min. The auto-sampler used was an AI/AS 3000, the injection size was 1 µL and the detector temperature was 300°C. Gaseous products were monitored using online GC-MS (Agilent 6890 series) and an Al_2O_3/Na_2SO_4 column (25 m in Length, 0.53 mm i.d. and film thickness of 10 µm).

Standard solutions of known concentrations were prepared by the following method. Firstly 1 mL of furfural was measured out using a syringe and added to

a 250 mL volumetric flask and mixed with 2-propanol (IPA) to make the 100% solution. From this 250 mL solution a 10 mL sample was taken and added to a 100 mL volumetric flask with IPA to make a 10% solution. A 30 mL sample was then taken from the original 250 mL solution using a pipette and put into a 100 mL volumetric flask. IPA was added to this flask to make the solution up to a 100 mL solution to make a 30% solution. This process was repeated until a series of standards representing 10, 30, 50 and 70% solutions made from the original 250 mL solution was obtained. A 2 mL sample was taken from each of these solutions analysed by gas chromatography. The whole process was repeated for each individual product using IPA as a solvent. The peak areas of these solutions were then plotted against their known concentrations to produce calibration graphs. The graph below shows the correlation between peak area and concentration of standard solutions.

Figure 3.5 Calibration of GC for furfural analysis

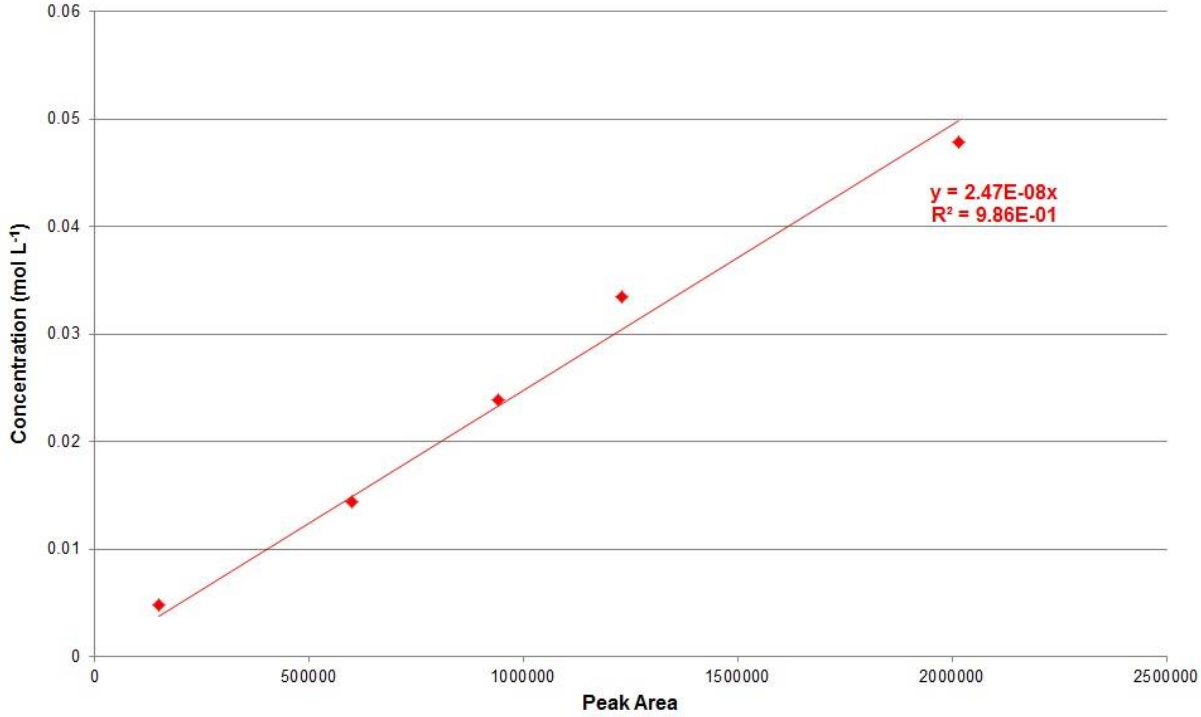

Figure 3.6 Calibration of GC for furfuryl alcohol analysis

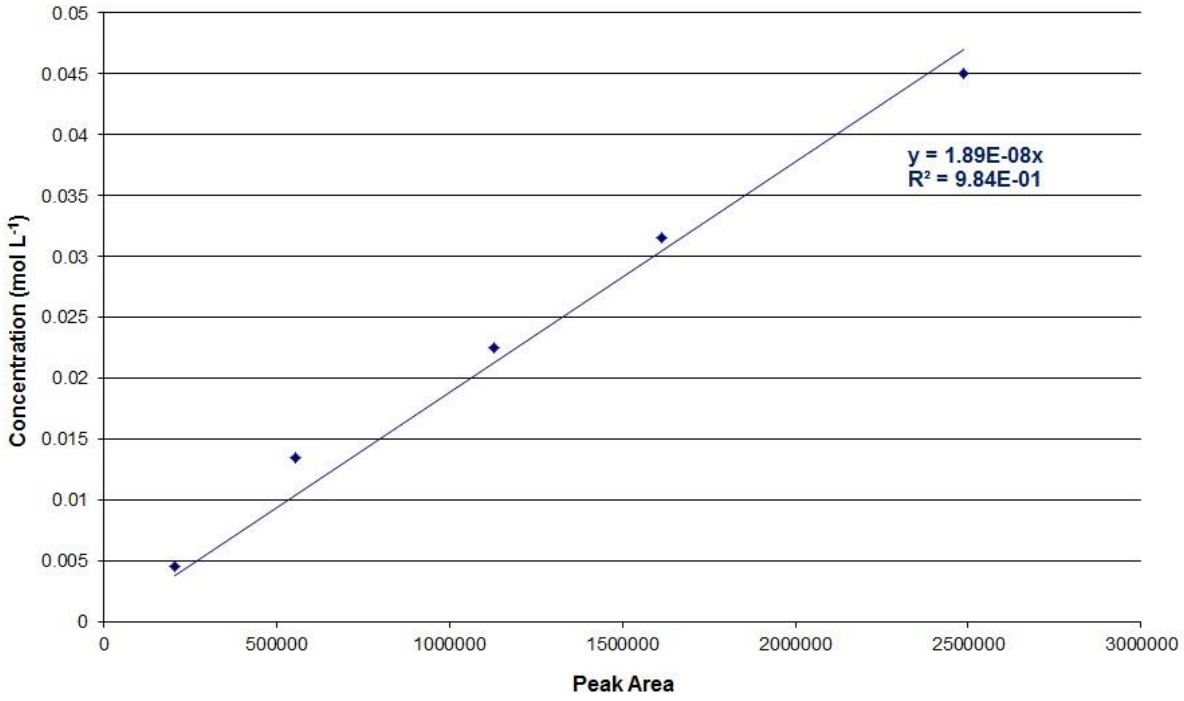

3.1.7 Deactivation studies

Analysis of post-reaction catalyst samples was conducted to investigate the extent and cause of deactivation. Samples were analysed both online (within reactor tube) and offline (removed from reactor).

At the end of the reaction, the liquid flow was stopped and the HPLC pump isolated. The gas was switched to nitrogen, the gas flow switched to bypass and the system was depressurised. The reactor and trace heating was left on overnight to allow removal of any reactants still present in the system. The following day all heating was switched off and the reactor cooled to room temperature. The knock-out pot was cleared of any condensed vapour and the gas flow was switched off.

The boiling chips and catalyst bed were removed from the reactor tube and stored in a glove box under nitrogen prior to analysis. Surface area determination, TGA and XRD were used to investigate the extent and cause of catalyst deactivation.

3.2 Liquid-phase hydrogenation

Liquid phase hydrogenation of 4-nitroacetophenone (4-NAP) was carried out and the following section describes the catalysts, reactor and reaction conditions used in this study.

3.2.1 Catalysts

The catalysts used for the hydrogenation of 4-nitroacetophenone were silica supported rhodium catalysts. The silica support material was supplied and characterised by Davison Catalysts and the rhodium catalysts were prepared by incipient wetness and characterised by Johnson Matthey. Table 3.3 shows the physical properties of the rhodium/silica catalysts.

Table 3.3 Catalysts for Liquid-phase hydrogenation

Catalyst code	Surface area (m^2g^{-1})	Average pore diameter (nm)	Pore volume (cm^3g^{-1})	Particle size (μm)	Average metal crystallite size (nm)
M01035	321	13.2	1.06	96.3	3.5
M01038	321	13.2	1.06	49.9	2.7
M01074	321	13.2	1.06	24	2.6
M01078	321	13.2	1.06	241	2.2
M01079	344	11.1	0.96	9.5	1.2

3.2.2 Materials

The following materials, shown in table 3.4, were used in all liquid-phase hydrogenation reactions without further purification.

Table 3.4 Materials used for liquid phase hydrogenation

Material	Supplier	Purity
4-nitroacetophenone	Sigma Aldrich	98%
4-aminoacetophenone	Sigma Aldrich	99%
4-(1-aminophenyl)ethanol	Sigma Aldrich	98%
4-ethylaniline	Sigma Aldrich	98%
cyclohexylamine	Fisher Scientific	98%
4-methylcyclohexylamine	Fisher Scientific	97%
2-propanol	Sigma Aldrich	>99.5%
H_2	BOC	99%
N_2	BOC	99.98%
D_2	BOC	99.9%

3.2.3 Reactor

Hydrogenation reactions were conducted using a 0.5 L stirred Büchi autoclave equipped with an oil-jacket and a hydrogen-on-demand delivery system. The design of the reactor was advantageous as it allowed for *in situ* reduction of the catalyst prior to the reaction and made the regulation of temperature, pressure and stirring speed accessible. Figure 3.7 shows a schematic of the stirred tank reactor used.

Figure 3.7 Schematic of stirred tank reactor

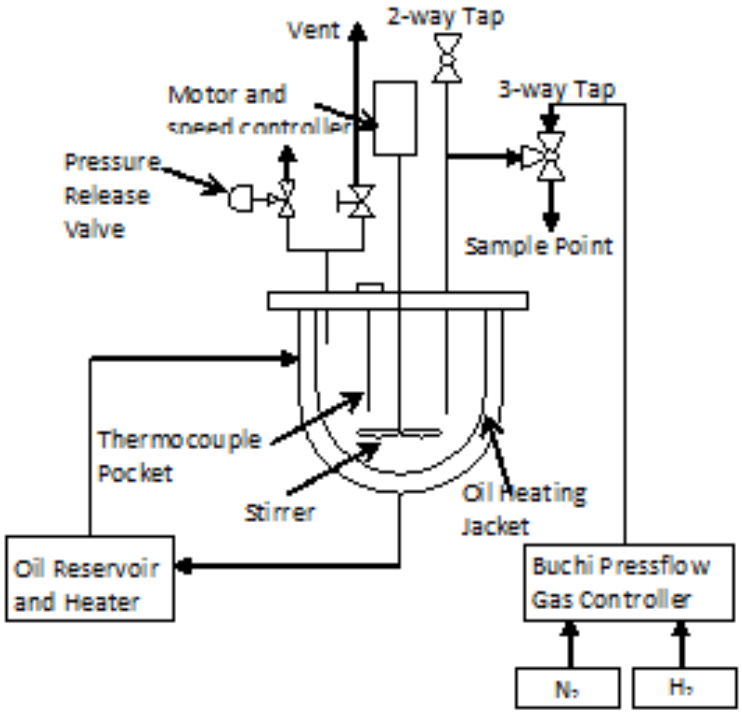

3.2.4 Experimental method

0.05 g of 2.5% Rh/SiO_2 catalyst and 310 mL 2-propanol (IPA) were added to the reactor vessel and brought to a temperature of 70°C, stirring at ~300 rpm. An *in situ* reduction of the catalyst was performed at 70°C by sparging hydrogen gas, at a flow rate of 280 cm^3 min^{-1}, through the mixture for 0.5 h while stirring at 300 rpm. The reaction mixture was allowed to cool after reduction to the desired reaction temperature.

0.45 g (2.7 mmol) of 4-nitroacetophenone (4-NAP) were added to 25 mL of IPA in a conical flask and heated until all of the 4-NAP was dissolved. After the reduction process was complete, the reaction mixture was allowed to cool to the desired reaction temperature under slow stirring. After reaching the desired temperature, the stirrer was turned off and 20 mL of the 4-NAP solution (2.16 mmol 4-NAP) was added to the reactor vessel through the reactor inlet; then flushed with 20 mL of IPA to give a total reaction volume of 350 mL and an initial 4-NAP concentration of 0.0062 mol L^{-1}. The solution was stirred at 1000 rpm for 5 seconds to allow mixing. The stirrer was then switched off and the reactor pressurised with nitrogen to 1 barg. A sample of 2.5 mL was withdrawn. The

reactor was de-pressurised, before being purged twice with hydrogen then pressurised with hydrogen to the desired reaction pressure. Once the vessel was pressurised the reaction was started by switching the stirrer on at 1000 rpm and the timer started. The progress of the reaction was followed by withdrawing 2.5 mL samples at regular intervals over 4 h. The moles of hydrogen consumed during the reaction were also monitored and recorded.

3.2.4.1 Average crystallite size

To investigate the effect of metal crystallite size on the rate of hydrogenation of 4-nitroacetophenone, reactions were conducted at 60°C and 4 barg using the catalysts Listed in table 3.3.

3.2.4.2 4-NAP reactions

Reactions were conducted to investigate the effect of temperature and pressure on the rate of hydrogenation of 4-nitroacetophenone. Reactions were carried out at temperatures from 30-60°C at 4 barg and at 60°C using pressures from 2-5 barg. From these reactions, an activation energy and order of reaction with respect to hydrogen pressure were calculated.

In addition, reactions were carried out using different initial concentrations of 4-NAP to investigate its effect on the rate of hydrogenation and to determine an order of reaction with respect to reactant concentration.

3.2.4.3 4-AAP reactions

Reactions were conducted to investigate the effect of temperature on the rate of hydrogenation of 4-aminoacetophenone (4-AAP). 0.36 g of 4-AAP (2.7 mmol) was dissolved in 25 mL of IPA then 20 mL of this solution (2.16 mmol 4-AAP) was added to the reactor vessel through the reactor inlet; then flushed with 20 mL of IPA to give a total reaction volume of 350 mL. The experimental procedure for 4-NAP reactions was followed and reactions were carried out at temperatures from 30-60°C at 4 barg.

3.2.4.4 4-NAP and 4-AAP reactions

To investigate the effect of the presence of the 4-AAP intermediate on the rate of hydrogenation of 4-NAP, reactions were conducted at 60˚C and 4 barg using 1:1, 2:1 and 1:2 molar ratios of 4-NAP:4-AAP as reactant. The concentration of 4-NAP was the same as reactions involving 4-NAP alone, the concentration of 4-AAP was altered to achieve the desired ratios and the same experimental procedure was followed.

3.2.4.5 Addition of an alicyclic amine

To investigate the effect of the presence of an alicyclic amine on the rate of hydrogenation of 4-NAP, 4-methylcyclohexylamine (4MCHA) was introduced to the reactant feed solution in 1:1, 2:1 and 1:2 molar ratios of 4-NAP:4MCHA. As before, the concentration of 4-NAP in all reactions remained constant and the concentration of aliphatic amine was changed to give the desired ratios. Reactions were also carried out to investigate the effect of 4-methylcyclohexylamine (4-MCHA) on the hydrogenation of 4-AAP. The same concentration of 4-AAP was used as in the reactions involving 4-AAP only and the concentration of 4-MCHA added was varied to achieve molar ratios of 1:1, 1:2 and 2:1.

3.2.4.6 Deuterium reactions

A series of reactions employing the use of deuterium in place of hydrogen were conducted to investigate whether hydrogen bond breaking or forming is involved in the rate determining step. The reactions were conducted at a pressure of 4 barg and a temperature of 60˚C using 2.7 mmol of 4-NAP alone, 2.7 mmol 4-AAP and finally 2.7 mmol of each to give a 1:1 ratio.

3.2.5 Analysis

A Thermo Finnigan Focus single column and flame ionization detector was used in the analysis of the samples obtained from reaction. The column used was an HP-1701 with length 30 m, 0.25 mm ID, and film thickness 1 μm. The parameters of the GC programme were set as follows: an injection temperature

of 240˚C, split ratio 150 with a column flow 2 mL min^{-1} and the detector temperature set at 300˚C. The oven temperature was 160˚C for 7 min and then increased at a rate of 10˚C min^{-1} to 200˚C for 6 min.

Standard solutions of known concentrations were prepared as described in section 3.1.6, and were used to calibrate the GC for analysis of reactants and all possible products.

Figure 3.8 Calibration of GC for 4-nitroacetophenone analysis

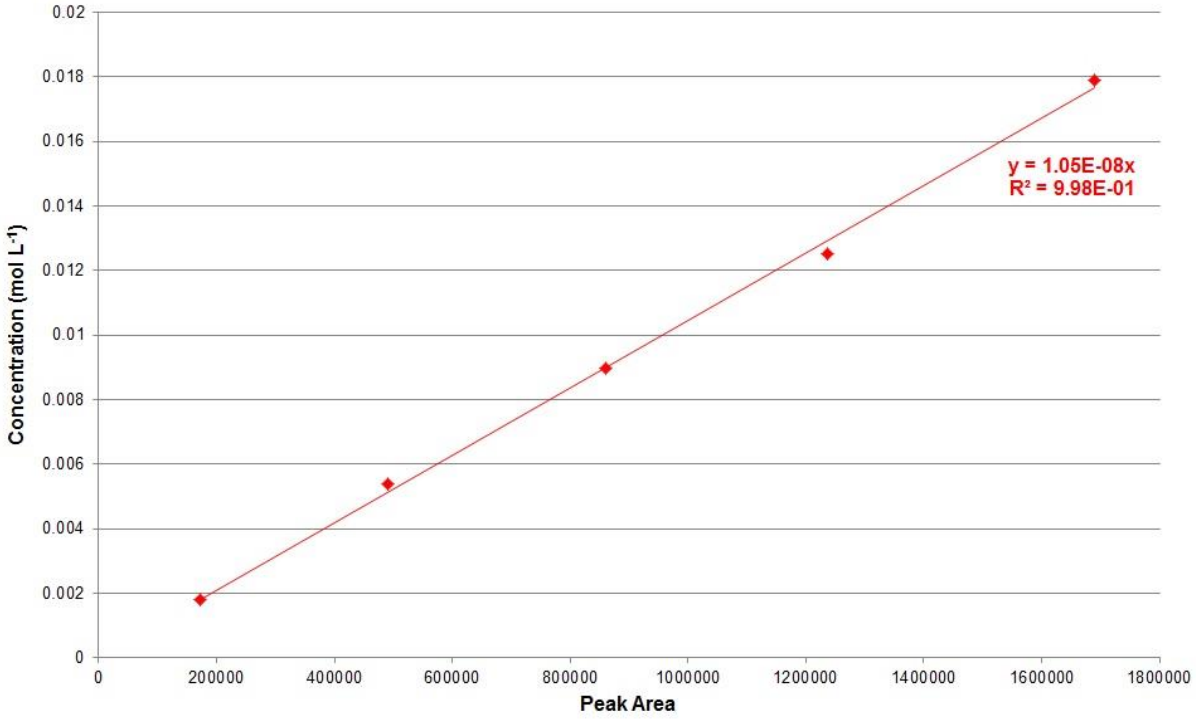

4 Gas-phase hydrogenation results

The following chapter shows the results for gas-phase hydrogenation of furfural (FFRAL) to furfuryl alcohol (FFRYL).

4.1 Catalyst characterisation

Firstly, pre-reaction characterisation was carried out on all catalysts. The surface area of the catalysts was determined by BET, while TGA and powder x-XRD were used to investigate the physical properties of the catalysts.

4.1.1 Surface area determination

Surface area determination was carried out as described in section 3.1.2.1 and the measurements obtained are shown in table 4.1.

Table 4.1 Surface area determination of gas-phase hydrogenation catalysts

Catalyst	BET		Single Point
	Surface area (m^2g^{-1})	Average pore diameter (nm)	Pore volume (cm^3g^{-1})
Cariact Q10 silica	276	14.6	1.01
5% Cu/SiO_2	236	13.9	0.82
5% CeO_x/SiO_2	254	15.1	0.96
5% Cu + 5% CeO_x/SiO_2	215	14.5	0.78
5% Cu + 1% CeO_x/SiO_2	232	14.9	0.87
10% Cu/SiO_2	235	13.1	0.77
10% Cu + 5% CeO_x/SiO_2	154	13.2	0.51
10% Cu+ 5% CeO_x + 0.05% Pd/SiO_2	190	14.5	0.69
Cu1132	45	8.8	0.10

The majority of the catalysts had a surface area around 200 m^2g^{-1} however the surface area of 10% Cu + 5% CeO_x/SiO_2 was slightly lower at 154 m^2g^{-1}. The surface area of 10% Cu + 5% CeO_x + 0.05% Pd/SiO_2 was higher than 10% Cu + 5% CeO_x/SiO_2 suggesting that presence of palladium inhibited structural change in

the silica. The commercial catalyst, Cu1132, had a significantly lower surface area compared to the rest of the catalysts.

4.1.2 Thermogravimetric analysis

TGA was carried out on pre-reaction samples of all catalysts. Temperature programmed oxidation (TPO), temperature programmed reduction (TPR) of as-prepared catalyst samples and TPR of pre-oxidised catalyst samples were carried out to investigate the effect of pre-treatment conditions on the structure and composition of the catalyst.

4.1.2.1 Temperature programmed oxidation

Firstly, temperature programmed oxidation (TPO) of the silica support material was carried out using the method described in section 3.1.2.2, and the results are shown in figure 4.1.

Figure 4.1 Pre-reaction TPO of Cariact Q10 silica support

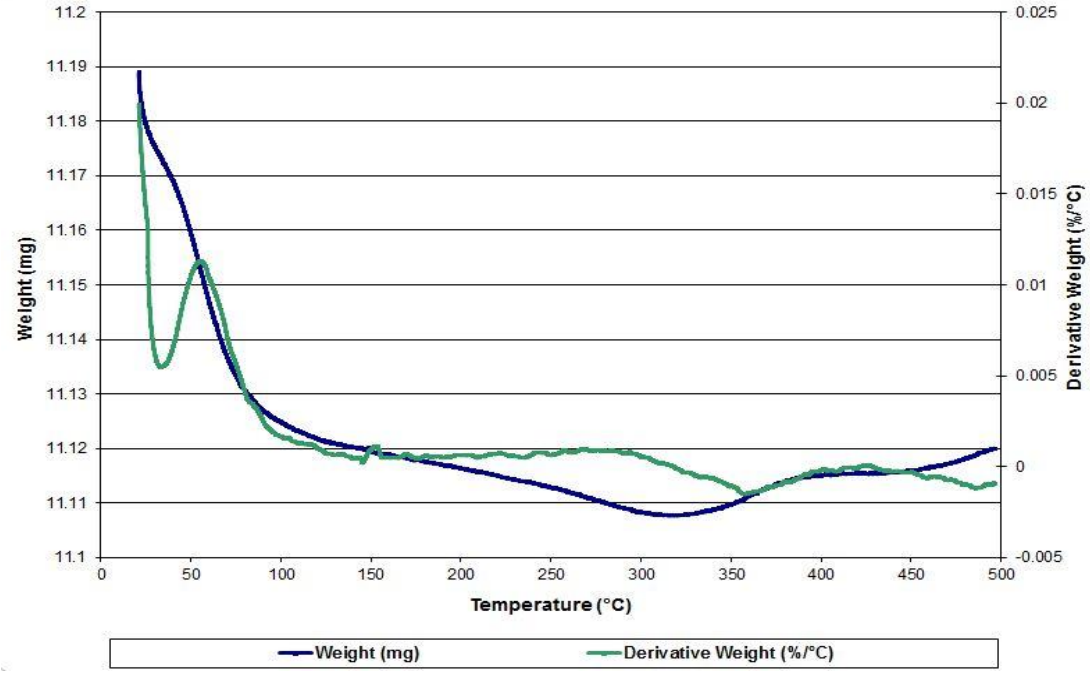

TPO of Cariact Q10 silica shows a small weight Loss at around 60˚C which could be due to the loss of physisorbed water from the surface. As little weight is Lost from the support, it can be assumed that any significant weight lost by catalyst samples is due to the presence of the active phase. TPO was carried out on all

catalysts to investigate the effect of calcination and TPO of 5% CeO_x/SiO_2 is shown in figure 4.2.

Figure 4.2 Pre-reaction TPO of 5% CeO_x/SiO_2

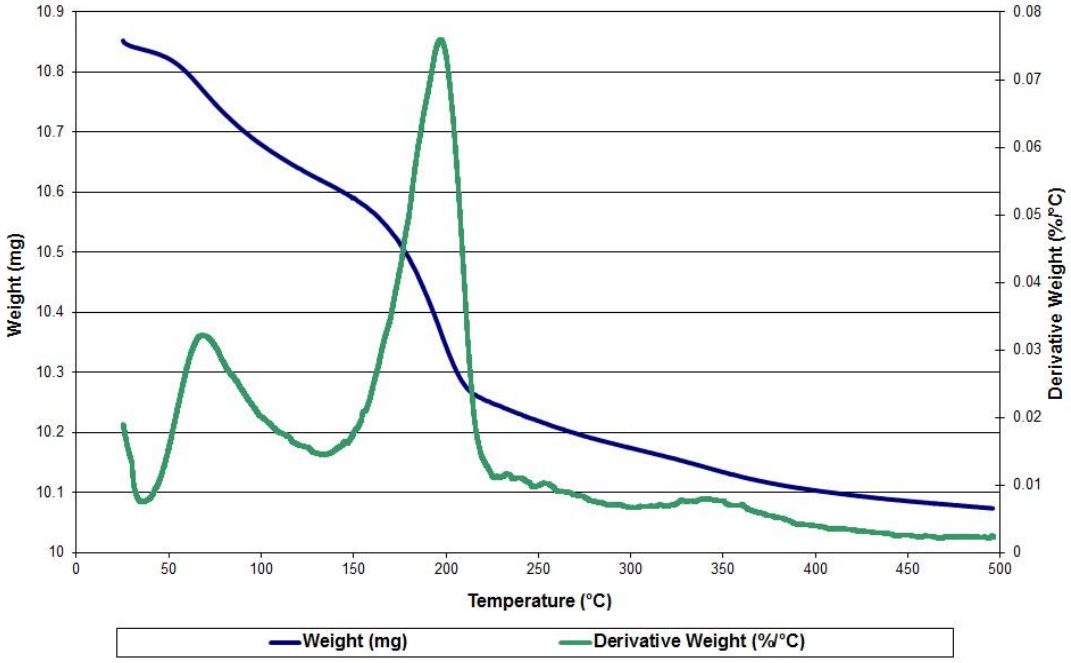

TPO of 5% CeO_x/SiO_2 from room temperature to 500˚C showed three weight losses, one at 70˚C, the largest at around 200˚C and a small loss at 340˚C. Heat flow was measured and plotted with the derivative weight against temperature to determine if the weight losses were endo- or exothermic.

Figure 4.3 Heat flow during pre-reaction TPO of 5% CeO_x/SiO_2

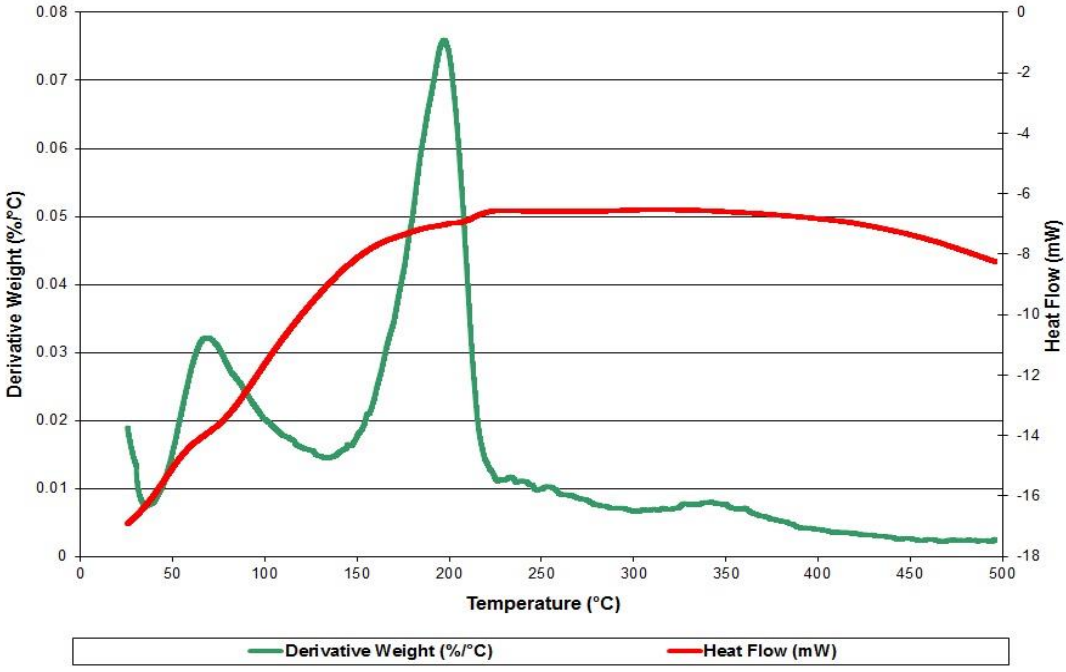

Heat flow data showed a small dip associated with each peak indicating that all weight losses were endothermic. Mass spectrometry was used to try to identify the species evolved at these temperatures.

Figure 4.4 Mass spectrometry data for 5% CeO_x/SiO_2

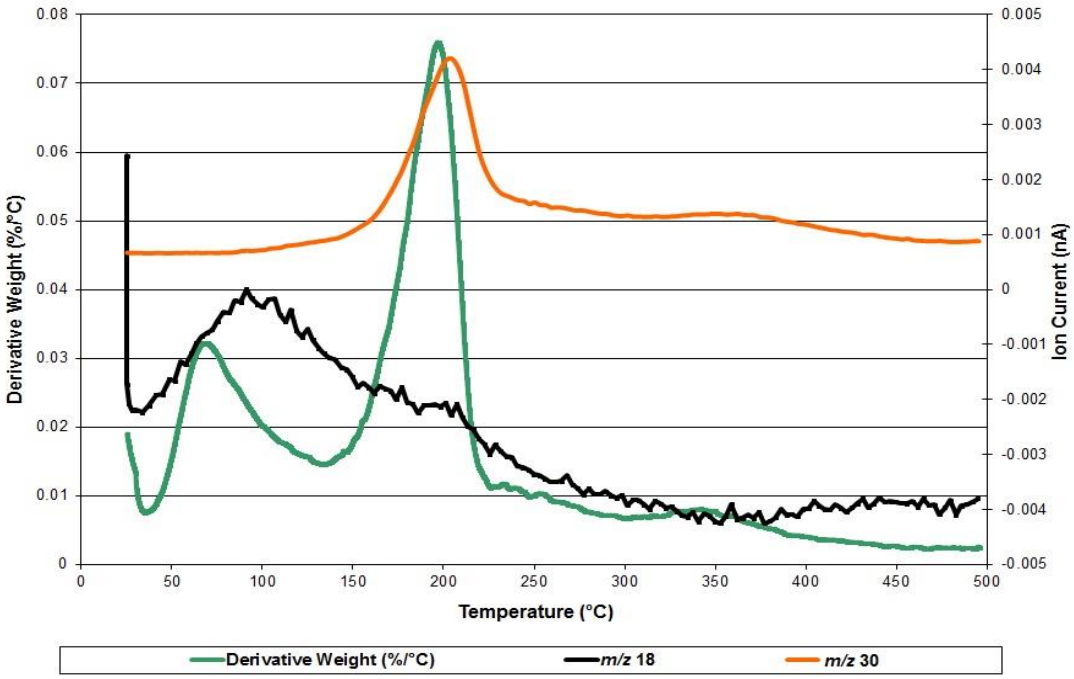

Two fragments were identified by mass spectrometry namely *m*/*z* 18 and *m*/*z* 30. The evolution of *m*/*z* 18 corresponded to the weight loss at 70˚C and was likely due to loss of physisorbed water from the surface. At 200 and 340˚C *m*/*z* 30 was detected and attributed to the evolution of NO as a result of the decomposition of the nitrate precursor.

TPO of 5% Cu/SiO_2 showed some similarities to TPO of 5% CeO_x/SiO_2 however the greatest weight loss was around 100˚C.

Figure 4.5 Pre-reaction TPO of 5% Cu/SiO_2

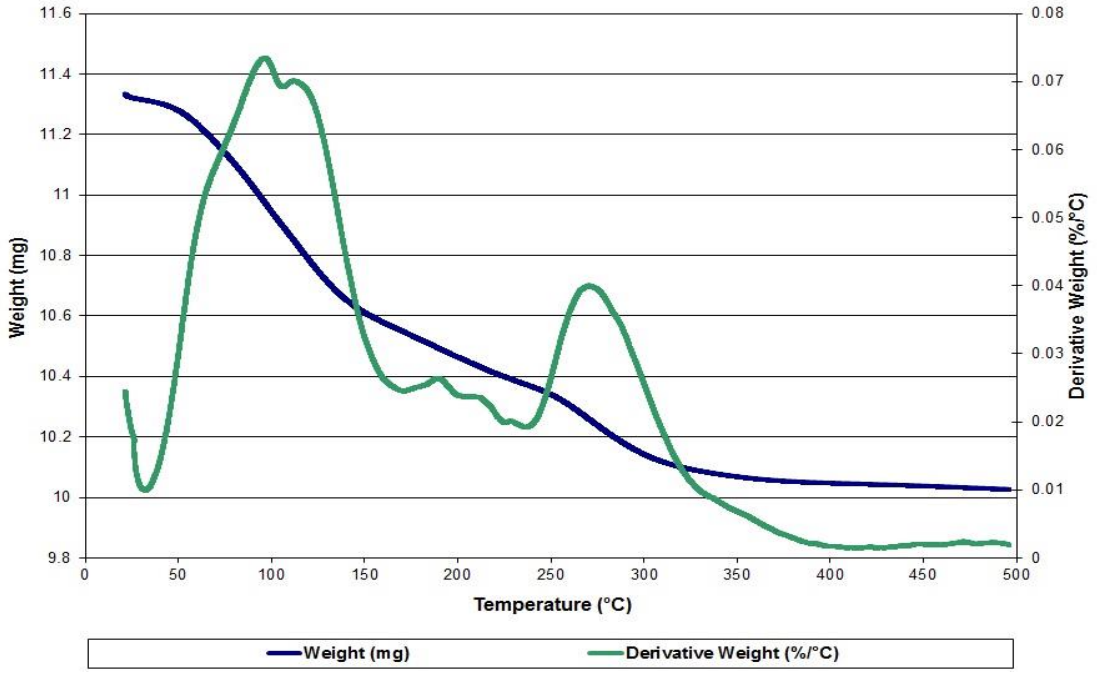

Figure 4.5 shows a pair of peaks around 100˚C and between room temperature and 170˚C, ~7% of the original sample weight is lost. Further weight was lost between 170 and 350˚C shown by peaks at 190, 215 and 230˚C. Heat flow data, not shown, confirmed all weight losses were endothermic. Like 5% CeO_x/SiO_2, mass spectrometry identified *m*/*z* fragments 18 and 30 but also showed a signal for *m*/*z* 44.

Figure 4.6 Mass spectrometry data for 5% Cu/SiO_2

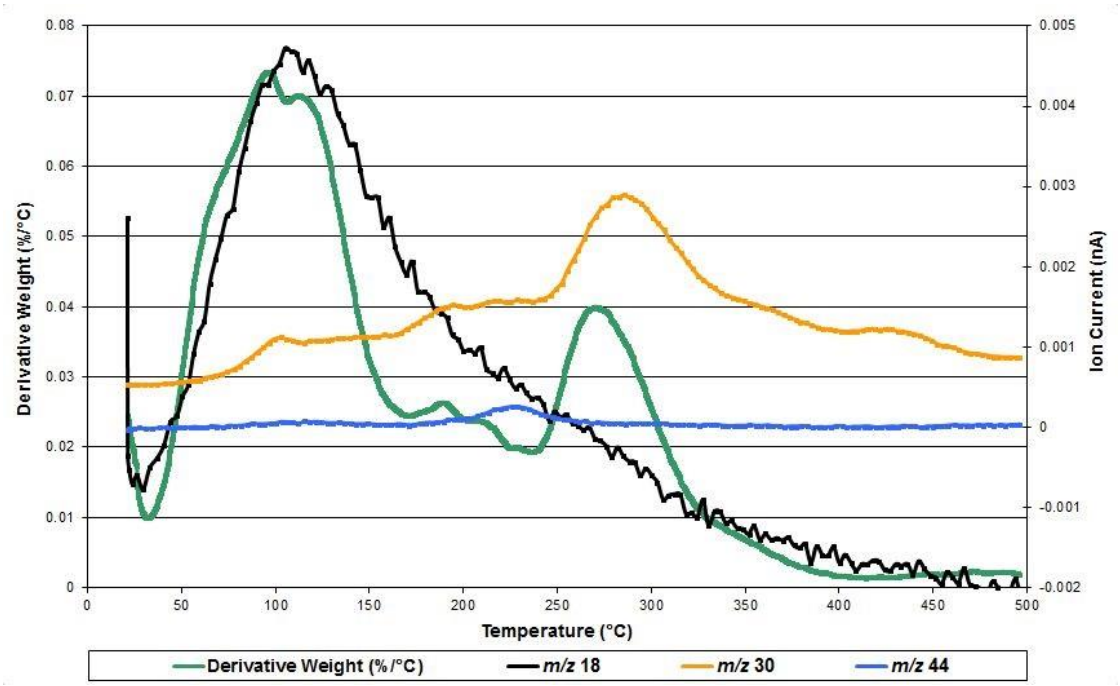

The peaks at ~100˚C corresponded to *m/z* 18 which suggests they corresponded to the loss of water from the surface. In addition, *m/z* 30 showed a small peak at 100 and 190˚C and a larger peak at 280˚C. As previously mentioned, this could be attributed to NO species lost during decomposition of the nitrate precursor which is common for all catalysts. At 230˚C *m/z* 44 was evolved which could correspond to CO_2 adsorbed from the atmosphere or N_2O species as a result of nitrate precursor decomposition.

For the higher loading copper catalyst, the TPO pattern obtained was very similar to that of 5% Cu/SiO_2.

Figure 4.7 Pre-reaction TPO of 10% Cu/SiO_2

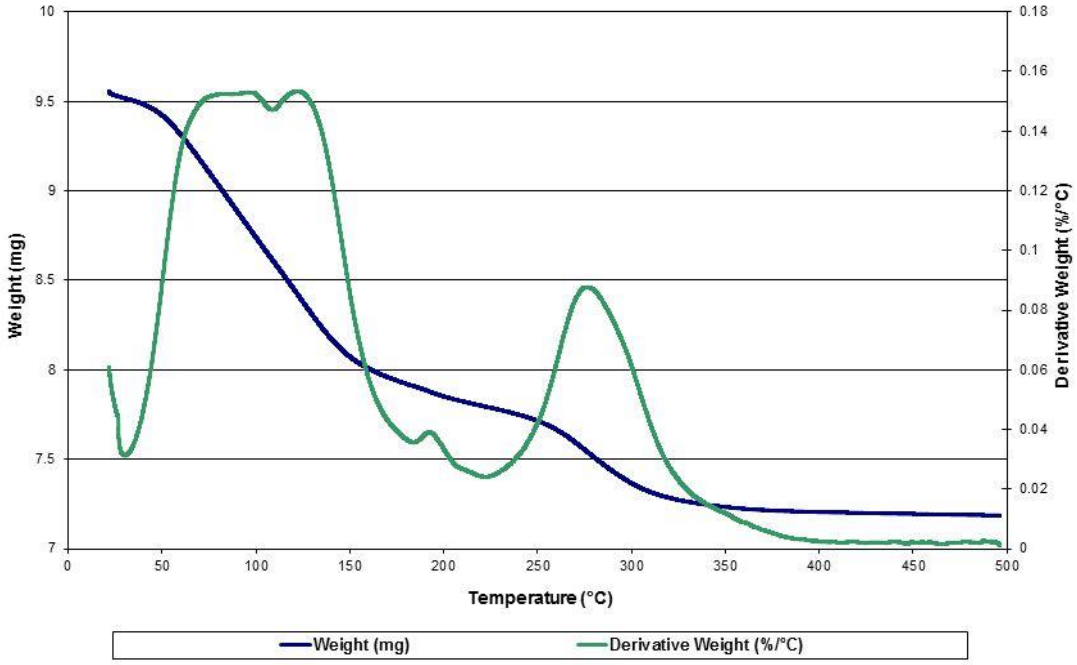

The weight loss around 100˚C was very broad and again looked like more than one peak. There was a small weight Loss at 195˚C and a larger peak shown at 280˚C. Heat flow data, not shown, shows that the weight losses around 100 and 280˚C were endothermic meanwhile the weight loss at 195˚C was exothermic. Like 5% Cu/SiO_2, the mass spectrometry data showed *m/z* 18 corresponding to the weight loss around 100˚C suggesting the loss of physisorbed water and the evolution of *m/z* 30 at 195˚C.

The presence of 1% ceria in the catalyst had little effect on the TPO pattern produced or the *m/z* fragments detected. However, 5% Cu + 5% CeO_x/SiO_2 showed sharp weight loss around 190˚C.

Figure 4.8 Pre-reaction TPO of 5% Cu + 5% CeO_x/SiO_2

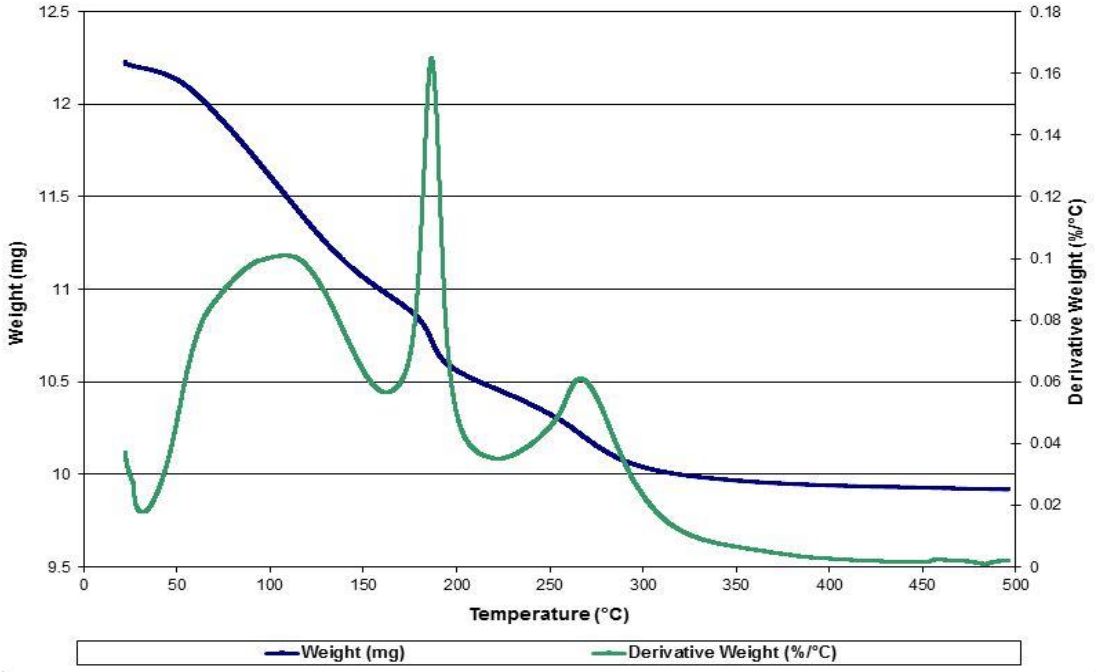

A weight loss at 270˚C and a very broad weight loss peak at 100˚C were observed and all the weight lost events were endothermic. Mass spectrometry data showed evolution of *m/z* 18 at 100˚C and *m/z* 30 at 190 and 270˚C. Additionally, *m/z* 44 and *m/z* 46; which could correspond to CO_2 or N_2O and NO_2, respectively, were also detected suggesting the loss of atmospheric CO2 from the surface and/or significant decomposition of nitrate precursor.

For 10% Cu + 5% CeO_x/SiO_2 catalysts similar TPO patterns were observed and the incorporation of low levels of palladium had little effect on the TPO pattern.

Figure 4.9 Pre-reaction TPO of 10% Cu + 5% CeO_x/SiO_2

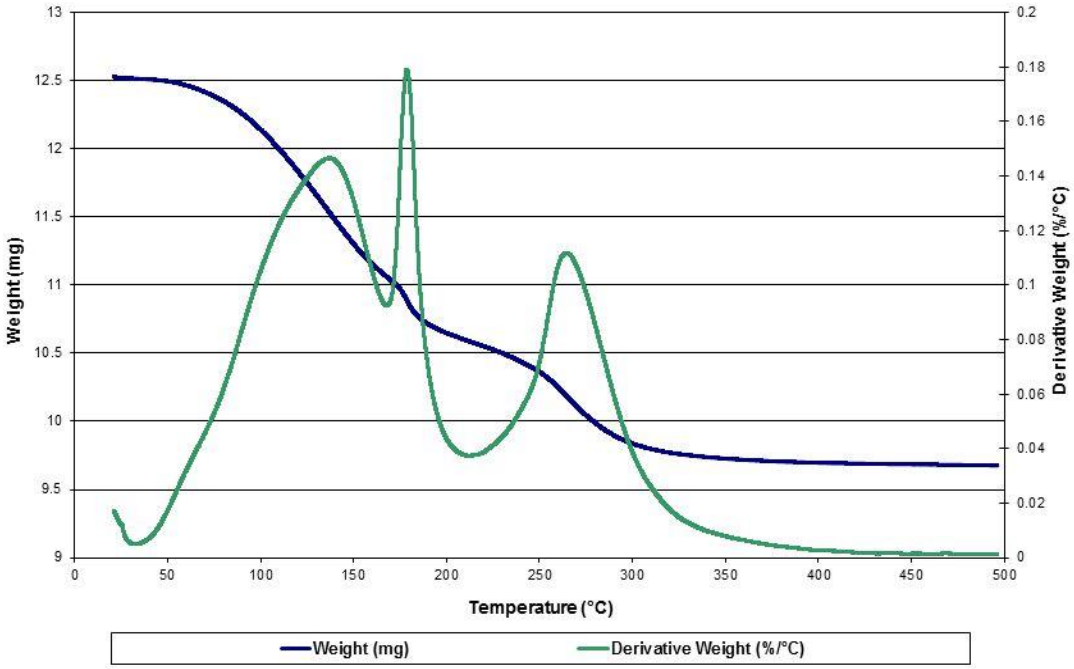

TPO of 10% Cu + 5% CeO_x/SiO_2 shows three clear weight loss peaks at 135, 175 and 265˚C. Heat flow data, not shown here, showed that all three weight losses were endothermic. A very similar TPO pattern was obtained for 10% Cu + 5% CeO_x + 0.05% Pd/SiO_2, with three endothermic weight losses at 130, 180 and 260˚C.

TPO was carried out on a sample of commercial catalyst Cu1132, the exact composition of which is not known.

Figure 4.10 Pre-reaction TPO of Cu1132

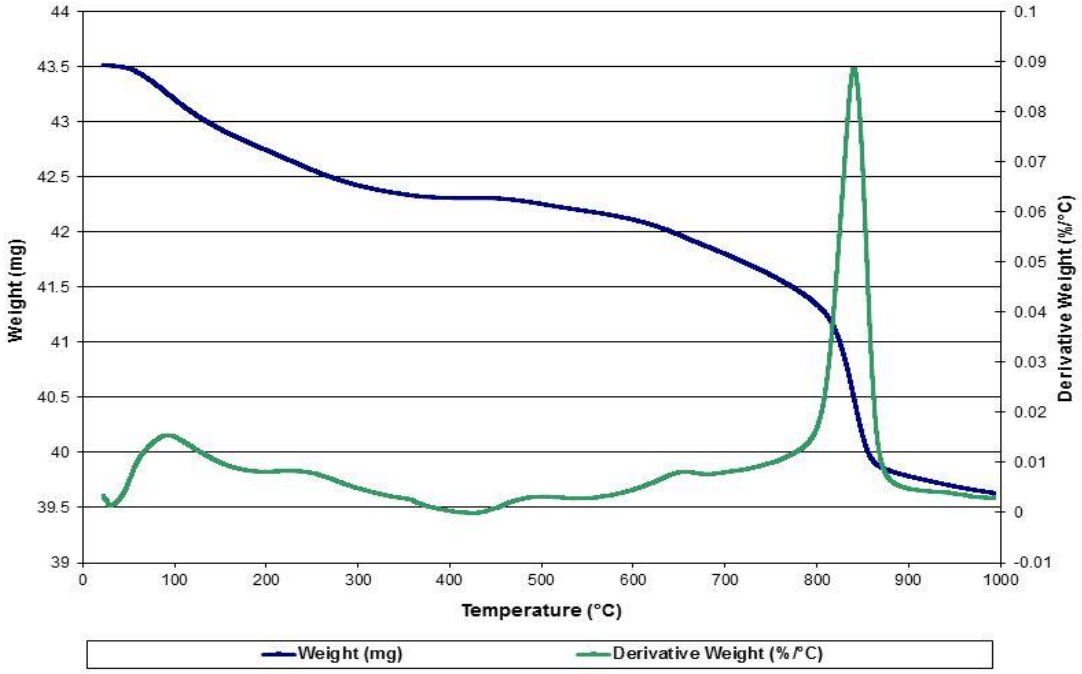

TPO of Cu1132 showed an initial small weight loss around 100˚C, with a main endothermic weight loss at 850˚C. Mass spectrometry data suggested that the first weight loss can be attributed to the loss of physisorbed water from the surface. Around 850˚C, oxygen is evolved suggesting that the chrome present undergoes a change in oxidation state.

4.1.2.2 Temperature programmed reduction

Temperature programmed reduction (TPR) was carried out on catalyst samples before and after oxidation to investigate the reducibility of the catalysts. TPR was carried out on as-prepared catalyst samples from room temperature to 500˚C. TPR of catalysts samples post TPO was also carried out to determine the effect of calcination followed by reduction.

Figure 4.11 Pre-reaction TPR of 5% CeO_x/SiO_2

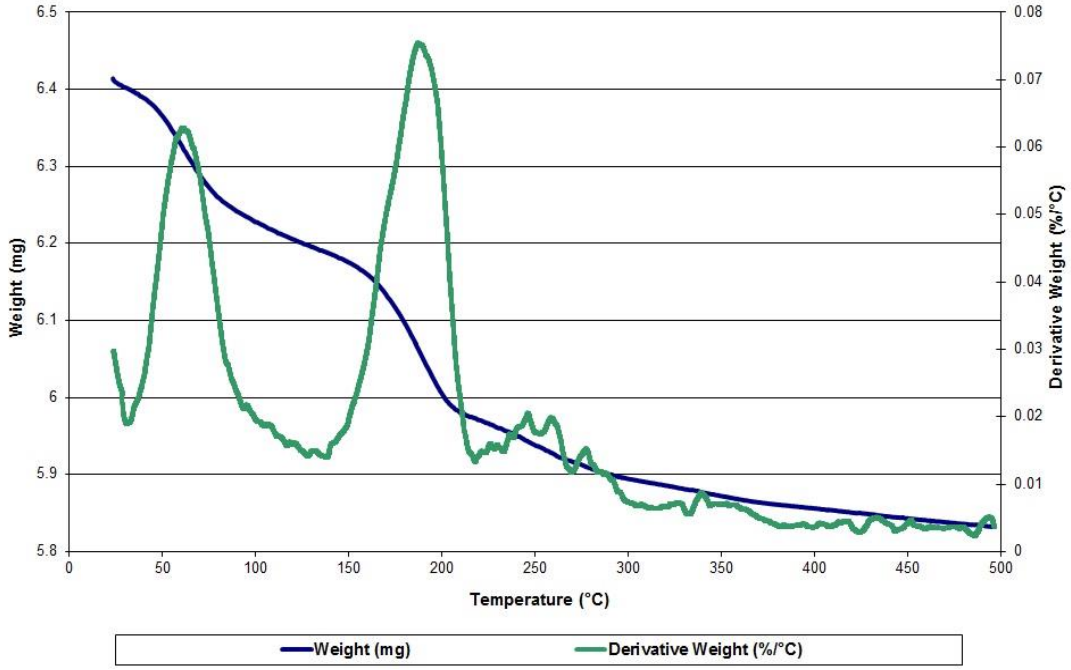

TPR of as-prepared 5% CeO_x/SiO_2 showed two prominent weight losses at 60 and 190˚C which were endothermic. Where the low temperature peak could correspond to the loss of surface water molecules, the reduction of the ceria active phase occurred at 190˚C. Figure 4.12 shows that the reduction temperature for 5% Cu/SiO_2 however, was much higher.

Figure 4.12 Pre-reaction TPR of 5% Cu/SiO_2

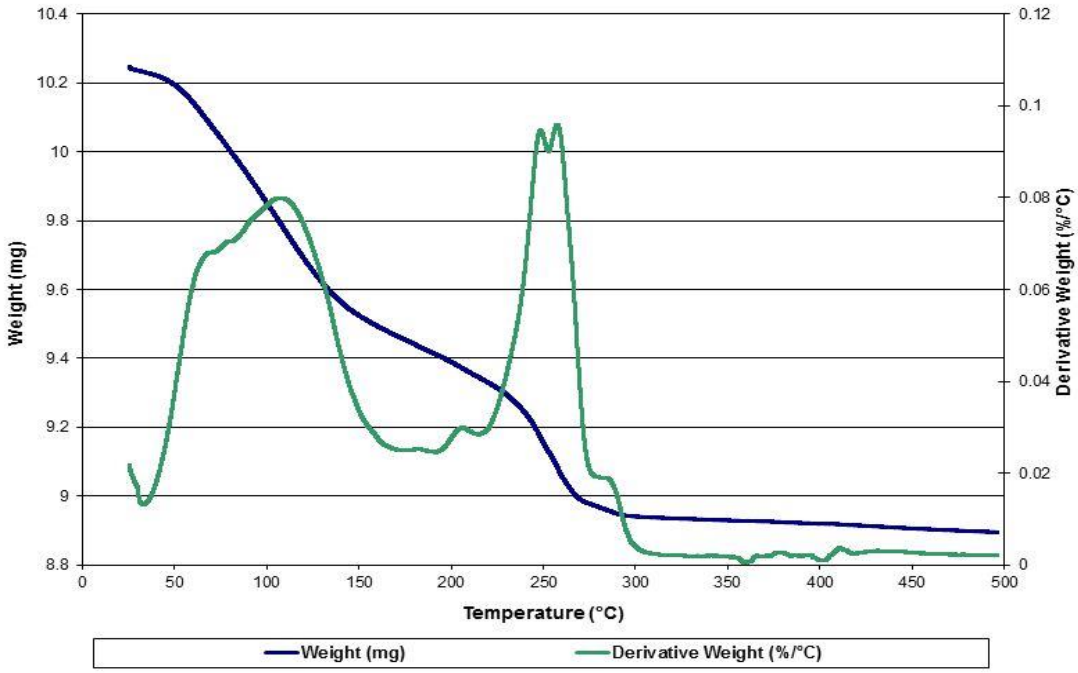

TPR of a pre-reaction sample of 5% Cu/SiO_2 shows a number of weight losses. There is a weight Loss at 100˚C with two preceding shoulders and a small peak at 210˚C. There is a pair of peaks around 250˚C and a small shoulder before 300˚C.

Figure 4.13 Pre-reaction TPR heat flow data for 5% Cu/SiO_2

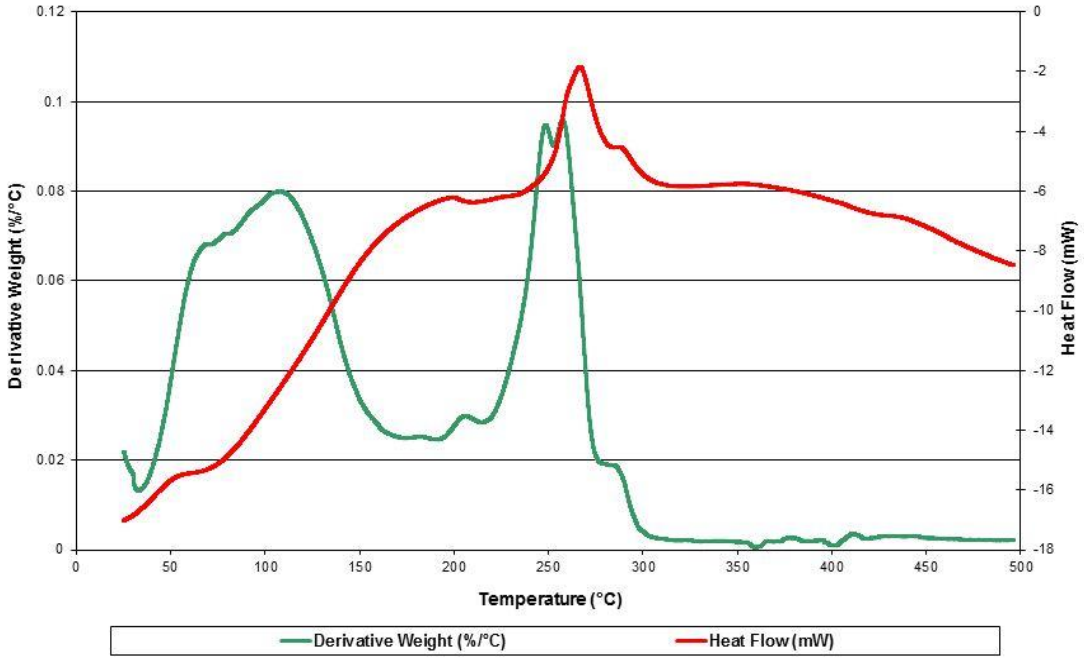

From heat flow data the weight loss ~100˚C, the small peak at 210˚C and the first of the pair of peaks are endothermic. However, the second peak at 250˚C and the small shoulder before 300˚C are exothermic.

Higher copper loading resulted in a shift of the reduction peak to a higher temperature and produced more defined peaks.

Figure 4.14 Pre-reaction TPR of 10% Cu/SiO_2

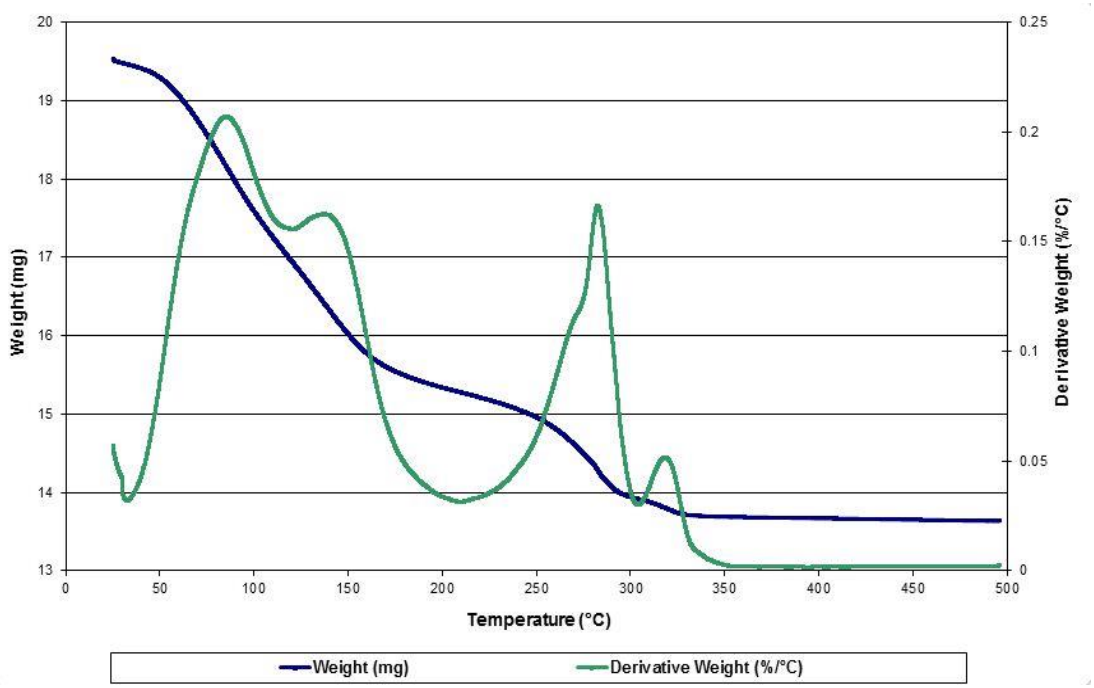

An initial weight loss from room temperature to 160˚C was shown by two peaks at 85 and 140˚C which were endothermic. Whereas, between 250 and 350˚C there were peaks shown at 280, 320, and a shoulder at 270˚C corresponding to exothermic weight losses.

The low loading of ceria in the catalyst had little effect on the reduction pattern obtained however 5% Cu + 5% CeO_x/SiO_2 showed a distinct weight loss at 190˚C as shown in figure 4.15.

Figure 4.15 Pre-reaction TPR of 5% Cu + 5% CeO_x/SiO_2

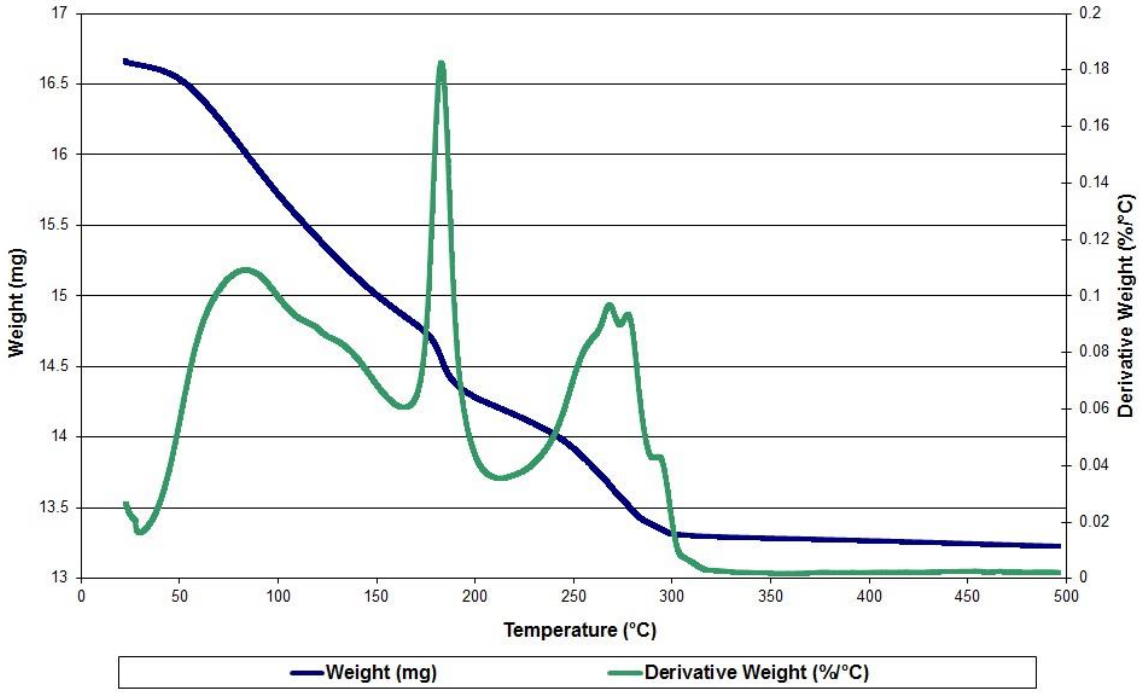

TPO of 5% Cu + 5% CeO_x/SiO_2 also showed a sharp endothermic weight loss at 190˚C which suggests that this weight was lost as a result of thermal treatment. A very broad peak at 80˚C, a sharp peak at 180˚C and a pair of peaks at 270˚C with shoulders at 260 and 290˚C. The broad low temperature peak was endothermic and the higher temperature reduction peaks exothermic.

For catalysts with the same ceria loading but a higher copper loading similar TPR patterns were observed and the incorporation of low levels of palladium had little effect on the TPR pattern. Temperature programmed reduction of Cu1132 however, produced a completely different reduction pattern compared to all of the other catalysts.

Figure 4.16 Pre-reaction TPR of Cu1132

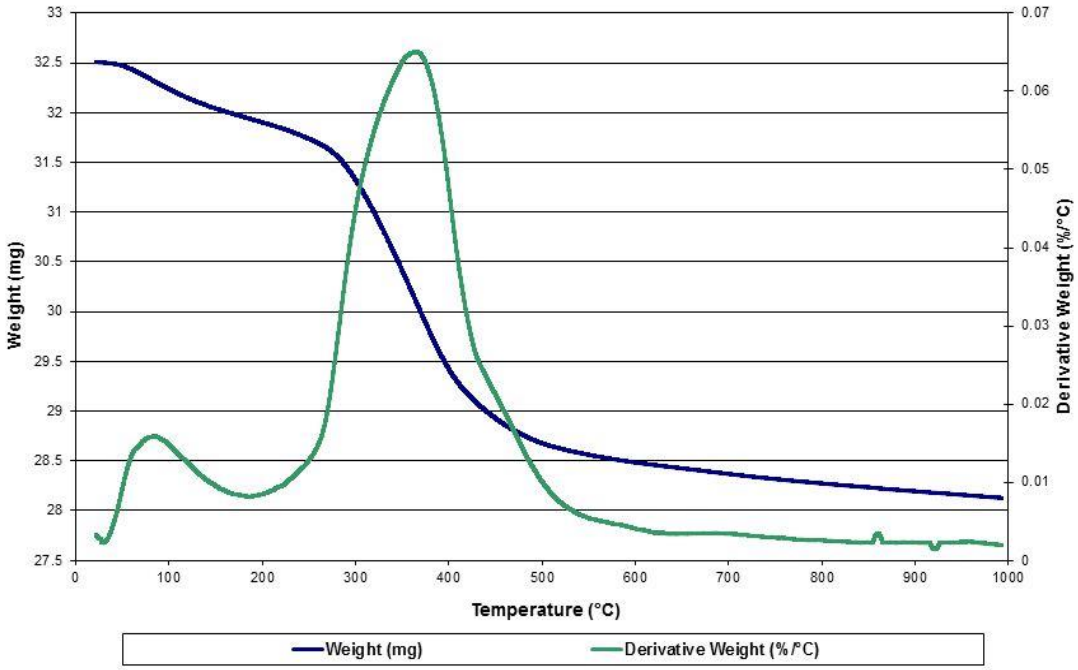

TPR of Cu1132 was conducted from room temperature to 1000˚C as reduction was incomplete at 500˚C. Two weight losses were observed at around 100 and the other at 365˚C. Heat flow data showed that the first weight loss was endothermic and the second was exothermic. Mass spectrometry data showed a low temperature evolution of *m/z* 17 and significant hydrogen consumption at 340˚C.

Pre-reaction catalyst samples underwent TPO and then TPR to investigate the effect of calcination followed by reduction. This treatment had the same effect on all of the catalysts which was a decrease in the overall weight lost as shown in figure 4.17 and 4.18.

Figure 4.17 TPR Comparison of calcined and uncalcined 5% Cu/SiO_2

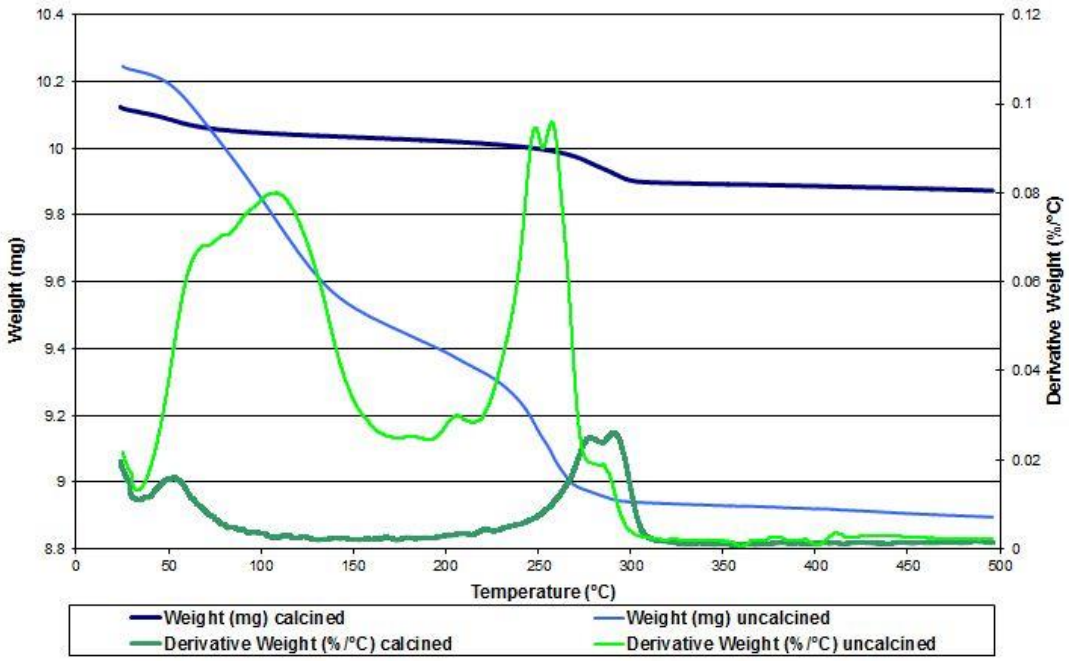

Reduction of the uncalcined sample showed a dramatic weight loss with a large broad peak around 100˚C and a pair of reduction peaks at 250˚C. The calcined sample showed a small weight loss around 50˚C and the reduction peaks were observed at a higher temperature of 290˚C. Heat flow data confirmed that as before, the low temperature weight loss was endothermic and the reduction peaks were exothermic.

Calcination of the 5% Cu + 1% CeO_x/SiO_2 followed by reduction altered the shape of the reduction peaks.

Figure 4.18 TPR comparison of calcined and uncalcined 5% Cu + 1% CeO_x/SiO_2

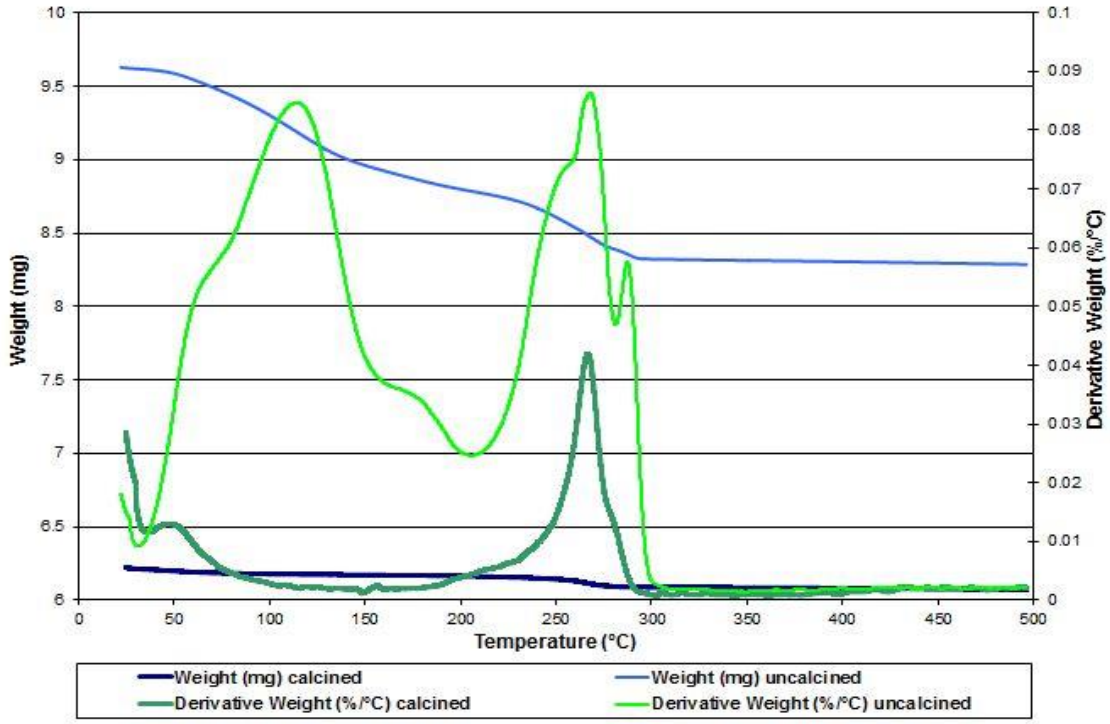

The calcined sample shows a much smaller weight loss at 50˚C, no peak at 190˚C and only one peak with a small shoulder around 260˚C.

Table 4.2 Weight Lost through pre-reaction TPO and TPR

Catalyst	Weight lost (% of original sample)		
	Pre-reaction TPO	Pre-reaction TPR calcined	Pre-reaction TPR uncalcined
5% Cu/SiO_2	11.5	2.5	13.2
5% CeO_x/SiO_2	7.2	1.7	9.1
5% Cu + 5% CeO_x/SiO_2	18.9	2.8	20.6
5% Cu + 1% CeO_x/SiO_2	13.6	2.4	13.9
10% Cu/SiO_2	24.8	4.5	30.2
10% Cu + 5% CeO_x/SiO_2	22.8	3.7	26.7
10% Cu+ 5% CeO_x + 0.05% Pd/SiO_2	24.2	3.8	25.2
Cu1132	8.9	NM	13.5

4.1.3 Powder x-ray diffraction

X-ray diffraction (XRD) was carried out for each catalyst pre-reaction. The pattern obtained for Cariact Q10 silica support material and 5% Cu/SiO_2 are shown in figure 4.19.

Figure 4.19 XRD pattern for Cariact Q10 silica and 5% Cu/SiO_2

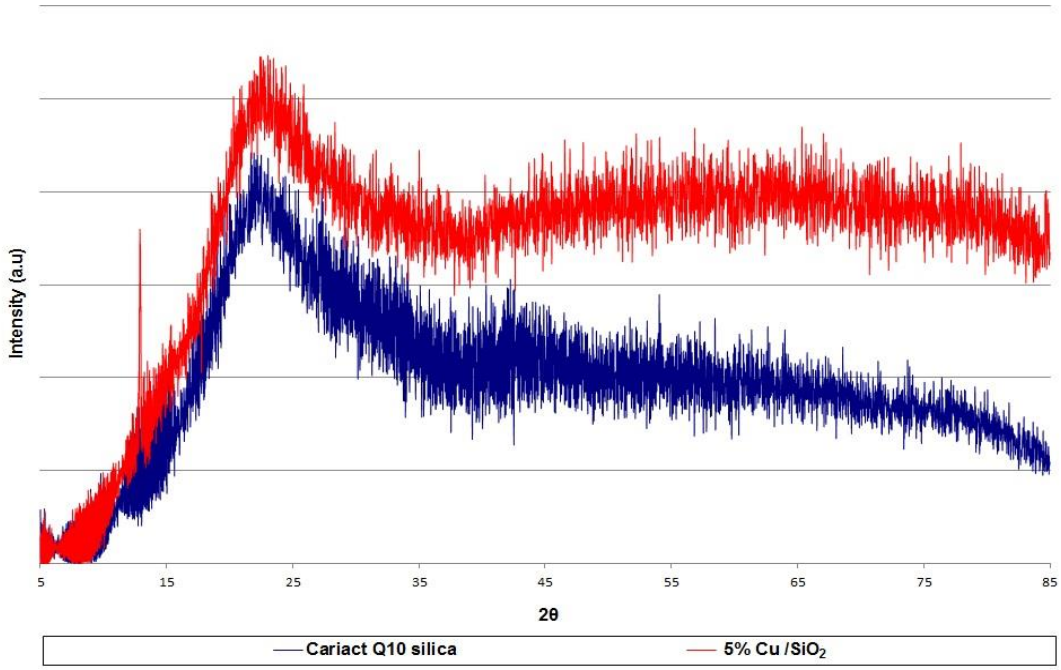

There is little to distinguish the catalyst pattern from the support material suggesting that impregnation of the support material using copper nitrate results in an amorphous solid. However, following calcination copper oxide is formed as shown in figure 4.20.

Figure 4.20 Fresh and calcined XRD patterns of 5% Cu/SiO_2

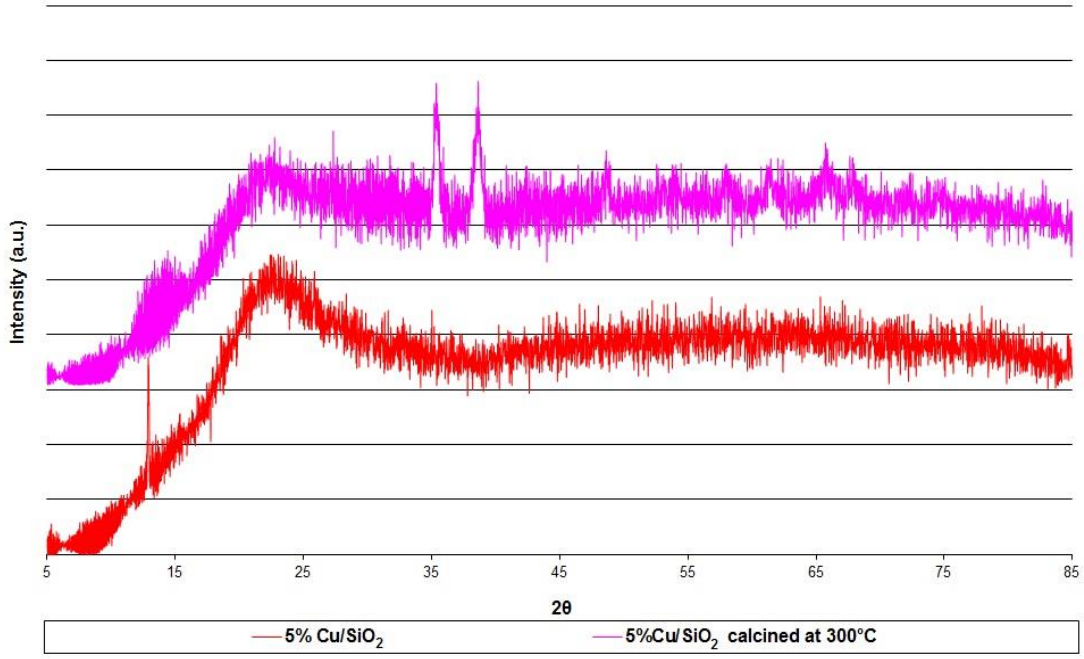

The peak at 22° is characteristic of silica and no other peaks were detected for 5% Cu/SiO_2 prior to pre-treatment. Calcination of the sample offline followed by XRD however, produces peaks at 35° and 38° corresponding to copper oxide in the tenorite form.

Figure 4.21 XRD patterns for calcined and reduced 5% Cu/SiO_2

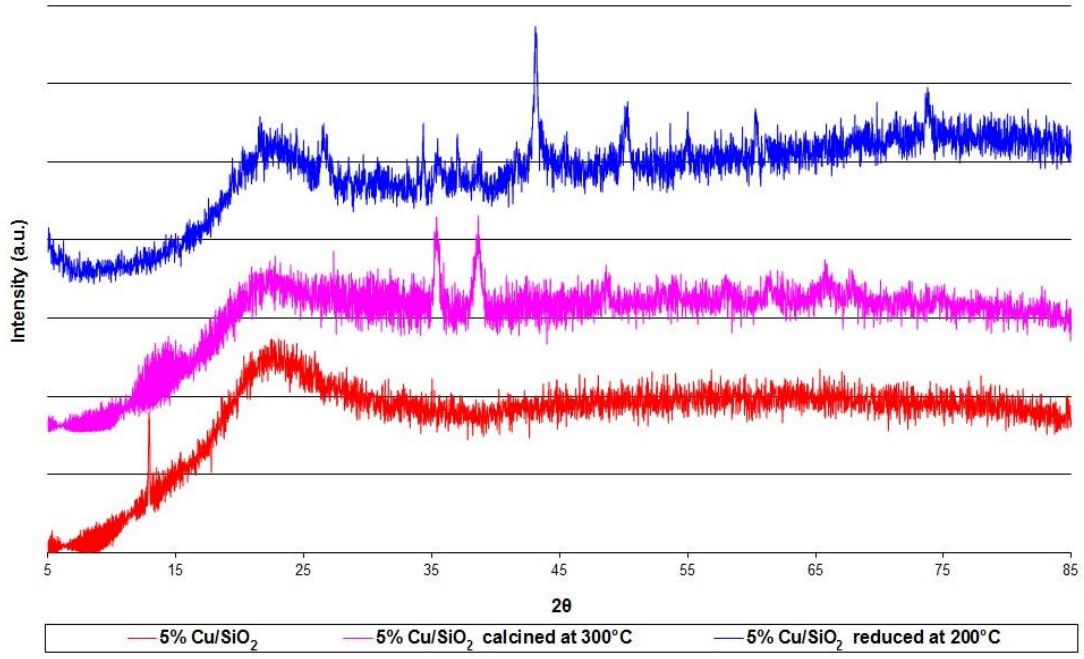

Reduction of the calcined sample was carried out using *in situ* hot stage XRD and shows the loss of copper oxide and the formation of copper particles, shown by the peaks at 43 and 50˚.

Catalysts involving ceria also gave an amorphous X-ray diffraction pattern showing that the catalytic surface is amorphous in character. However, calcination of these catalysts showed the formation of copper oxide (tenorite) and cerium oxide (Ce_2O_3).

Figure 4.22 XRD patterns for 5% Cu + 1% CeO_x/SiO_2

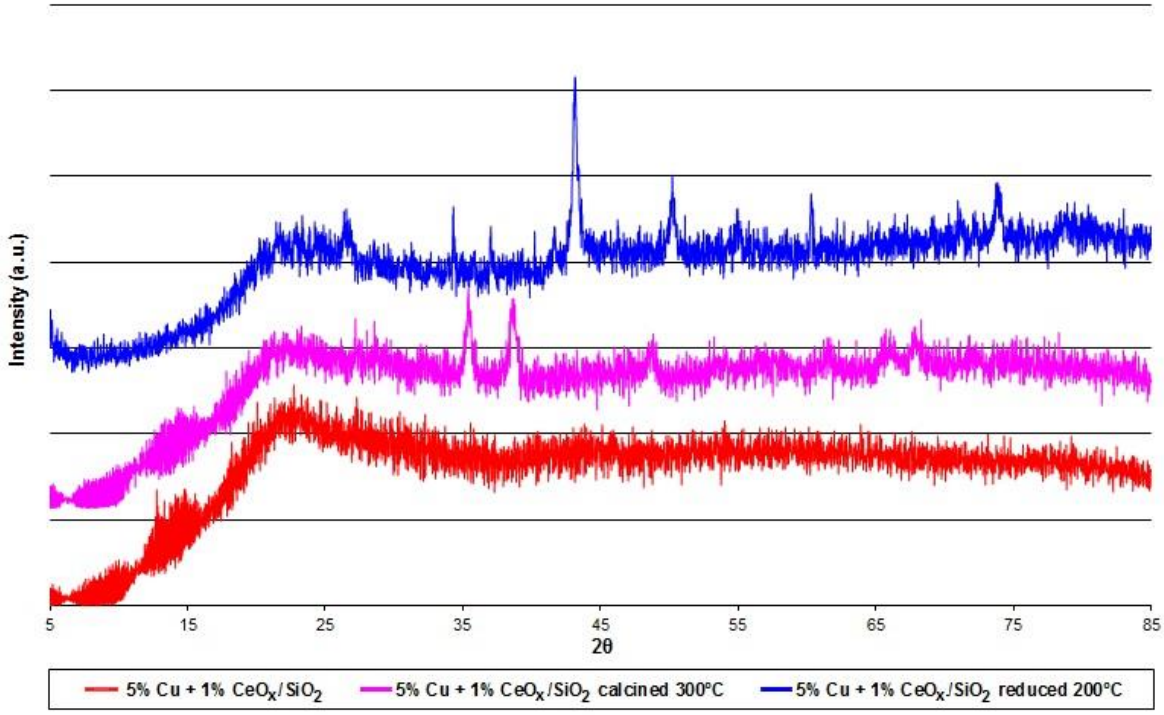

In situ reduction of the calcined sample showed the loss of these metal oxides and the production of copper particles. At low loading ceria the peaks associated with Ce_2O_3 at 28 and 47˚ are almost indistinguishable however, at 5% CeO_x the peaks are clear as shown in figure 4.23.

Figure 4.23 XRD patterns for 5% Cu + 5% CeO_x/SiO_2

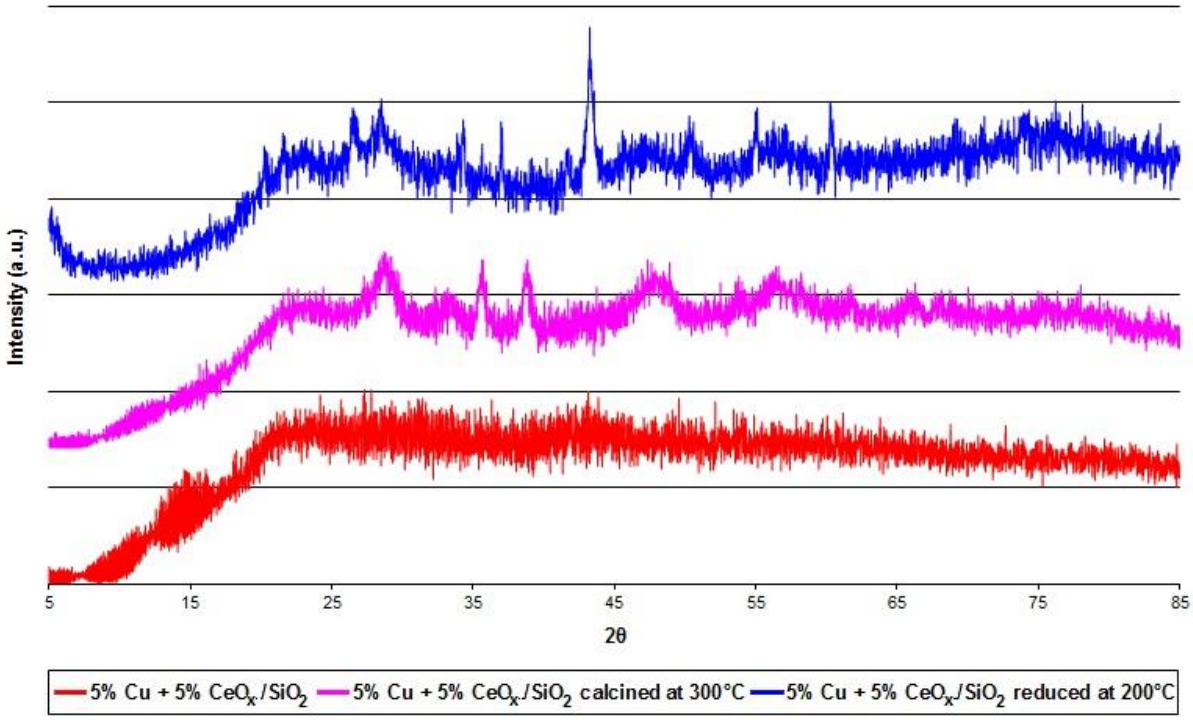

Similar patterns were obtained for 5% Cu + 5% CeO_x/SiO_2 and as expected the CeO_2 peaks at 28°, 47° and 56° were more intense corresponding to the increased amount of ceria present in the catalyst. For other catalysts such as 10% Cu + 5% CeO_x/SiO_2 and 10% Cu + 5% CeO_x + 0.05% Pd/SiO_2 showed very similar XRD patterns so will not be shown in this section and the results for 5% Cu/SiO_2, 5% Cu + 1% CeO_x/SiO_2 and 5% Cu + 5% CeO_x/SiO_2 will be used to show the effect of ceria on the structure of the catalysts.

The mean crystallite size was calculated using the Scherrer equation, where the Scherrer constant (particle shape factor) was taken as 0.89 and the full width at half maximum (FWHM) was in radians of the CuO(111) plane (35.6° in 2θ) or of the (111) for Cu (43° in 2θ). Crystallite sizes for CeO_2 were too small to be measured by this method but the estimated CuO and Cu crystallite sizes are shown in table 4.3.

Table 4.3 Average crystallite sizes for CuO and Cu

Catalyst	Average crystallite size (nm)	
	CuO (calcined)	Cu (reduced)
5% Cu/SiO_2	15.7	18.3
5% Cu + 1% CeO_x/SiO_2	32.8	14
5% Cu + 5% CeO_x/SiO_2	30.5	40.5
10% Cu + 5% CeO_x/SiO_2	14.6	n.m.[a]
10% Cu + 5% CeO_x + 0.05% Pd/SiO_2	9.8	n.m.

[a]n.m. not measured

The table shows that the presence of ceria increases the size of CuO crystals formed through calcination. Following reduction the presence of 1% CeO_x produced smaller Cu crystals compared to 5% Cu/SiO_2 and reduction of 5% Cu + 5% CeO_x/SiO_2 produced much larger copper crystals.

4.2 Catalyst testing

Catalysts were tested for the gas phase hydrogenation of furfural to furfuryl alcohol in a fixed bed reactor at 200˚C and 5 barg. Liquid samples were taken at regular intervals and analysed by gas chromatography (GC).

4.2.1 Cariact Q10 silica support

It was important firstly to establish whether the support material had any catalytic effect on the hydrogenation of furfural so a reaction was conducted using Cariact Q10 silica. Only trace levels of conversion of furfural to furfuryl alcohol (<3%) were observed over 50 h time on stream and so the silica was deemed to have no significant catalytic activity.

4.2.2 Ceria

5% CeO_x/SiO_2 showed poor activity for the hydrogenation of furfural to furfuryl alcohol. The following figure shows the distribution of reactant and products against time on stream.

Figure 4.24 Product distribution against time for 5% CeO_x/SiO_2

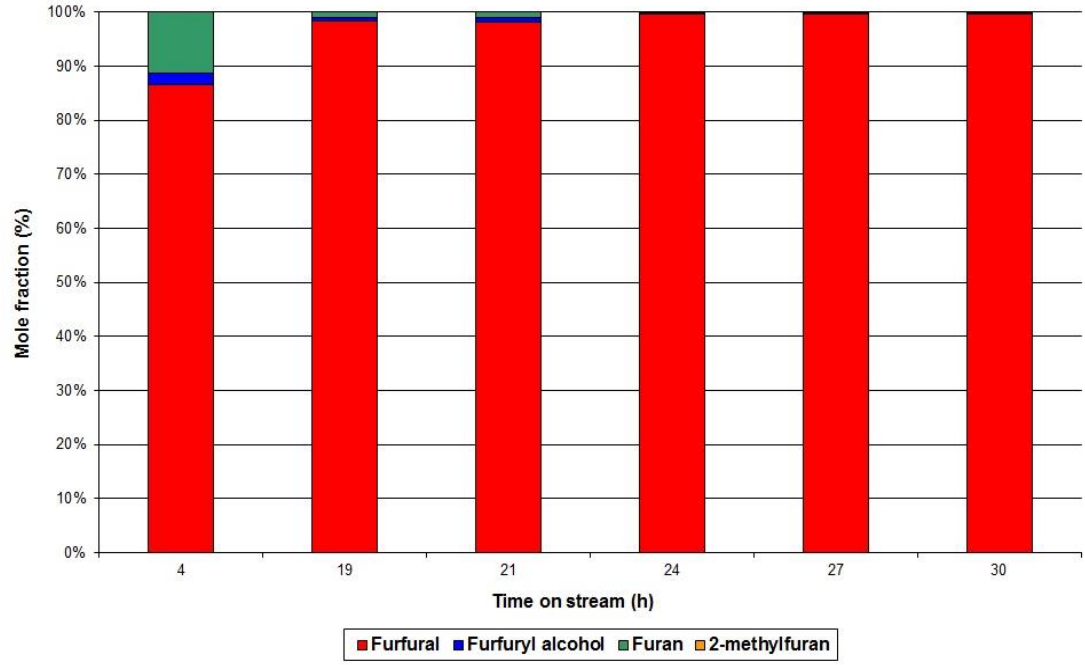

Figure 4.24 shows that very little furfural was converted (13%) to furfuryl alcohol and furan was the main by-product at 4 h time on stream (TOS). Over the observed reaction time the concentration of furfural in the product stream continued to increase and after 30 h TOS the catalyst was inactive and no furfural was being converted.

4.2.3 Copper catalysts

Silica supported copper catalysts however, proved far more active for the hydrogenation of furfural. Figure 4.25 shows the molar fraction of reactants and products over the total reaction time.

Figure 4.25 Product distribution against time for 5% Cu/SiO_2

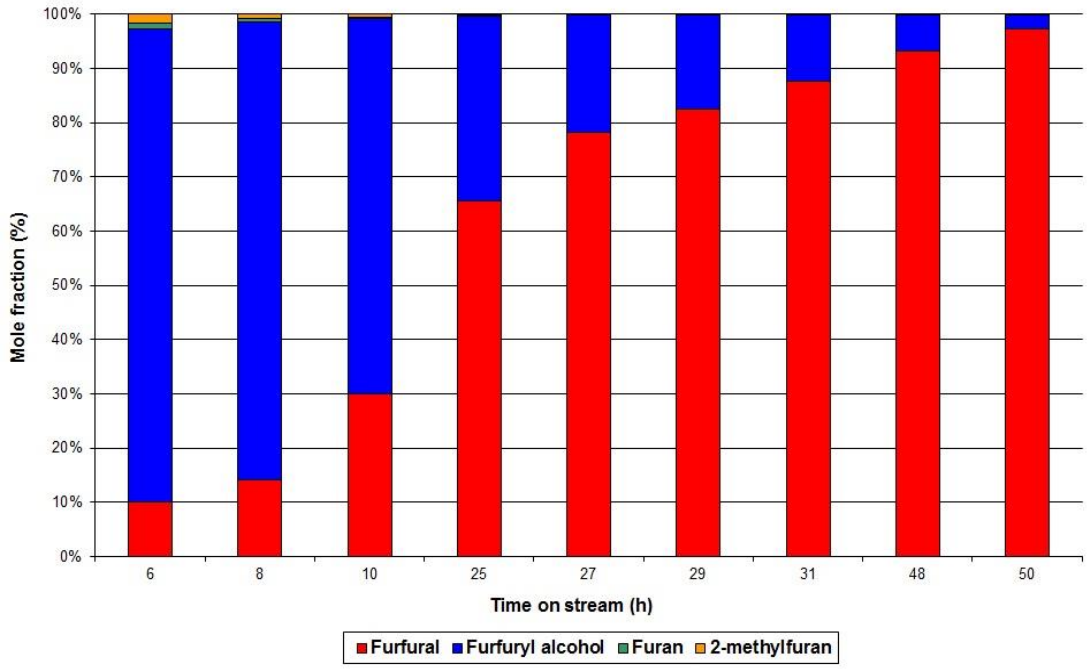

In the early stages of the reaction, high conversions of furfural were achieved and the main product was furfuryl alcohol with low levels of 2-methylfuran and furan as by-products. After 25 h TOS however, the conversion of furfural was remarkably lower and the conversion of furfural continued to decrease over the remaining TOS.

An inlet sample was taken periodically and analysed by GC to provide an inlet concentration $[FFRAL]_{in}$ used to calculate furfural conversion as shown below:

$$\textbf{Conversion} = ([FFRAL]_{in} - [FFRAL]_{out} / [FFRAL]_{in}) \times 100\%$$

This inlet concentration was also used to calculate the selectivity to furfuryl alcohol and the yield:

$$\textbf{Selectivity} = ([FFRYL]_{out} / [FFRAL]_{in} - [FFRAL]_{out}) \times 100\%$$

$$\textbf{Yield} = ([FFRYL]_{out} / [FFRAL]_{in}) \times 100\%$$

5% Cu/SiO_2 catalyst exhibited high activity for the hydrogenation of furfural with 90% conversion achieved at 6 h TOS and 98% selectivity towards furfuryl alcohol at 27 h TOS. 10% Cu/SiO_2 exhibited a lower activity achieving ~70% conversion

of furfural at 22 h TOS however, the activity of the catalyst slowly decreased over the remaining h on stream as shown in figure 4.26.

Figure 4.26 Product distribution against time for 10% Cu/SiO_2

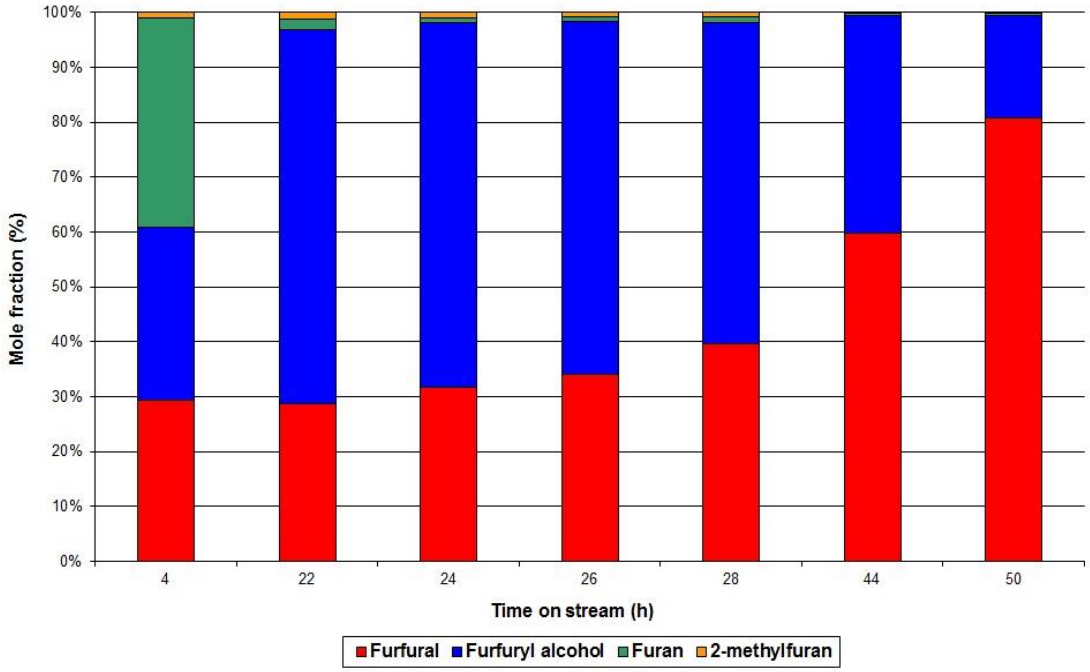

The figure shows furfural conversion slowly decreases with time on stream and in the early stages the selectivity to furan (34%) was higher than that of furfuryl alcohol (28.5%). 2-methylfuran was also present as a by-product at 4 h TOS (8×10^{-3} mol L^{-1}) but at 44 h TOS the only product of the reaction was furfuryl alcohol.

4.2.4 Copper and ceria catalysts

5% Cu + 1% CeO_x/SiO_2 was tested under the same conditions for the hydrogenation of furfural to furfuryl alcohol. The following figure shows the progress of the reaction over 50 h time on stream (TOS).

Figure 4.27 Product distribution against time for 5% Cu + 1% CeO_x/SiO_2

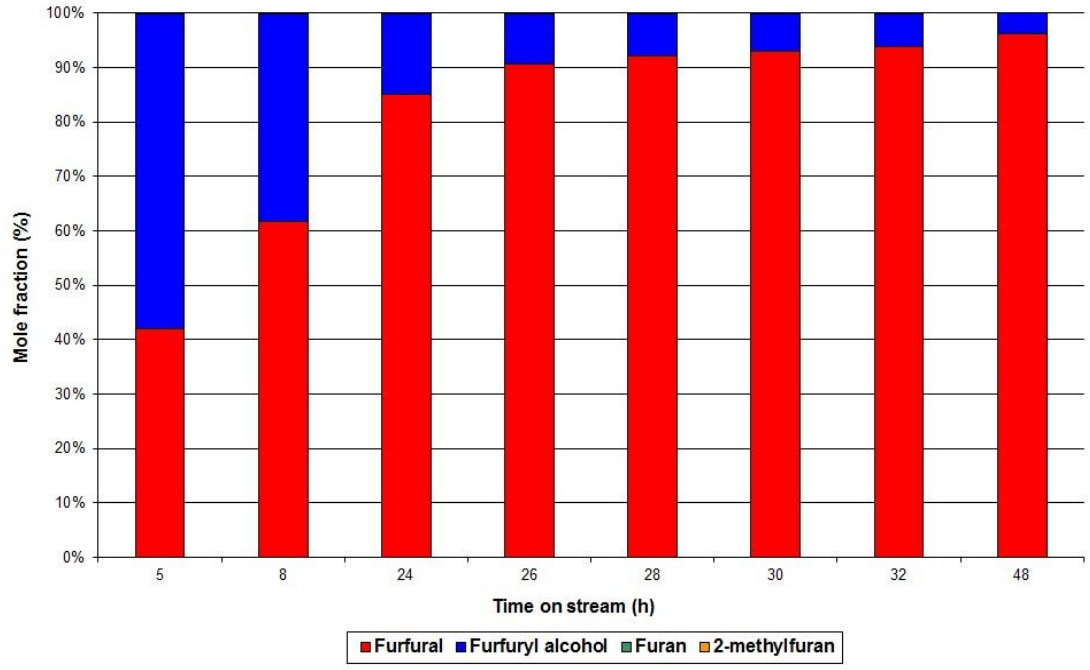

The conversion of furfural was high in the early stages of reaction however this rapidly decreased within the first 24 h and then remained low. The only by-product detected was low levels of 2-methylfuran (1.5×10^{-3} mol L^{-1}) and therefore the selectivity to furfuryl alcohol was high.

5% Cu + 5% CeO_x/SiO_2 was also tested to investigate the effect of higher loadings of ceria on the activity and selectivity of the catalyst for the reaction.

Figure 4.28 Product distribution against time for 5% Cu + 5% CeO_x/SiO_2

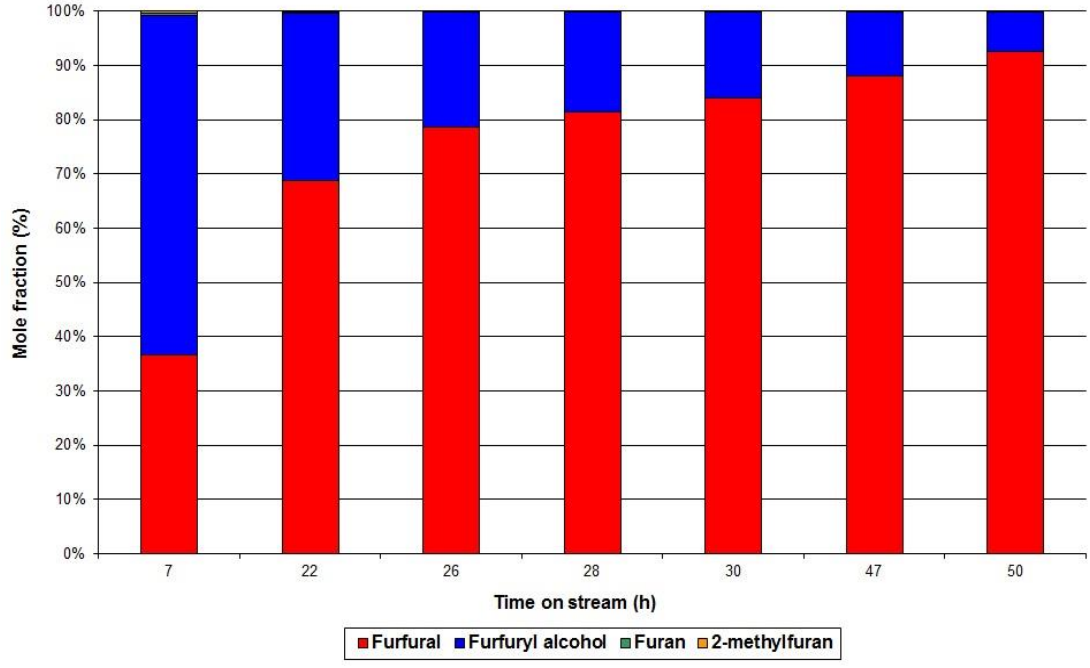

From figure 4.28 it appears that the higher ceria loading has enhanced the activity and lifetime of the catalyst as the fraction of furfural converted to furfuryl alcohol decreased more slowly over the TOS. 10% Cu + 5% CeO_x/SiO_2 was also tested to investigate the relationship between copper and ceria Loadings and their effect on activity and selectivity (Fig. 4.29).

Figure 4.29 Product distribution against time for 10% Cu + 5% CeO_x/SiO_2

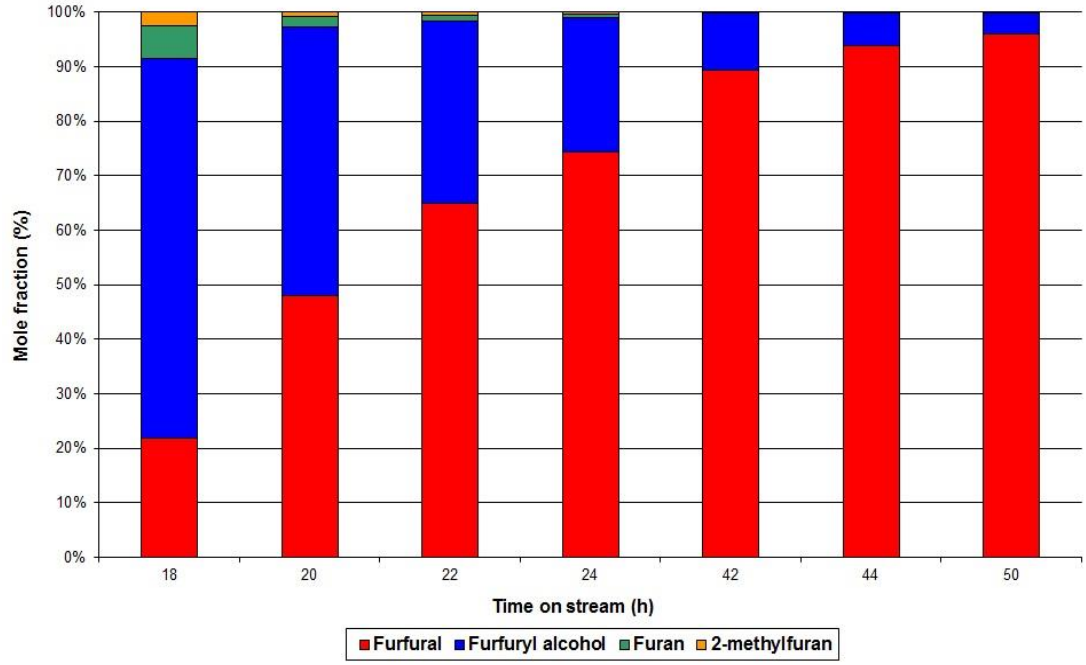

Nearly 80% conversion of furfural was achieved at 18 h TOS but the activity of the catalyst decreased rapidly to 5% conversion at 50 h. Selectivity to furan was 6% and furfuryl alcohol was ~70% at 18 h TOS however at 20 h TOS selectivities were 3.5% and ~90% respectively.

4.2.5 Pd promoter

10% Cu + 5% CeO_x + 0.05% Pd/SiO_2 was tested to investigate if incorporating a small amount of palladium had an effect on activity or selectivity.

Figure 4.30 Product distribution against time for 10% Cu + 5% CeO_x + 0.05% Pd/SiO_2

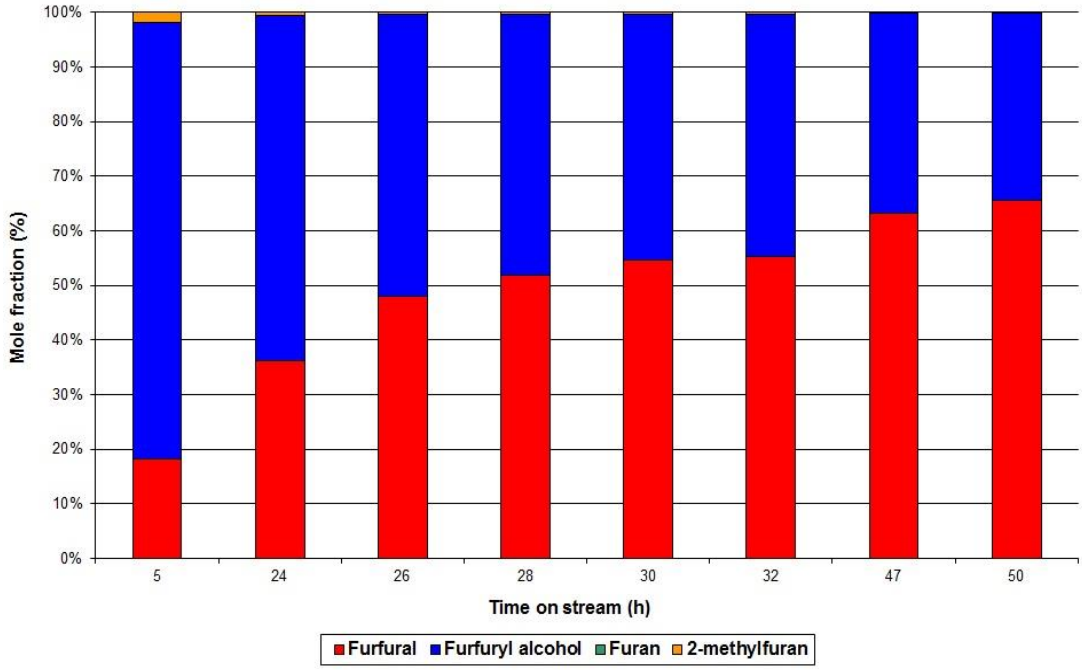

10% Cu + 5% CeO_x + 0.05% Pd/SiO_2 showed excellent activity in the early stages of reaction with conversion of furfural at ~80% and selectivity to furfuryl alcohol in excess of 80%. The only by-product detected was 2-methylfuran however as with previous catalysts, the production of 2-methylfuran decreased over time.

4.2.6 Commercial catalyst

Cu1132 exhibited moderate activity but excellent selectivity to furfuryl alcohol with only trace levels of 2-methylfuran produced. The activity started to decline around 23 h TOS.

Figure 4.31 Product distribution against time for Cu1132

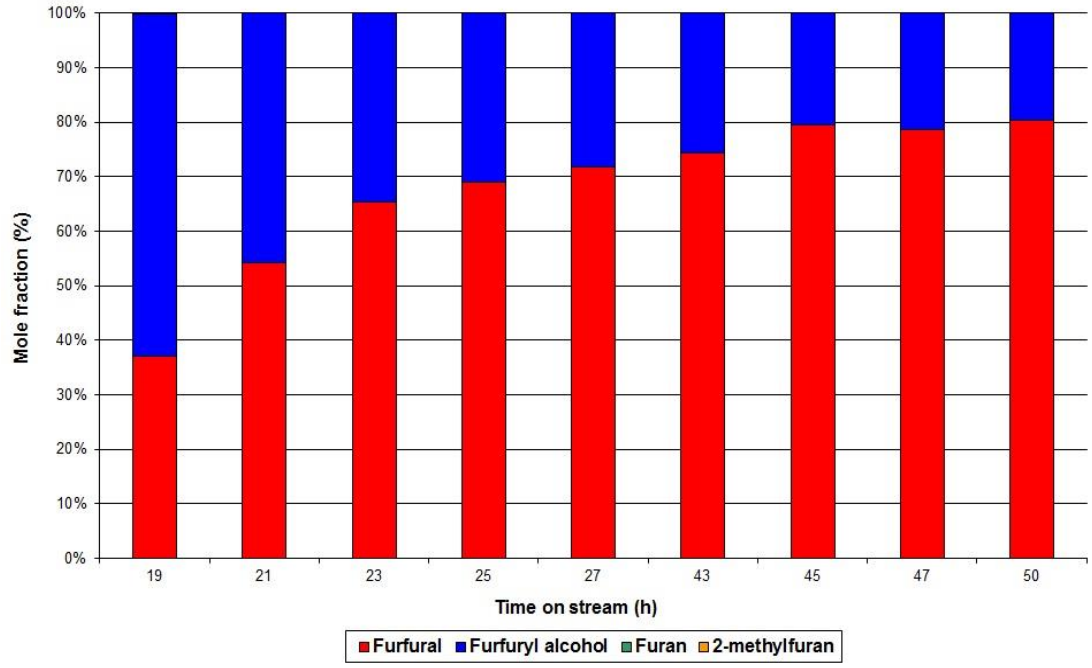

Conversion of 54% was achieved in the early stages of reaction with selectivity to furfuryl alcohol at almost 100% however the catalyst slowly deactivated with time on stream.

4.3 Post-reaction catalyst characterisation

Post-reaction catalyst samples were analysed to determine the extent and cause of catalyst deactivation. Surface area determination, TGA and powder XRD were carried out on a post-reaction sample of each catalyst.

4.3.1 Surface area determination

Surface area determination was carried out on catalyst samples after 50 h on stream (TOS) to investigate the effect of the reaction on the catalyst surface. Table 4.4 shows the pre-reaction surface area measurements in plain text and the post-reaction measurements in bold text.

Table 4.4 Surface areas of catalysts post 50 h TOS

Catalyst	BET				Single Point	
	Surface area (m^2g^{-1})		Average pore Diameter (nm)		Pore volume (cm^3g^{-1})	
Cariact Q10 silica	263	**187**	14.6	**14.1**	1.01	**0.66**
5% Cu/SiO_2	236	**128**	13.9	**12.6**	0.82	**0.40**
5% CeO_x/SiO_2	254	**193**	15.1	**15.1**	0.96	**0.73**
5% Cu + 5% CeO_x/SiO_2	215	**126**	14.5	**13.7**	0.78	**0.43**
5% Cu + 1% CeO_x/SiO_2	232	**224**	14.9	**14.1**	0.87	**0.70**
10% Cu/SiO_2	235	**90**	13.1	**12.2**	0.77	**0.28**
10% Cu + 5% CeO_x/SiO_2	154	**150**	13.2	**13.8**	0.51	**0.52**
10% Cu+ 5% CeO_x + 0.05% Pd/SiO_2	190	**152**	14.8	**13.5**	0.69	**0.53**
Cu1132	45	**<1**	8.8	**n.m.**[a]	0.10	**0.02**

[a]n.m. not measured

The majority of the catalysts show a dramatic reduction in surface area after 50 h on stream (TOS). This is the result of pore blocking by coke/coke precursors. The pore diameters do not change greatly but the surface area is reduced because whole pores are becoming blocked. Two of the catalysts showed little change; 5% Cu + 1% CeO_x/SiO_2 and 10% Cu + 5% CeO_x/SiO_2 showed less than 5% reduction in surface area after 50 h TOS. 10% Cu/SiO_2 however exhibited a 60% reduction in available surface area. Cu1132, with the lowest measured BET surface area, was difficult to analyse post-reaction. It is thought that all of the pores had become blocked making surface area measurements difficult and the results very low.

4.3.2 Thermogravimetric analysis

TGA was carried out on all catalysts post-reaction. Samples were taken from the reactor and stored in a glove box under a nitrogen atmosphere prior to analysis. TPO and TPD were carried out on each sample to determine whether there were any chemical species left on the catalyst surface post-reaction.

4.3.2.1 Temperature programmed oxidation

TPO of each catalyst was conducted from room temperature to 1000˚C under 100 mL min^{-1} flow of O_2/Ar. Figure 4.32 shows the TPO of a post-reaction sample of 5% CeO_x/SiO_2.

Figure 4.32 Post-reaction TPO of 5% CeO_x/SiO_2

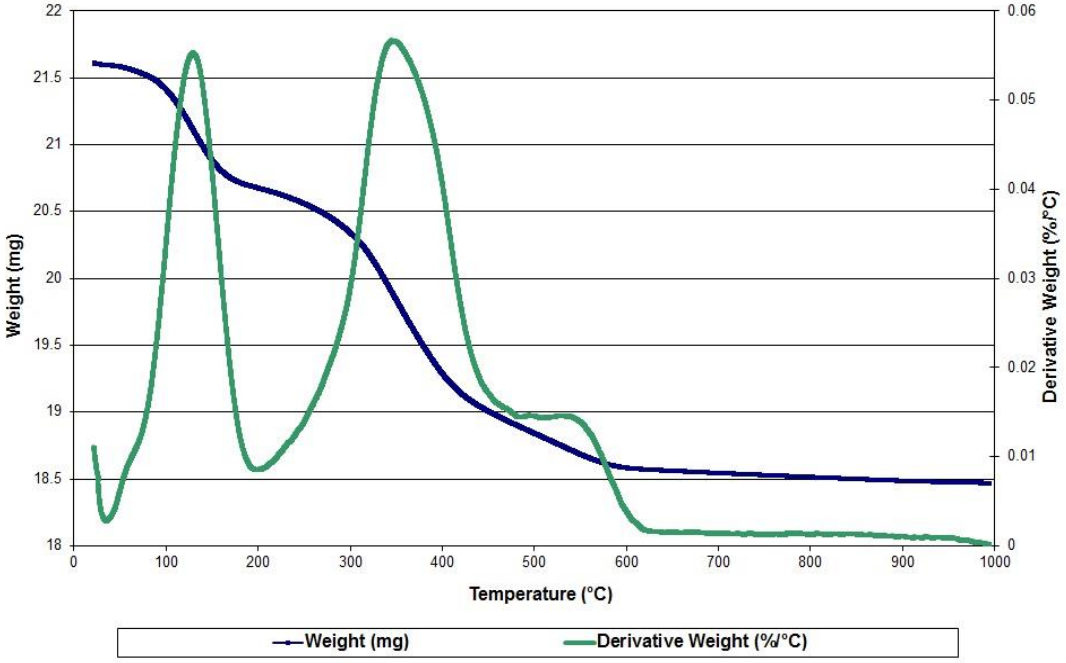

Post-reaction TPO of 5% CeO_x/SiO_2 showed a weight loss around 100˚C and two weight losses at around 360 and 550˚C. Heat flow data showed that the low temperature weight loss was endothermic and the weight lost at 360 and 550˚C was exothermic. Figure 4.33 shows mass spectrometry results for TPO of 5% CeO_x/SiO_2.

Figure 4.33 Mass spectrometry data for post-reaction TPO of 5% CeO_x/SiO_2

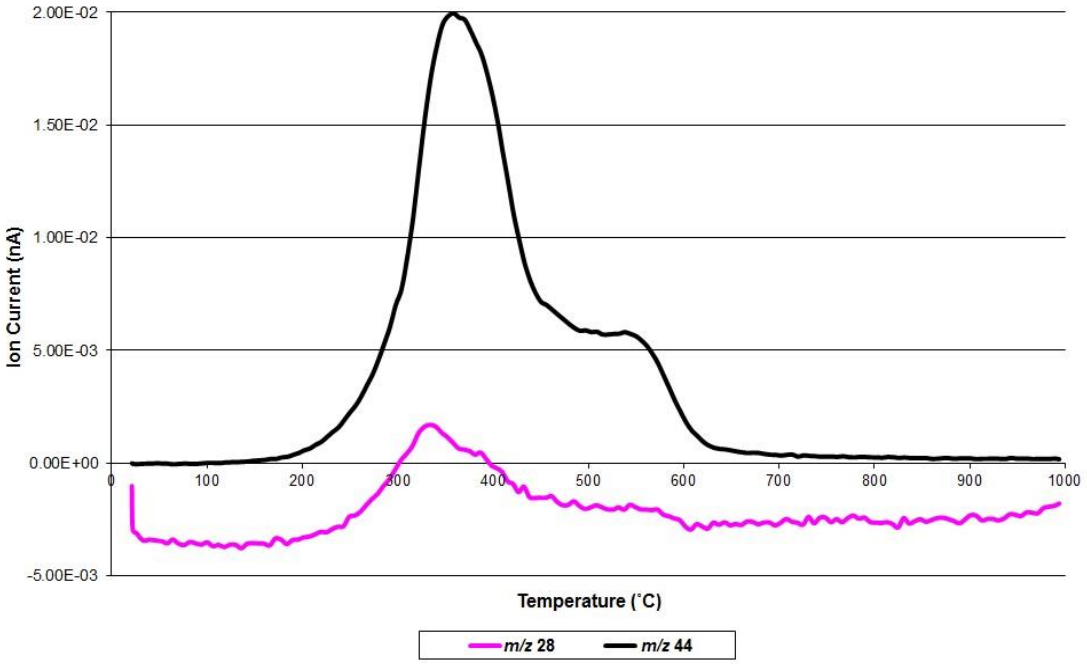

Mass spectrometry data showed that *m/z* 28 and *m/z* 44 were detected at 360 and 550˚C. This corresponds to the loss of CO and CO_2 from the surface of the catalyst at these temperatures. The loss of water from the surface was not observed. Post-reaction TPO of 5% Cu/SiO_2 showed much broader weight losses from 400–800˚C.

Figure 4.34 Post-reaction TPO of 5% Cu/SiO_2

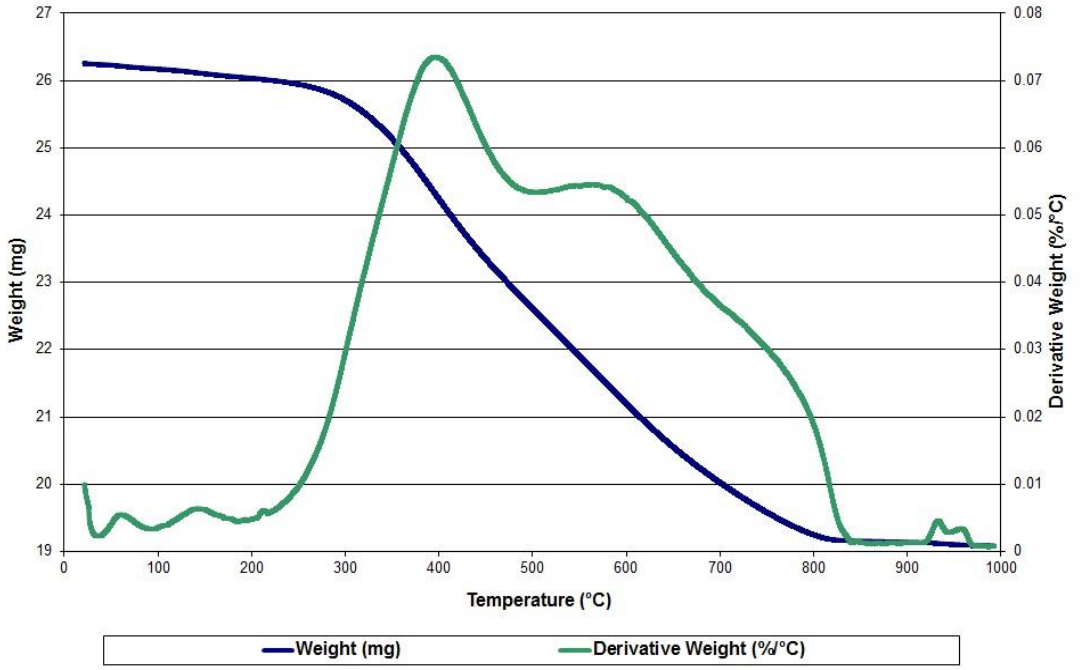

TPO of 5% Cu/SiO_2 after 50 h time on stream (TOS) shows several weight losses with the most prominent at 390, 570 and a shoulder at 750°C. Heat flow data, not shown here, showed that all weight losses were exothermic.

Figure 4.35 Mass spectrometry data for post-reaction TPO of 5% Cu/SiO_2

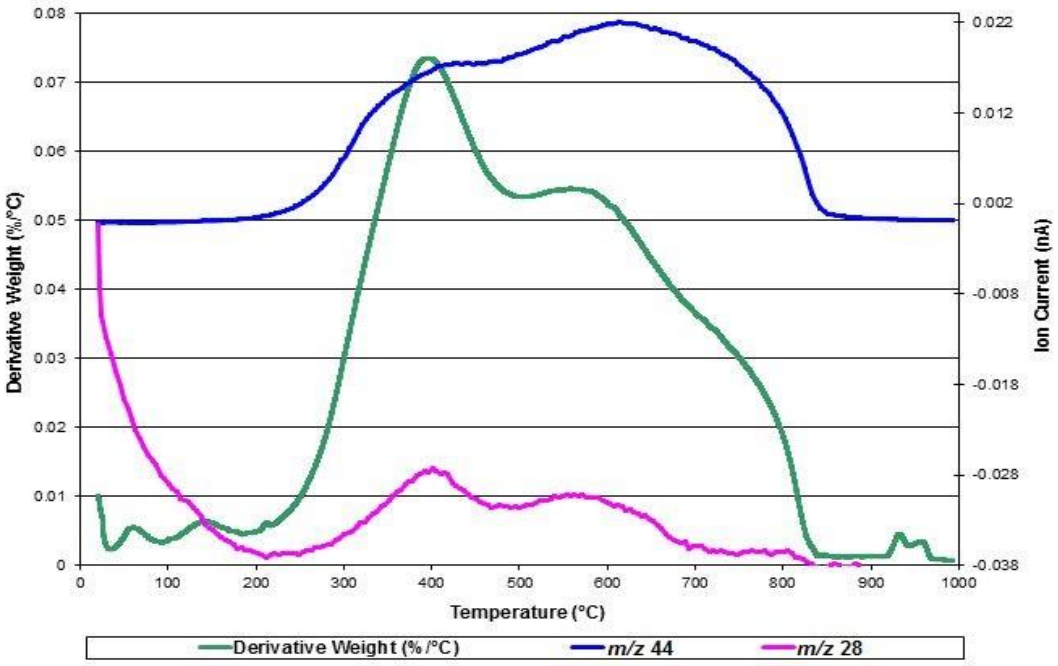

Mass spectrometry data shows that the weight Losses at 390, 570 and 750°C can be attributed to an evolution of CO_2; CO was also detected at these temperatures however fragments associated with the Loss of water were not detected. Figure 4.36 shows the post-reaction TPO of 5% Cu + 1% CeO_x/SiO_2.

Figure 4.36 Post-reaction TPO of 5% Cu + 1% CeO_x/SiO_2

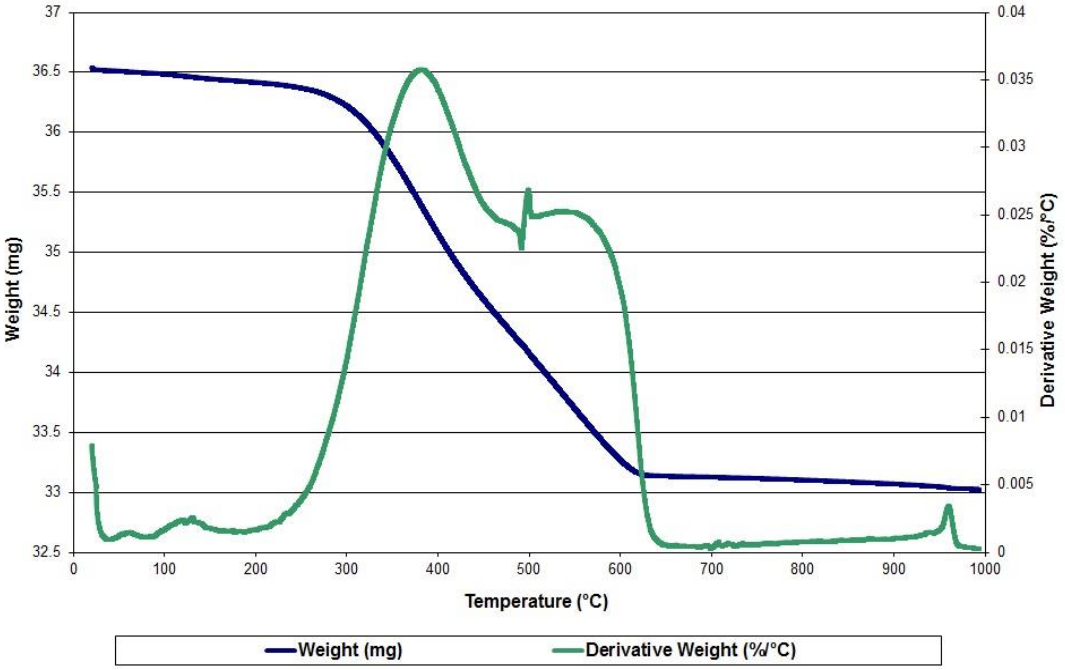

TPO of 5% Cu + 1% CeO_x/SiO_2 post 50 h TOS shows two sharper weight losses at 430 and 550˚C which were exothermic.

Figure 4.37 Post-reaction TPO mass spectrometry data for 5% Cu + 1% CeO_x/SiO_2

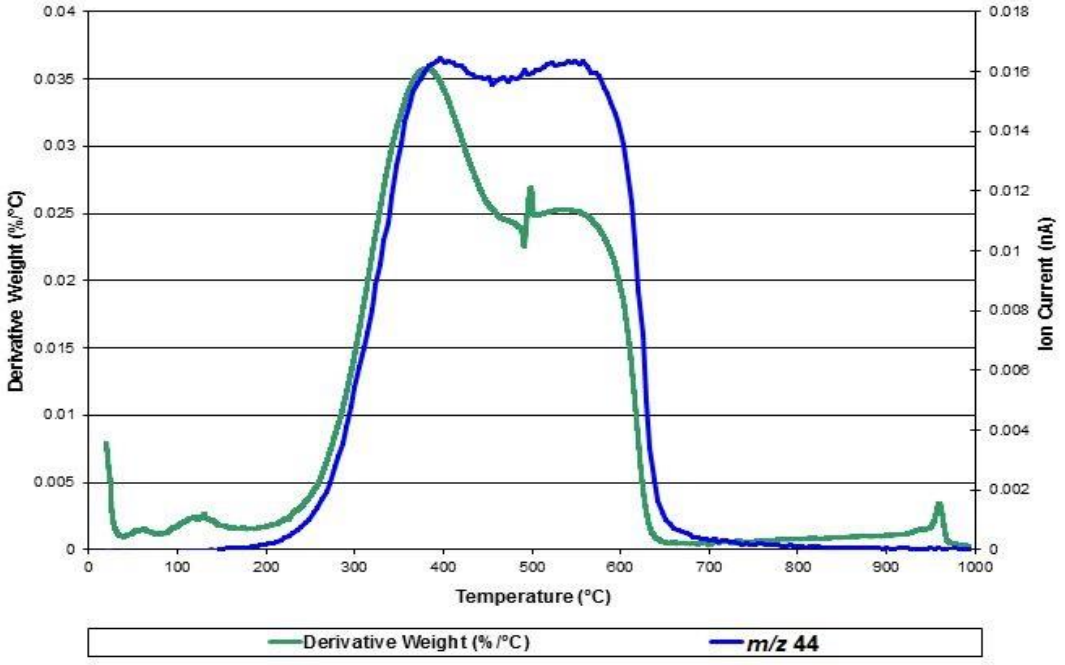

Mass spectrometry data showed *m/z* 44 corresponded to these weight losses. Figure 4.38 shows much broader weight losses were observed for TPO of 5% Cu + 5% CeO_x/SiO_2.

Figure 4.38 Post-reaction TPO of 5% Cu + 5% CeO_x/SiO_2

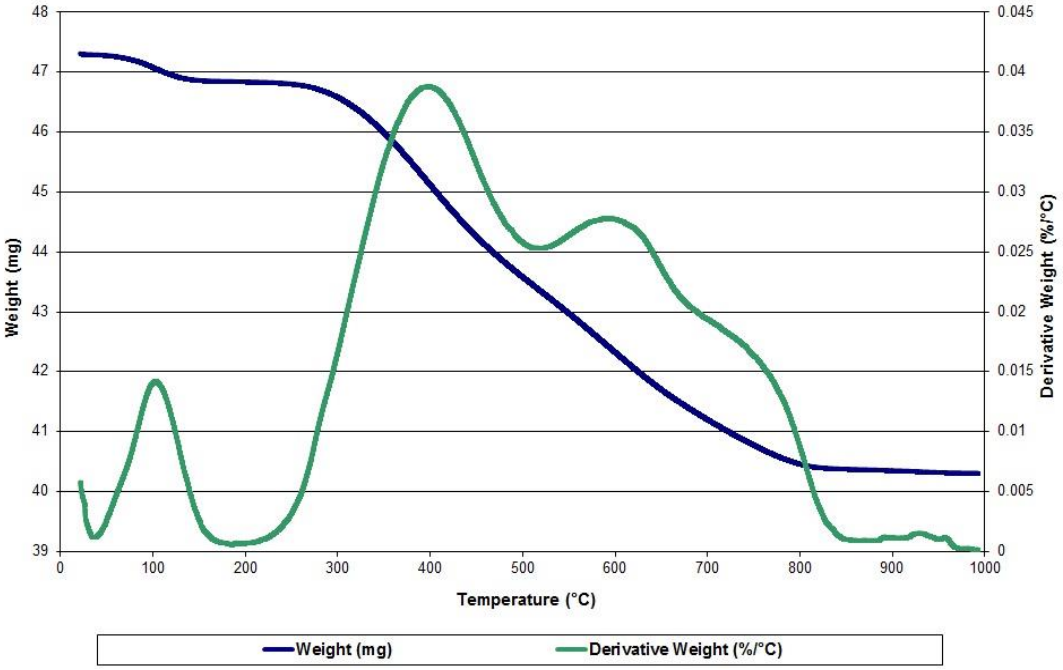

TPO of 5% Cu + 5% CeO_x/SiO_2 showed a similar pattern of peaks, and in addition to the broad peaks at 420, 630 and 750˚C, a sharp peak at 100˚C. Heat flow data showed that the weight loss between 200- 850˚C was exothermic and the weight lost at 100˚C was endothermic. Like 5% Cu + 1% CeO_x/SiO_2, mass spectrometry data showed *m*/*z* 44 detected between 200 and 850˚C which corresponds to the evolution of CO_2. 10% Cu/SiO_2 showed an extremely similar post-reaction TPO pattern, heat flow and mass spectrometry data and so is not shown here.

Figure 4.39 Post-reaction TPO of 10% Cu + 5% CeO_x/SiO_2

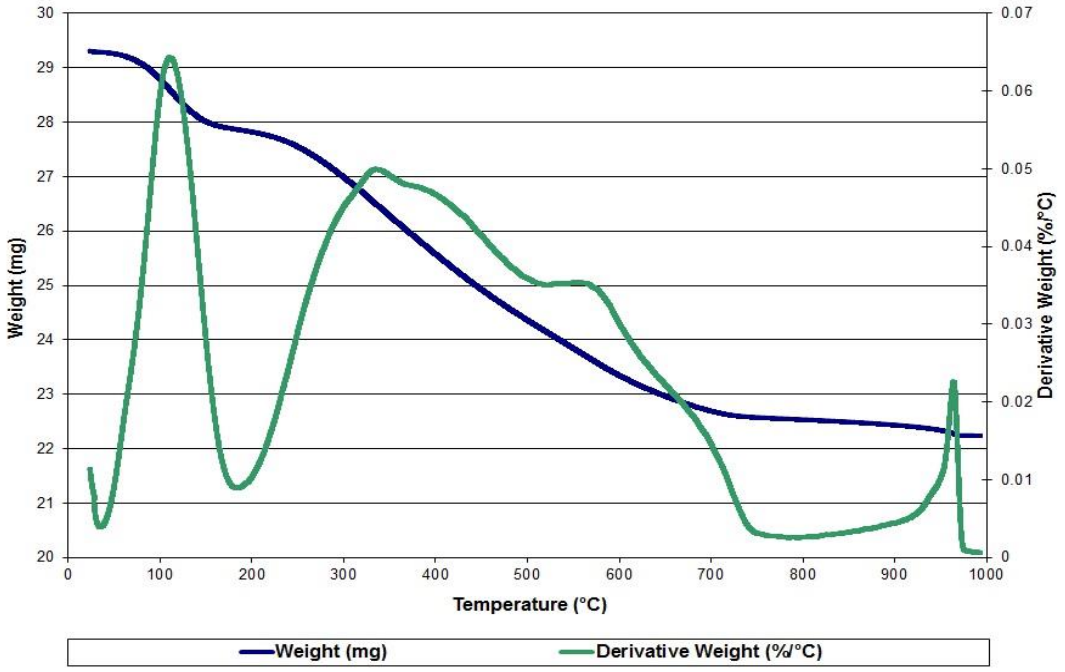

TPO of 10% Cu + 5% CeO_x/SiO_2 however showed a sharp peak at 100˚C, broad weight loss between 200 and 750˚C, and a small peak at 950˚C and the incorporation of low levels of palladium altered this pattern further as shown in figure 4.40.

Figure 4.40 Post-reaction TPO of 10% Cu + 5% CeO_x + 0.05% Pd/SiO_2

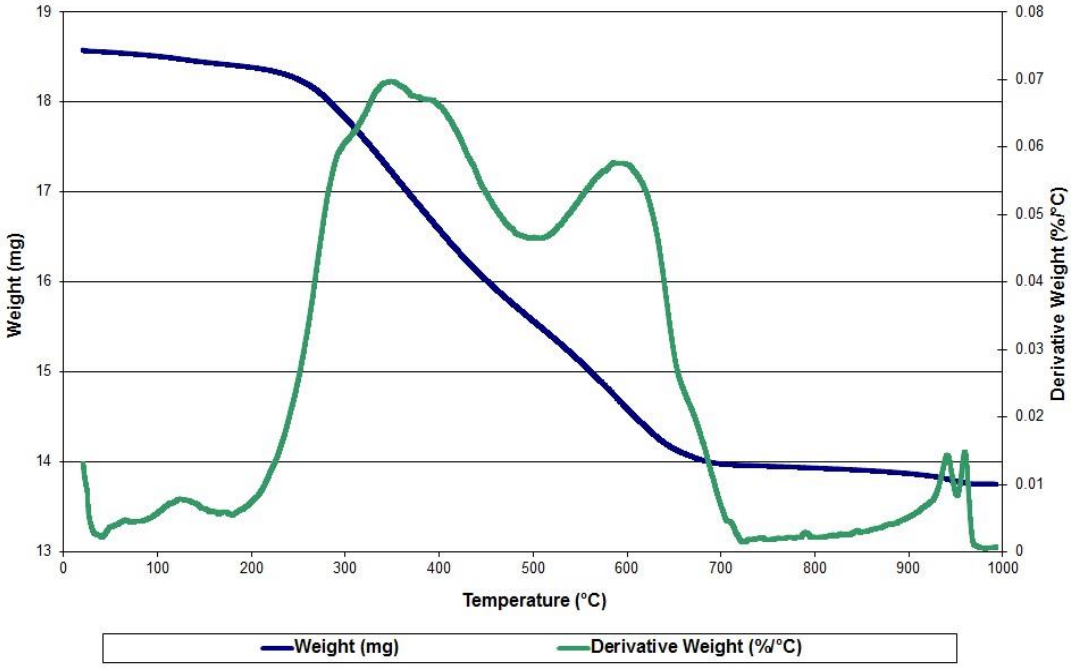

TPO of 10% Cu + 5% CeO_x + 0.05% Pd/SiO_2 showed a very small peak at 120˚C, a large peak at 360˚C with shoulders at 300˚C and 380˚C, another peak at 600˚C

and a small pair of peaks around 950˚C. As before, the weight lost between 200 and 700˚C was exothermic and all other weight losses endothermic.

Post-reaction TPO of commercial catalyst Cu1132 showed two main weight losses at 300˚C and 800˚C as shown in figure 4.41.

Figure 4.41 Post-reaction TPO of Cu1132

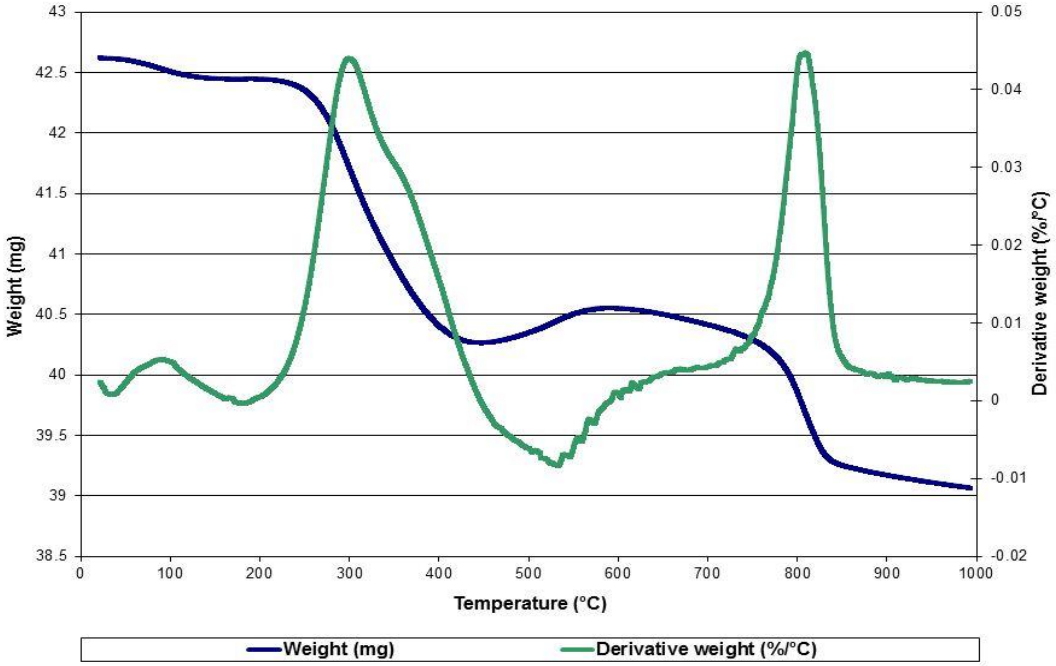

There was also a shoulder peak at 350˚C and heat flow data showed that the weight losses ~300˚C were exothermic, whereas the weight loss at 800˚C was endothermic. Mass spectrometry was used to try to identify which species contributed to these weight losses.

Figure 4.42 Post-reaction TPO mass spectrometry data for Cu1132

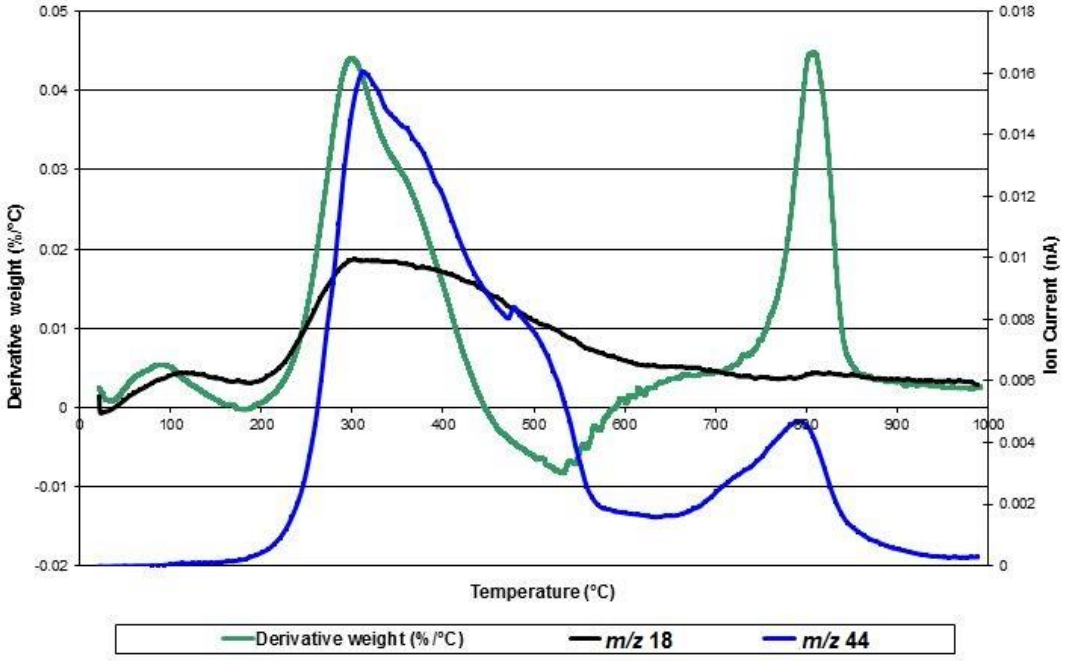

In figure 4.42, two fragments were observed with *m/z* 18 corresponding to water evolved ~300°C contributing to the exothermic weight loss and *m/z* 44 corresponding to CO_2 evolved at both 300 and 800°C.

4.3.2.2 Temperature programmed desorption

TPD was carried out from room temperature to 1000°C using argon. Mass spectrometry was used to determine species evolved between these temperatures. TPD of 5% Cu/SiO_2 showed a large weight loss between 200 – 700°C as shown in figure 4.43.

Figure 4.43 Post-reaction TPD of 5% Cu/SiO_2

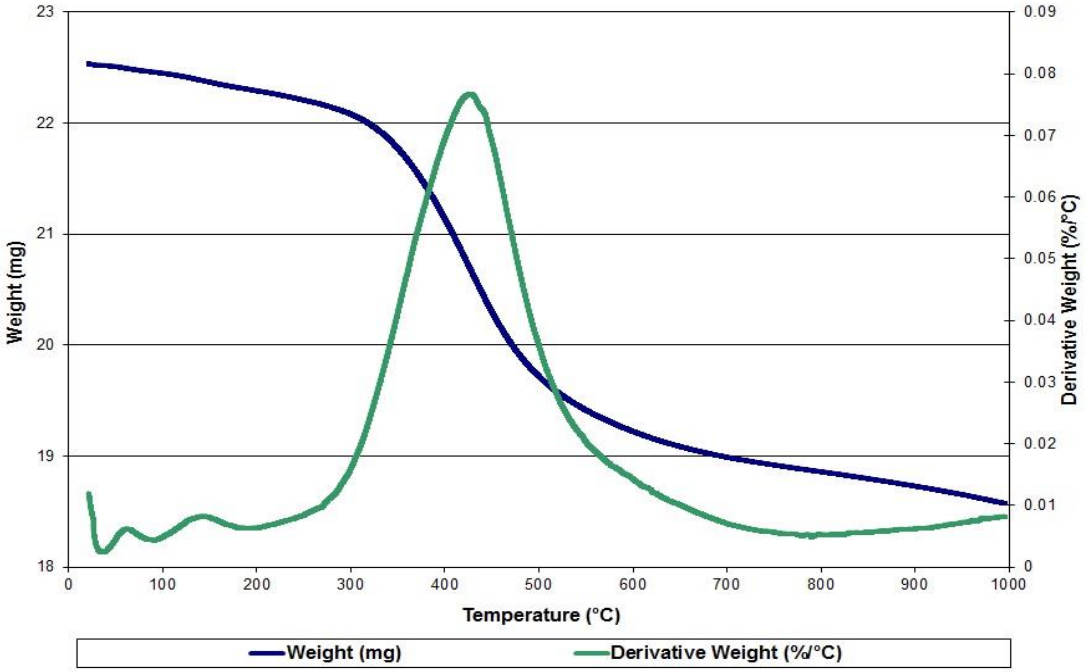

The weight loss between 200 and 700˚C was equal to 17% of the original sample weight and heat flow data, not shown here, showed that this was exothermic. Mass spectrometry was used to try to identify species evolved at these temperatures corresponding to the weight lost.

Figure 4.44 Mass spectrometry results from TPD of 5% Cu/SiO_2

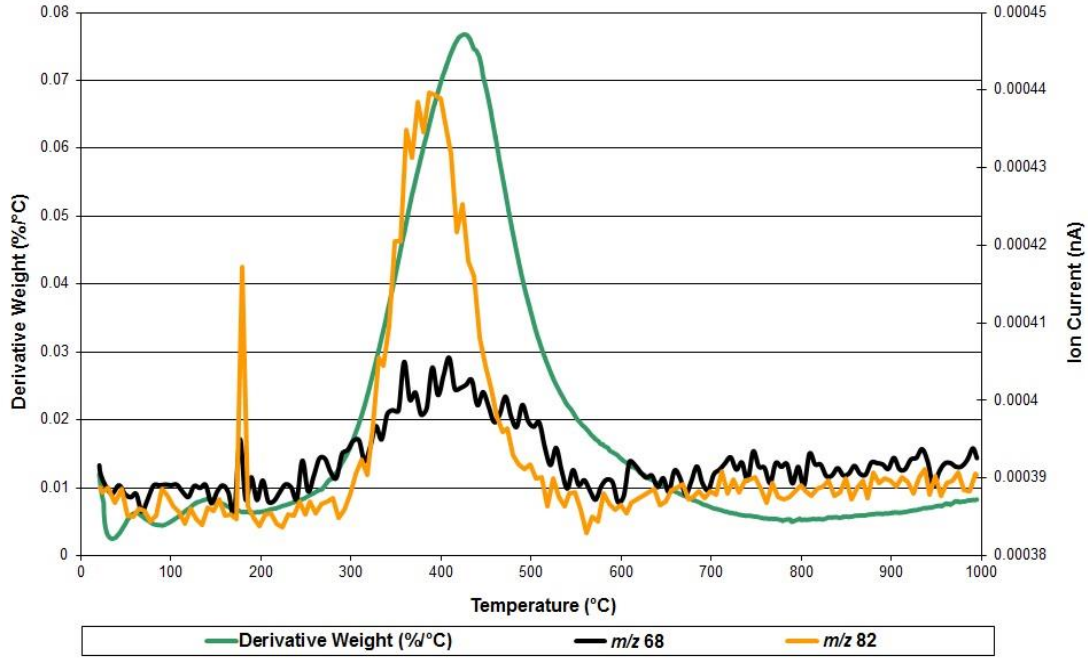

Mass spectrometry results showed peaks for *m/z* 68 and 82 characteristic of furan and 2-methyfuran respectively, suggesting that by-products are left on the

catalyst surface post-reaction. During TPD of 5% Cu + 1% CeO_x/SiO_2 only 7% of the original sample weight was lost between 200 and 600˚C with a peak at 420˚C. TPD of 5% Cu + 5% CeO_x/SiO_2 however showed an additional weight loss at 100˚C as shown in figure 4.43.

Figure 4.45 Post-reaction TPD of 5% Cu + 5% CeO_x/SiO_2

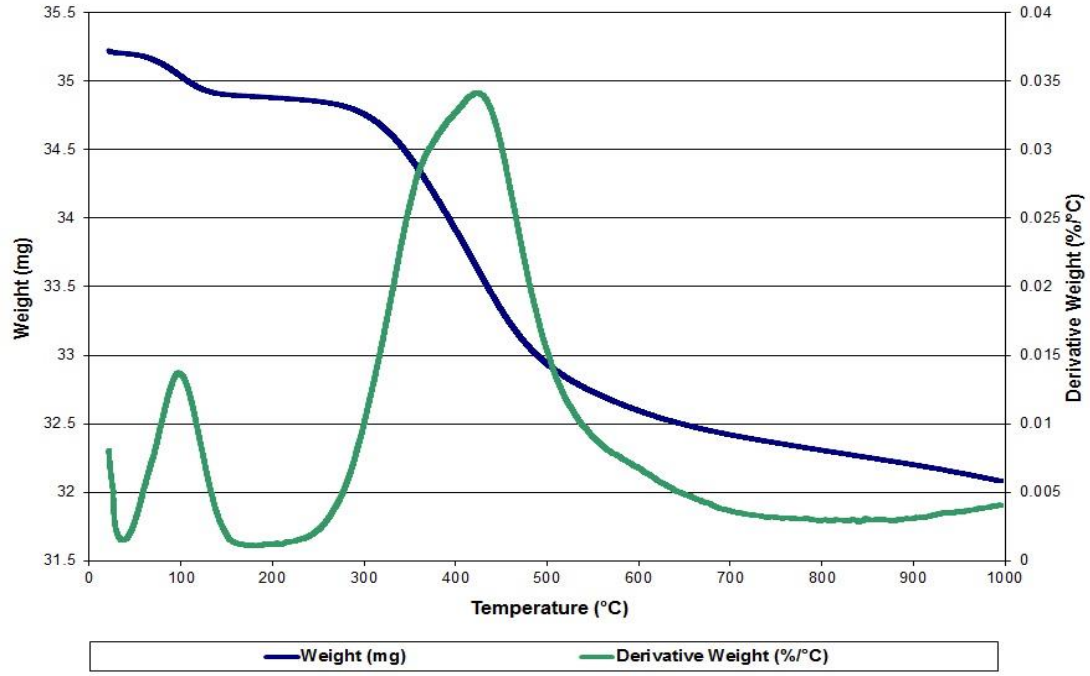

Results showed a large peak at 420 with a shoulder peak at 390˚C and almost 9% of the original sample weight was lost during TPD. Mass spectrometry results are shown in figure 4.46.

Figure 4.46 Mass spectrometry results from TPD of 5% Cu + 5% CeO_x/SiO_2

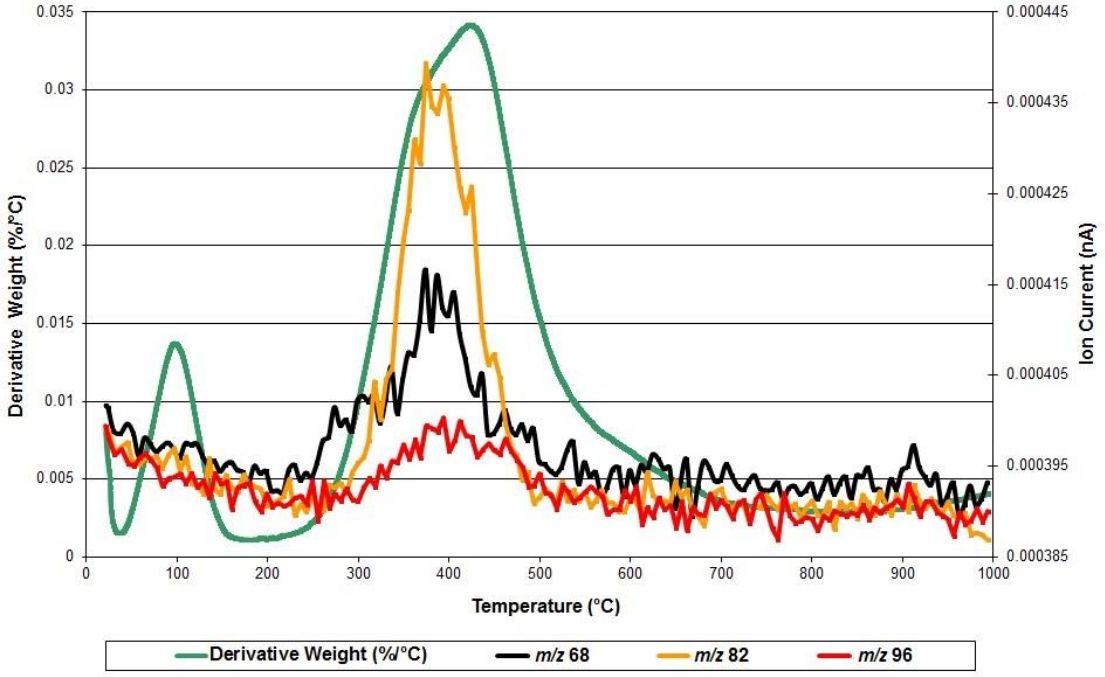

Mass spectrometry results showed evolution of *m/z* 96 corresponding to furfural, *m/z* 82 corresponding to 2-methylfuran and *m/z* 68 corresponding to furan. CO_2 was also observed at 420°C. TPD of the commercial catalyst, Cu1132, showed several weight loss peaks.

Figure 4.47 Post-reaction TPD of Cu1132

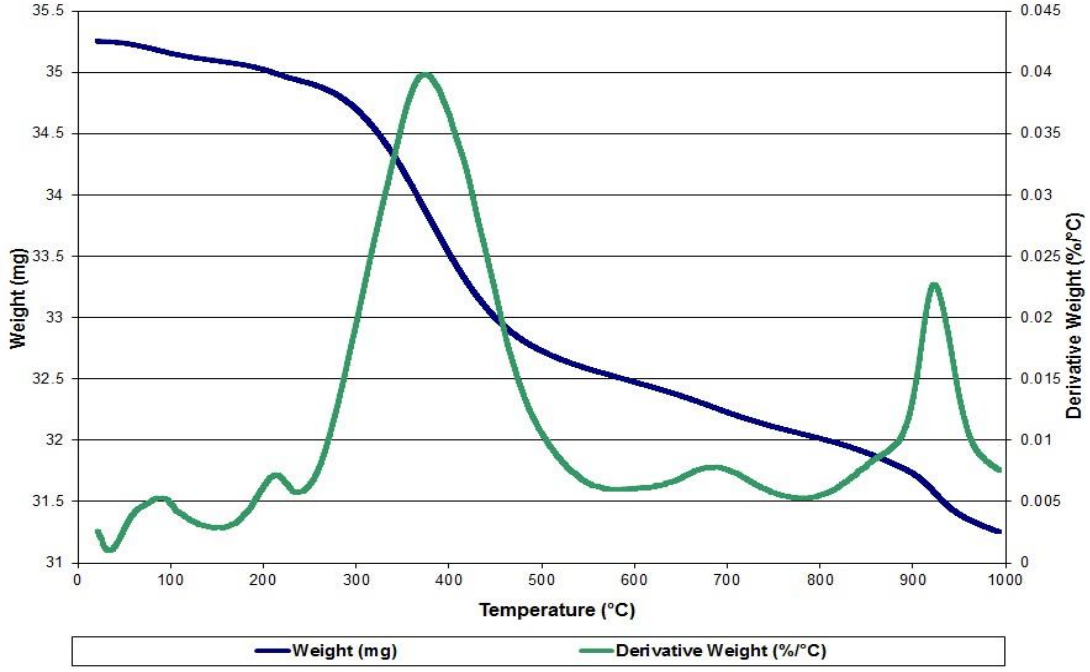

TPD of a post-reaction sample of Cu1132 lost ~11% of its original sample weight between room temperature and 800°C however most the weight was lost

between 250 and 550°C. Weight losses below 800°C were exothermic according to heat flow data, not shown here, and the weight loss at 900°C was endothermic. Mass spectrometry results showed water evolved at around 100°C and also at 450°C and CO2 evolved at 380 and 600°C.

Additionally, *m/z* 68 was evolved at 350°C corresponding to furan as well as *m/z* 41, 42, 45 and 46 which could correspond to products such as tetrahydrofuran and 2-pentanol.

Table 4.5 below shows the weight lost through post-reaction TPO and post-reaction TPD. In general, more weight was lost through post-reaction TPO compared to post-reaction TPD, the exception was Cu1132 which lost more weight through post-reaction TPD.

Table 4.5 Weight lost through post-reaction TPO and TPD

Catalyst	Weight lost (% of original sample)	
	Post-reaction TPO	Post-reaction TPD
5% Cu/SiO_2	27.3	17.6
5% CeO_x/SiO_2	14.5	n.m.[a]
5% Cu + 5% CeO_x/SiO_2	14.8	8.9
5% Cu + 1% CeO_x/SiO_2	9.6	7.5
10% Cu/SiO_2	34.3	22.0
10% Cu + 5% CeO_x/SiO_2	24.1	18.1
10% Cu+ 5% CeO_x + 0.05% Pd/SiO_2	26.0	17.6
Cu1132	8.3	11.3

[a]n.m. not measured

4.3.3 Powder X-ray diffraction

XRD was performed on post-reaction samples and the compared to patterns produced by calcined and reduced catalyst samples.

Figure 4.48 XRD patterns for pre- and post-reaction 5% Cu/SiO_2

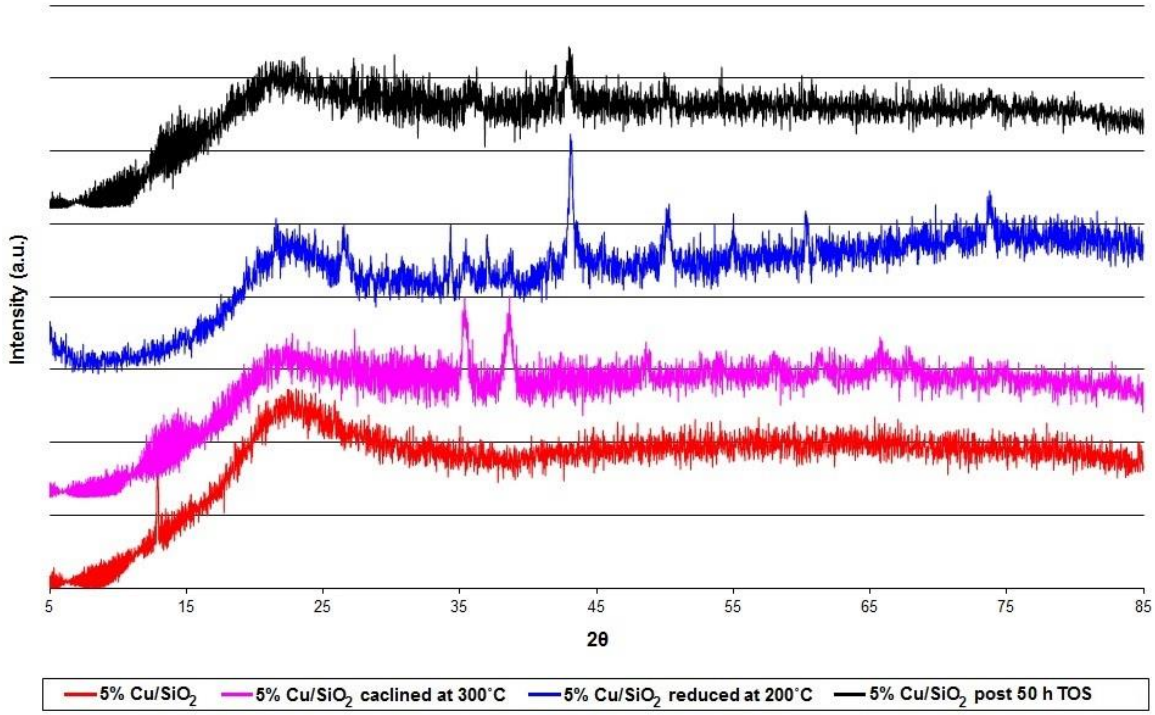

The figure shows that pre-treatment of the catalysts produces copper oxide firstly which can then be reduced to copper metal. Post-reaction the peak at 43° has a lower intensity than the reduced sample. All catalyst samples produced a similar result.

Figure 4.49 XRD patterns for pre- and post-reaction 5% Cu + 1% CeO_x/SiO_2

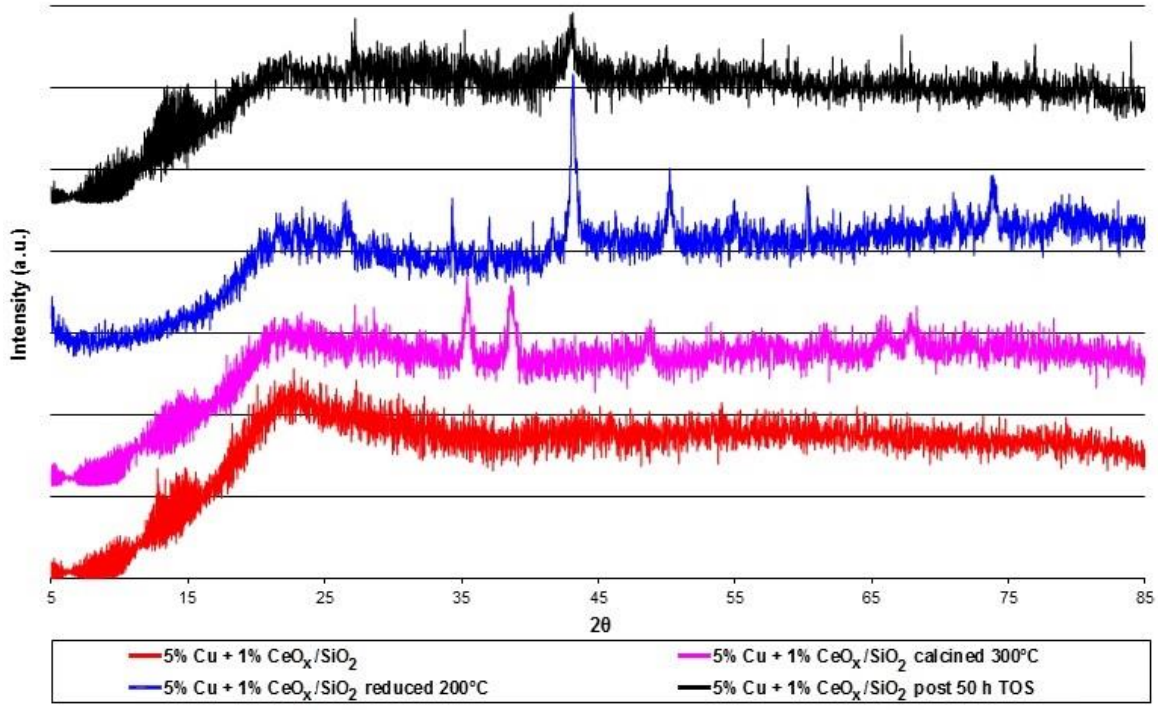

For 5% Cu + 1% CeO_x/SiO_2 a similar pattern is seen firstly for the fresh sample and for the post-reaction samples. The calcined sample however shows peaks for both copper oxide in the tenorite form and cerium oxide in the 3+ oxidation state (Ce_2O_3). Post-reaction, the peak at 43° corresponding to copper particles is less intense.

Table 4.6 Average crystallite sizes of reduced and post-reaction catalysts

Catalyst	Average crystallite size (nm)	
	Cu (reduced)	Cu (post-reaction)
5% Cu/SiO_2	18.3	11.8
5% Cu + 1% CeO_x/SiO_2	14	8.3
5% Cu + 5% CeO_x/SiO_2	40.5	172.8
10% Cu + 5% CeO_x/SiO_2	n.m.[a]	9.3
10% Cu + 5% CeO_x + 0.05% Pd/SiO_2	n.m.	7.8

[a]n.m. not measured

The results show that post-reaction samples of 5% Cu/SiO_2 and 5% Cu + 1% CeO_x/SiO_2 showed smaller copper crystallites compared to the reduced samples. This suggests that sintering is not the cause of catalyst deactivation. However the results for 5% Cu + 5% CeO_x/SiO_2 show a dramatic increase in copper crystallite size post-reaction suggesting sintering has caused catalyst deactivation.

5 Liquid-phase hydrogenation results

The results obtained from liquid-phase hydrogenation of 4-nitroacetophenone (4-NAP) are reported in this chapter.

5.1 Support only

Hydrogenation of 4-NAP was conducted over silica support to establish whether or not it had any catalytic effect on the reaction. Trace levels of 4-aminoacetophenone (4-AAP) were detected after 4 h reaction time showing that the silica did not have any significant catalytic activity for the hydrogenation of 4-nitroacetophenone.

5.2 Hydrogenation of 4-nitroacetophenone (4-NAP)

Hydrogenation of 4-NAP using each catalyst showed the conversion of 4-NAP to 4-aminoacetophenone (4-AAP) and the conversion of 4-AAP to 1-(4-aminophenyl)ethanol (4-APE) as shown in figure 5.1.

Figure 5.1 Reaction scheme for hydrogenation of 4-NAP over 2.5% Rh/SiO_2

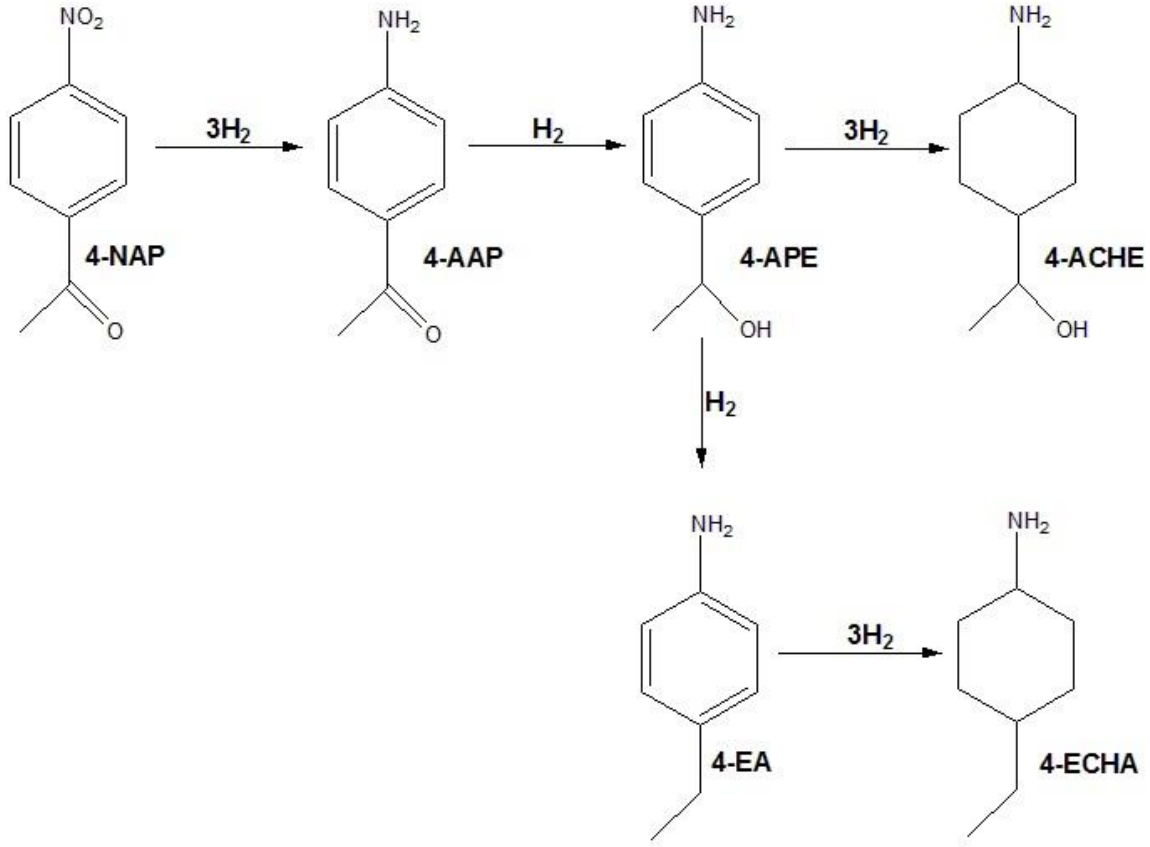

Further hydrogenation of 4-APE produced traces of 4-ethylaniline (4-EA) and hydrogenation of the aromatic ring produced low levels of 1-(4-aminocyclohexyl)ethanol (4-ACHE). Figure 5.2 shows the concentration of 4-NAP, 4-AAP and 4-APE against reaction time using catalyst M01074.

Figure 5.2 4-NAP hydrogenation over Rh/SiO_2 (M01074) at 60°C and 4 barg

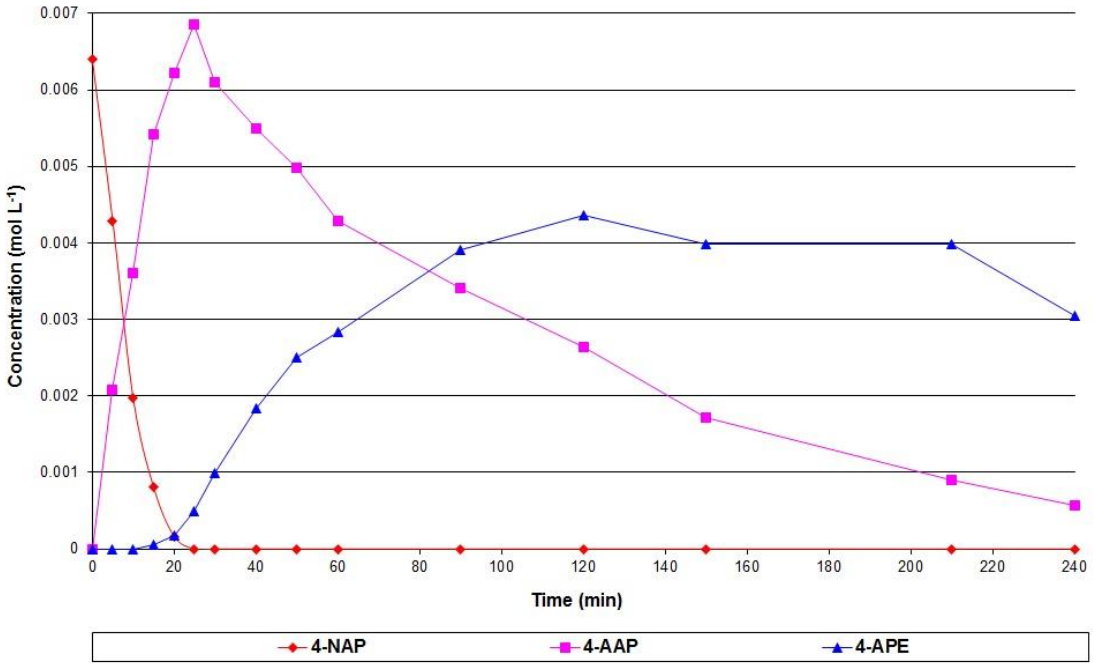

The figure shows that the subsequent hydrogenation of 4-AAP was limited until the conversion of 4-NAP was nearly complete. Similarly, although not shown here, the conversion of 4-APE to 4-ACHE and 4-EA only occurred once nearly all of the 4-AAP had been converted to 4-APE.

5.3 Effect of metal crystallite size

Reactions were carried out to investigate the effect of average crystallite size on the hydrogenation of 4-NAP. The following ~2.5% Rh/SiO_2 catalysts, shown in table 5.1, were used in hydrogenation reactions carried out at 60˚C and 4 barg.

Table 5.1 Catalysts used for liquid phase hydrogenation reactions

Catalyst code	Surface area (m^2g^{-1})	Average pore diameter (nm)	Pore volume (cm^3g^{-1})	Particle size (μm)	Average metal crystallite size (nm)
M01035	321	13.2	1.06	96.3	3.5
M01038	321	13.2	1.06	49.9	2.7
M01074	321	13.2	1.06	24	2.6
M01078	321	13.2	1.06	241	2.2
M01079	344	11.1	0.96	9.5	1.2

The catalysts had very similar metal loadings however the rates of reaction differed for each catalyst. To investigate the effect of catalyst particle size on activity, catalyst M01078 was sieved to give two particle size ranges; 450-250 μm and 125-75 μm and these were tested under the same conditions. Figure 5.3 shows the hydrogen uptake against time for the two catalyst samples.

Figure 5.3 Hydrogen uptake for catalysts with different particle sizes

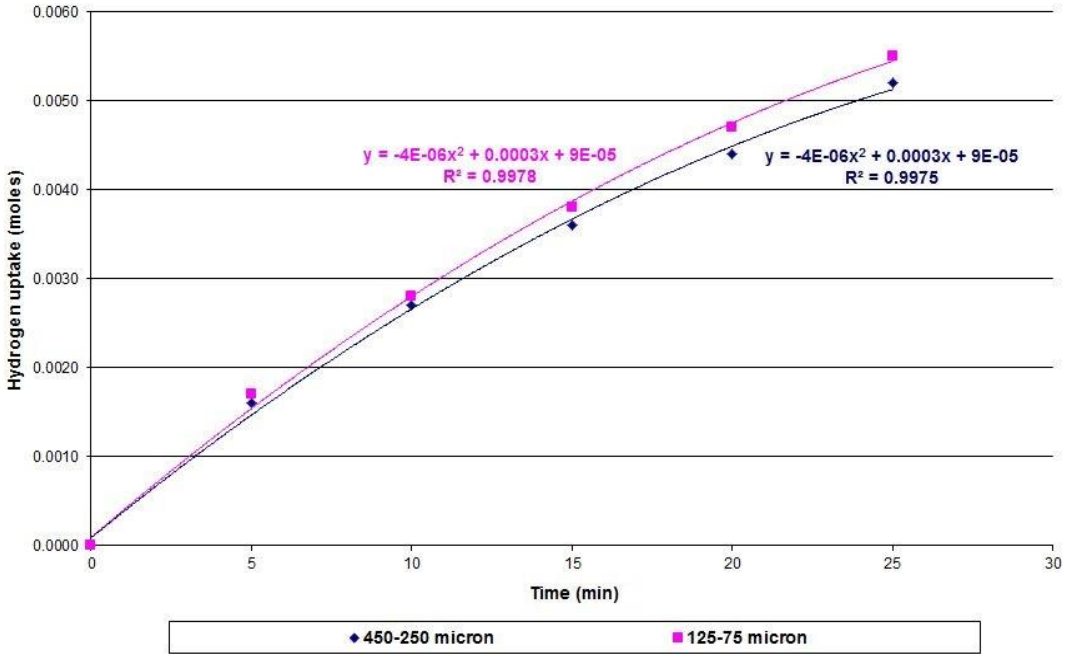

The figure shows that both catalyst samples exhibited the same level of activity suggesting that particle size does not have a significant effect on the rate of reaction. A turnover frequency (TOF) was calculated for each catalyst by dividing the rate of reaction (mol min^{-1}) by the moles of surface Rh on the catalysts. A plot of TOF against average crystallite size showed a linear relationship, shown in figure 5.4.

Figure 5.4 TOF versus crystallite size

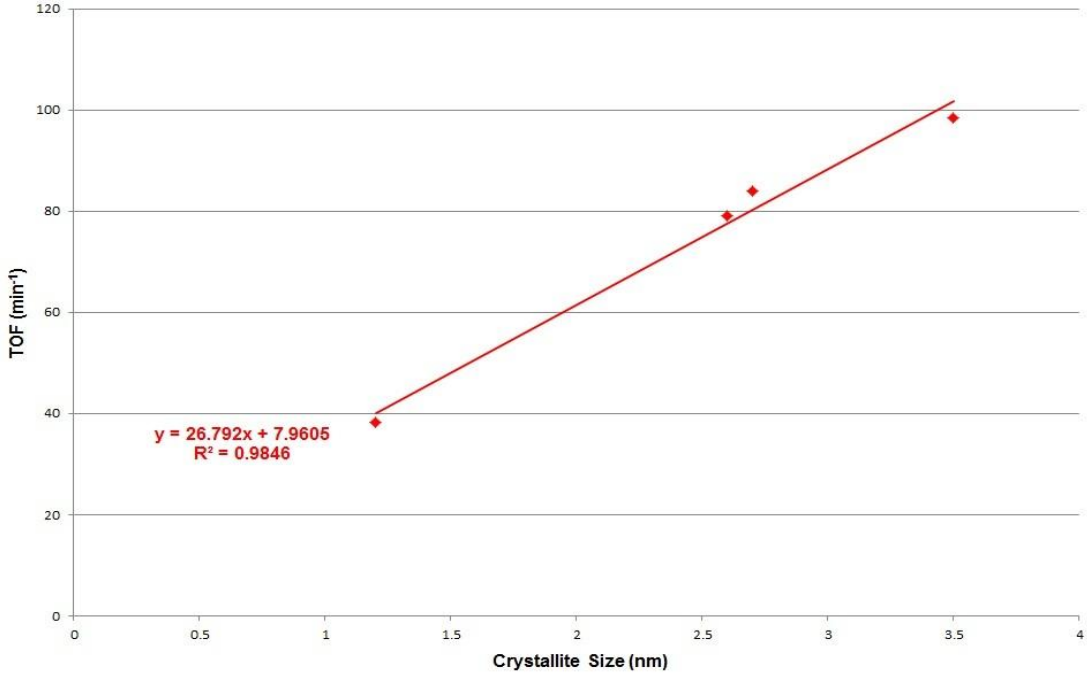

The graph shows a linear relationship between TOF and crystallite size and that the activity of the catalyst for the given reaction increases with crystallite size.

Catalyst M01079 was used for all further hydrogenation reactions as it exhibited the fastest conversion of 4-NAP and complete conversion of 4-AAP as shown in figure 5.5.

Figure 5.5 4-AAP concentration against time

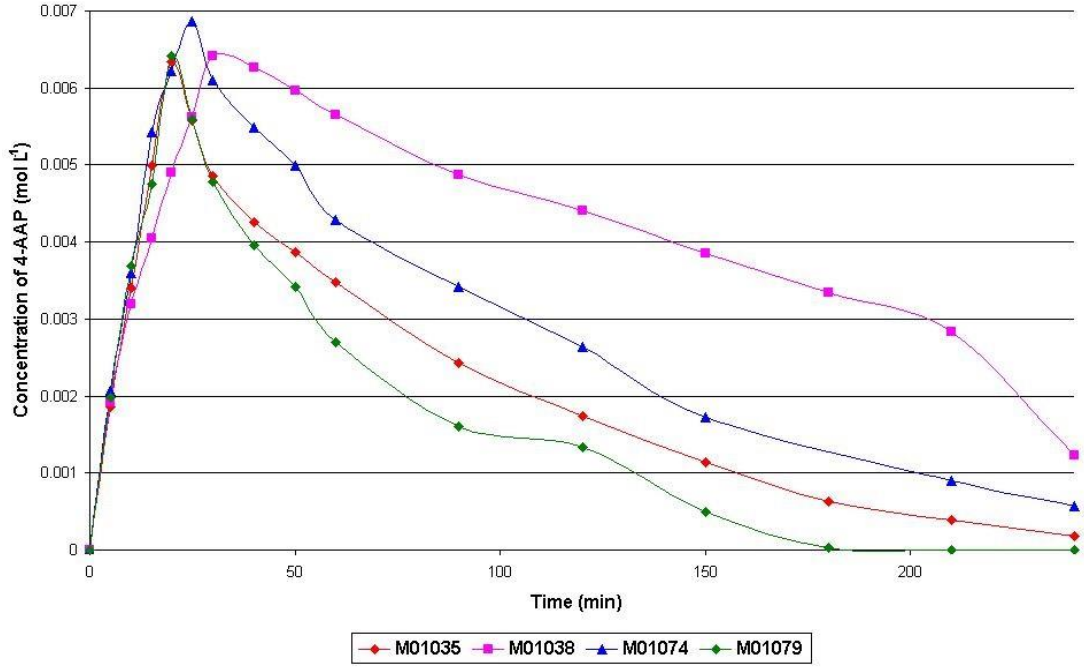

Using this catalyst allowed observation of further hydrogenation products such as 1-(4-aminocyclohexyl)ethanol (4-ACHE) and 4-ethylaniline (4-EA).

5.4 4-NAP reactions

Reactions using catalyst M01079 were conducted to investigate the effect of temperature and pressure on the rate of hydrogenation of 4-nitroacetophenone (4-NAP). Reactions were carried out over the temperature range 30-60°C at 4 barg and at 60°C using pressures between 2-5 barg. From these reactions, an activation energy and order of reaction with respect to hydrogen pressure were calculated.

5.4.1 Effect of temperature on 4-NAP hydrogenation

Reactions were conducted at 4 barg and temperatures of 30-60°C and the rate of hydrogenation increased with increasing temperature as shown in figure 5.6.

Figure 5.6 4-NAP concentration against time at different temperatures

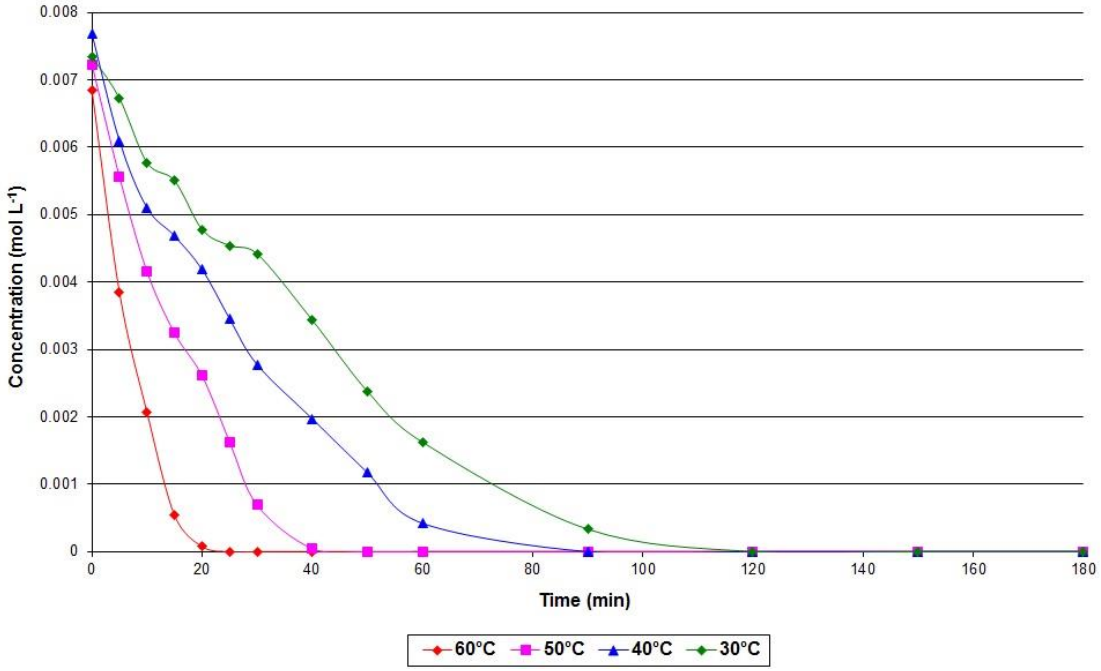

As hydrogen is supplied to the reaction in excess, pseudo first order kinetics may be used to determine the rate of reaction as this is dependent on the concentration of 4-NAP.

For a first order reaction the rate law is $-d[A]/dt = k.dt$, and so the integrated rate law can have the following form: $-\ln([A]/[A]_0) = k.t$ or $\ln([A]_0/[A]) = k.t$, so a plot of $\ln([A]_0/[A])$ against time will produce a linear plot with gradient equal to k. Figure 5.7 shows plots of $\ln([4\text{-NAP}]_0/[4\text{-NAP}])$ against time for each reaction temperature.

Figure 5.7 Determining rate constants for 4-NAP hydrogenation

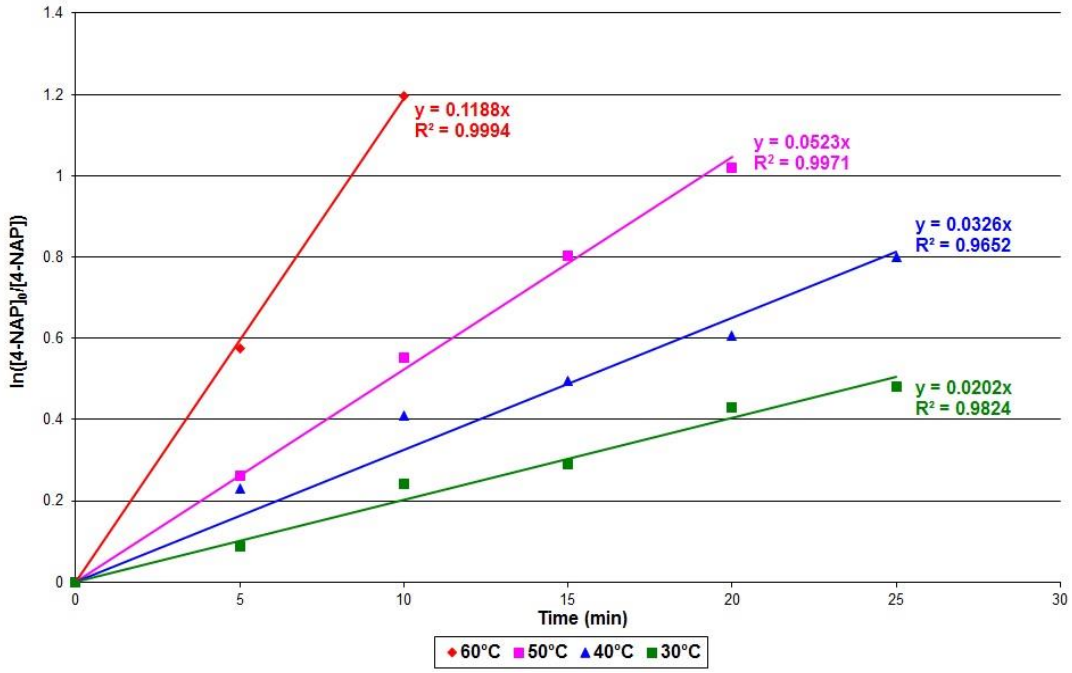

The activation energy was calculated using the Arrhenius equation shown below:

$$k = Ae^{-E_a/(RT)}$$

Where k = rate constant

A = pre-exponential factor

E_a = activation energy

R = ideal gas constant (8.314 J K^{-1} mol^{-1})

T = temperature (K)

Taking the natural logarithm of the Arrhenius equation yields:

$$\ln(k) = \frac{-E_a}{RT} + \ln(A)$$

So an Arrhenius plot of ln(k) against 1/T will give a straight Line with a gradient equal to E_a/R, where R is the ideal gas constant and E_a is the activation energy of the reaction.

Figure 5.8 Activation energy for 4-NAP hydrogenation

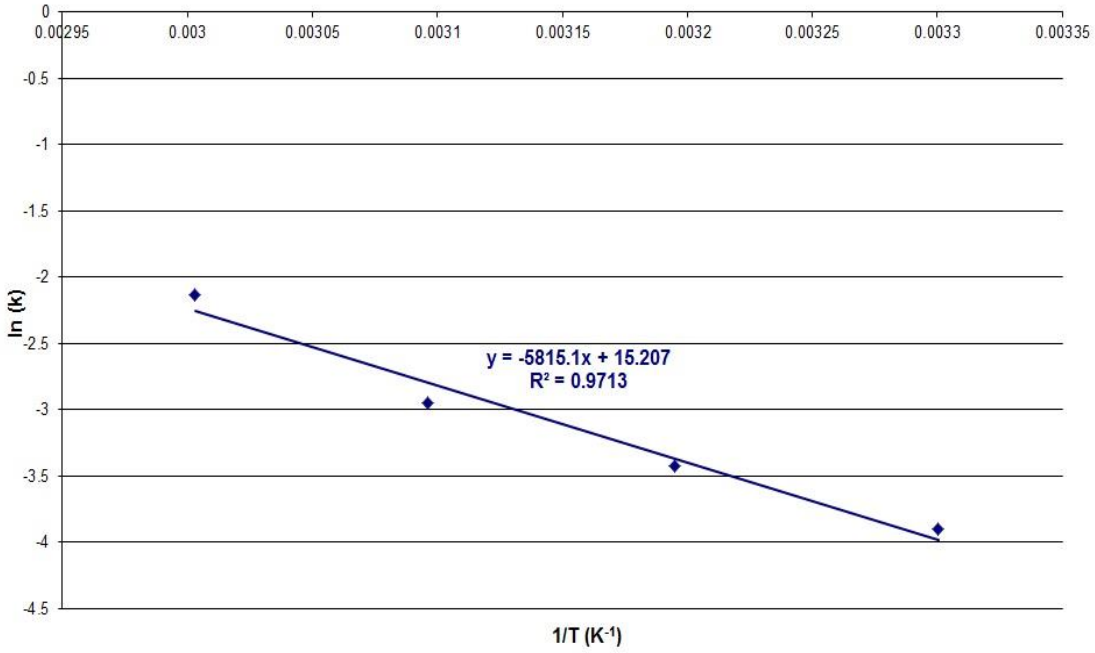

From this gradient the activation energy for hydrogenation of 4-NAP was calculated to be 50 ± 4 kJ mol^{-1}.

It was possible to calculate a first order rate constant for the hydrogenation of 4-AAP once all of the 4-NAP had reacted and then to use these values to calculate an activation energy for 4-AAP hydrogenation. Calculated in this way an activation energy of 61 ± 6 kJ mol^{-1} was determined.

5.4.2 Effect of 4-NAP concentration on 4-NAP hydrogenation

In addition, reactions were carried out using different initial concentrations of 4-NAP to investigate its effect on the rate of hydrogenation and to determine an order of reaction with respect to reactant concentration. Reactions were carried out using initial concentrations of 0.0062, 0.0031 and 0.0047 mol L^{-1} of 4-NAP and a rate of reaction determined by the rate of disappearance of 4-NAP against time.

The initial concentration of 4-NAP did not have a significant effect on the rate of reaction and therefore a zero order of dependence with respect to 4-NAP concentration was determined.

5.4.3 Effect of pressure on 4-NAP hydrogenation

Reactions were carried out at 40°C and 1-5 barg to determine the effect of hydrogen pressure on the hydrogenation of 4-NAP. The rates of hydrogenation of 4-NAP and of 4-AAP once all of the 4-NAP had been converted are shown in table 5.2.

Table 5.2 Rate of hydrogenation at different reaction pressures

P (barg)	Rate of 4-NAP hydrogenation (mol L^{-1} min^{-1} g^{-1})	Rate of 4-AAP hydrogenation (mol L^{-1} min^{-1} g^{-1})
1	2.9×10^{-3}	5×10^{-4}
2	7.2×10^{-3}	1.2×10^{-3}
3	9.9×10^{-3}	1.8×10^{-3}
4	1.5×10^{-2}	2.4×10^{-3}
5	n.m.[a]	3.7×10^{-3}

[a]n.m. not measured

The initial rate of the reaction was measured over the first few min because in the early stages of the reaction the concentration of reactants was known before they were quickly converted to products. If the elementary reaction between 4-NAP and hydrogen is considered then the rate equation can be written in the form:

$$\textbf{Rate} = k[\text{4-NAP}]^x[H_2]^y$$

where x is equal to the order of reaction with respect to [4-NAP] and y is the order of reaction with respect to $[H_2]$. However, in the previous section a zero order dependence was determined, i.e. x = 0, with respect to [4-NAP]. Therefore the rate equation may be expressed in the following way: Rate = $k[H_2]^y$ or $\ln(\text{rate}) = \ln(k) + y \ln[H_2]$.

The ideal gas equation can be used to explain the relationship between the concentration and pressure of an ideal gas in the following way.

The ideal gas equation, PV = nRT where P is the pressure, V the volume, n is the number of moles of gas, R the ideal gas constant and T is the absolute temperature may also be expressed:

$$P = nRT/V$$

where n/V is equal to concentration therefore the pressure is directly proportional to concentration. This means that ln(rate) = ln(k) + y ln[H_2] can be expressed: ln(rate) = ln(k) + y ln(P), where P is equal to the hydrogen pressure, and a plot of ln(rate) vs. ln(P) will produce a Linear relationship with gradient equal to the order of reaction, y. In this case, a first order of reaction was determined with respect to hydrogen pressure of 1.1 ± 0.1.

5.4.4 Second addition of 4-NAP

To investigate the whether there was any deactivation during use of the catalyst, a second measure of 4-NAP was added to the reaction mixture after 3 h reaction time. Figure 5.9 shows the concentration of the reactants and products over 6 h reaction time.

Figure 5.9 Second addition of 4-NAP

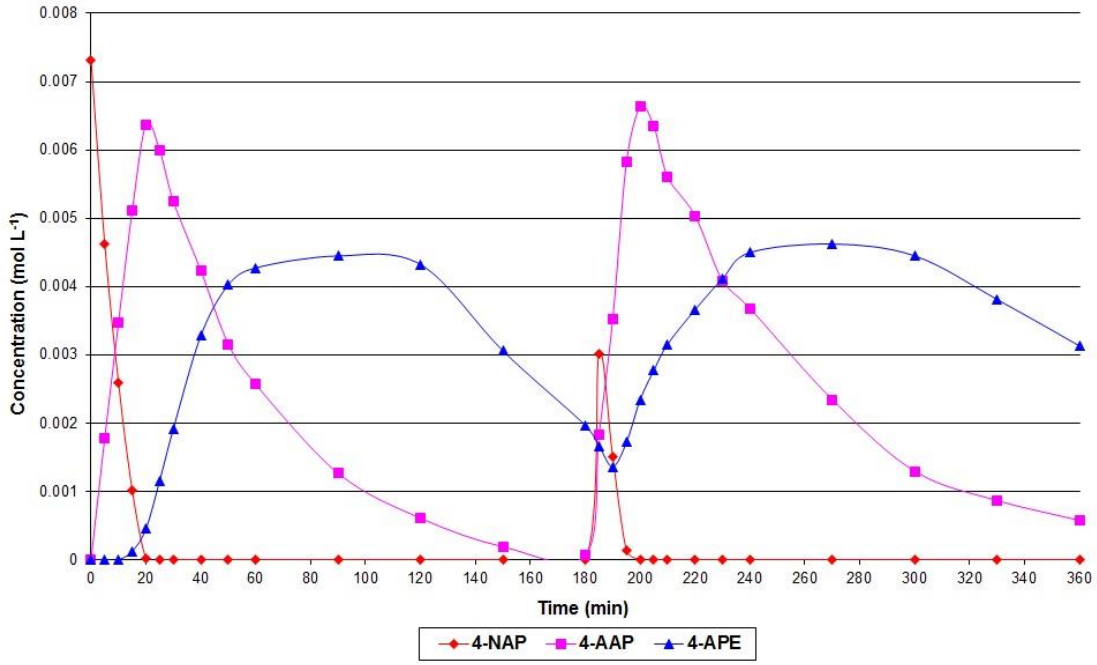

The graph shows that after a second addition of 4-NAP, the catalyst exhibited a similar activity and the same competitive hydrogenation is observed. The

second addition of 4-NAP must be hydrogenated to 4-AAP before the carbonyl hydrogenation will occur to produce the alcohol product. Although the concentration of second addition of 4-NAP was the same as the first, the initial 4-NAP measurement is much less than expected. The reason for this is thought to be because of the time it takes to add a second solution to the reactor it has quickly hydrogenated to 4-AAP by the time a sample is taken. The rate of hydrogenation of 4-NAP was comparable after each addition suggesting that the activity of the catalyst was maintained and the catalyst can be recycled.

5.5 4-AAP reactions

Reactions were conducted to investigate the effect of temperature on the rate of hydrogenation of 4-aminoacetophenone (4-AAP). A typical reaction profile is shown in figure 5.10. It shows the hydrogenation of 4-AAP to 4-APE and then to 4-ACHE with only trace levels of 4-EA produced.

Figure 5.10 Hydrogenation of 4-AAP at 60°C and 4 barg

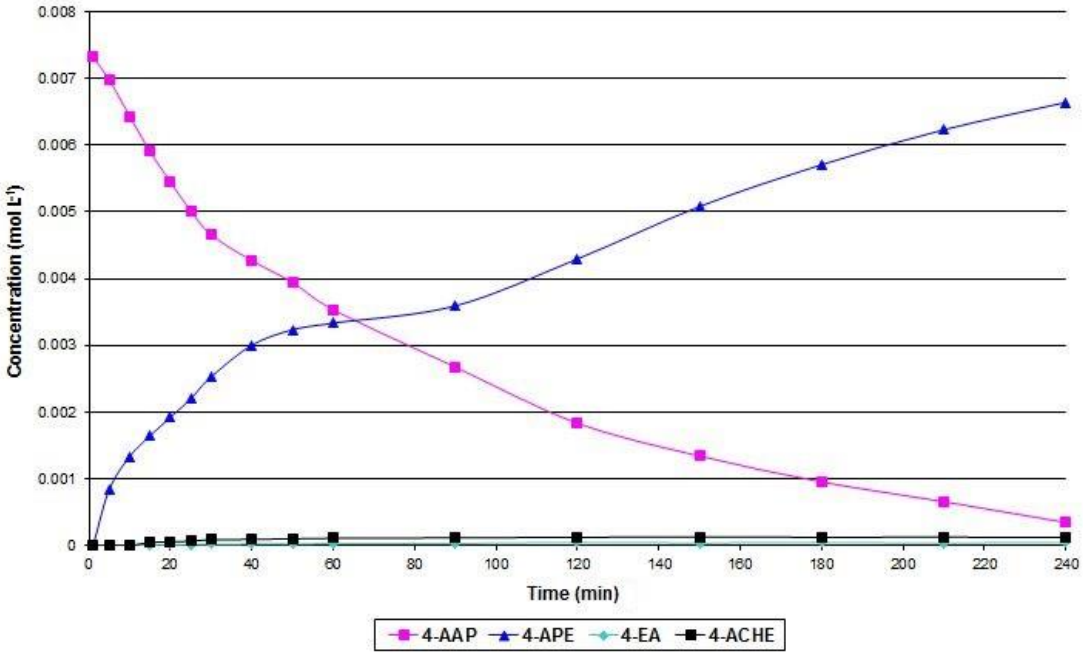

Reactions were carried over the temperature range 30-60°C at 4 barg and results were used to calculate the activation energy for the reaction. The method described in 5.4.1 was used to determine rate constants for 4-AAP hydrogenation at each temperature and the results are shown in figure 5.11.

Figure 5.11 Determining rate constants for 4-AAP hydrogenation

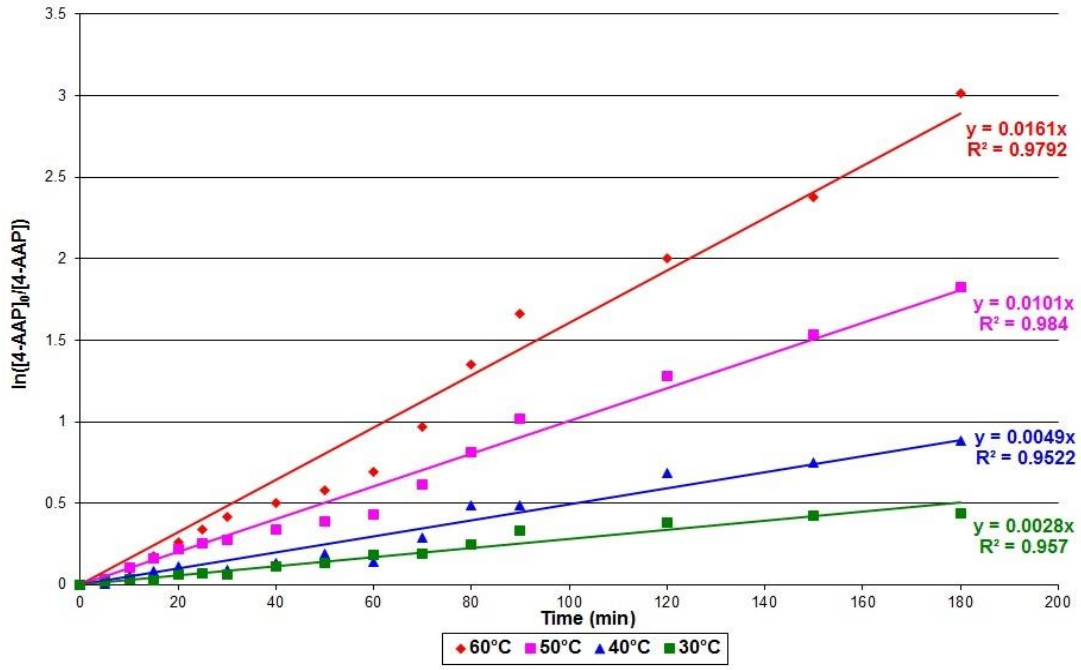

These rate constants, k, were then used to determine an activation energy for the hydrogenation of 4-AAP alone. The activation energy for the hydrogenation of 4-AAP alone was calculated to be 48 ± 2 kJ mol^{-1} which is much lower than the activation energy determined for 4-AAP hydrogenation following 4-NAP hydrogenation (61 kJ mol^{-1}). This suggests that the presence of 4-NAP affects the activation energy for 4-AAP hydrogenation.

5.6 4-NAP and 4-AAP reactions

To investigate the effect of the presence of 4-AAP intermediate on the rate of hydrogenation of 4-NAP, reactions were conducted at 60˚C and 4 barg using 1:1, 2:1 and 1:2 molar ratios of 4-NAP:4-AAP as reactant. The concentration of 4-NAP remained constant at 0.062 mol L^{-1}; the same concentration used in single reactant reactions, and the concentration of 4-AAP reactant varied to achieve different molar ratios. Figure 5.12 shows the distribution of products against time for hydrogenation of 4-NAP.

Figure 5.12 Hydrogenation of 4-NAP using M01079 catalyst at 60˚C and 4 barg

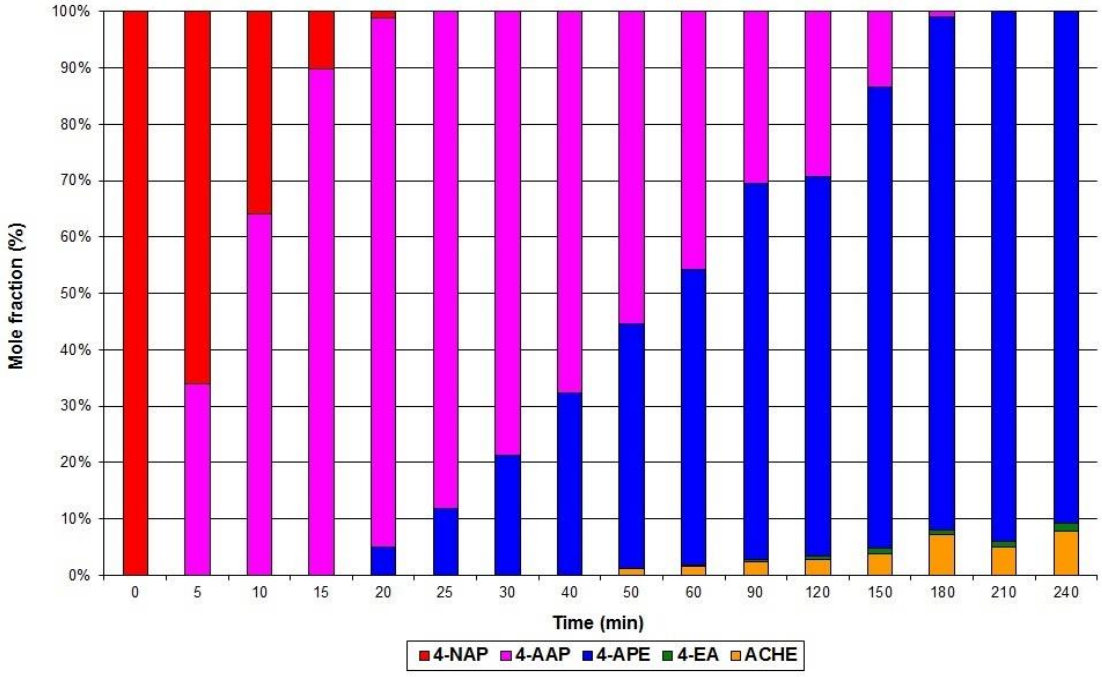

After 5 min, almost 35% of the 4-NAP present at the beginning of the reaction (0.0062 mol L^{-1}) has been converted to 4-AAP and by 20 min almost all of the 4-NAP present has been converted to 4-AAP. After 240 min all of the 4-AAP has been converted to 4-APE and 9% of the 4-APE produced has been further hydrogenated to 4-EA (1.5%) and 4-ACHE (7.5%). When a 2:1 molar ratio of 4-NAP:4-AAP is used, there is a difference in the rate of conversion as shown in figure 5.13.

Figure 5.13 Hydrogenation of 2:1 molar ratio 4-NAP:4-AAP

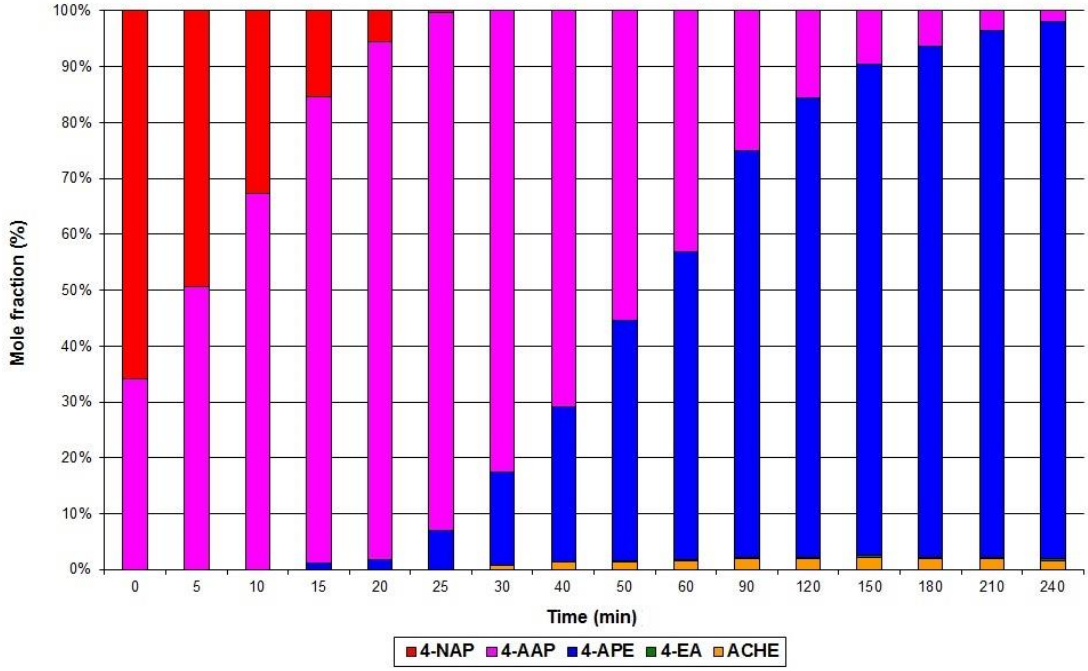

At time zero there is ~33% 4-AAP and ~66% 4-NAP present as they were added in this ratio as reactants. After 5 min, only 15% of the 4-NAP present at the beginning of the reaction has been converted to 4-AAP and it takes 25 min to convert 0.062 mol L^{-1} 4-NAP when 0.0031 mol L^{-1} 4-AAP is present at the beginning of the reaction. Conversion of 4-AAP to 4-APE begins at 15 min and is slow until all of the 4-NAP has been converted to 4-AAP. After 240 min only 2% of 4-APE had been hydrogenated to 4-EA and 4-ACHE combined which shows that the presence of 4-AAP at the beginning of the reaction has reduced the overall yield of final hydrogenation products. Figure 5.14 shows the concentration of 4-NAP and 4-AAP against time for the hydrogenation of 4-NAP alone and molar equivalents of 4-NAP and 4-AAP.

Figure 5.14 Hydrogenation of 1:1 molar ratio 4-NAP:4-AAP

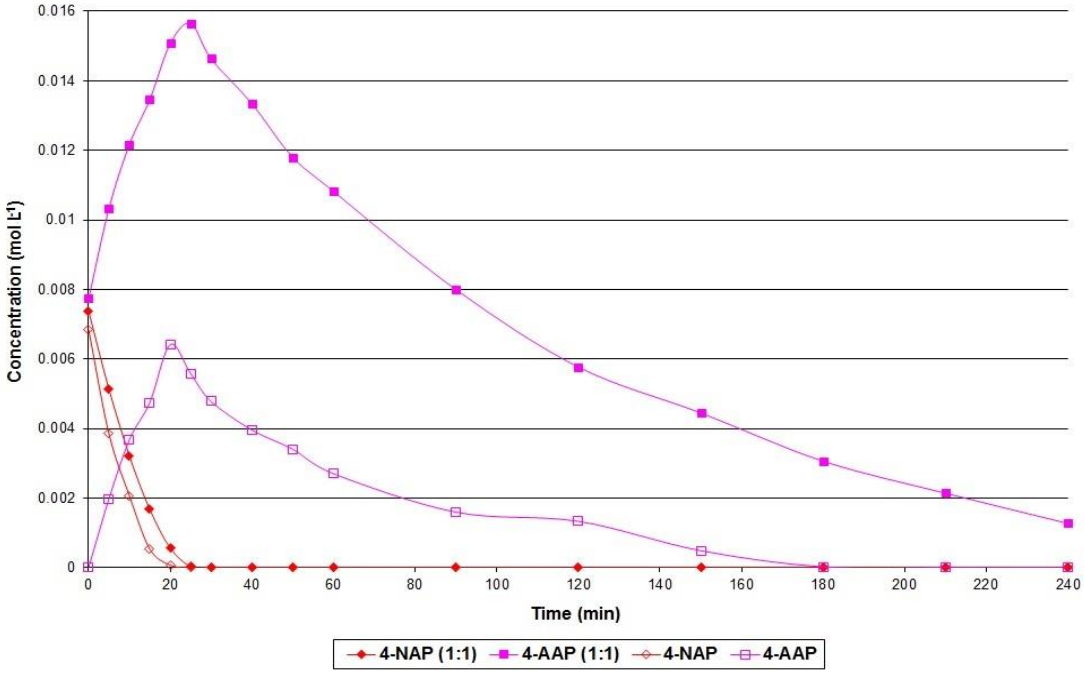

With a 1:1 molar ratio of 4-NAP:4-AAP the conversion of 4-NAP to 4-AAP is much slower than the reaction of only 4-NAP. Rate constants were calculated for 4-NAP hydrogenation and for 4-AAP hydrogenation at different molar ratios of reactants. Overall the rate of hydrogenation of 4-NAP was slightly slower when 4-AAP was present but this was independent of the concentration of 4-AAP present. The rate of hydrogenation of 4-AAP however varied depending on the concentration of 4-AAP present relative to the 4-NAP present at the beginning of the reaction. Figure 5.15 shows the rate constants calculated for 4-AAP

hydrogenation at relative molar equivalents of 4-NAP, i.e. 4-NAP concentration constant for all reactions so 4-AAP × 0.5 indicates a 2:1 molar ratio 4-NAP:4-AAP.

Figure 5.15 Determination of rate constants for 4-AAP hydrogenation

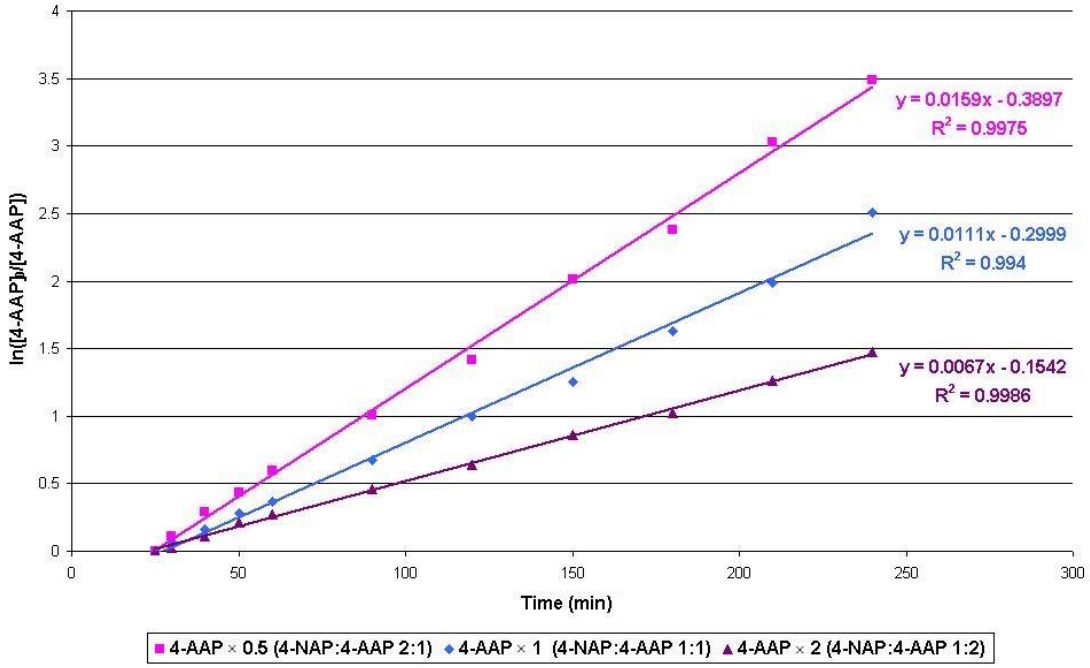

The graph shows that as the concentration of 4-AAP present as reactant increases the overall rate of hydrogenation of 4-AAP decreases suggesting a negative order of reaction.

5.7 Addition of an alicyclic amine

To investigate the effect of the presence of an alicyclic amine on the hydrogenation of 4-NAP and 4-AAP, both were independently hydrogenated with 4-methylcyclohexylamine (4-MCHA) present in a 1:1 molar ratio. The 4-MCHA did not react under the reaction conditions used and its concentration remained constant throughout the reaction. Figure 5.16 shows the hydrogenation of 4-NAP in the presence of a molar equivalent of 4-MCHA at 60˚C and 4 barg.

Figure 5.16 Hydrogenation of 1:1 4-NAP : 4-MCHA

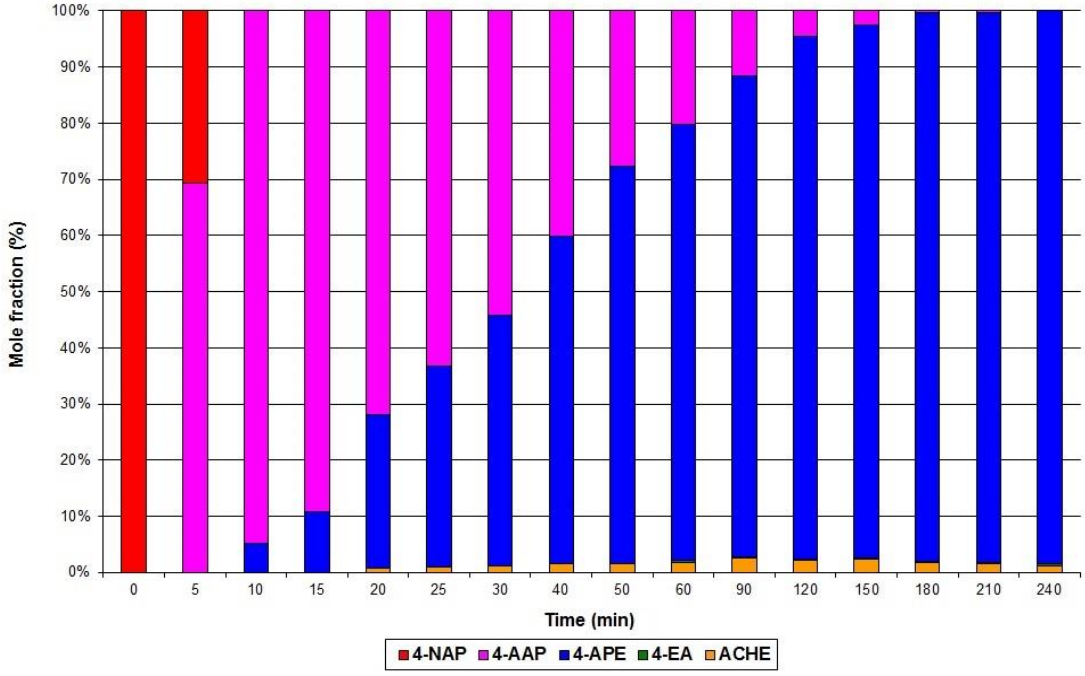

Figure 5.12 showed the hydrogenation of 4-NAP alone and in that reaction all of the 4-NAP was converted to 4-AAP after 20 min. Figure 5.16 shows that the introduction of 4-MCHA promoted the hydrogenation of 4-NAP with 100% conversion achieved after 10 min. Figure 5.17 shows increasing the concentration of 4-MCHA present increases the rate of hydrogenation of 4-NAP.

Figure 5.17 1:2 4-NAP : 4-MCHA

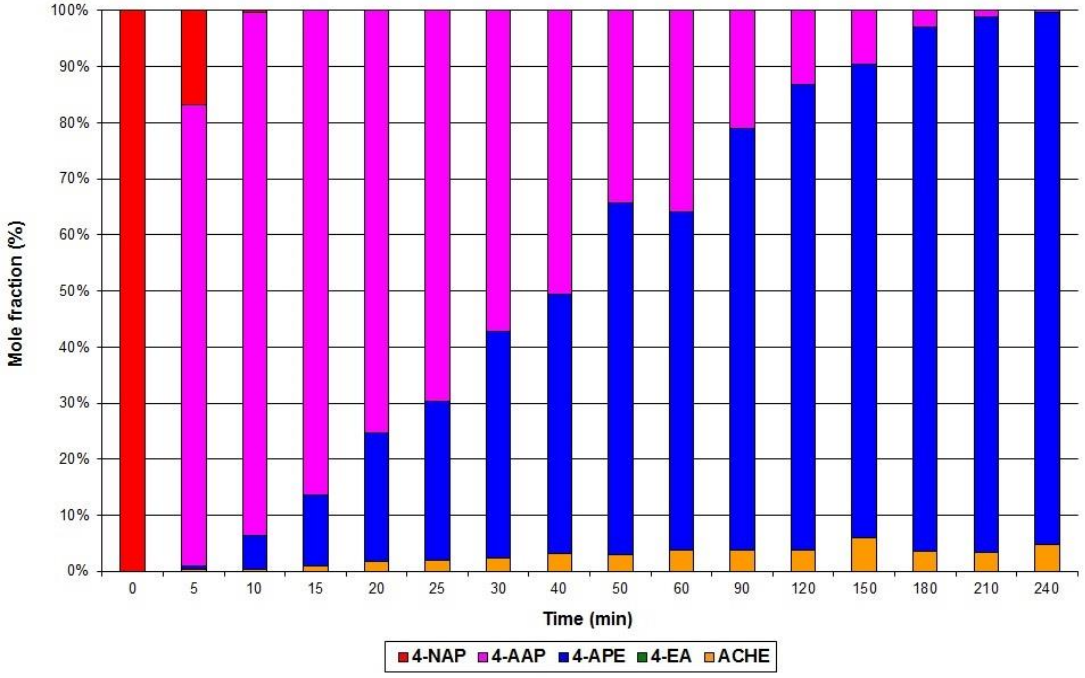

A 2:1 molar ratio of 4-MCHA:4-NAP promotes the conversion of 4-NAP to 4-AAP, and subsequently the hydrogenation 4-AAP to 4-APE. Table 5.3 shows the calculated rate constants for both hydrogenation of 4-NAP and 4-AAP after 4-NAP with and without 4-MCHA present as a reactant.

Table 5.3 Rate constants for hydrogenation of 4-NAP and 4-NAP with 4-MCHA

Reactants present	Rate constant (min^{-1})	
	4-NAP hydrogenation	**4-AAP hydrogenation**
4-NAP	1.51×10^{-1}	1.95×10^{-2}
4-NAP and 4-MCHA (1:1)	2.63×10^{-1}	2.67×10^{-2}
4-NAP and 4-MCHA (1:2)	4.06×10^{-1}	2.18×10^{-2}

The results show that the addition of 4-MCHA has a greater influence on the rate of 4-NAP hydrogenation than on 4-AAP hydrogenation after the 4-NAP had been converted.

Reactions were carried out using different molar ratios of 4-AAP:4-MCHA to determine if the presence of an alicyclic amine has an effect on the intermediate hydrogenation. Figure 5.18 shows the hydrogenation of 4-AAP alone at 60˚C and 4 barg.

Figure 5.18 Hydrogenation of 4-AAP using M01079 catalyst at 60˚C and 4 barg

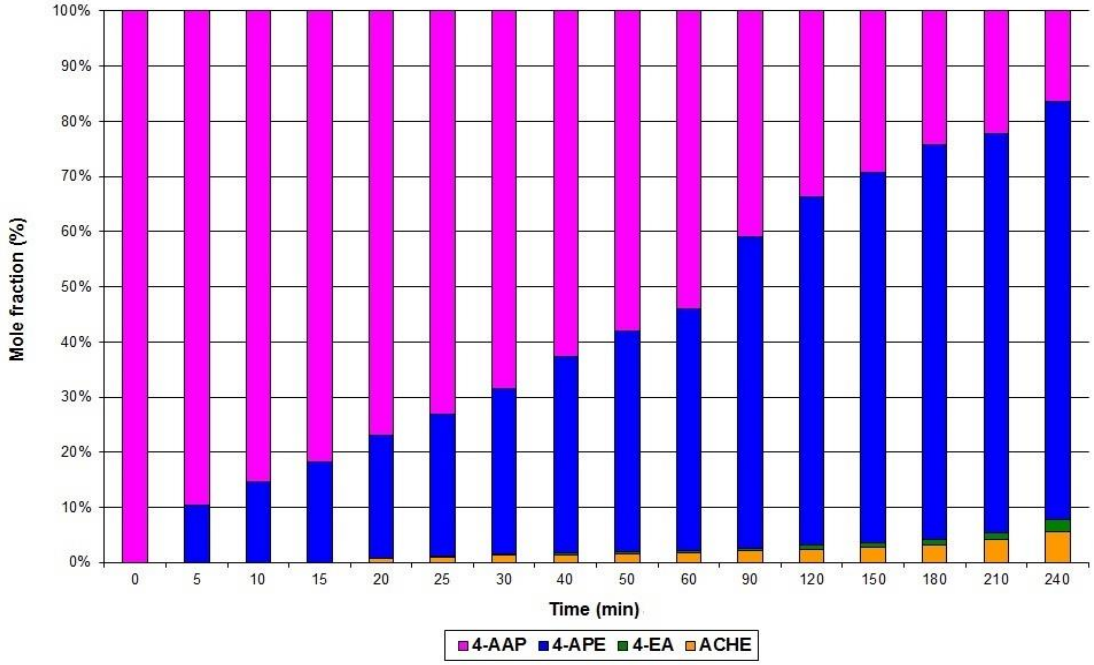

Hydrogenation of 4-AAP is much slower than the hydrogenation of 4-NAP under these conditions. After 5 min only 10% 4-AAP was converted to 4-APE. Hydrogenation of 4-APE to 4-ACHE and 4-EA began after 20 min but by 240 min reaction time, less than 10% 4-APE had been hydrogenated to 4-ACHE and 4-EA. The presence of a molar equivalent of 4-MCHA affected the rate of hydrogenation of 4-AAP, as shown in figure 5.19.

Figure 5.19 Hydrogenation of 1:1 4-AAP:4-MCHA

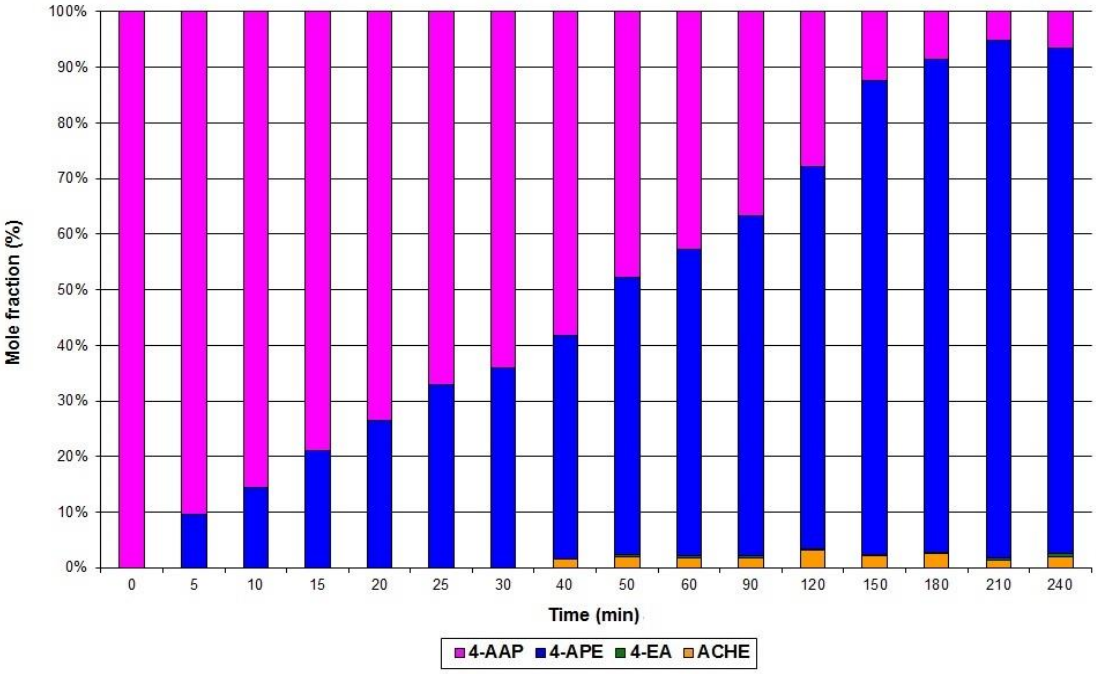

In the early stages of the reaction there appears to be little difference due to the presence of 4-MCHA however, after 20 min an enhancement in rate is apparent. For the hydrogenation of 4-AAP without 4-MCHA, the conversion at 30 min was ~32% and in the presence of 4-MCHA this was increased to 36% and at 180 min the conversion without 4-MCHA was 76% but with 4-MCHA it was 91%. Rate constants were calculated for the hydrogenation of 4-AAP with and without 4-MCHA.

Table 5.4 Rate constants for hydrogenation of 4-AAP and 4-AAP with 4-MCHA

Reactants present	Rate constant (min^{-1})
4-AAP	1.16×10^{-2}
4-AAP and 4-MCHA (1:1)	2.09×10^{-2}
4-AAP and 4-MCHA (1:2)	1.79×10^{-2}

5.8 Deuterium reactions

Reactions using deuterium were carried out to investigate the role of hydrogen in the rate determining step. Three reactions were carried out at 60˚C and 4 barg using 2.7 mmol of 4-NAP, 2.7 mmol 4-AAP and finally 2.7 mmol of each to give a 1:1 ratio. The rate of hydrogenation of 4-NAP was much slower when deuterium was employed as shown in figure 5.20.

Figure 5.20 4-NAP reaction with hydrogen and deuterium

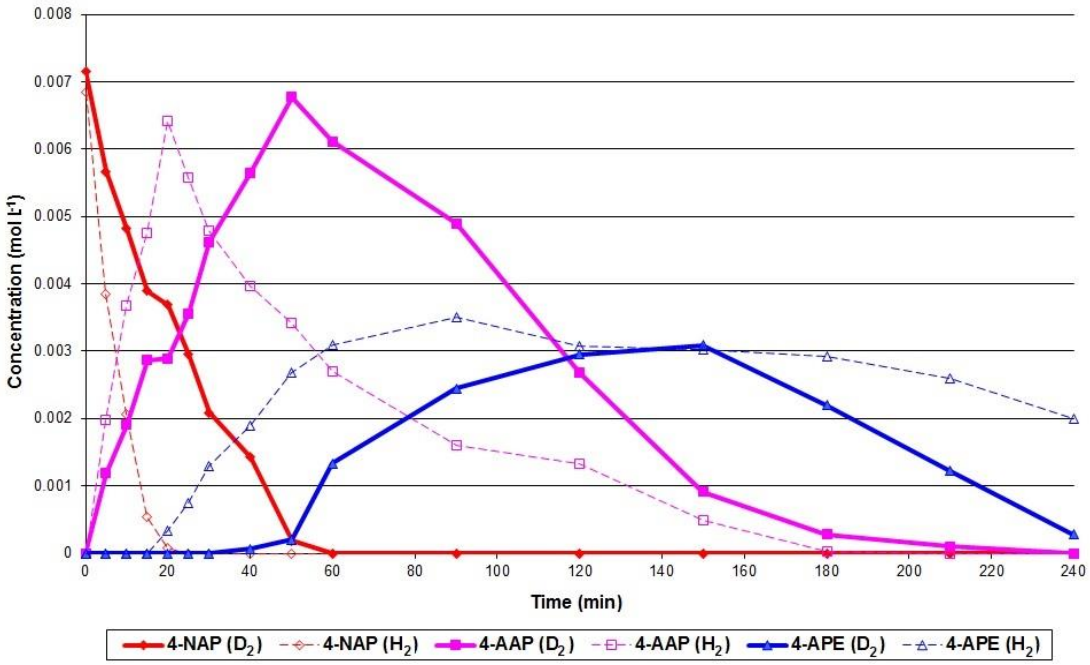

Under hydrogen, complete conversion of 4-NAP to 4-AAP took about 20 min however, complete conversion of 4-NAP under deuterium took thrice as long. A first order rate constant was calculated for the reaction of 4-NAP with hydrogen and deuterium respectively by plotting the change in concentration of 4-NAP as shown in figure 5.21.

Figure 5.21 Rate constants for 4-NAP under H_2 and D_2

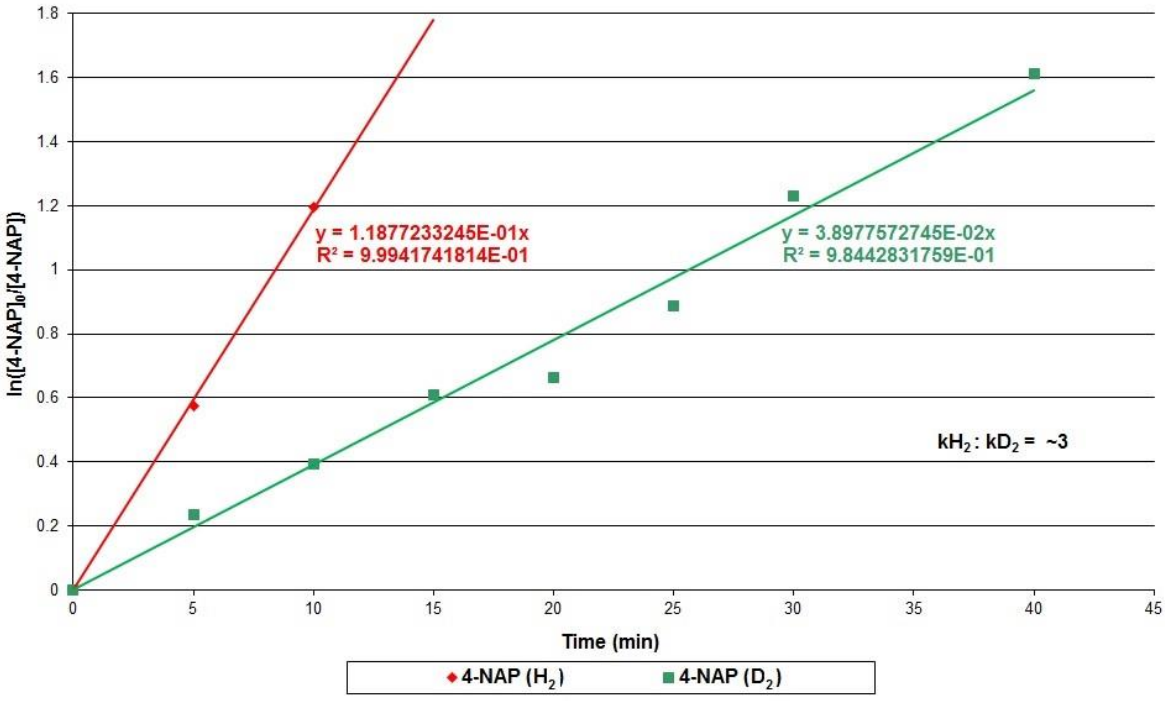

Reaction of 4-AAP with deuterium was carried out and the first order rate constants plotted as above. A primary kinetic isotope effect (KIE) of ~3 was observed for the hydrogenation of 4-NAP. Rate constants were also calculated for the hydrogenation of 4-AAP once all of the 4-NAP had been converted. Figure 5.22 shows the rate of hydrogenation of 4-AAP under hydrogenation and deuterium.

Figure 5.22 Rate constants for 4-AAP after 4-NAP under H_2 and D_2

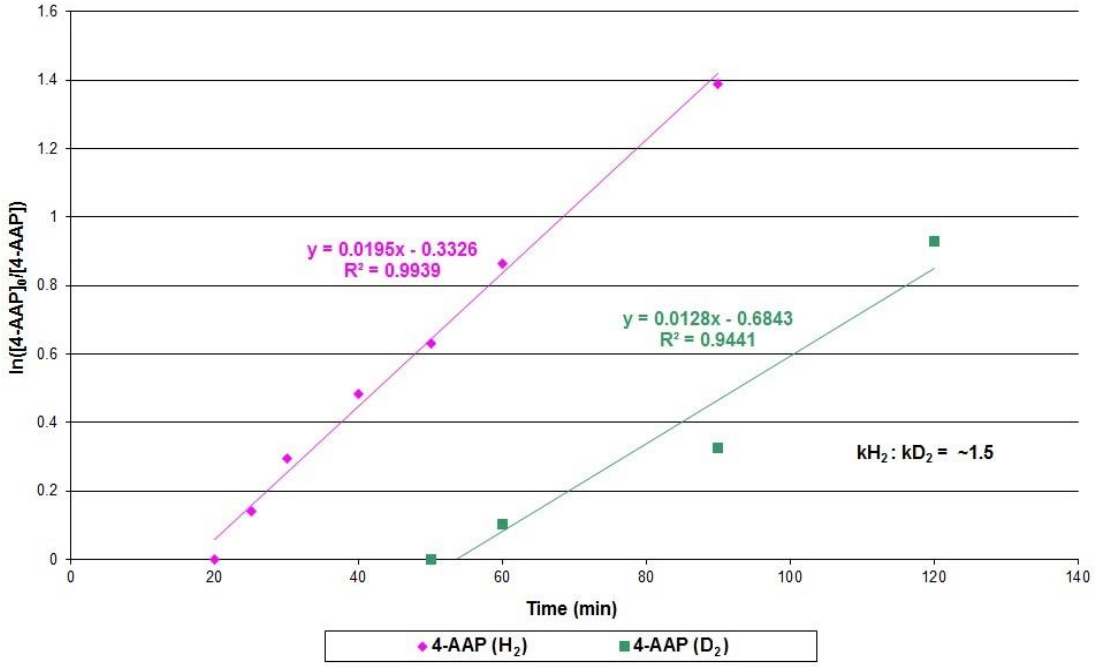

In this case a KIE of ~1.5 was calculated. Reaction of 4-AAP with deuterium was also carried out and first order rate constants calculated as before as shown in figure 5.23.

Figure 5.23 Rate constants for 4-AAP under H_2 and D_2

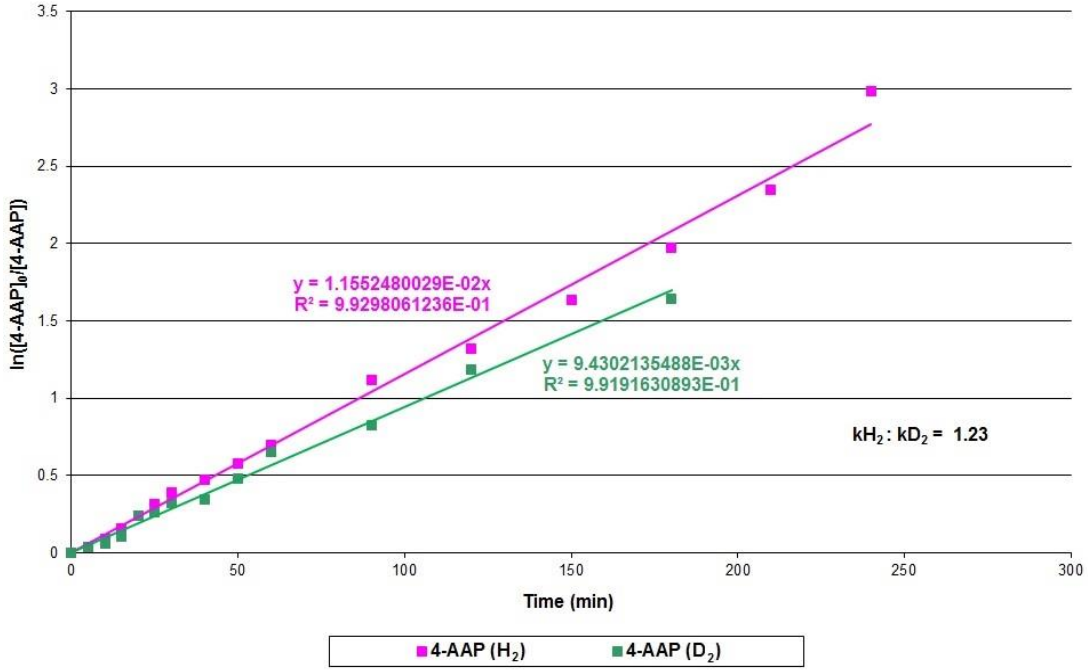

A small KIE of 1.2 was observed for hydrogenation of 4-AAP as the deuterium reaction was only slightly slower than the reaction conducted using hydrogen. Finally, the reaction was carried out using 1:1 molar ratios of 4-NAP and 4-AAP as reactants with deuterium instead of hydrogen. The rate of hydrogenation of both 4-NAP and 4-AAP was slower using deuterium rather than hydrogen and a KIE was observed and calculated for 4-NAP hydrogenation as ~1.8 and 4-AAP hydrogenation as ~1.5. The results contained in this chapter will be discussed in the following chapter.

6 Discussion

6.1 Gas-phase hydrogenation

In this chapter, the results from gas-phase hydrogenation reactions will be discussed. It was found that all of the catalysts tested exhibited different activity and selectivity to furfuryl alcohol and so each catalyst will be discussed separately.

6.1.1 Ceria catalyst

Cerium(III) nitrate hexahydrate ($Ce(NO_3)_3.6H_2O$) was used to prepare 5% CeO_x/SiO_2 by wet impregnation of Cariact Q10 silica support. BET surface area measurements for the silica support and the resulting supported ceria catalyst are shown in table 6.1.

Table 6.1 BET measurements for Cariact Q10 silica and 5% CeO_x/SiO_2 catalyst

Catalyst	BET		Single Point
	Surface area (m^2g^{-1})	Average pore diameter (nm)	Pore volume (cm^3g^{-1})
Cariact Q10 silica	276	14.6	1.01
5% CeO_x/SiO_2	254	15.1	0.96

The table shows that impregnation of the silica reduced the pore volume and surface area as the cerium salt blocked the silica pores. TPO and TPR were carried out to determine the effect of pre-treatments of the catalysts prior to testing. Figure 6.1 shows the pre-reaction TPO for 5% CeO_x/SiO_2.

Figure 6.1 Pre-reaction TPO of 5% CeO_x/SiO_2

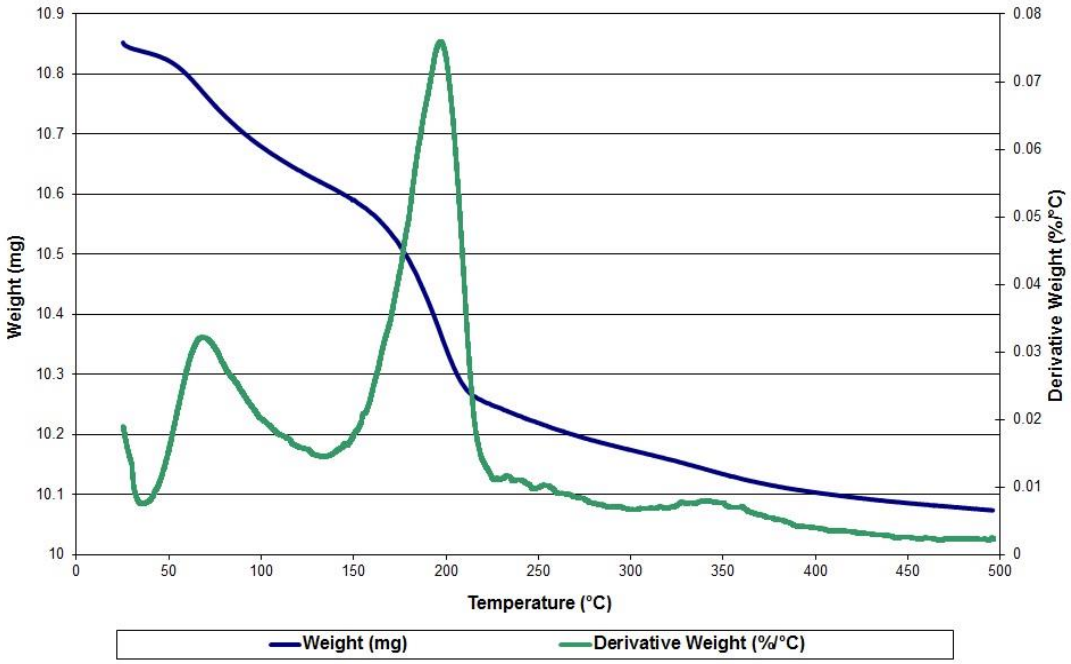

TPO showed three endothermic weight losses at 70, 200 and 340˚C. $Ce(NO_3)_3 \cdot 6H_2O$ loses water of crystallisation to produce the trihydrate at around 150˚C [105] and then decomposes around 200˚C by the following redox reaction [106]:

$$2Ce(NO_3)_3 \rightarrow 2CeO_2 + 6NO_2 + O_2$$

For complete decomposition of the cerium nitrate present, the theoretical weight loss would be 5.5%. As the observed weight loss for this sample was 7.17%, of which ~2% represented the loss of physically adsorbed water and water of crystallisation, it is reasonable to conclude that most of the cerium nitrate has formed CeO_2. XRD confirmed the presence of CeO_2 after calcination at 300˚C with peaks at 28, 47, and 56˚; characteristic of CeO_2 [107].

TPR of unsupported CeO_2 shows three peaks at 416˚C, due to the removal of adsorbed oxygen [108], 680 and 940˚C which are attributed to surface and bulk ceria reduction respectively [109-111].

$$2CeO_2 + H_2 \rightarrow Ce_2O_3 + H_2O$$

For ceria dispersed on alumina, removal of adsorbed oxygen and surface ceria reduction requires a higher temperature than that of pure ceria [112]. On the contrary, bulk ceria reduction is facilitated when dispersed on alumina however this occurs at temperatures in excess of 800°C [112].

TPR of pre-calcined 5% CeO_x/SiO_2 catalyst showed three weight loss peaks at 55, 200 and 280°C, shown in figure 6.2, and 1.67% of the original sample weight was lost.

Figure 6.2 Pre-reaction TPR of calcined 5% CeO_x/SiO_2

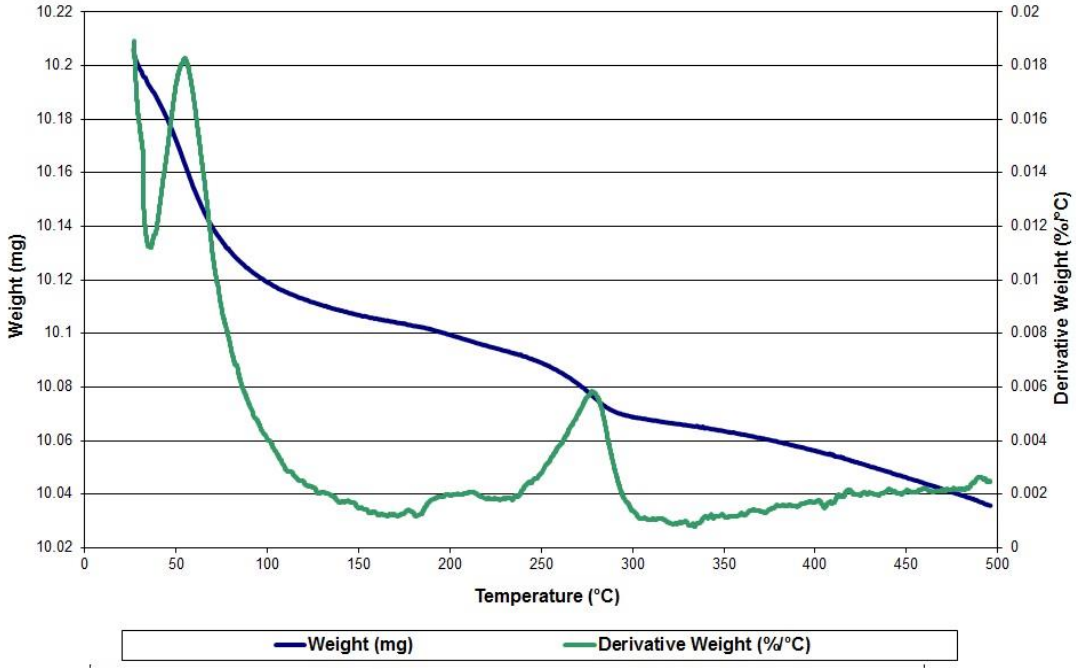

The theoretical weight loss associated with reduction of CeO_2 to form Ce_2O_3 for 5% CeO_x/SiO_2 catalyst is only 0.32%, and the experimental value was much higher. This difference can be attributed to the loss of physisorbed water and mass spectrometry also showed the evolution of *m/z* 30 and *m/z* 44 at temperatures below 180°C. The evolution of *m/z* 30 corresponded to desorption of any remaining NO species as a result of decomposition of the nitrate precursor, and *m/z* 44 can be attributed to desorption of atmospheric CO_2. From the experimental weight lost it is likely that the active phase present on the catalytic surface was Ce_2O_3; formed as a result of pre-treatment conditions.

5% CeO_x/SiO_2 exhibited low activity for the hydrogenation of furfural showing 13% conversion after 4 h on stream. It was also noted that at this stage in the

reaction 5 times as much furan was produced compared to furfuryl alcohol and no 2-methylfuran was detected.

Figure 6.3 Product distribution at 4 h on stream using 5% CeO_x/SiO_2

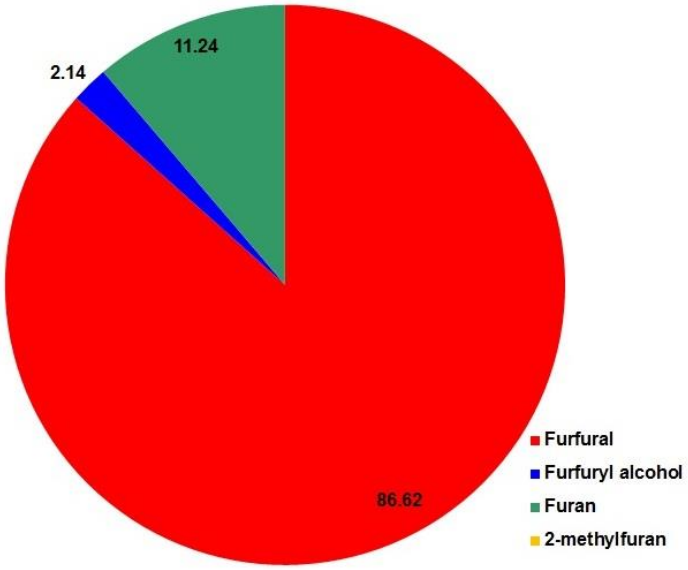

Previous studies have suggested that ceria is an inactive catalyst and unsuitable support for the hydrogenation of aldehydes to alcohols [62,113]. The results observed in this study are in accordance with prior reports. Additionally, the production of furan by decarbonylation can form polymeric carbon by-products which foul the catalyst surface [114]. Catalyst deactivation was observed and after just 30 h on stream 5% CeO_x/SiO_2 was inactive.

BET measurements were carried out on a post-reaction sample of 5% CeO_x/SiO_2 and table 6.2 shows a comparison between pre-reaction and post-reaction (in bold text) samples.

Table 6.2 BET measurements pre- and post-reaction

Catalyst	BET				Single Point	
	Surface area (m^2g^{-1})		Average pore Diameter (nm)		Pore volume (cm^3g^{-1})	
5% CeO_x/SiO_2	254	**193**	15.1	**15.1**	0.96	**0.73**

The table shows that there was a 24% reduction in surface area after 30 h on stream and although the pore diameter was unchanged there was a significant impact on the pore volume. These results suggest that as a result of the reaction, carbonaceous material was left on the surface blocking the pores.

TPO of post-reaction 5% CeO_x/SiO_2 showed three weight loss peaks as seen in figure 6.4.

Figure 6.4 Post-reaction TPO of 5% CeO_x/SiO_2

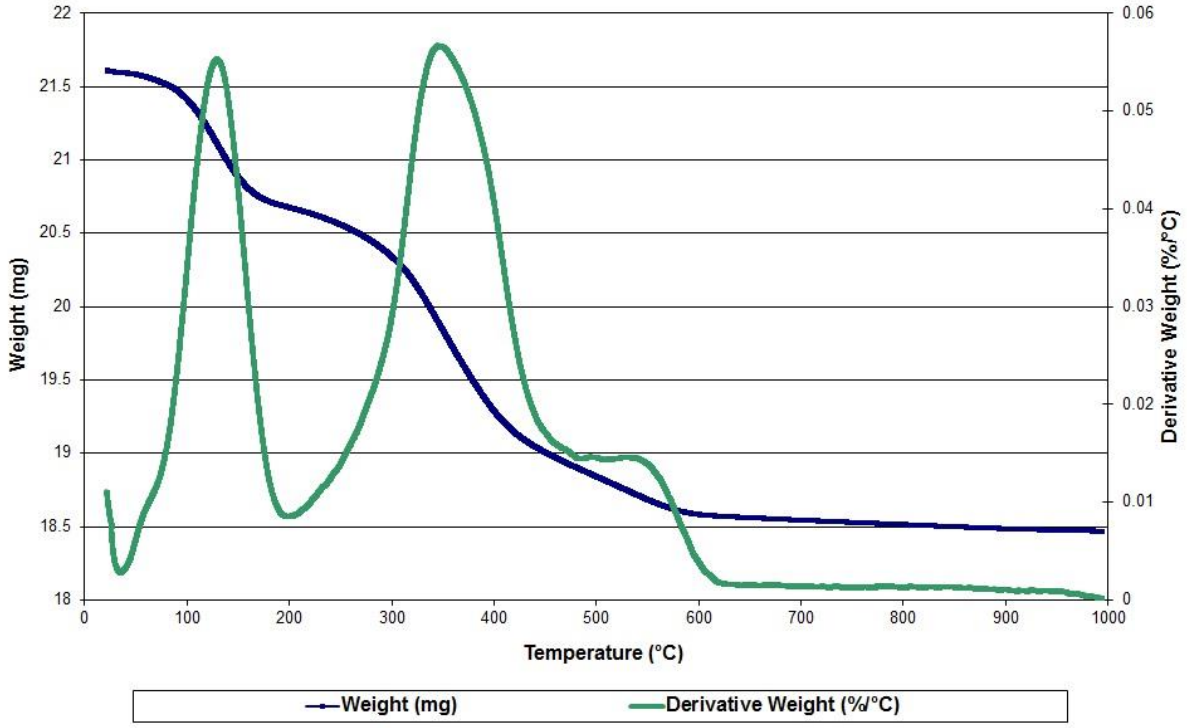

The low temperature peak at 100°C was endothermic while the peak at 360°C and the shoulder peak at 550°C were exothermic. Mass spectrometry data confirmed the evolution of water from the surface of the catalyst around 100°C. However, water was not detected at the higher temperatures.

Figure 6.5 Mass spectrometry data for post-reaction TPO of 5% CeO_x/SiO_2

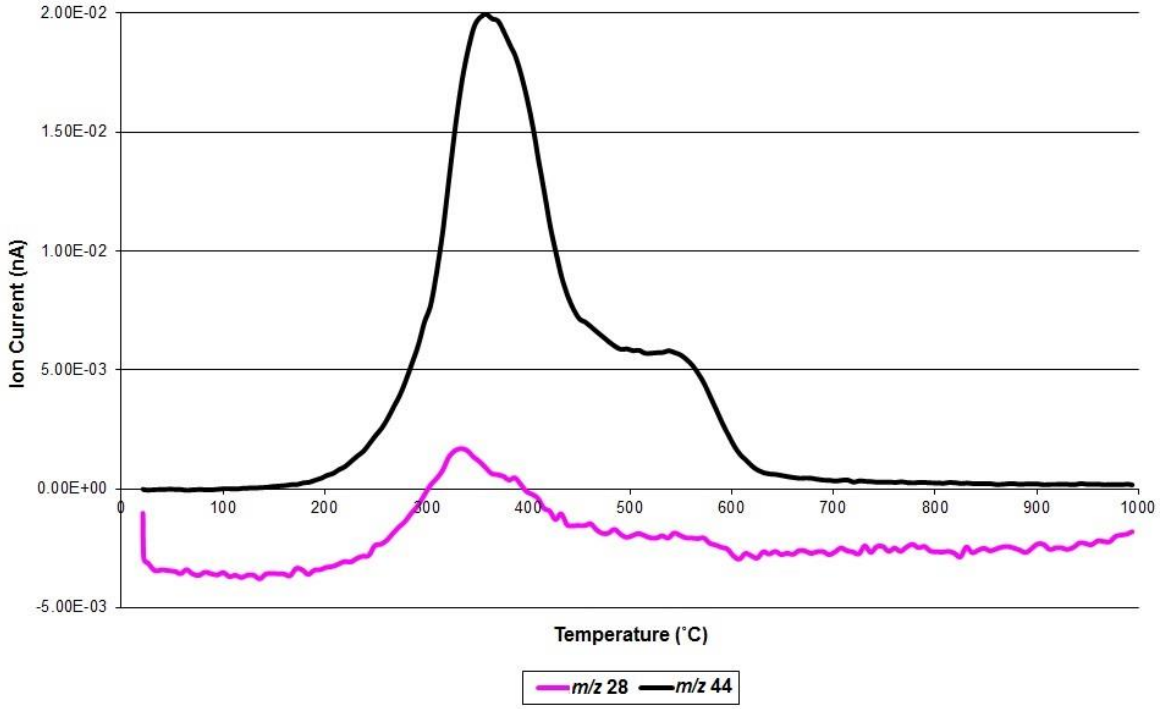

Mass spectrometry data showed that *m/z* 28 and *m/z* 44 were detected at 360 and 550°C respectively. This corresponds to the loss of CO and CO_2 from the surface of the catalyst. The weight lost during post-reaction TPO was 14.5% which represents significant carbon laydown.

Additionally, *m/z* 68 was detected at around 300°C and could correspond to furan. Extensive research has shown that unsaturated aromatic compounds are excellent precursors for coke formation [115-117]. It is feasible that furan by-product acts as a precursor to coke formation.

In general, supported ceria proved to be an inactive catalyst for the hydrogenation of furfural to furfuryl alcohol, and instead was active for the decarbonylation reaction producing furan. Furan on the surface may have acted as a precursor for coke formation which clogged the catalyst pores inhibiting any further reaction.

6.1.2 Copper catalysts

Copper(II) nitrate hemipentahydrate ($Cu(NO_3)_2 \cdot 2.5H_2O$) was used to prepare 5% and 10% Cu/SiO_2 by wet impregnation of Cariact Q10 silica support. BET surface

area measurements for the silica support and the resulting supported copper catalysts are shown in table 6.3.

Table 6.3 BET measurements for Cariact Q10 silica, 5% Cu/SiO_2 and 10% Cu/SiO_2

Catalyst	BET		Single Point
	Surface area (m^2g^{-1})	Average pore diameter (nm)	Pore volume (cm^3g^{-1})
Cariact Q10 silica	276	14.6	1.01
5% Cu/SiO_2	236	13.9	0.82
10% Cu/SiO_2	235	13.1	0.77

The table shows that impregnation using the copper salt caused a reduction in surface area, pore volume and pore diameter. Additionally, the higher the copper loading the greater the reduction in pore volume and pore diameter. This suggests that pores become blocked reducing the surface area of the catalyst. TPO and reduction TPR were carried out to determine the effect of pre-treatments of the catalysts prior to testing. Figure 6.6 shows the pre-reaction TPO profile obtained for 5% Cu/SiO_2.

Figure 6.6 Pre-reaction TPO of 5% Cu/SiO_2

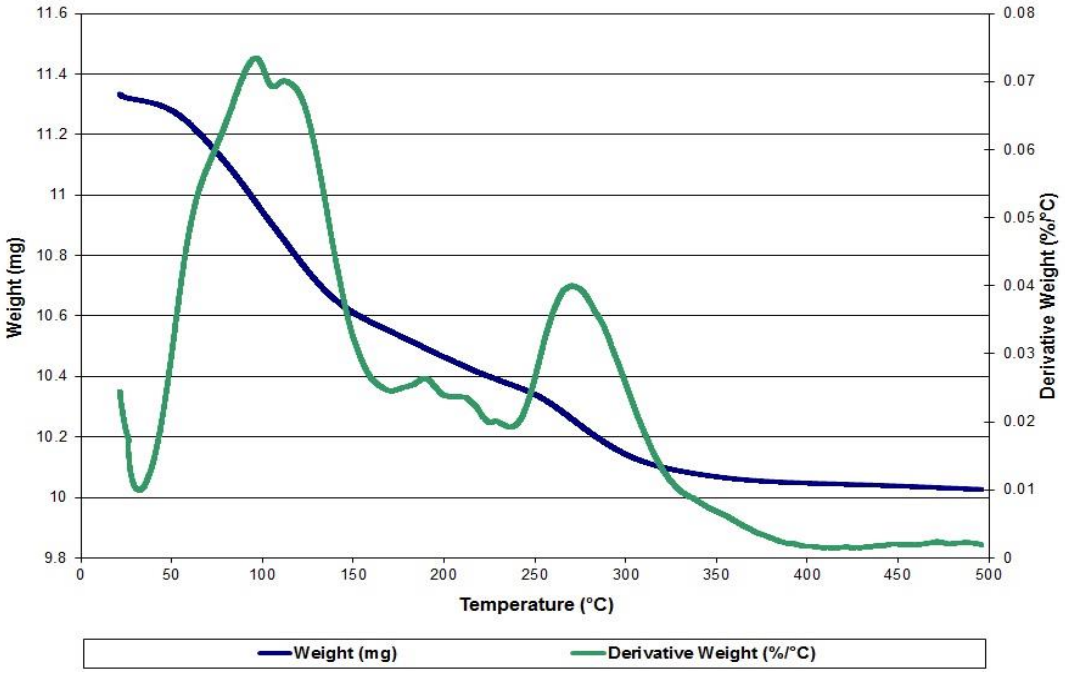

The results showed endothermic weight losses between 50 and 400°C. A pair of peaks at 100°C represents the release of physically adsorbed water from the catalyst surface, evidenced by mass fragment *m*/*z* 18 detected at this temperature using mass spectrometry. Further weight loss peaks were observed at 190, 215 and 230°C, and mass fragments *m*/*z* 30 and *m*/*z* 44 were observed at these temperatures, corresponding to NO and N_2O species, respectively. Decomposition of copper nitrate can occur as follows:

$$2Cu(NO_3)_2 \rightarrow 2CuO + 4NO_2 + O_2$$

For complete decomposition of the copper nitrate present in a 5% Cu/SiO_2 catalyst the theoretical weight loss would be 8.5%. The experimental weight loss for this sample was 11.54% which is higher than the theoretical value as it includes the loss of physically adsorbed water and water of crystallisation. Therefore, significant nitrate decomposition occurred during TPO and XRD results confirm the presence of CuO after calcinations at 300°C, as shown in figure 6.7.

Figure 6.7 XRD patterns for as-prepared and calcined samples of 5% Cu/SiO_2

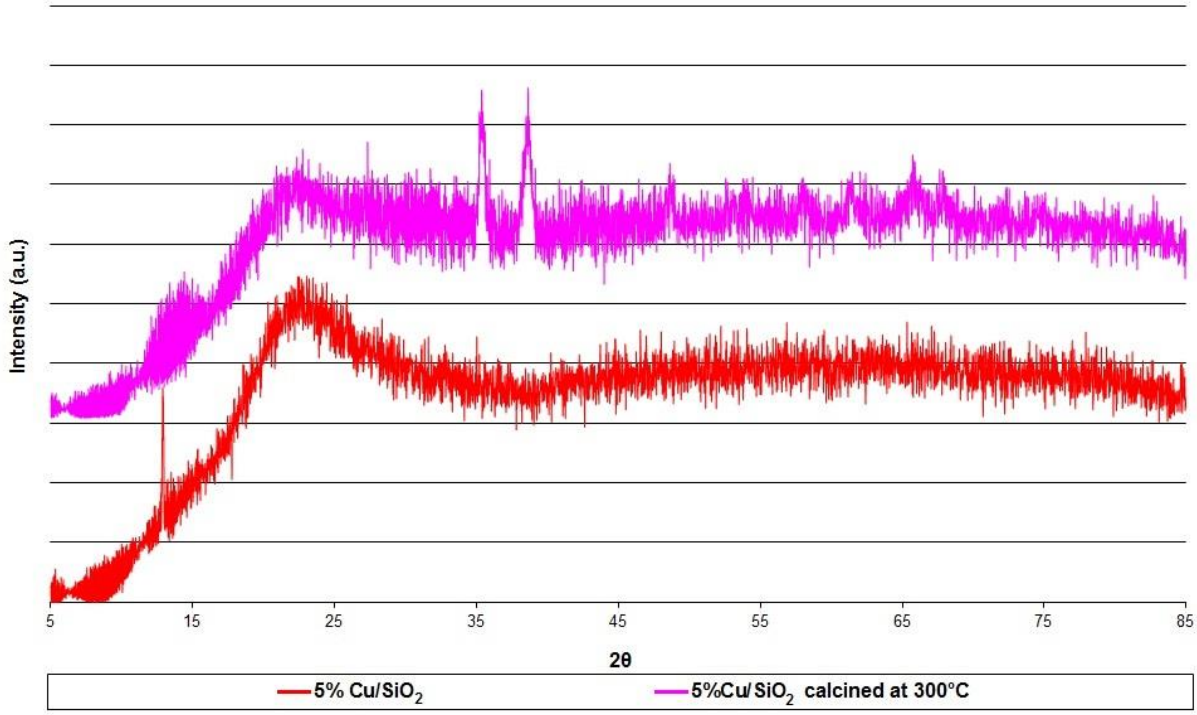

The peak at 22° is characteristic of silica and no other peaks were detected for 5% Cu/SiO_2 prior to pre-treatment suggesting an amorphous character. A peak associated with copper(II) nitrate hydrate or hydroxide was not detected for this

catalyst and suggests that the sample was mainly amorphous to X-rays [104]. Calcination of the sample however, generated peaks at 35° and 38° and confirms the presence of some cupric oxide (CuO) in the tenorite form. Similar results were observed for 10% Cu/SiO_2 where the theoretical weight Loss for the decomposition of twice as much nitrate is 17% and the experimental value was much higher at 24.81%.

TPR was used to investigate the reducibility of copper catalysts and the effect of copper loading on the reduction profile. Both catalysts showed more than one hydrogen consumption peak as shown in figure 6.8.

Figure 6.8 Effect of copper loading on reduction temperature

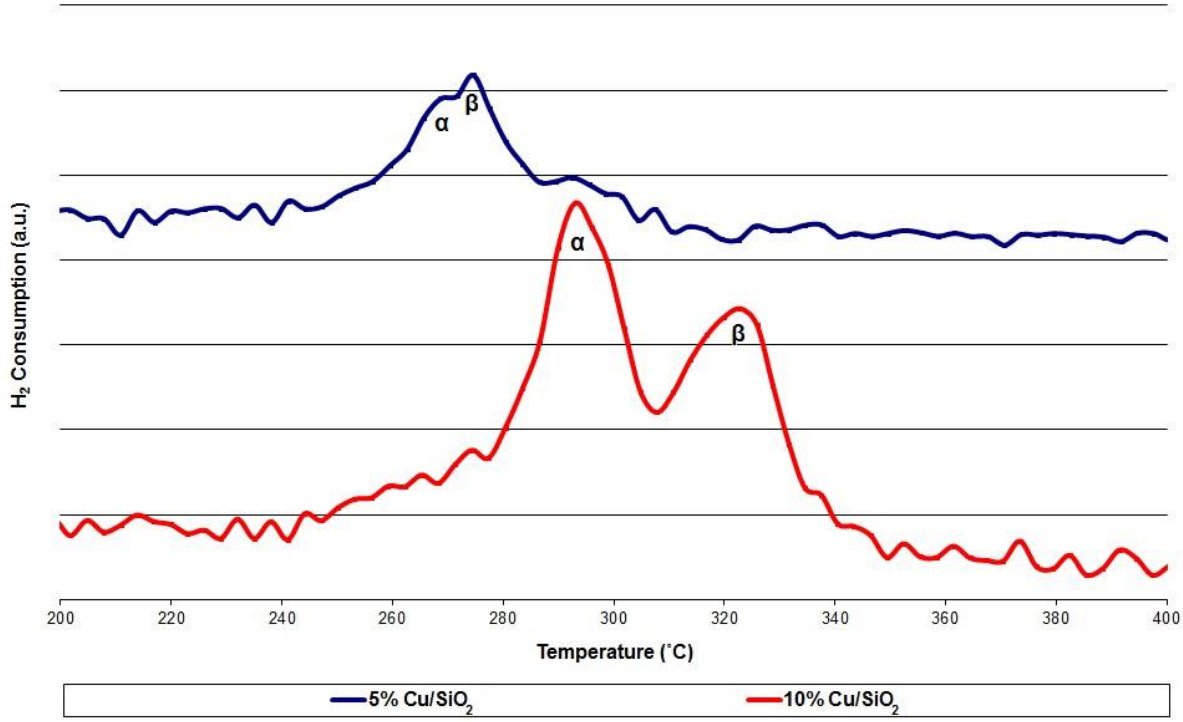

For 5% Cu/SiO_2, reduction peaks were observed at 268°C and 274°C but for 10% Cu/SiO_2, the reduction peaks were slightly higher at 293°C and 323°C. This suggests that at lower copper loadings, the copper(II) species was well dispersed, providing a large surface area for reaction to occur [118] and also producing smaller, more easily reducible CuO particles. It has been suggested that the reduction of higher loaded copper catalysts is controlled by the rate of diffusion of hydrogen through the CuO particles [24].

Pure CuO supported on silica can be reduced in one step at ~290°C however, supported copper can exist as isolated ions, clusters and bulk CuO, and

aggregates can be reduced at ~200°C [112]. More than one peak in a TPR profile can indicate either a single stage reduction ($Cu^{2+} \rightarrow Cu^{0}$) of more than one type of Cu(II) species or a two-stage reduction ($Cu^{2+} \rightarrow Cu^{1+} \rightarrow Cu$) of a single Cu(II) species present. The overall reduction of copper oxide has a theoretical weight loss of 20% and follows:

$$\mathbf{CuO + H_2 \rightarrow Cu + H_2O}$$

Table 6.4 shows the theoretical and experimental weight Losses associated with the reduction of 5% Cu/SiO_2 and 10% Cu/SiO_2 catalysts.

Table 6.4 Theoretical and experimental weight Lost through TPR

Catalyst	Theoretical weight loss for reduction (%)	Experimental weight loss for reduction (%)
5% Cu/SiO_2	1.42	1.22
10% Cu/SiO_2	2.83	2.52

The experimental weight loss was calculated for the reduction region for each catalyst and was found to be slightly lower than the expected weight loss for complete reduction of 5% and 10% CuO, respectively.

The reduction of uncalcined copper nitrate/silica catalysts has been studied and it was found that copper nitrate decomposed to $Cu(NO_3)_2{\cdot}2Cu(OH)_2$ between 100–150°C [119]. Under nitrogen, weight was lost between 300 and 400°C corresponding to the decomposition of copper nitride, decomposition of NO and decomposition of $Cu(NO_3)_2.2Cu(OH)_2$. An additional weight loss was observed under hydrogen between 200-250°C due to the reduction of $Cu(NO_3)_2{\cdot}2Cu(OH)_2$ to form metallic copper. Two reduction routes were proposed:

$$\mathbf{Cu(NO_3)_2.2Cu(OH)_2 + 11H_2 \rightarrow 3Cu + 2NH_3 + 10H_2O}$$

$$\mathbf{Cu(NO_3)_2 + 9H_2 \rightarrow Cu + 2NH_3 + 6H_2O}$$

It is reasonable that a combination of these reactions occurred on the catalyst as a result of calcination and reduction to form metallic copper. The production of ammonia would have been difficult to detect as water was also formed. XRD patterns confirmed the presence of Cu crystals post-reaction as shown in figure 6.9.

Figure 6.9 XRD patterns for calcined and reduced 5% Cu/SiO_2

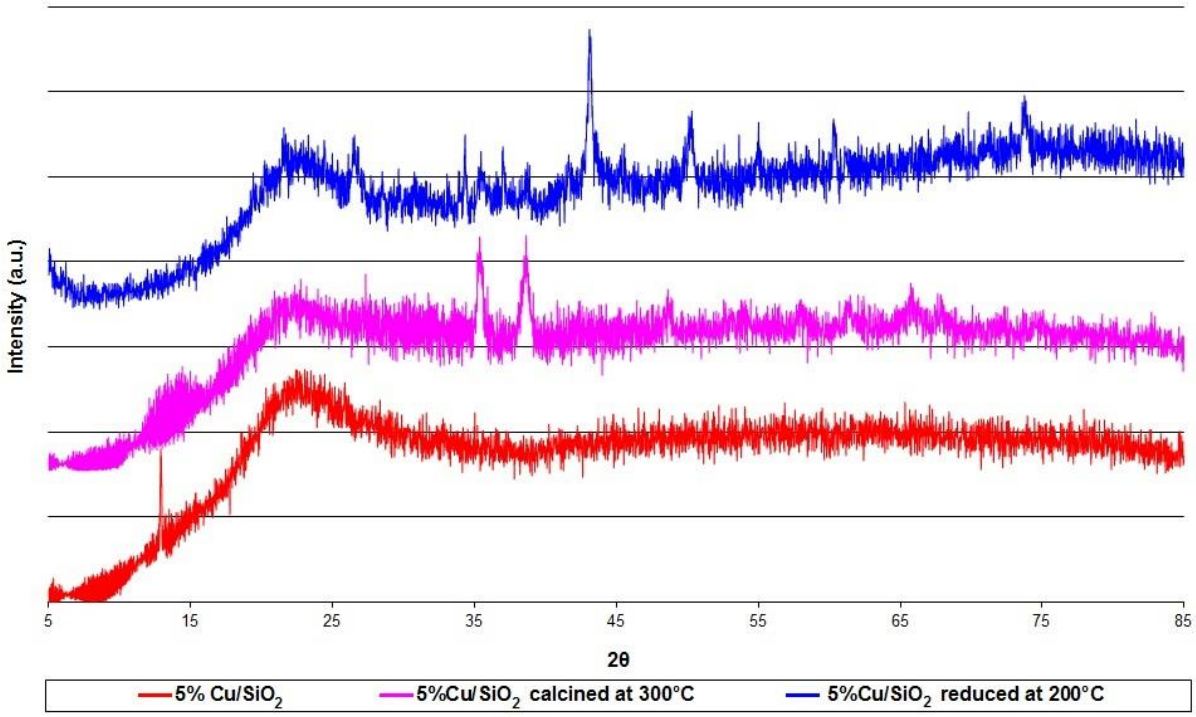

The peaks present in the calcined sample at 35° and 38° corresponding to CuO are not detectable in the reduced sample, however peaks at 43° and 50° corresponding to Cu were observed. Using the Scherrer equation, the size of the resulting Cu crystals was calculated to be 18 nm.

Silica supported copper catalysts proved to be active catalysts for the hydrogenation of furfural and the higher the copper loading, the greater the activity for furfural conversion as shown in figure 6.10.

Figure 6.10 Product distribution at 25 h on stream

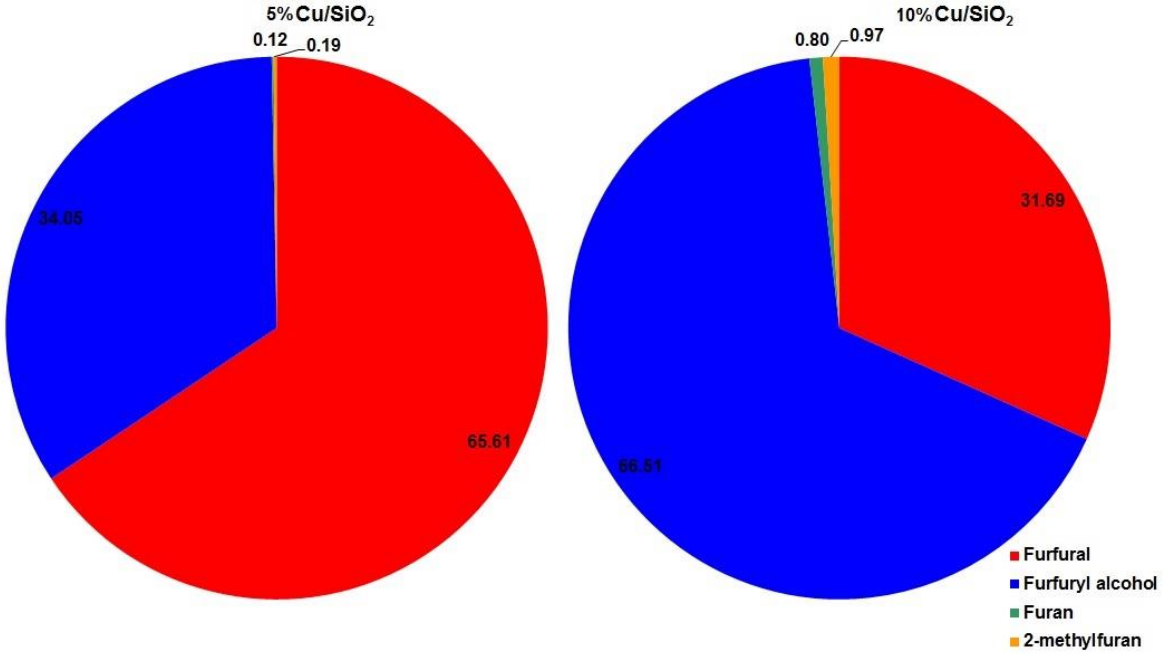

10% Cu/SiO_2 exhibited improved activity compared to that of 5% Cu/SiO_2 for the reaction with 68% furfural conversion at 25 h on stream. Nagaraja *et al.* proposed that the presence of more Cu, or Less CuO, resulted in a high catalytic activity toward the formation of furfuryl alcohol through hydrogenation of furfural [39]. However, both catalysts achieved 98% selectivity towards furfuryl alcohol at around 27 h on stream.

BET measurements were carried out on post-reaction samples of 5% Cu/SiO_2 and 10% Cu/SiO_2. Table 6.5 shows a comparison between pre and post-reaction (in bold text) samples.

Table 6.5 BET measurements pre- and post-reaction of 5% and 10% Cu/SiO_2

Catalyst	BET				Single Point	
	Surface area (m^2g^{-1})		Average pore Diameter (nm)		Pore volume (cm^3g^{-1})	
5% Cu/SiO_2	236	**128**	13.9	**12.6**	0.82	**0.40**
10% Cu/SiO_2	235	**90**	13.1	**12.2**	0.77	**0.28**

Both catalysts show a dramatic reduction in both surface area and pore volume with 5% Cu/SiO_2 having lost 45% surface area and 10% Cu/SiO_2 lost 62%. Post-reaction XRD patterns showed a Cu peak and smaller average crystallite sizes than the corresponding reduced samples, so significant sintering did not occur. Catalyst deactivation was most likely caused by the build-up of carbonaceous material on the surface of the catalyst which subsequently blocked pores. Post-reaction TPD and TPO with mass spectrometry were used to try to identify any species that remained on the surface of the catalysts post-reaction. For TPD, argon flow was used and the mass spectrometry results for TPD of 5% Cu/SiO_2 are shown in figure 6.11.

Figure 6.11 Mass spectrometry results from TPD of 5% Cu/SiO_2

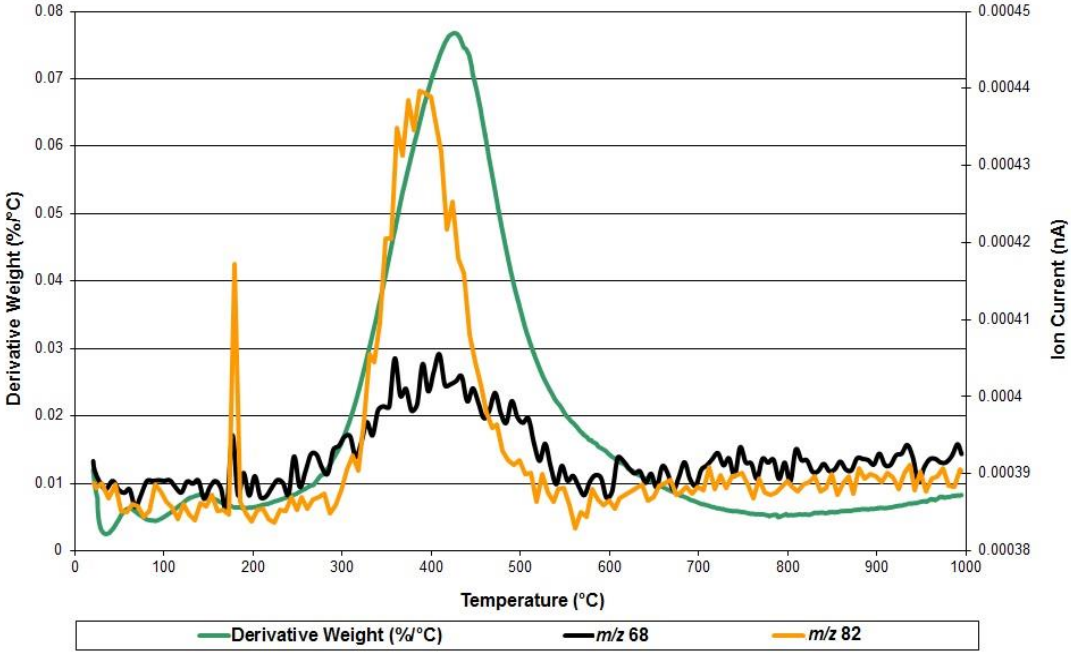

Mass spectrometry results showed peaks for *m/z* 68 and 82 characteristic of furan and 2-methyfuran, respectively, suggesting that by-products are left on the catalyst surface post-reaction. These by-products could lead to coke formation as aromatic molecules are known for their coke forming tendencies [115] and a study conducted by Voge *et al.* [116] reported a direct relationship between the aromatic content of the feed solution and the amount of coke deposited on a silica-alumina catalyst.

Figure 6.12 Mass spectrometry data for post-reaction TPO of 10% Cu/SiO_2

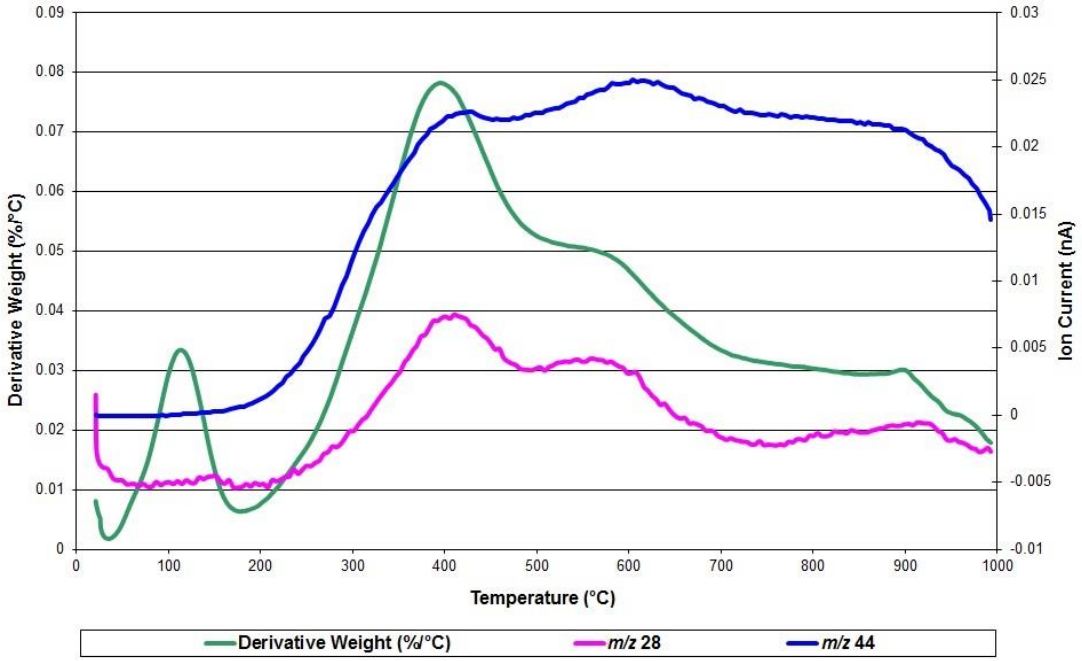

During post-reaction TPO, 10% Cu/SiO_2 Lost over 34% of its original sample weight and mass fragments *m/z* 28 and 44 were detected. A study of coke formation over a copper catalyst identified three weight loss regions pertaining to different species present on the catalyst surface [120]. Simón *et al*. reported the removal of water and volatile materials from the surface at temperatures up to 200°C [120]. Weight lost above 200°C but below 370°C was attributed to desorption of more mobile carbonaceous residues or physisorbed products/side-products. This type of coke is referred to as soft coke and can comprise of mainly high molecular weight aliphatic oligomers. In the third weight loss region (>370°C) hard coke, or bulkier carbonaceous compounds such as polynuclear aromatics were desorbed [121]. These results suggest the presence of both soft and hard coke on the surface of the catalyst. Table 6.6 shows the % weight lost in each temperature region for both 5% Cu/SiO_2 and 10% Cu/SiO_2.

Table 6.6 Coke content of post-reaction 5% Cu/SiO_2 and 10% Cu/SiO_2

Catalyst	Coke content (wt.%)		
	Soft coke[a]	Hard coke[b]	Total coke
5% Cu/SiO_2	13.12	12.67	25.79
10% Cu/SiO_2	14.58	14.85	29.43

[a] 180 – 500°C, [b] >500 – 1000°C

The table shows that both catalysts have significant coke content with almost equal quantities of soft and hard coke present. Mass spectrometry data showed the desorption of furan and 2-methylfuran at ~400°C suggesting that these species act as poisons or as precursors to coke formation. Hard type coke was formed on the surface clogging pores as seen in post-reaction BET measurements and most likely consisted of polynuclear aromatic compounds [121].

Silica supported copper catalysts proved to be active and selective catalysts for the hydrogenation of furfural to furfuryl alcohol. Calcination caused decomposition of the nitrate precursor to form CuO which was subsequently reduced to Cu prior to reaction. The higher the copper loading the greater the furfural conversion as more Cu sites were present and both catalysts achieved 98% selectivity for furfuryl alcohol. However catalyst deactivation was observed and post-reaction characterisation showed a dramatic reduction in surface area and pore volume and TPO confirmed that there was significant carbon laydown as result of the reaction.

6.1.3 Copper and ceria catalysts

Co-impregnation of Cariact Q10 silica using copper(II) nitrate hemipentahydrate ($Cu(NO_3)_2 \cdot 2.5H_2O$) and cerium(III) nitrate hexahydrate ($Ce(NO_3)_3 \cdot 6H_2O$) was used to prepare catalysts with different levels of Cu and CeO_x present. Table 6.7 shows the BET measurements for each of the catalysts prepared by this method.

Table 6.7 BET measurements for Cu/SiO_2 and $Cu + CeO_x/SiO_2$ catalysts

Catalyst	Molar $Cu:CeO_x$	BET		Single Point
		Surface area (m^2g^{-1})	Average pore diameter (nm)	Pore volume (cm^3g^{-1})
Cariact Q10 silica	/	276	14.6	1.01
5% Cu/SiO_2	0	236	13.9	0.82
10% Cu/SiO_2	0	235	13.1	0.77
5% Cu + 1% CeO_x/SiO_2	11	232	14.9	0.87
5% Cu + 5% CeO_x/SiO_2	2.2	215	14.5	0.78
10% Cu + 5% CeO_x/SiO_2	4.4	154	13.2	0.51

Table 6.7 shows that both an increase in metal loading and the addition of more than one metal reduced the surface area and pore volume. The reduction in pore volume indicates that the pores of the support were blocked during catalyst preparation. Ceria can act as a promoter and a reducible support and has proven to improve the dispersion of supported metals [122,123]. By comparison of the catalysts containing 5% Cu and varying levels of CeO_x it can be seen that 1% CeO_x had little effect on the surface area, pore volume or pore diameter. Further investigation of the effect of cerium addition to support copper catalysts was carried out by TPO and TPR.

Figure 6.13 Pre-reaction TPO for Cu-CeO_x catalysts

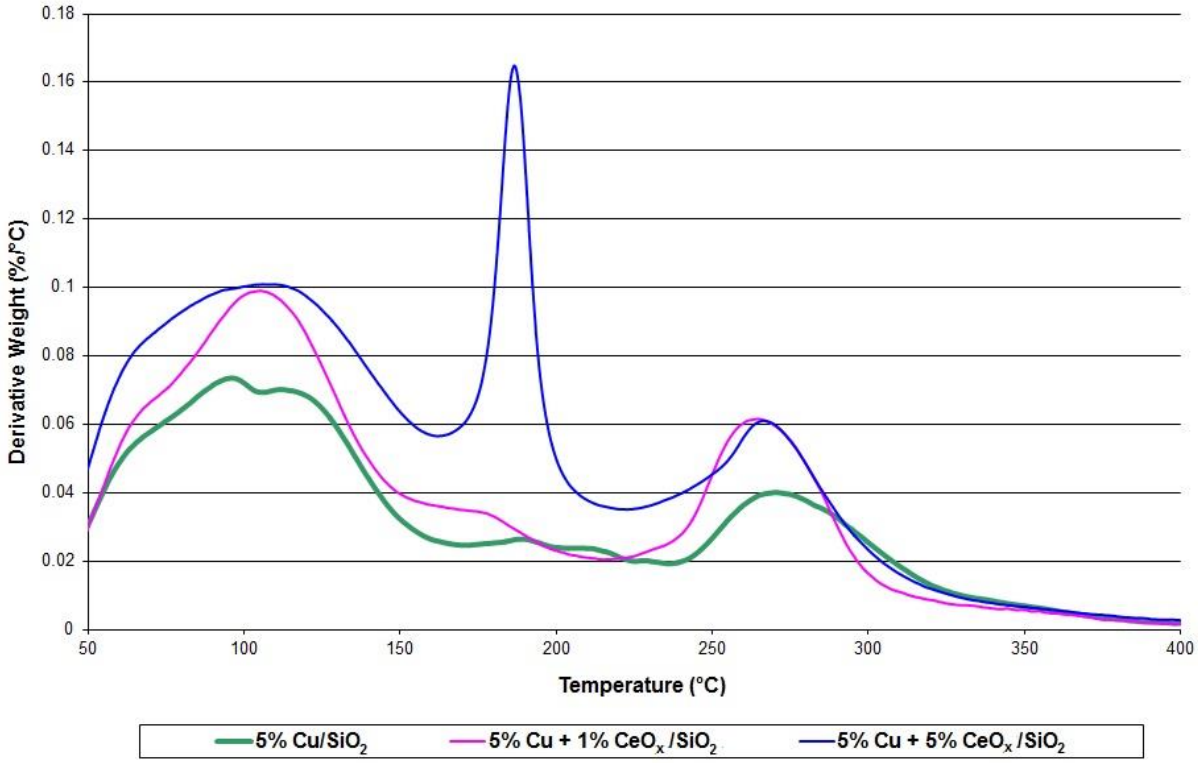

Pre-reaction TPO profiles for 5% Cu/SiO_2, 5% Cu + 1% CeO_x/SiO_2 and 5% Cu + 5% CeO_x/SiO_2 are shown above. Weight losses were observed at ~100°C, 180–220°C and 270°C and these corresponded to the evolution of *m/z* 18, *m/z* 30 and *m/z* 44, respectively. From the TPO, it was observed that 5% Cu + 5% CeO_x/SiO_2 exhibited a significantly larger peak at 190°C compared to the other catalysts, which may correspond to decomposition of more nitrate present. Mass spectrometry data for pre-reaction TPO of 5% Cu + 5% CeO_x/SiO_2 is shown in figure 6.14.

Figure 6.14 Mass spectrometry results for pre-reaction TPO of 5% Cu + 5% CeO_x/SiO_2

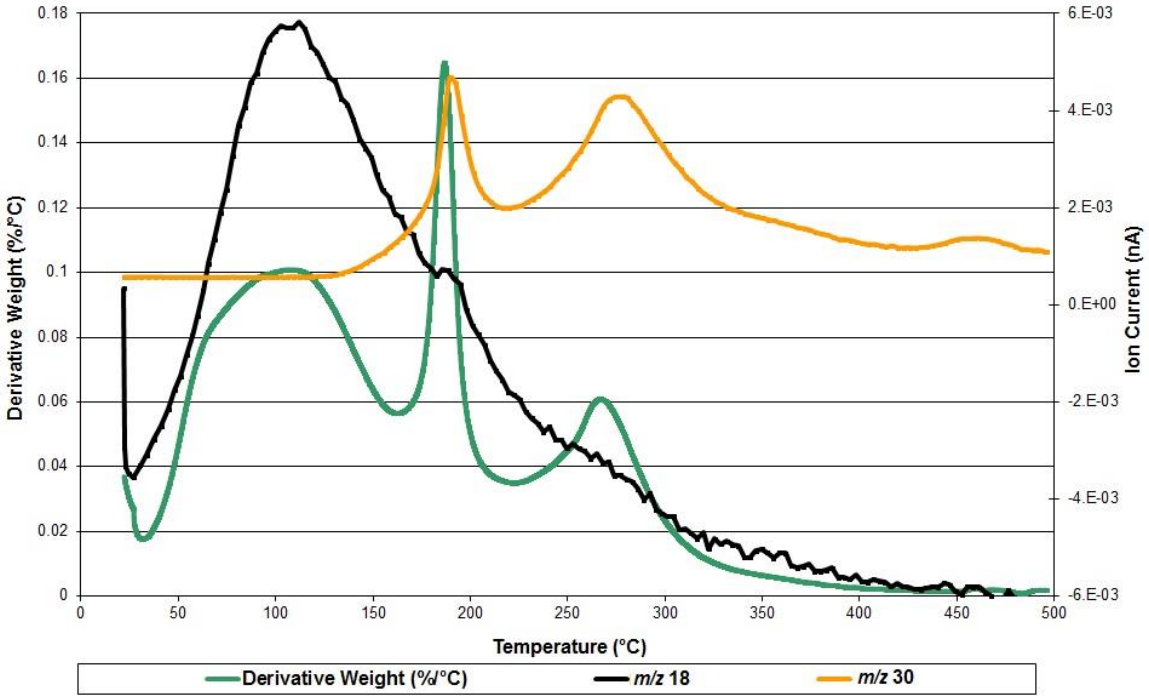

The weight loss at ~100˚C corresponded to the release of physisorbed water from the catalyst surface. Mass fragment *m/z* 30 and also *m/z* 46 were detected at 190 and 270˚C indicating decomposition of the nitrate precursor to form copper oxide. Table 6.8 shows the theoretical weight loss for each catalyst if assuming all $Cu(NO_3)_2$ and $Ce(NO_3)_3$ decompose to produce CuO and CeO_2, respectively.

Table 6.8 BET measurements for Cu/SiO_2 and Cu + CeO_x/SiO_2 catalysts

Catalyst	Theoretical weight loss (%)	Experimental weight Loss (%)	
	$Cu(NO_3)_2 \rightarrow CuO$ and $Ce(NO_3)_3 \rightarrow CeO_2$	< 150˚C	150–400˚C
5% Cu + 1% CeO_x/SiO_2	9.60	7.68	5.96
5% Cu + 5% CeO_x/SiO_2	14.0	9.51	9.38
10% Cu + 5% CeO_x/SiO_2	22.50	9.79	12.71

The table also shows the experimental weight loss below 150˚C and between 150-400˚C corresponding with the loss of physisorbed water and the

decomposition of nitrate precursor. The results show a significant loss associated with the evolution of water from the catalyst and the reduction weight losses were lower than the theoretical values. This suggests that the nitrate precursor is not fully decomposed through calcination, however the XRD patterns shown in figure 6.15 show the presence of some CuO and CeO_2.

Figure 6.15 XRD patterns for calcined Cu and Cu-CeO_x catalysts

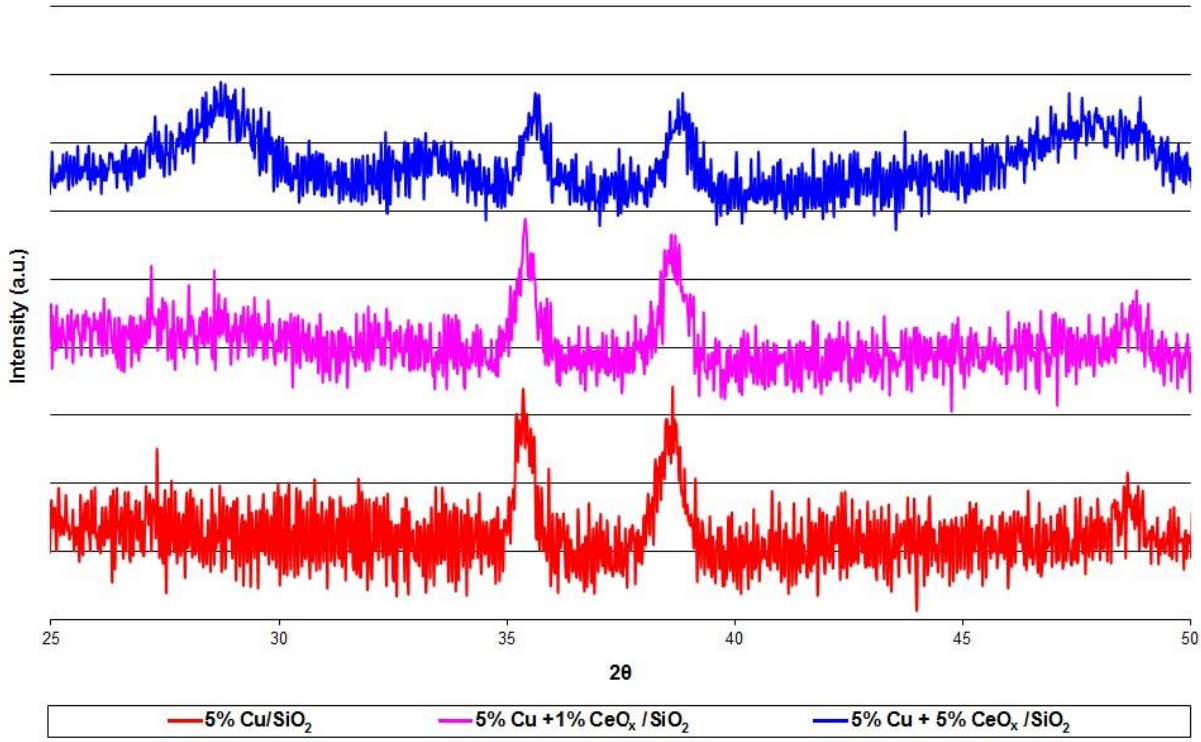

The XRD patterns show the presence of CuO as a result of calcination pre-treatment. Additionally, with increasing ceria content the intensity of the CuO peaks decreases. For a supported crystalline oxide, particle size is proportional to its signal intensity and therefore the presence of ceria has reduced CuO particle size [107]. Similarly, 10% Cu/SiO_2 and 10% Cu + 5% CeO_x/SiO_2 catalysts differed in that the weight Loss peak at 190°C was more intense for the catalyst containing CeO_x.

The effects of CeO_x on the reducibility of the catalysts was investigated by TPR and figure 6.16 shows the reduction peaks for 5% Cu/SiO_2 and catalysts containing 1% and 5% CeO_x.

Figure 6.16 Effect of CeO_x on the reducibility of 5% Cu catalysts

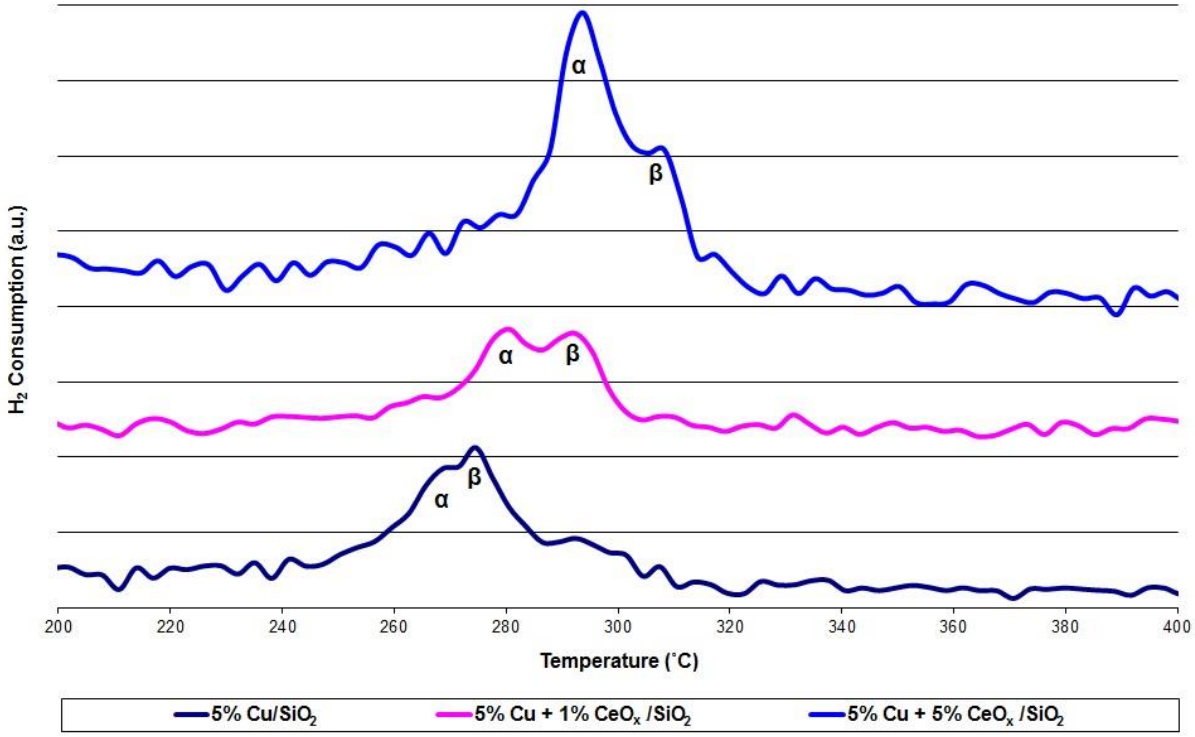

The figure shows the reduction peaks for 5% Cu/SiO_2, 5% Cu + 1% CeO_x/SiO_2 and 5% Cu + 5% CeO_x/SiO_2. Firstly, the presence of ceria in the catalyst increased the reduction temperature, which was unexpected as a previous study by Liu *et al*. showed that association of copper and ceria resulted in enhanced reducibility of $Cu\text{-}CeO_2$ catalysts [124]. Secondly, the presence of ceria altered the intensity of the lower temperature, α peak compared to the higher temperature ß peak. This can be seen most clearly in the reduction trace for 5% Cu + 5% CeO_x/SiO_2 where the α-peak has a much greater intensity than that of the higher temperature ß peak. According to literature data [125,126] the lower temperature α-peak is attributed to the reduction of highly dispersed copper oxide, which includes isolated copper ions and well dispersed clusters. The higher temperature ß-peak was attributed to the reduction of bulk CuO [127-132].

For 10% Cu/SiO_2 and 10% Cu + 5% CeO_x/SiO_2 the presence of CeO_x has less an effect on the reducibility of the catalyst. In figure 6.17, the reduction peaks for 10% Cu/SiO2 at 290˚C and 325˚C are more defined than the peaks for 10% Cu + 5% CeO_x/SiO_2.

Figure 6.17 Effect of CeO_x on the reducibility of 10% Cu catalysts

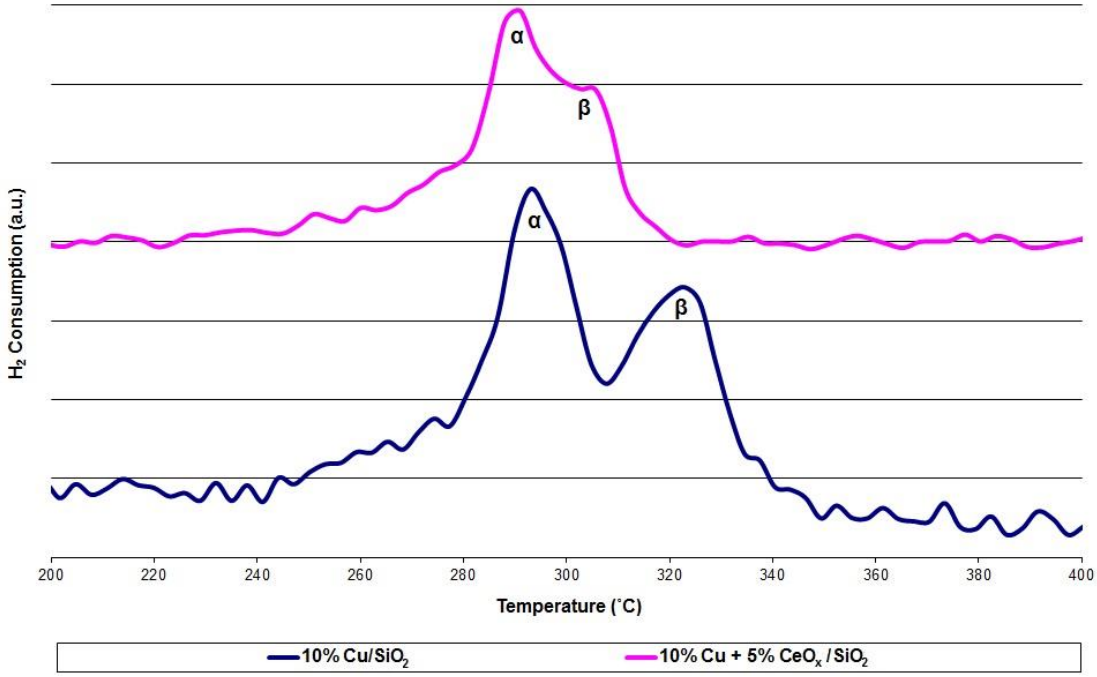

For the reduction of 10% Cu + 5% CeO_x/SiO_2, the ß-peak is less intense suggesting less bulk CuO is present. This peak is also at a slightly lower temperature suggesting that any CuO present is more easily reduced in the presence of CeO_x. Many authors have studied mixed Cu-Ce oxides with various copper contents [133-138], and reported that strong interaction occurs easily at the interface between highly dispersed copper oxide and ceria due to their close contact with each other. This strong interaction can lead to low temperature reduction of copper oxide, and concurrently, to partial reduction of ceria at low temperature [135,138].

XRD patterns for Cu-CeO_x catalysts show the presence of Cu post reduction and for 5% Cu + 5% CeO_x/SiO_2, peaks corresponding to Ce_2O_3 can also be seen. Figure 6.18 shows the hot-stage XRD results for the reduction of 5% Cu/SiO_2, 5% Cu + 1% CeO_x/SiO_2 and 5% Cu + 5% CeO_x/SiO_2.

Figure 6.18 XRD patterns for reduced Cu and Cu-CeOx catalysts

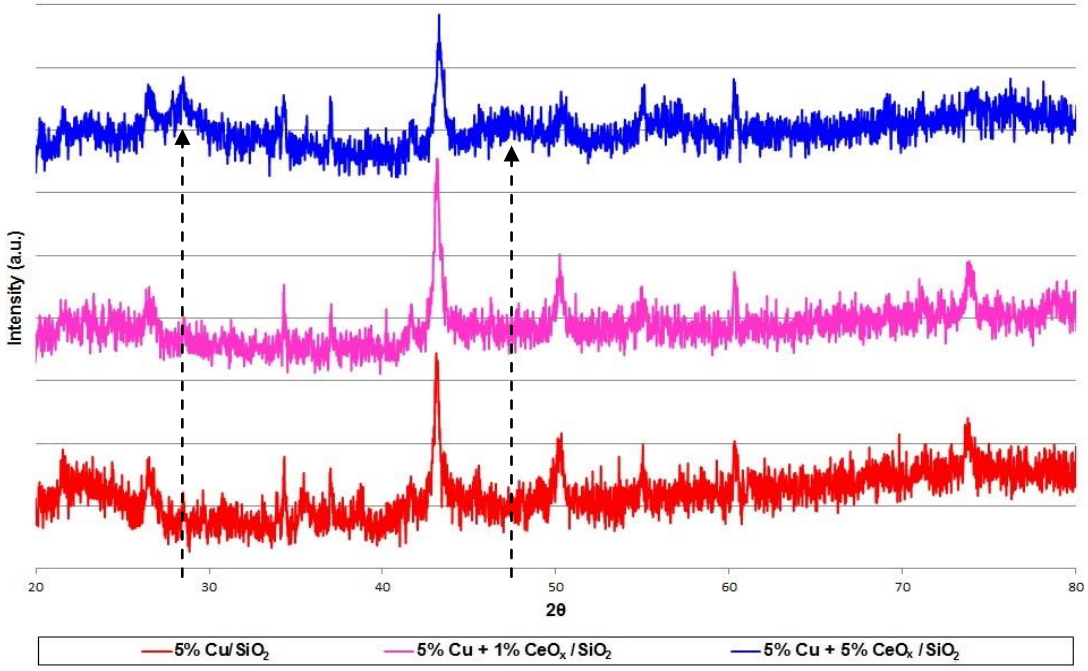

Peaks at 28.57° and 47.51° are characteristic of Ce_2O_3 and these can be seen in the reduction pattern for 5% Cu + 5% CeO_x/SiO_2 suggesting that reduction of some CeO_2 takes place during reduction conditions.

Table 6.9 shows the weight lost through pre-reaction TPO and TPR or Cu and Cu-CeO_x catalysts and good correlation can be seen as the sum of the weight lost through TPO followed by TPR almost equals the weight lost through TPR of an uncalcined sample.

Table 6.9 Weight Lost through pre-reaction TPO and TPR

Catalyst	Weight Lost (% of original sample)		
	Pre-reaction TPO	Pre-reaction TPR calcined	Pre-reaction TPR uncalcined
5% Cu/SiO_2	11.5	2.5	13.2
10% Cu/SiO_2	24.8	4.5	30.2
5% Cu + 1% CeO_x/SiO_2	13.6	2.4	13.9
5% Cu + 5% CeO_x/SiO_2	18.9	2.8	20.6
10% Cu + 5% CeO_x/SiO_2	22.8	3.7	26.7

Ceria doped copper catalyst proved to be active and selective catalysts for furfural hydrogenation. Their catalytic performance was compared, in figure 6.19, to that of copper only catalysts to determine the effect of the presence of ceria dopant.

Figure 6.19 Furfural conversion against time for Cu and Cu-CeO_x catalysts

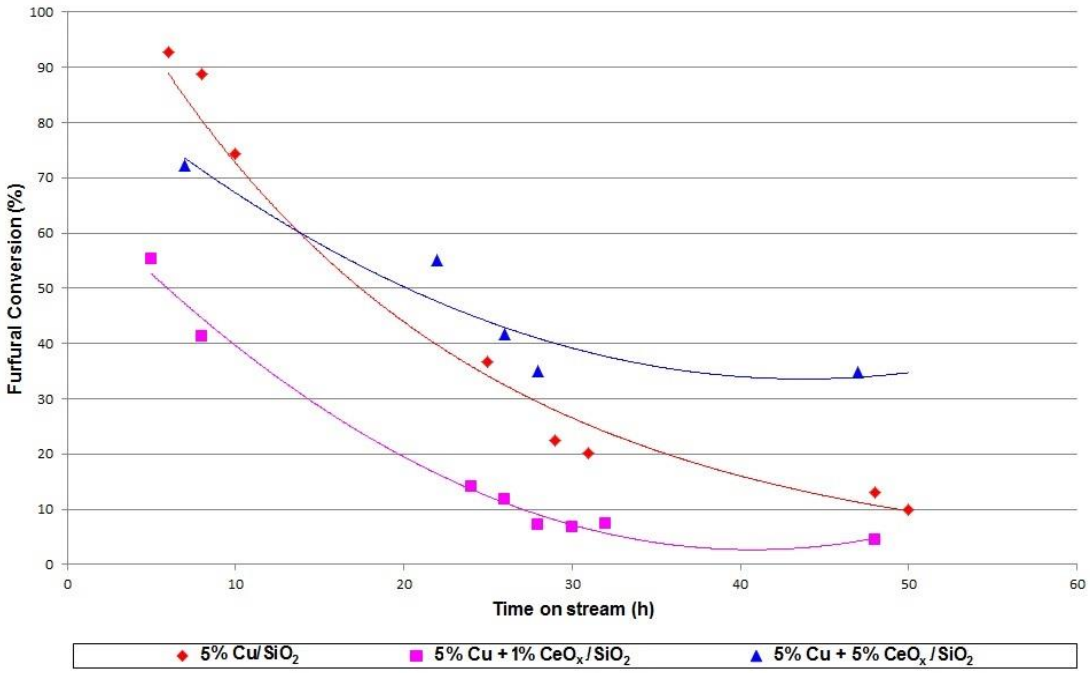

The figure shows that 5% Cu + 1% CeO_x/SiO_2 exhibited the lowest activity and 5% Cu/SiO_2 showed the highest activity. Both of these catalysts however, deactivated rapidly with time on stream. 5% Cu + 5% CeO_x/SiO_2 achieved moderate activity and a much slower deactivation.

A study of Ce promoted Ni-B amorphous alloy catalysts for furfural hydrogenation [62] reported an optimum ceria content of 1.28% and found that higher levels had a detrimental impact on the activity of the catalyst. It is thought that the furfural molecule adsorbs in both the pyranic and linear form and that the Ce^{3+} present could act as Lewis acid sites. Furfural could become adsorbed via donation of a lone electron pair from the oxygen of the carbonyl group which would polarised the C=O bond making it more the carbon more susceptible to nucleophilic attack. It is reasonable that the presence of both Cu active sites for hydrogen adsorption and the surface Ce^{3+} species for C=O adsorption allowed for high furfural hydrogenation activity. A higher than

optimum Ce^{3+} surface concentration could block Cu active sites and cause a reduction in activity [15].

Figure 6.20 Furfuryl alcohol concentration against furfural conversion

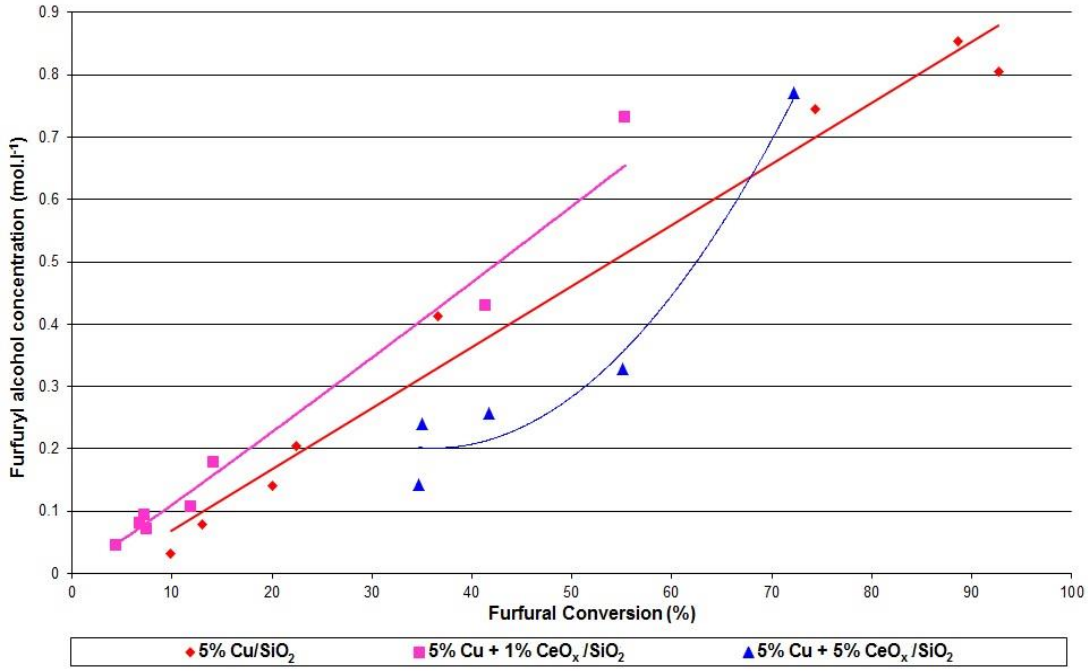

Figure 6.20 shows furfuryl alcohol concentration against furfural conversion and indicates how selective the catalysts were towards the formation of the unsaturated alcohol product. At a given conversion, the catalyst that exhibited the highest furfuryl alcohol concentration was the most selective and inversely at that same conversion, the catalyst that exhibited the lowest furfuryl alcohol concentration was the least selective. In this case, 5% Cu + 1% CeO_x/SiO_2 appeared to be the most selective catalyst, followed by 5% Cu/SiO_2 and 5% Cu + 5% CeO_x/SiO_2 was the least selective.

Figure 6.19 shows furfural conversion against time on stream and all catalysts showed deactivation as furfural conversion decreased with time on stream. 5% Cu + 5% CeO_x/SiO_2 showed the slowest deactivation post-reaction analysis was used to identify the cause and extent of catalyst deactivation.

Table 6.10 BET measurements pre- and post-reaction

Catalyst	BET				Single Point	
	Surface area (m^2g^{-1})		Average pore Diameter (nm)		Pore volume (cm^3g^{-1})	
5% Cu/SiO_2	236	**128**	13.9	**12.6**	0.82	**0.40**
10% Cu/SiO_2	235	**90**	13.1	**12.2**	0.77	**0.28**
5% Cu + 1% CeO_x/SiO_2	232	**224**	14.9	**14.1**	0.87	**0.70**
5% Cu + 5% CeO_x/SiO_2	215	**126**	14.5	**13.7**	0.78	**0.43**
10% Cu + 5% CeO_x/SiO_2	154	**150**	13.2	**13.8**	0.51	**0.52**

Table 6.10 shows that all catalysts exhibited a reduction in surface area and pore volume with 10% Cu/SiO_2 showing over 60% reduction in surface area and pore volume. Contrastingly, however 10% Cu + 5% CeO_x/SiO_2 showed only a slight reduction in surface area and 50 h on stream and little effect on the pore volume or diameter. Additionally, where 5% Cu/SiO_2 and 5% Cu + 5% CeO_x/SiO_2 exhibited a similar reduction in both surface area and pore volume, 5% Cu + 1% CeO_x/SiO_2 retained much of its surface area, pore diameter and pore volume.

The post-reaction XRD pattern for 5% Cu + 1% CeO_x/SiO_2 showed a peak at 43°corresponding to Cu which was less intense than the peak observed for the reduced sample. The Scherrer equation was used to calculate the average Cu crystallite size for reduced and post-reaction samples of Cu and Cu-CeO_x catalysts and the results are shown in table 6.11.

Table 6.11 Average crystallite sizes from XRD

Catalyst	Average crystallite size (nm)	
	Cu (reduced)	Cu (post-reaction)
5% Cu/SiO_2	18.3	11.8
5% Cu + 1% CeO_x/SiO_2	14	8.3
5% Cu + 5% CeO_x/SiO_2	40.5	172.8
10% Cu + 5% CeO_x/SiO_2	n.m.	9.3

The table shows that post-reaction Cu crystal sizes are slightly smaller than Cu crystals present after reduction of 5% Cu/SiO_2 and 5% Cu + 1% CeO_x/SiO_2. 5% Cu + 5% CeO_x/SiO_2 however, shows much larger Cu crystals post-reaction which is indicative of sintering and the most likely cause of catalyst deactivation.

Post-reaction TPD of 5% Cu + 5% CeO_x/SiO_2 shows a large weight loss at 420°C and almost 9% of the original sample weight was lost during TPD. Mass spectrometry results are shown in figure 6.21.

Figure 6.21 Mass spectrometry results from TPD of 5% Cu + 5% CeO_x/SiO_2

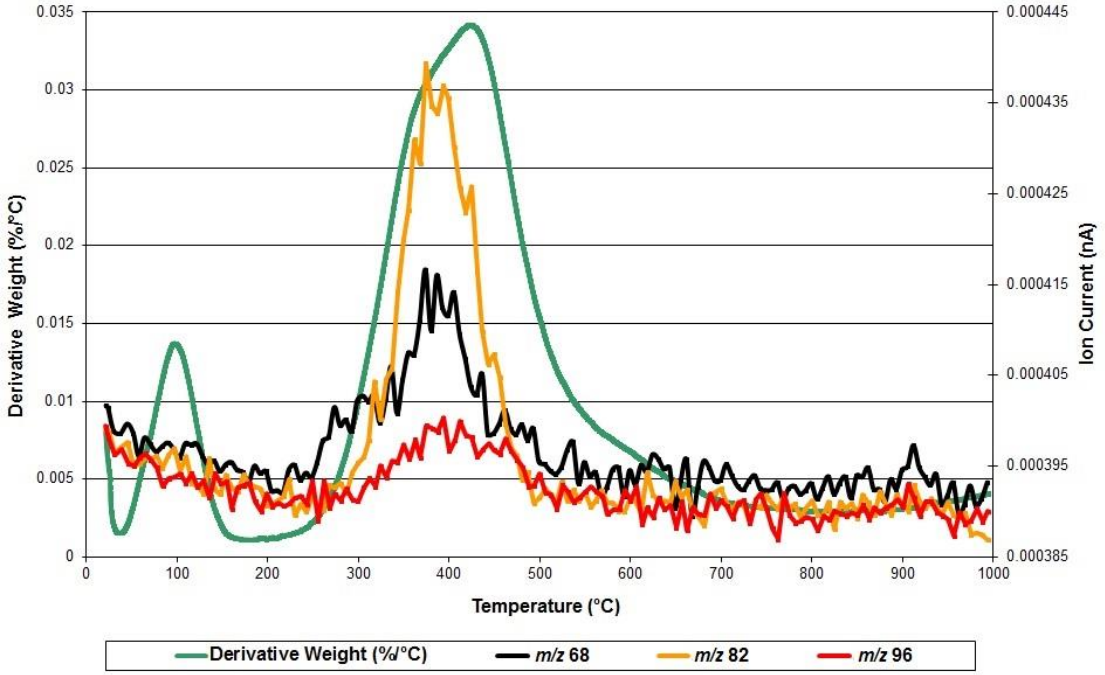

Evolution of *m/z* 96 corresponding to furfural, *m/z* 82 corresponding to 2-methylfuran and *m/z* 68 corresponding to furan were detected at 420°C. Post-reaction TPD of 5% Cu + 1% CeO_x/SiO_2 also showed a 5% weight loss at 420°C corresponding to desorption of *m/z* 68, 82, 96, suggesting that catalyst deactivation was the result of furfural and by-products which poisoned the catalyst surface.

Silica supported copper catalysts have been shown to be selective towards furfuryl alcohol and 1% CeO_x was found to enhance the selectivity. 5% CeO_x was found to reduce the selectivity of the catalyst possibly by the blocking Cu active sites. Previous studies have shown an optimum CeO_x content promotes activity and more than this has a detrimental impact on the selectivity of the catalyst. 5% Cu + 5% CeO_x/SiO_2 catalyst showed a slow deactivation and post-reaction XRD suggested sintering was the cause of deactivation. TPD of 5% Cu + 1% CeO_x/SiO_2 showed desorption of furfural, 2-methylfuran and furan suggesting that the catalyst was poisoned causing deactivation.

6.1.4 Palladium promoter

Co-impregnation of Cariact Q10 silica was used to prepare a 10% Cu + 5% CeO_x + 0.05% Pd/SiO_2 catalyst using a solution of the corresponding metal nitrate salts. BET surface area measurements for the silica support and the resulting supported copper catalysts are shown in table 6.12.

Table 6.12 BET measurements for Cariact Q10 silica and 10% Cu catalysts

Catalyst	BET		Single Point
	Surface area (m^2g^{-1})	Average pore diameter (nm)	Pore volume (cm^3g^{-1})
Cariact Q10 silica	276	14.6	1.01
10% Cu/SiO_2	235	13.1	0.77
10% Cu + 5% CeO_x/SiO_2	154	13.2	0.51
10% Cu+ 5% CeO_x + 0.05% Pd/SiO_2	190	14.5	0.69

Comparison of 10% Cu + 5% CeO_x/SiO_2 and 10% Cu + 5% CeO_x + 0.05% Pd/SiO_2 catalysts shows both an increased surface area and pore volume when Pd was present. TPO was used to investigate the effect of calcinations on the active phase of the catalyst and table 6.13 shows the theoretical and experimental weight losses for 10% Cu and Pd–promoted Cu catalysts.

Table 6.13 TPO weight Losses for Cu-Ce and Pd promoted Cu-Ce catalysts

Catalyst	Theoretical weight loss (%)	Experimental weight loss (%)
10% Cu + 5% CeO_x/SiO_2	22.50	22.77
10% Cu + 5% CeO_x + 0.05% Pd/SiO_2	22.55	24.23

The experimental weight loss for 10% Cu + 5% CeO_x/SiO_2 was very similar to the theoretical weight loss, however physisorbed water has been included in the experimental value so it is likely that not all of the nitrate precursor decomposed. For the 10% Cu + 5% CeO_x + 0.05% Pd/SiO_2 the experimental value was slightly higher than the theoretical which suggests that more of the nitrate precursor decomposed.

TPR was carried out using hydrogen and the resulting TPR profiles are shown in figure 6.22. For all samples, two reducing peaks were seen between 270-330°C which is in agreement with results reported by Shimokawabe *et al*. [139].

Figure 6.22 Effect of CeO_x and Pd on the reducibility of Cu catalysts

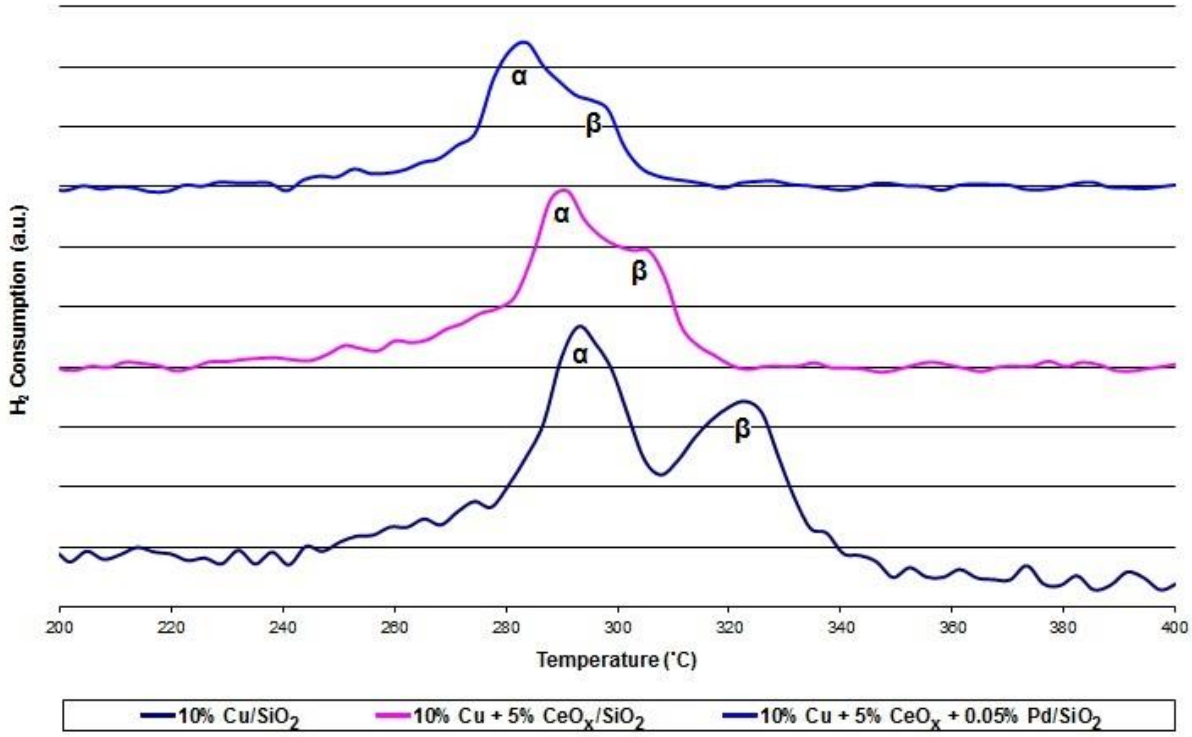

The figure shows the reduction peaks for 10% Cu/SiO_2, 10% Cu + 5% CeO_x/SiO_2 and 10% Cu + 5% CeO_x + 0.05% Pd/SiO_2. There were two well defined reduction peaks observed for 10% Cu/SiO_2 at 290°C and 325°C. Previous studies have reported two reduction peaks corresponding to the reduction of CuO particles at lower temperatures and the reduction of bulk CuO at higher temperatures. Here we can see that the α peak is more intense than the ß peak for each of the catalysts. However, when 5% CeO_x is incorporated the reduction peaks become less defined with greater overlap as a result of the ß peak shifting to a lower temperature of 315°C. With the further addition of 0.05% Pd both the α peak and the ß peak have shifted to a lower temperature and the intensity of the ß peak is greatly reduced. A higher intensity lower temperature reduction peak was also observed for Pd-promoted copper/zirconia catalysts by Lin *et al.* [140]. This has been attributed to hydrogen spillover from Pd to support and also in the interface between copper and support. Dissociation of hydrogen occurred on Pd and spread over the silica support and facilitated the reduction of the CuO species present [141]. Theoretical and experimental weight losses as a result of TPR are shown in table 6.14 and suggest that significant reduction of Cu and CeO_x have occurred.

Table 6.14 Weight loss through TPR

Catalyst	Theoretical loss of mass (%)	Experimental loss of mass (%)
10% Cu/SiO_2	2.83	4.49
10% Cu + 5% CeO_x/SiO_2	3.16	3.73
10% Cu + 5% CeO_x + 0.05% Pd/SiO_2	3.16	3.79

10% Cu + 5% CeO_x + 0.05% Pd/SiO_2 was tested to investigate if incorporating a small amount of palladium had an effect on activity or selectivity.

Figure 6.23 Product distribution using 10% Cu + 5% CeO_x/SiO_2 (±Pd) at 24 h TOS

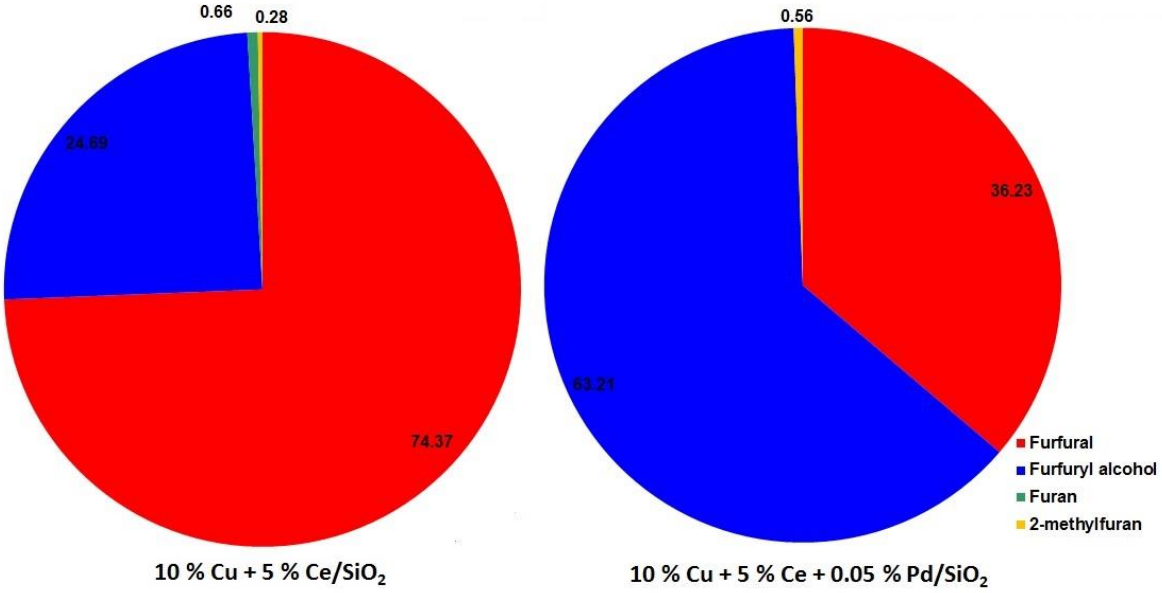

The results show a dramatic difference in furfural conversion when Pd is present with only half as much furfural converted over 10% Cu + 5% CeO_x/SiO_2 catalyst. The Pd-promoted catalyst was also more selective towards furfuryl alcohol as fewer and lower levels of by-products were formed. Seo and Chon observed enhanced conversion to furfuryl alcohol over Pd-CuY catalyst [142]. They proposed an interaction between Cu^{2+} and the furan ring inhibited hydrogenation of the aromatic ring and the role of Pd was activation of hydrogen.

The effect of catalyst deactivation was investigated by comparing BET measurements for pre-reaction and post-reaction samples as shown in table 6.15.

Table 6.15 BET measurements pre- and post-reaction

Catalyst	BET				Single Point	
	Surface area (m^2g^{-1})		Average pore Diameter (nm)		Pore volume (cm^3g^{-1})	
10% Cu/SiO_2	235	**90**	13.1	**12.2**	0.77	**0.28**
10% Cu + 5% CeO_x/SiO_2	154	**150**	13.2	**13.8**	0.51	**0.52**
10% Cu+ 5% CeO_x + 0.05% Pd/SiO_2	190	**152**	14.8	**13.5**	0.69	**0.53**

The inclusion of Pd promoter did not however improve the post-reaction BET measurements as 10% Cu + 5% CeO_x + 0.05% Pd/SiO_2 showed a 20% reduction of surface area whereas the Cu-CeO_x catalyst without Pd showed only a 2.5% reduction. TPO of post-reaction samples showed evolutions of *m/z* 44 corresponding to CO2 formed as a result of combustion of carbonaceous species on the surface of the catalyst. No water was detected for either catalyst and ~25% of the original sample weight was lost for both catalysts. Therefore, the presence of Pd provided little improvement to the lifetime of the catalyst.

Incorporation of a palladium promoter was found to enhance the activity and selectivity of the catalyst as it activated hydrogen allowing for more facile hydrogenation of the carbonyl group. This catalyst rapidly deactivated through carbon laydown.

6.1.5 Commercial copper-chrome catalyst (Cu1132)

The preparation route for Cu1132 is unknown and its exact composition is not clear however the type of catalyst suggests that it may have been prepared by co-precipitation instead of impregnation.

Table 6.16 BET measurements for 5% Cu/SiO_2 and Cu1132

Catalyst	BET		Single Point
	Surface area (m^2g^{-1})	Average pore diameter (nm)	Pore volume (cm^3g^{-1})
5% Cu/SiO_2	236	13.9	0.82
Cu1132	45	8.8	0.10

As expected there is a significant difference in BET surface area, pore volume and diameter between 5% Cu/SiO_2 and the commercial copper-chrome catalyst (table 6.16). TGA was carried out to try to determine the effect of pre-treatment conditions on the Cu1132. TPO showed one main endothermic weight loss at 850°C and initially this was thought to be due to the reduction of Cr present. To investigate whether thermal treatment had an effect on the catalyst, TPD using argon was carried out and the results are shown in figure 6.24.

Figure 6.24 Pre-reaction TPD of Cu1132

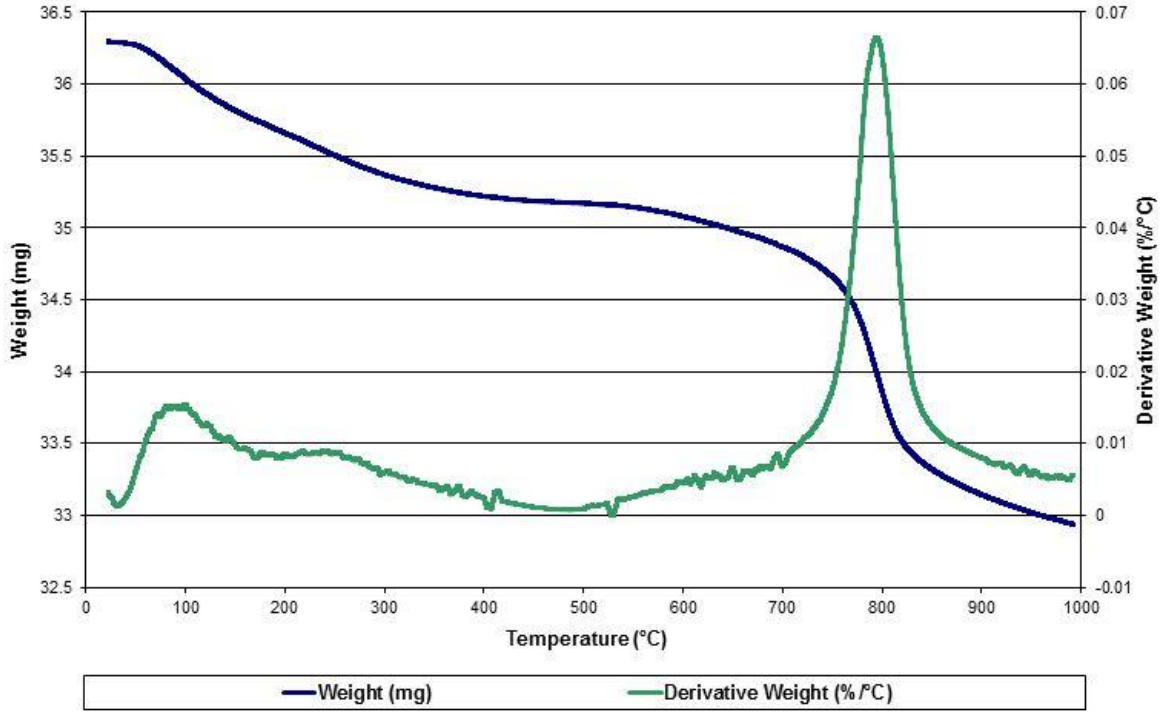

Thermal treatment of Cu1132 in argon shows similar weight Loss peaks at 100˚C and ~800˚C. Plech *et al*. observed a weight loss of 3.5% above 750˚C during thermal treatment of a copper-chromium oxide catalyst and reported the product of the reaction was $CuCrO_2$, observed by XRD [143]. An endothermic weight loss at 820˚C has been attributed to the reduction of Cu^{2+} to Cu^{+} and the following reaction proposed [144]:

$$CuO + CuCr_2O_4 \rightarrow 2CuCrO_2 + Cu_2O + \tfrac{1}{2}O_2$$

The results obtained for Cu1132 correlate well with previous observations as the sample lost ~4% of its original weight above 750˚C and mass spectrometry detected *m*/*z* 16 corresponding to the evolution of oxygen. Unfortunately, XRD analysis of this commercial catalyst was not permitted and so the presence of $CuCrO_2$ or CuO_2 could not be confirmed.

TPR of Cu1132 was conducted from room temperature to 1000˚C as reduction was incomplete at 500˚C. Two weight losses were observed; an endothermic loss at 100˚C and an exothermic loss at 365˚C, as shown in figure 6.26.

Figure 6.25 Pre-reaction TPR of Cu1132

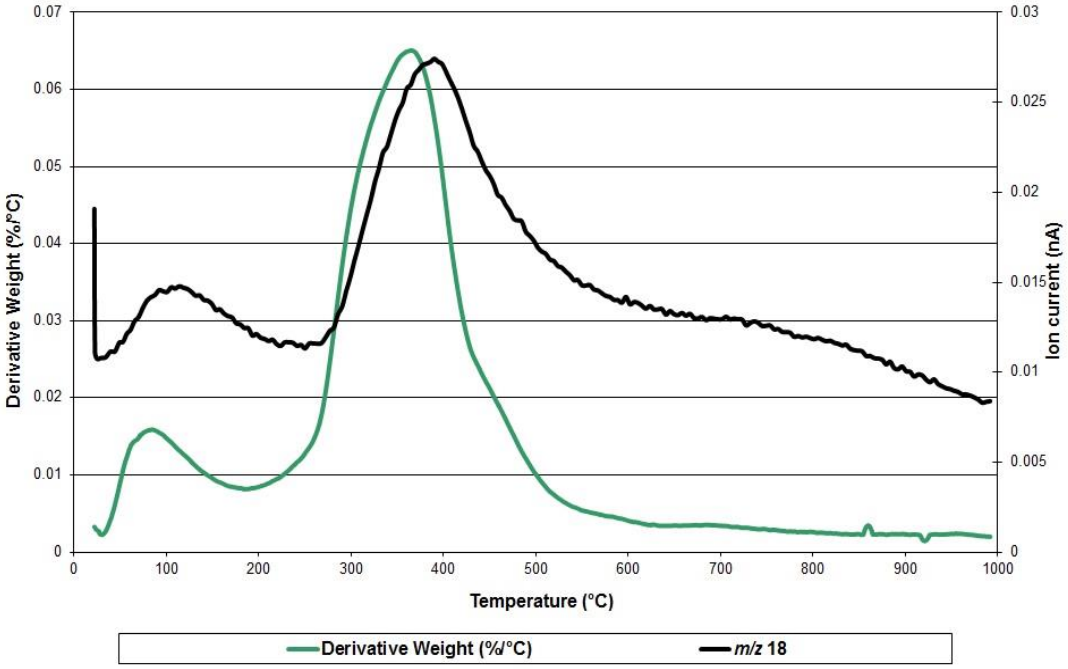

Mass spectrometry was used to try and determine species evolved at these temperatures. Figure 6.25 shows that *m/z* 18 was evolved at both temperatures and that hydrogen was consumed at 365°C suggesting a reduction took place. A two stage reduction of CuO to Cu was observed by Nagaraja *et al*. who studied Cu-MgO-Cr_2O_3 catalyst for furfuryl alcohol production [54]. Most of the oxidic copper present in the catalyst was reduced in the temperature range 250-290°C but complete reduction was achieved ~400-440°C. It was thought that the first temperature range corresponded to the reduction of CuO to Cu_2O and the higher temperature reduction corresponded to further reduction of Cu_2O to Cu. The reduction 10% CuO to Cu, as described in section 6.1.2 occurred ~300°C but without knowing the catalyst composition it is difficult to determine is the weight lost at 365°C corresponds to the formation of elemental Cu.

Cu1132 exhibited moderate activity but excellent selectivity to furfuryl alcohol with only trace levels of 2-methylfuran produced as shown in figure 6.26.

Figure 6.26 Product distribution for 5% Cu/SiO_2 and Cu1132 at 25 h on stream

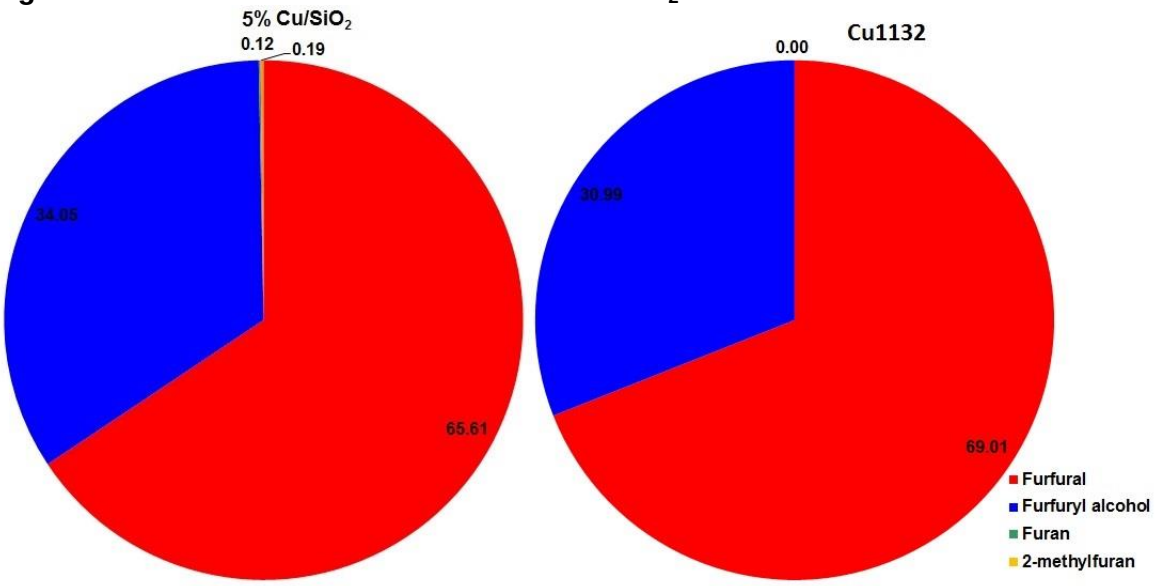

However, the activity of the catalyst decreased with time on stream and figure 6.27 shows the product distribution at 50 h on stream.

Figure 6.27 Product distribution for 5% Cu/SiO_2 and Cu1132 at 50 h on stream

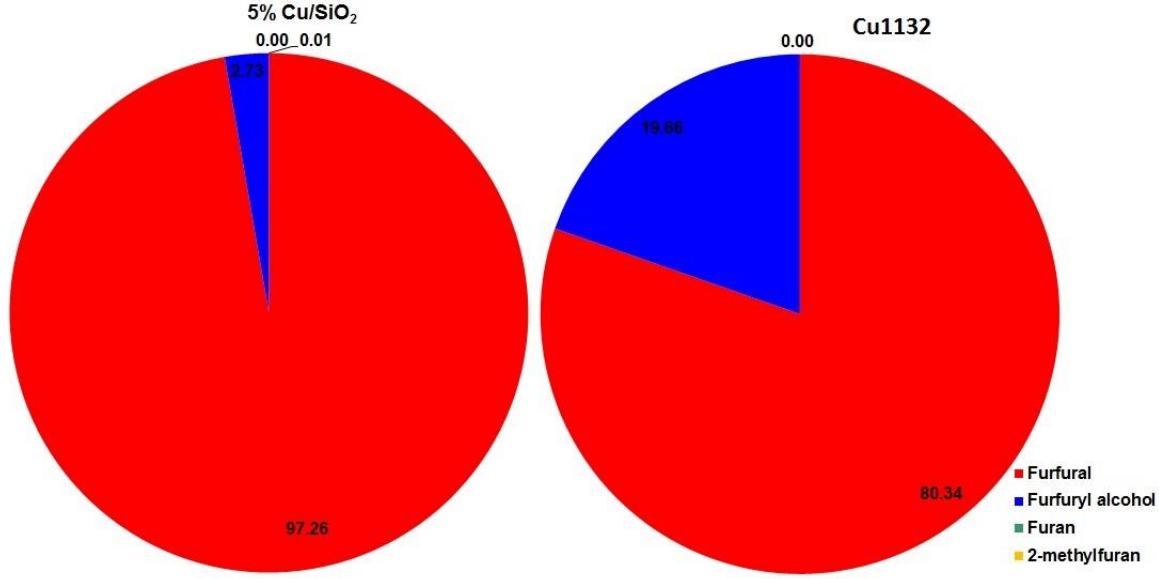

Controversy exists over the type of copper species acting as active sites for certain hydrogenation reactions with some reports that only Cu^+ and some that both Cu^+ and Cu act as active sites [39,42]. A Langmuir-Hinshelwood model [42] suggested either one type of site and competitive adsorption of furfural and hydrogen or the presence of two different sites, one for each reactant. It has been proposed that the presence of both Cu^+ and Cu is required for optimum selectivity to furfuryl alcohol [14]. From pre-reaction characterisation results

the presence of Cu^+ and Cu could not be confirmed but it is feasible that these species are present in Cu1132.

Severe deactivation of the copper chromite catalyst used for vapour-phase hydrogenation of furfural has been reported by others [34]. Several possible mechanisms have been proposed, such as (a) loss of the active Cu^+ species by reduction, (b) Cu Particle sintering, and (c) active Cu site coverage by coke or adsorbed reactants/products. Therefore post-reaction characterisation of the catalyst was carried out to try and identify the cause and extent of deactivation. Table 6.17 shows a comparison between pre-reaction and post-reaction surface areas for 5% Cu/SiO_2 and Cu1132.

Table 6.17 BET measurements for pre- and post-reaction 5% Cu/SiO_2 and Cu1132

Catalyst	BET				Single Point	
	Surface area (m^2g^{-1})		Average pore Diameter (nm)		Pore volume (cm^3g^{-1})	
5% Cu/SiO_2	236	**128**	13.9	**12.6**	0.82	**0.40**
Cu1132	45	**<1**	8.8	**/**	0.10	**0.02**

Cu1132, with the lowest measured BET surface area, was difficult to analyse post-reaction. It is thought that all of the pores had become blocked making surface area measurements difficult and the results very low. TGA and mass spectrometry was used to try to identify any species left on the catalyst surface as a result of the reaction.

TPO of a post-reaction sample of Cu1132 showed two main weight losses and mass spectrometry showed the evolution of water and CO_2 as shown in figure 6.28.

Figure 6.28 Post-reaction TPO and mass spectrometry data for Cu1132

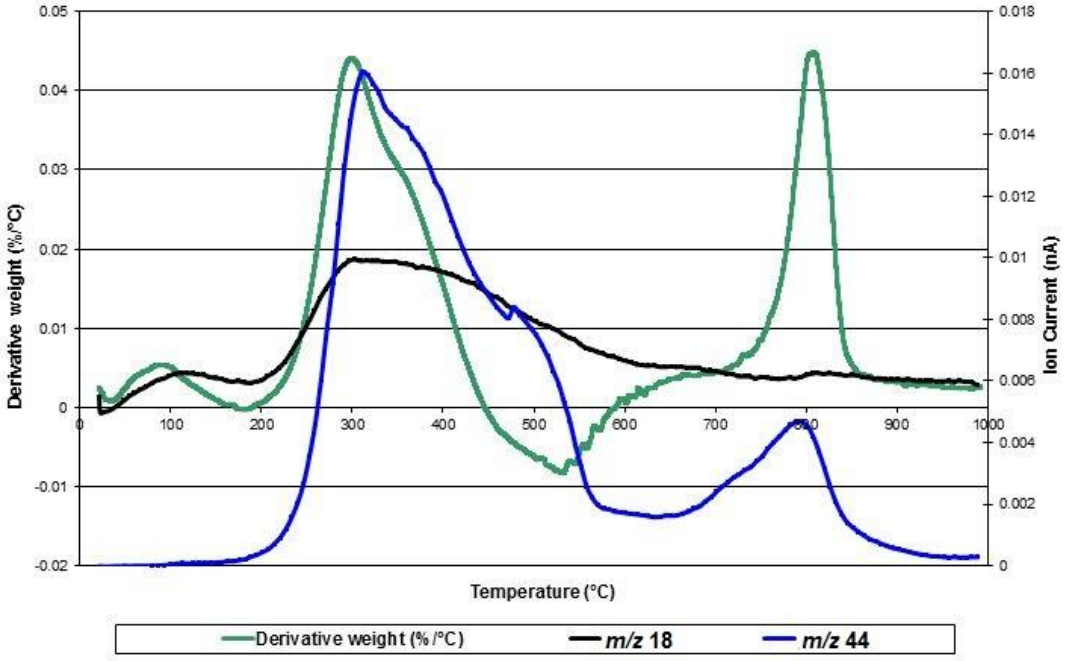

These results are characteristic of coke formation and correlate well with previous studies of [120,121]. It is thought that the first weight lost corresponds to the combustion of soft coke which comprises mainly high-molecular weight aliphatic oligomers. The higher temperature weight loss corresponds to the combustion of hard coke or bulkier carbonaceous compounds [121].

Additionally, post-reaction TPD of a sample showed the evolution of *m*/*z* 68 around 300°C corresponding to furan which may have acted as a precursor to coke formation. Unlike all of the other catalysts in this study, Cu1132 showed a greater weight Loss through post-reaction TPD (11.3%) rather than TPO (8.3%). The reason for this is there is a weight gain during TPO due to reoxidation of the catalyst. This means that the overall weight loss is apparently much less than the TPD whereas in fact it could easily be more as the weight gain cannot be accurately measured because of simultaneous weight loss.

Cu1132, a commercial catalyst used for the hydrogenation of furfural to furfuryl alcohol showed excellent selectivity (almost 100%) to furfuryl alcohol with only traces of 2-methylfuran detected. As the composition of this catalyst was unknown and XRD analysis was not permitted, identification of the active species was difficult however it is likely that some Cu^{+} and Cu was present on the catalyst as a result of calcination and reduction. Deactivation of the catalyst

occurred through the formation of coke which blocked the pores and showed a reduction in activity and post-reaction analysis showed the presence of aliphatic and aromatic coke.

6.1.6 Hydrogenation of furfural

In general, supported ceria proved to be an inactive catalyst for the hydrogenation of furfural to furfuryl alcohol and instead was active for the decarbonylation reaction producing furan. Furan on the surface may have acted as a precursor for coke formation which clogged the catalyst pores inhibiting any further reaction.

Silica supported copper catalysts proved to be active and selective catalysts for the hydrogenation of furfural to furfuryl alcohol. Calcination caused decomposition of the nitrate precursor to form CuO which was subsequently reduced to Cu prior to reaction. The higher the copper loading the greater the furfural conversion as more Cu sites were present with both catalysts achieving 98% selectivity for furfuryl alcohol. However catalyst deactivation was observed and post-reaction characterisation showed a dramatic reduction in surface area and pore volume and TPO confirmed that there was significant carbon laydown as result of the reaction.

Promotion of copper catalysts using 1% CeO_x was found to enhance the selectivity towards furfuryl alcohol. 5% CeO_x was found to reduce the selectivity of the catalyst possibly by the blocking Cu active sites. 5% Cu + 5% CeO_x/SiO_2 catalyst showed a slow deactivation and post-reaction XRD suggested sintering was the cause of deactivation. TPD of 5% Cu + 1% CeO_x/SiO_2 showed desorption of furfural, 2-methylfuran and furan suggesting that the catalyst was poisoned causing deactivation.

Incorporation of a palladium promoter was found to enhance the activity and selectivity of the catalyst as it activated hydrogen allowing for more facile hydrogenation of the carbonyl group. This catalyst rapidly deactivated through carbon laydown.

The commercial catalyst, Cu1132, exhibited moderate activity but excellent selectivity (almost 100%) and deactivated slowly over 50 h compared to 5% Cu/SiO_2. From pre-reaction characterisation, it is possible that some Cu^+ and Cu was present which may have improved selectivity to furfuryl alcohol. Through post-reaction analysis the cause of deactivation was formation of soft and hard coke which blocked pores and reduced the activity.

6.2 Liquid-phase hydrogenation

The results obtained from Liquid-phase hydrogenation reactions will be discussed in this chapter. Catalyst properties and reaction parameters were found to significantly affect the rate of hydrogenation and product distribution.

6.2.1 4-NAP hydrogenation

The aim of this project was to study the hydrogenation of 4-nitroacetophenone (4-NAP) using different Rh/SiO_2 catalysts and a range of reaction conditions. It was observed that hydrogenation of the $-NO_2$ group to form 4-aminoacetophenone (4-AAP) took place before the hydrogenation of the carbonyl group to give 1-(4-aminophenol)ethanol (4-APE). Further hydrogenation of 4-APE Led to the production of 4-ethylaniline (4-EA), 4-ethylcyclohexylamine (4-ECHA) and ring saturation produced 1-(4-aminocyclohexyl)ethanol (4-ACHE) as shown in figure 6.29.

Figure 6.29 Hydrogenation of 4-NAP

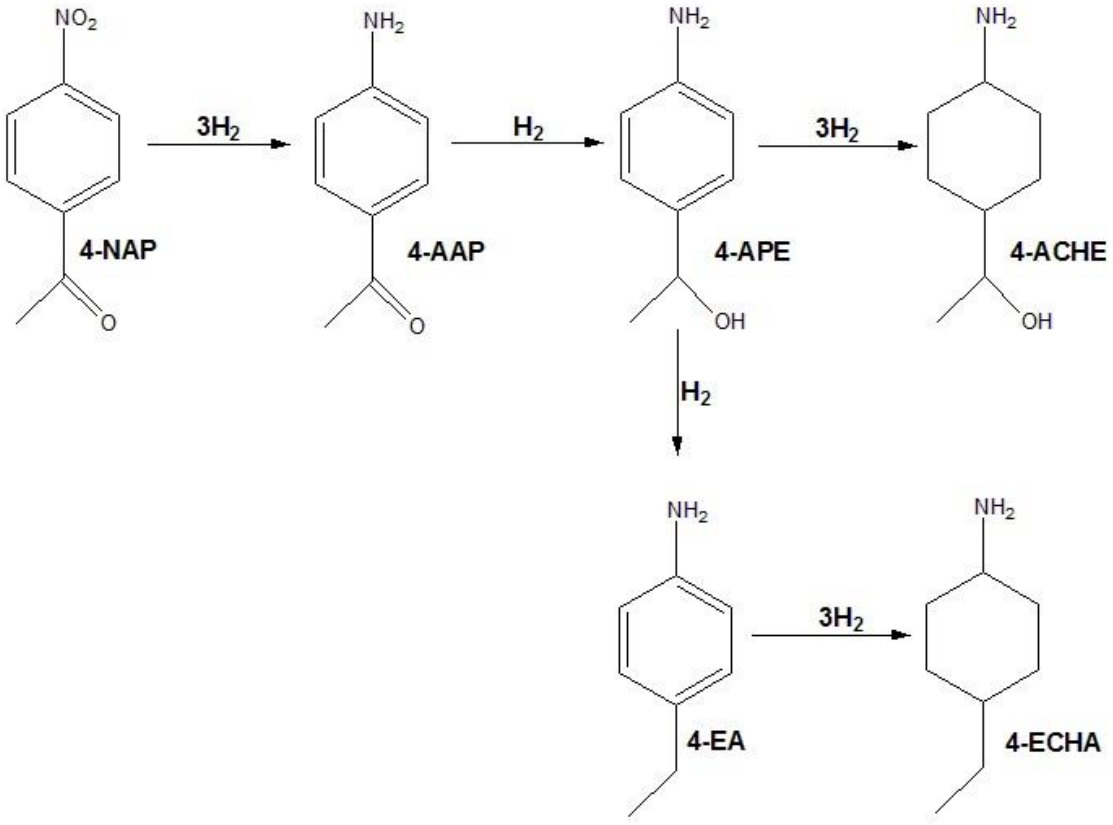

The consecutive hydrogenation of the functional groups followed the order NO_2 >> C=O > Ph > OH, and was independent of catalyst choice or reaction

conditions. It was observed that the hydrogenation of the carbonyl group was an order of magnitude slower than that of the nitro group, and the hydrogenation of the phenyl ring or the OH group was at least a factor of 2 slower than that of the carbonyl group as shown in table 6.18.

Table 6.18 Consecutive hydrogenation rate constants

Reaction	Rate constant (min^{-1})
4-NAP → 4-AAP	1.188×10^{-1}
4-AAP → 4-APE	1.61×10^{-2}
4-APE → 4-ACHE /4-EA	5.9×10^{-3}

Hydrogenation of the nitro group occurs readily due to its strong electronegativity, with two electron deficient oxygen atoms bonded to a partially positive nitrogen atom. Whereas, hydrogenation of 4-AAP is more complex due to the potential for competitive hydrogenation between the phenyl and carbonyl groups. Hydrogenation of acetophenone has shown that the products formed are related to the catalyst used. For example, over Pd-based catalysts reduction of the carbonyl group occurs followed by hydrogenation of the OH [93]. Whereas, when a Pt-based catalyst is used, reduction of the phenyl group can occur and lead to ring saturation products [26]. Likewise, for substituted acetophenones the choice of active metal was found and more prominent geometric and steric effects were observed for metals with high d-electron densities [26]. Examination of the reaction profiles for 4-NAP hydrogenation reveals that no 4-APE is formed until virtually all the 4-NAP has reacted. The nitro group becomes strongly adsorbed to the catalyst surface and is reduced to form the amine group. The strength of the interaction of the amine group is much lower than the strength of adsorption of the carbonyl group as hydrogenation only occurs if the molecule is oriented to allow C=O access to the surface. In the competitive hydrogenation of acetophenone and meta-substituted acetophenones, the rate was found to be higher for the meta-

substituted molecule as it was more strongly adsorbed to the catalyst than acetophenone [26]. The electron-withdrawing or electron-donating properties of substituents have been shown to affect the strength of the interaction with the catalyst [26]. Once the nitro group has been reduced, the electron-donating properties of the amine group attenuates the strength of adsorption of this group to the surface. Whereas, the electron-withdrawing properties of the carbonyl group means it becomes more strongly bound to the catalyst surface.

Reactions were conducted at temperatures in the range 30-60°C and kinetic analysis showed an activation energy of 48 ± 6 kJ mol^{-1} for the reduction of the nitro group. This result was in good agreement with the activation energy determined for 3-NAP hydrogenation (44 kJ mol^{-1}) [103]. This suggests that the position of the aceto-group does not influence the strength of adsorption of the nitro group. A Lower value of ~35 kJ mol^{-1} has been reported using a palladium catalyst [96] as may be expected when using a different metal. Hydrogenation of substituted nitrobenzenes using rhodium catalysts has also shown similar activation energies between 53 and 57 kJ mol^{-1} [144] again suggesting that other groups do not affect the energetics of nitro adsorption.

The initial concentration of 4-NAP did not significantly affect the rate of reaction and therefore a zero order dependence with respect to 4-NAP concentration was determined. The reaction order in respect to hydrogen concentration for 4-NAP hydrogenation was calculated as first order. These orders suggest strong adsorption of 4-NAP and weak adsorption of hydrogen.

Using deuterium rather than hydrogen resulted in an overall reduction in rate of reaction and a reduced conversion to both aminoacetophenone and final hydrogenation products. Switching from hydrogen to deuterium represents a 100% increase in mass, therefore the isotopic rate change can be quite pronounced. Since deuterium is a heavier atom this leads to a lower vibration frequency of the chemical bonds or, in terms of quantum mechanics, lower zero-point energy. This means that more energy is required to break the bond, which results in higher activation energy for bond cleavage and in turn reduced the rate of reaction. When deuterium was used instead of hydrogen, the rate of 4-NAP hydrogenation was much lower and a KIE equal to 3 was measured. This result is indicative of a primary KIE in which hydrogen is actively involved in the

rate determining step. This KIE correlates well with the magnitude of the KIE found for nitrobenzene hydrogenation (~2) [146]. A much lower KIE (~1.5) was observed for the hydrogenation of 4-AAP after 4-NAP hydrogenation which suggests hydrogen has less of an effect on the rate determining step.

A series of Rh/SiO_2 catalysts, shown in table 5.1, were tested and although they had very similar metal loadings, the rates of reaction differed for each catalyst. Testing of catalyst M01078 sieved to give two particle size ranges (450-250 μm and 125-75 μm) were tested to first establish if the catalyst particle size had an effect on the activity of the catalyst. As both catalyst samples exhibited the same level of activity, it was concluded that particle size does not have a significant effect on the rate of reaction.

An antipathetic relationship with respect to crystallite size was observed as the larger the crystallite the higher the TOF as shown in figure 6.30.

Figure 6.30 TOF for reduction of nitro and carbonyl functions against crystallite size

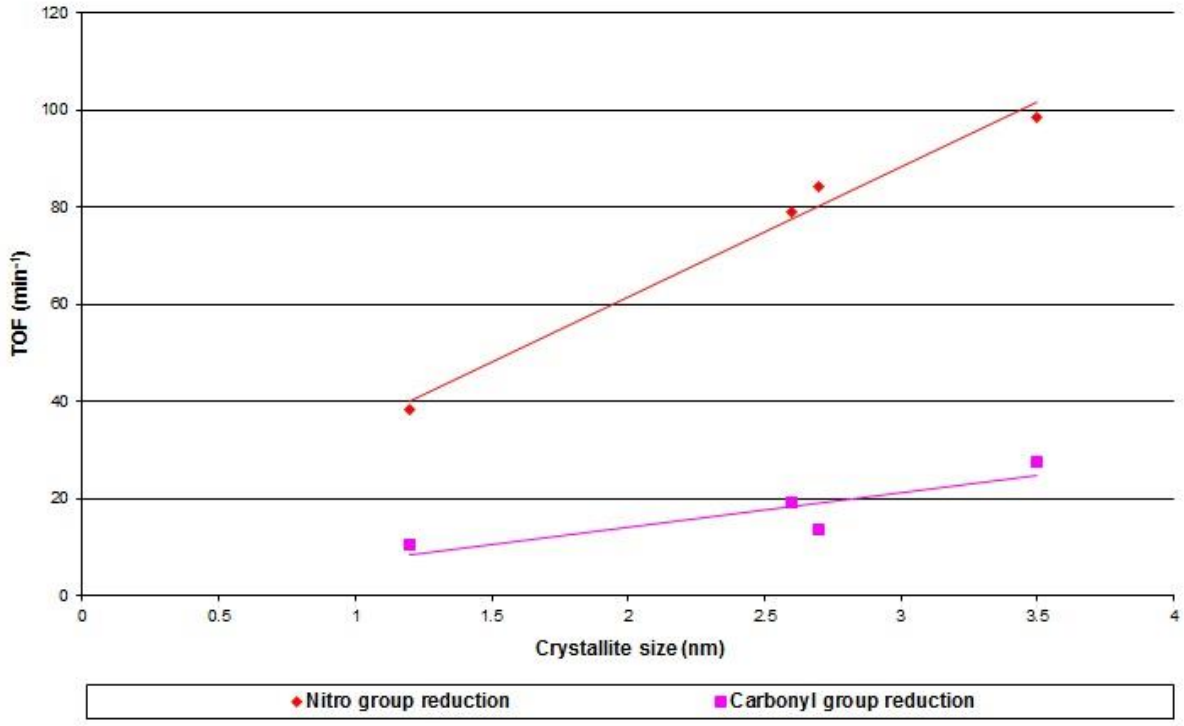

A similar but weaker effect was observed for 3-NAP hydrogenation over the same catalysts [103]. An antipathetic particle size effect has been observed for nitrobenzene hydrogenation over Pd/C catalysts [146], and this behaviour is consistent with the hydrogenation of p-chloronitrobenzene to p-chloroaniline

over Pt/Al_2O_3 catalysts [147]. The hydrogenation of p-toluidine and 4-tert-butylaniline over Rh/SiO_2 also showed a decrease in catalyst activity with an increase in metal dispersion [98,148]. Rhodium has a face-centred cubic (fcc) closed packed arrangement so as the size of the crystal increases, the number of face surface atoms increases at the expense of edge and corner sites [26]. This result suggests that the hydrogenation reaction took place on the plane face surface opposed to edge or corner sites.

For the hydrogenation of the nitro group, geometrically a plane face could accommodate the various components and this is consistent with an antipathetic particle size effect. However, many crystallites will have defects and will not have complete crystal structures hence the change in the ratio of face:edge:corner atoms is not straightforward. In addition, as the size of a metal particle decreases the electronic structure of the metal changes [20]. Recently [21], it has been proposed that below 10 nm the electronic factor will have the largest effect on a surface sensitive reaction rather than the geometric factor and in this study the metal crystallites are well below 10 nm. Such changes in the electronic structure will influence the strength of reactant bonding and so changes in reactivity may be expected. This has been demonstrated in 4-NAP hydrogenation in the presence of 4-methylcyclohexylamine; a molecule known to bind strongly to rhodium [98]. The rate of 4-NAP hydrogenation increased due to a weakening of the metal to 4-NAP bond. In the hydrogenation of nitrobenzene over Pd/C [145] the particle size effect was solvent dependent suggesting that the electronic effect may be the dominant feature.

The particle size effect on carbonyl reduction was smaller than that observed for nitro group reduction. Hydrogenation of cinnamaldehyde showed that larger metal particles were found to give a higher selectivity to cinnamyl alcohol and this was attributed to steric effects [22]. The phenyl group present hinders the close approach of the C=C bonds to the surface of a large particle so the molecule is tilted with the C=O bond closer to the surface which means it is more easily activated [24]. For smaller particles, the approach of the phenyl group is not hindered and therefore more easily hydrogenated resulting in a lower selectivity to cinnamyl alcohol. This suggests that a geometric factor has the greatest effect on the rate of 4-AAP hydrogenation.

Complete conversion of 4-NAP was achieved in only 20 min however, complete conversion of 3-NAP using the same catalyst reportedly took 90 min [103]. The rate of hydrogenation of 4-NAP has been reported to be faster than the hydrogenation of 3-NAP and 2-NAP [149]. This could be due to electron-withdrawing properties of the functional groups and their relative positions. In a previous study of hydrogenation of nitroacetophenones using 1% Pd/Al_2O_3, the meta-isomer exhibited the fastest rate as the cooperative position of the nitro and carbonyl groups facilitated hydrogenation [96]. Whereas, in a study of 3-NAP hydrogenation over an Ir/ZrO_2 catalyst, the carbonyl group competed with the hydrogenation of the nitro group which had a deactivating effect on the reaction [150]. In this study, over rhodium catalysts there was no evidence of carbonyl hydrogenation in the presence of the nitro group. Through hydrogenation of the carbonyl group, 94% selectivity to 4-APE is achieved whereas a selectivity of only 80% for 3-APE was obtainable due to rapid conversion of 3-APE to 3-ACHE.

Deactivation of Rh/SiO_2 catalysts has been reported upon catalyst recycling for the hydrogenation of p-toluidine [97]. In this study, a second addition of 4-NAP was used to investigate any catalyst deactivation. As the catalyst exhibited a similar activity to that of a fresh sample, no catalyst deactivation was evident after this reaction time. Additionally, good mass balances were observed which is concurrent with the lack of catalyst deactivation. Upon second addition of 4-NAP, the same consecutive reaction was observed in that the nitro group was reduced prior to carbonyl reduction.

6.2.2 4-AAP hydrogenation

Reactions were carried out using 4-AAP as the main reactant to investigate the activity of the catalyst for carbonyl hydrogenation without a nitro group present. Table 6.19 shows the rate constants for the hydrogenation of 4-AAP as a single reactant and the rate constant calculated for the hydrogenation of 4-AAP following 4-NAP hydrogenation.

Table 6.19 Rate constants for 4-AAP reactions

Reactant	4-AAP	
	Single	After 4-NAP
k (min^{-1})	1.1×10^{-2}	2.3×10^{-2}

The table shows that the rate constant for 4-AAP hydrogenation after 4-NAP hydrogenation is double that found for the hydrogenation of 4-AAP as the main reactant. This is a remarkable effect as there is no 4-NAP in the system when 4-AAP is being hydrogenated. It is this enhancement in rate that allows the high selectivity to 4-APE, when 4-AAP was the main reactant the differential in rate of hydrogenation between 4-AAP and 4-APE was not sufficiently large to allow high selectivity to 4-APE. However, the rate enhancement seen for 4-AAP hydrogenation after 4-NAP hydrogenation allowed a high selectivity to 4-APE. A similar effect has been observed for the hydrogenation of 1-pentene following hydrogenation of 1-pentyne [151] as the rate was found to be faster by a factor of twenty compared to hydrogenation of 1-pentene as a single reactant. It was proposed that this rate enhancement was due to more facile hydrogen transfer as a result of carbon laydown [151]. In this study there was little evidence of carbon laydown as good mass balances were obtained. Nevertheless changes to the catalyst structure allowing an enhanced hydrogen concentration may be the cause of the rate increase as reactions involving deuterium showed a primary KIE in which hydrogen is actively involved in the rate determining step. Additionally, the order of reaction with respect to hydrogen was calculated to be first order showing that as the hydrogen concentration increases the rate of reaction increases. Recently, a study of allylbenzene hydrogenation over Rh/SiO_2 showed that the hydrogen concentration in the metal could be affected by hydrocarbon adsorption resulting in changes in reactivity [152]. Begley *et al.* showed that the adsorption of allylbenzene inhibited the fast diffusion of hydrogen to sub-surface which promoted isomerisation of internal alkenes rather than hydrogenation. Other studies have also compared Rh to Pd in its ability to adsorb hydrogen under certain conditions to form sub-surface hydrogen [153] and reconstruction of the surface through adsorption causing open diffusion channels to the sub-surface have been discussed [154].

For reactions where 4-AAP was the starting material, the activation energy for the reduction of the carbonyl group was calculated to be 48 ± 2 kJ $mol^{-1.}$ For the reduction of the carbonyl group after 4-NAP hydrogenation the activation energy was calculated to be 53 ± 8 kJ mol^{-1}. Considering the errors, these values cannot be considered significantly different and in a previous study the activation energy for hydrogenation of acetophenone was reported as ~50 kJ mol^{-1} [155]. This suggests that the presence of the amino group in the para position has little effect on the energetics of the carbonyl group hydrogenation. The KIE calculated for 4-AAP hydrogenation was lower than the KIE calculated for 4-NAP hydrogenation, at 1.6/1.2 which may suggest a mechanism involving an adsorbed enol form of 4-AAP as shown in figure 6.31.

Figure 6.31 Keto-enol tautomerisation

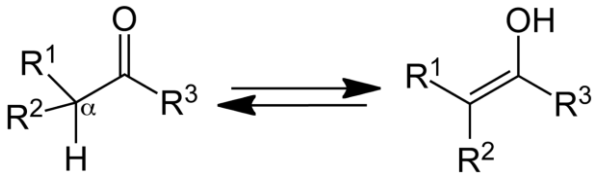

However, a study conducted by Bonnet *et al*. [156], using acetophenone-d^3, showed that hydrogenation over a Pt/Al_2O_3 catalyst proceeded through the keto-form and no significant keto-enol tautomerisation took place. A KIE value of 1.4 ± 2 obtained for 4-AAP hydrogenation is in keeping with the reported value for acetone hydrogenation over a platinum catalyst (~2) [157]. This has been interpreted as the addition of H/D to a π-adsorbed sp^2 hybridised C=O bond to form an sp^3 hybridised half-hydrogenated intermediate [157, 158].

6.2.3 Competitive hydrogenation

Competitive hydrogenation of 4-NAP and 4-AAP was investigated to determine the effect of 4-NAP on 4-AAP hydrogenation and vice versa in a competitive reaction as distinct from reactions involving a single reactant. Reactions were carried out using a 1:1 ratio at the same concentrations as the individual reactions and the rate constants are shown in table 6.20.

Table 6.20 Rate constants for 4-NAP and 4-AAP competitive hydrogenation

Reactant	4-NAP		4-AAP	
	Single	1:1 4-AAP	Single	1:1 4-NAP
k (min^{-1})	1.2×10^{-1}	1.25×10^{-1}	1.1×10^{-2}	1.0×10^{-2}

From the table it can be seen that the rate constant for the hydrogenation of 4-NAP was unchanged relative to 4-NAP hydrogenation in the absence of 4-AAP. Moreover, the rate constant for 4-AAP hydrogenation was also unchanged (within experimental variation) relative to 4-AAP as the sole reactant. On the basis of competition for space on the catalyst surface, a reduction in both rates would be expected; the antipathetic particle size effect observed for both 4-NAP and 4-AAP hydrogenation would suggest that both molecules would compete for the plane face surface of Rh crystallites, however the absence of a reduction in rate suggests that 4-NAP and 4-AAP are not competing for the same sites. Indeed although 4-AAP is present from the beginning of the reaction conversion does not take place until almost all of the 4-NAP has been converted which suggests that 4-NAP blocks 4-AAP hydrogenation.

Interestingly, the presence of 4-AAP in the reaction mix from the outset has an negative effect on the rate enhancement seen for 4-AAP hydrogenation after 4-NAP hydrogenation (1.1×10^{-2} min^{-1} c.f. 2.3×10^{-2} min^{-1}). This suggests that in a competitive reaction, the presence of 4-AAP during 4-NAP hydrogenation inhibits any changes to the catalyst that facilitates the rate enhancement. It is possible that adsorption of 4-AAP occurs on a site that does not facilitate hydrogenation yet may change the ability of the Rh to facilitate sub-surface hydrogen.

Aromatic amines, such as 4-AAP, are weak bases (pK_b 11.83) whereas alicyclic amines are much stronger bases (pK_b 3.42) and hence a much stronger interaction with the metal can be achieved. Therefore the addition of 4-methylcyclohexylamine (4-MCHA) was expected to hinder the hydrogenation of 4-NAP in line with previous studies, which reported it acting as a catalyst poison [159,160] as it becomes strongly adsorbed and blocks active sites [97,98].

However, instead the presence of 4-MCHA had a promoting effect on both 4-NAP and 4-AAP hydrogenation as shown by the rate constants in table 6.21.

Table 6.21 Rate constants for 4-NAP and 4-AAP hydrogenation with 4-MCHA

4-NAP (min^{-1})		4-AAP (min^{-1})			
Single	With 4-MCHA	Single	With 4-MCHA	After 4-NAP	After 4-NAP with 4-MCHA
1.2×10^{-1}	TF[a]	1.1×10^{-2}	2.1×10^{-2}	2.3×10^{-2}	2.7×10^{-2}

[a]reaction proceeded too fast to measure the rate

The presence of 4-MCHA was also found to promote the rate of 4-AAP hydrogenation following 4-NAP hydrogenation slightly. Rate enhancements due to the presence of an amine have been reported [161-163], and it was thought that the amine modified the surface through electron donation and so changed the surface-reactant bonding. In this study, it is clear that 4-NAP forms a strong bond to the surface as shown by the zero order kinetics and the inhibition of 4-AAP hydrogenation, so a reduction in the strength of 4-NAP adsorption would enhance the rate of 4-NAP hydrogenation. Hence a reduction in the strength of adsorption of the 4-NAP due to the alicyclic amine donating electron density to the rhodium is Likely to result in a rate enhancement

The rate hydrogenation of 4-AAP following 4-NAP hydrogenation was significantly enhanced compared to the rate of 4-AAP hydrogenation as a single reactant, however the rate of 4-AAP hydrogenation is equally enhanced in the presence of 4-MCHA. Given that 4-AAP is not strongly bound to the surface it is unlikely that weakening the carbonyl interaction would lead to an enhanced rate. It was proposed that the rate enhancement found for 4-AAP after 4-NAP hydrogenation was due to changes in hydrogen concentration in the rhodium facilitated by strong adsorption of 4-NAP resulting in structural changes which enabled routes for hydrogen to go sub-surface. Given that 4-MCHA is also strongly adsorbed it is not unreasonable to assume that it also causes a surface reconstruction that facilitates facile 4-AAP hydrogenation in a similar process to that of 4-NAP.

6.2.4 Hydrogenation of 4-nitroacetophenone

The hydrogenation of 4-nitroacetophenone has been investigated using a series of Rh/SiO_2 and different reaction conditions. Regardless of catalyst or conditions, the reduction of functional groups followed the order NO_2 >> C=O > Ph > OH. Reduction of the nitro group occurs readily due to its strong electronegativity with 4-NAP blocking the hydrogenation of 4-AAP.

As the rhodium crystallite increased the TOF for 4-NAP and 4-AAP also increased revealing an antipathetic relationship between crystallite size effect and TOF. The particle size effect on carbonyl reduction was smaller than that observed for nitro group reduction. As the carbonyl group was hydrogenated preferentially over the phenyl group it is thought that 4-AAP must approach the catalyst tilted with the C=O bond closer to the surface for reduction of this functional group to occur. This suggests that a geometric factor has the greatest effect on the rate of 4-AAP hydrogenation.

The rate constant for 4-AAP hydrogenation after 4-NAP hydrogenation is double that found for the hydrogenation of 4-AAP as the main reactant, and it is this enhancement in rate that gives the high selectivity to 4-APE. This rate enhancement may be due to a surface reconstruction allowing easier hydrogen transfer or the presence of sub-surface hydrogen as first order dependence for hydrogen was determined and a primary KIE showing that H_2 is actively involved in the rate determining step. In competitive reactions, it is thought that the presence of 4-AAP from the outset caused significant reduction to this rate enhancement by adsorbing to a site not used for hydrogenation yet changes the ability of Rh to facilitate sub-surface hydrogen.

The addition of the acyclic amine, 4-MCHA has a promoting effect on both 4-NAP and 4-AAP hydrogenation by modifying the surface of the catalyst by electron donation. Such a modification would reduce the surface-reactant bond strength and in this study, it is clear that 4-NAP forms a strong bond to the surface as shown by the zero order kinetics and the inhibition of 4-AAP hydrogenation, so a reduction in the strength of 4-NAP adsorption would enhance the rate of 4-NAP hydrogenation.

7 Conclusions

This study has successfully demonstrated that the control of selectivity during hydrogenation of multi-functional compounds can be modulated by a number of variables such as the interaction of the reactants and intermediates with the catalyst, particle size, promoters, steric factors and adsorption geometries.

For the selective hydrogenation of furfural to furfuryl alcohol, Cu/SiO_2 catalysts were investigated as an alternative to the traditional copper-chromite catalyst. Calcination caused decomposition of the nitrate precursor to form CuO which was subsequently reduced to Cu prior to reaction. The higher the copper loading the greater the furfural conversion as more Cu sites were present with both 5% Cu/SiO_2 and 10% Cu/SiO_2 achieving 98% selectivity for furfuryl alcohol. However catalyst deactivation was observed and post-reaction characterisation showed a dramatic reduction in surface area and pore volume and TPO confirmed that there was significant carbon Laydown as result of the reaction.

The addition of 1% CeO_x was found to enhance the selectivity of Cu/SiO_2 however 5% CeO_x blocked Cu sites and reduced activity. The presence of Ce^{3+} sites polarised the carbonyl bond in furfural promoting nucleophilic attack by hydrogen dissociated on Cu. Incorporation of a palladium promoter was found to enhance the activity and selectivity of the catalyst as it activated hydrogen allowing for easier hydrogenation of the carbonyl group.

Catalyst deactivation was observed for all catalysts and attributed mainly to the interaction of reactants and/or products with the catalyst. 5% CeO_x/SiO_2 was found to deactivate rapidly due to decarbonylation of furan by-product which led to coke formation, blocking catalyst pores. $Cu\text{-}CeO_x$ catalysts were found to deactivate by sintering, carbon laydown or by-products such as 2-methylfuran poisoning the catalyst.

The commercial copper-chrome catalyst (Cu1132) exhibited moderate activity but excellent selectivity (almost 100%) and deactivated slowly over 50 h compared to 5% Cu/SiO_2. From pre-reaction characterisation, it is possible that some Cu^+ and Cu was present, which may have improved selectivity to furfuryl

alcohol. Through post-reaction analysis the cause of deactivation was formation of soft and hard coke which blocked pores and reduced the activity.

As little literature exists surrounding the hydrogenation of 4-nitroacetophenone (4-NAP), a systematic study was carried out to investigate the effect of temperature, pressure, concentration and the presence of an aliphatic amine on the consecutive reaction. Reactions were conducted in the Liquid-phase, over a series of 2.5% Rh/SiO_2 catalysts, with both hydrogen and deuterium to ascertain the rate determining step.

Over Rh/SiO_2 catalysts the consecutive hydrogenation of 4-NAP was observed with functional group hydrogenation following the order of NO_2 >> C=O > Ph > OH. The nitro group was hydrogenated approximately an order of magnitude faster than the carbonyl group, while hydrogenation of either the phenyl ring or the alcohol function was a factor of two slower than carbonyl hydrogenation. This combination of kinetic controls allowed high selectivity to 4-AAP (99%) and 4-APE (94%) to be achieved at different times in the reaction.

Full kinetic analysis of the reaction system gave activation energies of ~48 kJ mol^{-1} for 4-NAP and 4-AAP hydrogenation, with orders of reaction of ~1 for hydrogen and a zero order dependence for 4-NAP.

The rate constant for 4-AAP hydrogenation after 4-NAP hydrogenation is double that found for the hydrogenation of 4-AAP as the main reactant and it is this enhancement in rate that allows the high selectivity to 4-APE. This rate enhancement may be due to a surface reconstruction allowing easier hydrogen transfer or the presence of sub-surface hydrogen as first order dependence for hydrogen was determined and a primary KIE showing that H_2 is actively involved in the rate determining step. In competitive reactions, it is thought that the presence of 4-AAP from the outset caused significant reduction to this rate enhancement by adsorbing to a site not used for hydrogenation yet changes the ability of Rh to facilitate sub-surface hydrogen.

The addition of the acyclic amine, 4-MCHA has a promoting effect on both 4-NAP and 4-AAP hydrogenation by modifying the surface of the catalyst by electron donation. Such a modification would reduce the surface-reactant bond strength

and in this study, it is clear that 4-NAP forms a strong bond to the surface as shown by the zero order kinetics and the inhibition of 4-AAP hydrogenation.

The rate hydrogenation of 4-AAP following 4-NAP hydrogenation was equally enhanced in the presence of 4-MCHA. As 4-AAP is not strongly bound to the surface it is unlikely that weakening the carbonyl interaction would lead to an enhanced rate. The rate enhancement observed for 4-AAP hydrogenation after 4-NAP hydrogenation has been attributed to changes in hydrogen concentration in the rhodium by strong adsorption of 4-NAP. As 4-MCHA is also strongly adsorbed it is not unreasonable to assume that it can also cause a reconstruction leading to easier 4-AAP hydrogenation by a similar process.

An antipathetic relationship of negative crystallite size effect was observed as the Larger the crystallite the higher the TOF for 4-NAP and 4-AAP. Rhodium crystals have a fcc arrangement, so as the size of the crystal increases, the number of face surface atoms increases at the expense of edge and corner sites [26]. This result suggests that the hydrogenation reaction took place on the plane face surface opposed to edge or corner sites.

The particle size effect on carbonyl reduction was smaller than that observed for nitro group reduction. As the carbonyl group was hydrogenated preferentially over the phenyl group it is thought that 4-AAP must approach the catalyst tilted with the C=O bond closer to the surface for reduction of this functional group to occur. This suggests that a geometric factor has the greatest effect on the rate of 4-AAP hydrogenation.

8 References

[1] P. Gallezot, D. Richard, Catal. Rev. -Sci. Eng., 40, (1998), 81

[2] P. Mäki-Arvela, J. Hájek, T. Salmi, D.Y. Murzin, Appl. Catal., A: Gen, 292 (2005), 1

[3] C. Mohr, H. Hofmeister, J. Radnik, P. Claus, J. Am. Chem. Soc., 125, (2003), 1905

[4] J. Jenck, J. E. Germain, J. Catal. 65, (1980), 141

[5] R. Hubaut, J. P. Bonnelle, M. Daage, J. Mol. Catal., 55, (1989), 170

[6] R. Hubaut, M. Daage, J. P. Bonnelle, Appl. Catal., 22, (1986), 231

[7] P. Rylander, 1967, *Catalytic Hydrogenation over Platinum Metals*, New York: Academic Press, p. 59

[8] H. Wei, C. Gomez, J. Liu, N. Guo, T. Wu, R. Lobo-Lapidus, C. L. Marshall, J. T. Miller, R. J. Meyer, J. Catal., 298, (2013), 18

[9] M. Englisch, A. Jentys, J. A. Lercher, J. Catal., 166, (1997), 25

[10] M. A. Vannice, Top. Catal., 4, (1997), 241

[11] A. Giroir-Fendler, 1988, *et al., Heterogeneous Catalysis and Fine Chemicals*, Amsterdam: Elsevier, p. 171

[12] T. B. L. W. Marinelli, S. Nabuurs, V. Ponec, J. Catal., 151, (1995), 431

[13] M. Englisch, V. S. Ranade, J. A. Lercher, J. Mol. Catal. A: Chem., 121, (1997), 69

[14] R. Rao, A. Dandekar, R. T. K. Baker, M. A. Vannice, J. Catal., 171, (1997), 406

[15] B. Bachiller-Baeza, I. Rodrigues-Ramos, A. Gerrero-Ruiz, Appl. Catal. A. Gen., 205, (2001), 227

[16] H. Liu, L. Ma, S. Shao, Z. Li, A. Wang, Y. Huand T. Zhang, Chin. J. Catal., 28, (2007), 1077

[17] D. Q. Yu, Y. Liu, Z. B. Wu, Catal Commun., 11, (2010), 788

[18] R.A.V. Santena, H.P.C.E. Kuipersa, Adv. Catal., 35 (1987), 265

[19] P. Claus, Top. Catal., 5 (1998), 51

[20] R. Hirschl, F. Delbecq, P. Sautet, J. Hafner, J. Catal., 217 (2003), 354

[21] D. Richard, P. Fouilloux, P. Gallezot, 1988, *Proceedings 9th International Congress on Cataysis*, Chemical Institute of Canada, p. 1074

[22] S. Galvagno, G. Capannelli, G. Neri, A. Donato, R. Pietropado, J. Mol. Catal, 64, (1991), 237

[23] Y. Nitta, K. Ueno, T. Imanaka, Appl. Catal., 56, (1989), 9

[24] A. Chambers, S.D. Jackson, D. Stirling, G. Webb, J. Catal., 168, (1997), 301

[25] C-S. Chen, H-W. Chen, W-H. Cheng, Appl. Catal. A. Gen., 248, (2003), 117

[26] M. Kajitani, N. Suzuki, T. Abe, Y. Kaneko, K. Kasuya, K. Takahashi, A. Sugimori, Bull. Chem. Soc. Jpn., 52, (1979), 2343

[27] D. Vargas-Hernandez, J. M. Rubio-Caballero, J. Santamaria-Gonzalez, R. Moreno-Tost, J. M. Merida-Robles, M. A. Perez-Cruz, A. Jimenez-Lopez, R. Hernandez-Huesca, P. Maireles-Torres, J. Mol. Catal. A., 383, (2014), 106

[28] X. Tong, Y. Ma, Y. Li, Appl. Catal. A. Gen., 385, (2010), 1

[29] M. E. Zakrzewska, E. Bogel-Łukasik, R. Bogel-Łukasik, Chem. Rev., 111, (2011), 397

[30] R. Karinen, K. Vilonen, M. Niemelä, ChemSusChem, 4, (2011), 1002

[31] J-P. Lange, E. van der Heide, J. van Buijtenen, R. Price, ChemSusChem, 5, (2012), 150

[32] C. Moreau, M. N. Belgacem, A. Gandini, Top. Catal., 27, (2004), 11

[33] J. Lewkowski, Arkivoc, 1, (2001), 17

[34] R-J. van Putten, J. C. van der Waal, E. de Jong, C. B. Rasrendra, H. J. Heeres, J. G. de Vries, Chem. Rev., 113, (2013), 1499

[35] K. Bauer, D. Garbe, 1985, *Common Fragrance and Flavour Materials*, Kyoto, Japan: VCH Publishers

[36] M. S. Li, W. Z. Ma, Hebai Ind. (1999), 6.

[37] B. M. Nagaraja, V. Siva Kumar, V. Shasikala, A. H. Padmasri, B. Sreedhar, B. David Raju, K. S. Rama Rao, Catal Commun., 4, (2003), 287

[38] J. Kijenski, P. Winiarek, T. Paryjczak, A. Lewicki, A. Mikolajska, Appl. Catal. A: Gen., 233, (2002), 171

[39] B. M. Nagaraja, A. H. Padmasri, B. David Raju, K. S. Rama Rao, J. Mol. Catal. A: Chem., 265, (2007), 90

[40] A. B. Merlo, V. Vetere, J. F. Ruggera, M. L. Casella, Cat. Comm., 10, (2009), 1665

[41] H. Y Zheng, Y. L. Zhua, B. T. Teng, Z. Q. Bai, C. H. Zhang, H. W. Xiang, Y. W. Li, J. Mol. Catal. A: Chem., 246, (2006), 18

[42] R. S. Rao, R. T. K. Baker, M. Vannice, Catal. Lett., 60, (1999), 51

[43] L. Baijun, L. Lianhai, W. Bingchun, C. Tianxi, K. Iwatani, Appl. Catal. A: Gen., 171, (1998), 117

[44] D. Liu, D. Zemlyanov, T. Wu, R. J. Lobo-Lapidus, J. A. Dumesic, J. T. Miller, C. L. Marshall, J. Catal., 299, (2013), 336

[45] US 2094975

[46] B.H. Wojcik, J. Ind. Eng. Chem. Res., 40, (1948), 210

[47] US 4302397

[48] US 4261905

[49] S. Sitthisa, T. Sooknoi, Y. Ma, P.B. Balbuena, D. E. Resasco, J. Catal., 277, (2011), 1

[50] S. Sitthisa, D.E. Resasco, Catal. Lett., 141, (2011), 784

[51] V. Vetere, A.B. Merlo, J.F. Ruggera, M. L. Casella, J. Braz. Chem. Soc., 21, (2010), 914

[52] W. Huang, H. Li, B. Zhu, Y. Feng, S. Wang, S. Zhang, Ultrason. Sonochem., 14, (2007), 67

[53] X. Chen, H. Li, H. Luo, M. Qiao, Appl. Catal. A., 233, (2002), 13

[54] B. M. Nagaraja, A. H. Padmasri, P. Seetharamulu, K. Hari Prasad Reddy. B. David Raju, K. S. Rama Rao, J. Mol. Catal. A., 278, (2007), 29

[55] S. P. Lee, Y. W. Chen, Ind. Eng. Chem. Res., 38, (1999), 2548

[56] A. Kaufman, J. C. Adams, J. Am. Chem. Soc., 45, (1923), 3029

[57] J. Wu, Y. Shen, C. Liu, H. Wang, C. Geng, Z. Zhang, Catal. Commun., 6, (2005), 633

[58] B. M. Nagaraja, A. H. Padmasri, B. David Raju, K. S. Rama Rao, Int. J. Hydrogen Energy, 36, (2011), 3417

[59] S. Sitthisa, W. An. D. E. Resasco, J. Catal., 284, (2011), 90

[60] N. R. Avery, Surf. Sci., 125, (1983), 771

[61] M. Mavrikakis, M. A. Barteau, J. Mol. Catal. A., 131, (1998), 135

[62] H. Li, S. Zhang, H. Luo, Mater. Lett., 58, (2004), 2741

[63] C.D. Bellefon, P. Fouilloux, Catal. Rev., -Sci. Eng., 36, (1994), 459

[64] J. G. M. Bremner, R. K. F. Keeys, J. Chem. Soc., (1947), 1068

[65] US 2754304

[66] R. M. Lukes, C. L. Wilson, J. Am. Chem. Soc., 73, (1951), 4790

[67] H. P. Thomas, C. L. Wilson, J. Am. Chem. Soc., 73 (1951), 4803

[68] C. L. Wilson, J. Chem. Soc., 52, (1945)

[69] P. Mäki-Arvela, N. Kumar, A. Nasir, T. Salmi, D. Y. Murzin, Ind. Eng. Chem. Res., 44, (2005), 9376

[70] EP 0400892A3

[71] N. Thakar, R. J. Berger, F. Kapteijn, J. A. Moulijn, Chem. Eng. Sci. 62, (2007), 5322

[72] G. J. Hutchings, F. King, I. P. Okoye, C. H. Rochester, Appl. Catal. A: Gen., 83, (1992), L7.

[73] G. J. Hutchings, F. King, I. P. Okoye, C. H. Rochester, Catal. Lett., 23, (1993), 127

[74] M. B. Padley, C. H. Rochester, G. J. Hutchings, F. King, J. Chem. Soc. Faraday Trans., 90, (1994), 203

[75] G. J. Hutchings, F. King, I. P Okoye, M. B. Padley, C. H. Rochester, J. Catal., 148, (1994), 464

[76] S. S. Ashour, J. E. Bailie, C. H. Rochester, J. Thomson, G. J. Hutchings, J. Mol. Catal. A: Chem., 123, (1997), 65

[77] G. J. Hutchings, F. King, I. P Okoye, M. B. Padley, C. H. Rochester, J. Catal., 148, (1994), 453

[78] CA 2495386

[79] US 3320312

[80] A.L. Schul'tsev, E.F. Panarin, Russ. J. Gen. Chem., 80, (2010), 1309

[81] L. Hernandez, F. F. Nord, J. Colloid Interface Sci., 3, (1948), 363

[82] P. S. Kumbhar, M. R. Kharkar, G. D. Yadav, R. A. Rajadhyaksha, J. Chem. Soc. Chem. Commun., (1992), 584

[83] M. A. Aramendia, V. Borau, J. F. Gómez, C. Jiménez, M. Marinas, Appl. Catal., 10, (1984), 347

[84] M. A. Aramendia, V. Borau, J. F. Gómez, A. Herrera, C. Jiménez, M. Marinas, J. Catal., 140, (1993), 335

[85] P. S. Kumbhar, Appl. Catal., 96, (1993), 241

[86] A. Alba, M. A. Aramendia, V. Borau, C. Jiménez, J. M. Marinas, Appl. Catal., 17, (1985), 223

[87] M. A. Aramendia, V. Borau, C. Jiménez, J. M. Marinas, M. E. Sempere, P. Urbnao, Appl. Catal., 43, (1998), 41

[88] S. D. Lin, D. K. Sanders, M. A. Vannice, Appl. Catal., 113, (1994), 59

[89] D. K. Sanders, S. D. Lin, M. A. Vannice, J. Catal., 147, (1994), 375

[90] T. Koscielski, J. M. Bonnier, J. P. Damon, J. Masson, Appl. Catal., 49, (1989), 91

[91] S. D. Lin, D. K. Sanders, M. A. Vannice, J. Catal., 147 (1994), 370

[92] J. Masson, S. Vidal, P. Cividino, P. Fouilloux, J. Court, Appl. Catal., 99, (1993), 147

[93] M. Freifelder *et al*. J. Pharm. Sci., 53, (1964), 967

[94] W. B. Wheatley *et al.*, J. Am. Chem. Soc., 76, (1954), 4490

[95] J. M. Hawkins, T.W. Makowski, Org. Proc. Res. Dev., 5, (2001), 328

[96] S.D. Jackson, R. McEwan, R.R. Spence, 2008, *Catalysis of organic reactions*, Boca Raton: CRC Press, p. 79

[97] K. T. Hindle, S. D. Jackson, D. Stirling, G. Webb, J. Catal., 241, (2006), 417

[98] K. F. Graham, K. T. Hindle, S. D. Jackson, D. J. M. Williams, S. Wuttke, Top. Catal., 53, (2010), 1121

[99] US 4021487

[100] US 2680136

[101] US 2797244

[102] US 3423462

[103] M. I. Abdul-Wahab, S. D. Jackson, Appl. Catal., A. Gen: 462-463, (2013), 121

[104] E. M. Vass, *Development of next generation methanol synthesis catalysts*, (phD thesis), Glasgow, University of Glasgow, 2005

[105] W. M. Latimer, J. H. Hildebrand, 1951, *Reference book of inorganic chemistry*, New York: Macmillan, p 581

[106] C. A. Stydom, C. P. J. van Vuuren, Journal Therm. Anal., 32, (1987), 157

[107] W-P. Dow, Y-P. Wang, T-J. Huang, Appl. Catal., 190, (2000), 25

[108] J. Z. Shyu, K. Otto, J. Catal., 115, (1989), 16

[109] H. C. Yao, Y. F. Yu Yao, J. Catal., 86, (1984), 254

[110] M. Haneda, T. Mizushima, N. Kakuta, A. Ueno, Y. Sato, S. Matsuura, K. Kasahara, M. Sato, Bull. Chem. Soc. Jpn., 66, (1993), 1279

[111] L. G. Appel, J. G. Eon, M. Schmal, Phys. Status Solidi A., 163, (1997), 107

[112] C. Decarne, E. Abi-Aad, B. G. Kostyuk, V. V. Lunin and A. Aboukals. J. Mater. Sci., 39, (2004), 2349

[113] L. Vivier, D. Duprez, ChemSusChem, 3, (2010), 645

[114] US 8710251

[115] P.G. Menon, J. Mol. Catal., 59, (1990), 207

[116] H. H. Voge, J. M. Good, B. J. Greensfelder, 1951, *Proceedings of the Third World Petroleum Congress*, p. 124

[117] B. C. Gates, J. R. Katzer, G.C. A. Schuit, 1979, *Chemistry of Catalytic Processes*, New York: McGraw-hill, p. 43

[118] CJ.G. Van Der Grift, A. Mulder, J. W. Geus, Appl. Catal., 60, (1990), 181

[119] S.D. Jackson, F.J. Robertson, J. Willis, J. Mol. Catal., 63, (1990), 255

[120] E. Simón, J M Rosas, A. Santis, A. Romero, Chem Eng J., 214, (2013), 119

[121] A. R. Pradhan, J. F. Wu, S. J . Jong, T.C. Tsia, S. B. Liu, Appl. Catal. A: Gen., 165, (1997), 489

[122] B. Harrison, A.F. Diwell, C. Hallett, Plat. Met. Rev., 32, (1988), 73

[123] E.C. Su, W.G. Rothschild, J. Catal., 99, (1986), 506

[124] M. Fernandez-Garcia, E. Gomez Rebollo, A. Guerra Ruiz, J. C. Conesa, J. Soria, J. Catal., 172, (1997), 146

[125] K. Pokrovski, A. T. Bell, J. Catal., 241, (2006), 276

[126] F. Arena, R. Giovenco, T. Torre, A. Venuto, A. Parmaliana, Appl. Catal. B, 45, (2003), 51

[127] F. Arena, K. Barbera, G. Italiano, L. Spadaro, F. Frusteri, J. Catal., 249, (2007), 183

[128] F. Arena, G. Italiano, K. Barbera, G. Bonura, L. Spadaro, F. Frusteri, Appl. Catal. A., 350, (2008), 16

[129] A. Trovarelli, Catal Rev. -Sci. Eng., 38, (1996), 439

[130] S. Bennici, A. Auroux, C. Guimon, A. Gervasini, Chem Mater., 18, (2006), 3641

[131] W.-P. Dow, Y.-P. Wang, T.-J. Huang, J. Catal., 160, (1996), 155

[132] J.-B. Wang, H.-K. Lee, T.-J. Huang, Catal. Lett., 83, (2002), 79

[133] W. Liu, M. Flytzani-Stephanopoulos, J. Catal., 153, (1995), 304

[134] A. Tschbpe, W. Liu, M. Flytzani-Stephanopoulos, J. Y Ying, J. Catal., 157, (1995), 42

[135] W. Liu, M. Flytzani-Stephanopoulos, Chem. Eng. J., 64, (1996), 283

[136] A. Aboukais, A. Bennani, C. F. Aissi, G. Wrobel, M. Guelton, J. Chem. Soc., Faraday Trans., 88, (1992), 1321

[137] E. Abi-ad, A. Bennani, J. P Bonnelle, A. Aboukais, J. Chem. Soc., Faraday Trans., 91, (1995), 99

[138] G. Wrobel, C. Lamenter, A. Bennani, A. D'Huysser, A. Aboukais, J. Chem. Soc. Faraday Trans., 92, (1996), 2001

[139] M. Shimokawabe, A. Ohi, N. Takezawa, Appl. Catal. A, 85, (1992), 129

[140] M. Lin, C. Yang, Y. Shan, W. Wei, Y. Sun, M. H, Prepr. Pap.-Am. Chem. Soc., Div. Fuel Chem., 48, (2003), 885

[141] R. Burch, S. E. Golunski, M. S. Spencer, J. Chem. Soc., Faraday Trans., 86, (1990), 2683

[142] G. Seo, H. Chon, J. Catal., 67, (1981), 424

[143] G. Plesch, F. Hanic, K. Putyera, Thermochim. Acta, 176, (1999), 267

[144] F. Hanic, I. Horvath and G. Plesch, Thermochim. Acta, 145, (1989), 19

[145] H.-C. Yao, P. H. Emme, J. Am. Chem. Soc., 81, (1959), 4125

[146] S. D. Jackson, E. A. Gelder, M. Lok, Catal. Lett., 84, (2012), 205

[147] B. Coq, A. Tijani, F. Figueras, J. Mol. Catal., 68, (1991), 331

[148] K. T. Hindle, S. D. Jackson, G. Webb, 2005, *Catalysis of Organic Reactions*, Boca Raton: CRC Press, p. 77

[149] C. Black, S. D. Jackson, unpublished results

[150] C. Campos, C. Torres, M. Oportus, M. A. Pena, J. L. G. Fierro, P. Reyes, Catal. Today, 213, (2013), 93

[151] A. S. Canning, S. D. Jackson, A. Monaghan, T. Wright, Catal. Today, 116, (2006), 22

[152] L. C. Begley, K. J. Kakanskas, A. Monaghan, S. D. Jackson, Catal. Sci. Tech., 2, (2012), 1287

[153] V. V. Gorodetskii, B. E. Nieuwenhuys, W. M. H. Sachtler, G. K. Boreskov, Surf. Sci., 108, (1981), 225

[154] W. Nichtl-Pecher, W. Stammler, K. Heinz, K. Muller, Pys. Rev. B: Condens Matter., 43, (1991), 6946

[155] N. M. Bertero, C. R. Apesteguia, A. J. Marchi, Appl. Catal. A, 349, (2008), 100

[156] M. Bonnet, P. Geneste, Y. Lozano, C.R. Acad. Sci., Ser. IIc: Chim., 282, (1976), 1009

[157] C. Kemball, C. T. H. Stoddart, Proc. R. Soc. London, Ser. A, 241, (1957), 208

[158] P. Geneste, M. Bonnet, M. Rodrigues, J. Catal., 57, (1979), 147

[159] E. L. Pitara, B. N'Zemba, J. Barbier, F. Barbot, F. Miginiac, J. Mol. Catal. A., 106, (1996), 235

[160] G, Mink, L. Horvath, React. Kinet. Catal. Lett., 65, (1998), 59

[161] P.E. Garcia, A. S. Lynch, A. Monaghan, S. D. Jackson, Catal. Today, 164, (2011), 548

[162] J. P. Boitiaux, J. Cosyns, S. Vasijdevan, Appl. Catal., 15, (1985), 317

[163] J. Yu, J. B. Spencer, Chem. Commun., (1998), 1103